Study of CP-properties of the Higgs sector of supersymmetric models

Biswaranjan Das

A thesis

submitted for the degree of

Doctor of Philosophy

Department of Physics

Indian Institute of Technology Guwahati

Guwahati-781039, India

December 2018

Study of CP-properties of the Higgs sector of supersymmetric models

Biswaranjan Das

A thesis
submitted for the degree of
Doctor of Philosophy

Supervisor
Prof. Poulose Poulose

Department of Physics
Indian Institute of Technology Guwahati
Guwahati - 781 039, India

December 2018

This thesis is dedicated to
the memory of my
mom and dad,
Junu Das
and
Dinesh Das.

Declaration

This thesis is based on my original research works carried out at the Department of Physics, Indian Institute of Technology Guwahati, India, under the supervision of Prof. Poulose Poulose. Whenever contributions of others are involved, it is clearly mentioned with due reference to the literature and acknowledgement. No part of this thesis has been submitted elsewhere for award of any other degree or qualification.

Date: **Biswaranjan Das**

Place: Guwahati

Prof. Poulose Poulose
Department of Physics
Indian Institute of Technology Guwahati
Guwahati - 781039, INDIA
Email: poulose@iitg.ac.in

CERTIFICATE

This is to certify that the work contained in the thesis entitled **"Study of CP-properties of the Higgs sector of supersymmetric models"** by **Mr. Biswaranjan Das**, a Ph.D student of the Department of Physics, Indian Institute of Technology Guwahati, was carried out under my supervision and has not been submitted elsewhere for award of any degree.

The thesis, in my opinion, has reached the standard fulfilling the requirement for the award of degree of **Doctor of Philosophy** in accordance with the regulations of Indian Institute of Technology Guwahati.

Date: **Prof. Poulose Poulose**

Place: Guwahati

Acknowledgements

I am strongly indebted to my thesis supervisor Prof. Poulose Poulose for giving me the opportunity to work with him, and for all his countless suggestions and support throughout my research career. I greatly acknowledge Prof. Stefano Moretti and Dr. Shoaib Munir for the wonderful research collaboration and their constant support and suggestions throughout this work. I extend my sincere thanks to our other collaboration members: Dr. Amit Chakraborty, Prof. Dilip Kumar Ghosh and Prof. J. L. Diaz-Cruz. I acknowledge my doctoral committee members: Prof. Bipul Bhuyan, Dr. Arunansu Sil and Dr. P. A. S. Sree Krishna.

I am very thankful to the former HoD Prof. Saurabh Basu and the present HoD Prof. Shubhradeep Ghosh of the Department of Physics for providing the full support and facilities at their best. I extend my hearty thanks to all the faculty members and staff of the Department of Physics, who supported me in several ways during this period. I also extend my thanks to all the members of the HEP Journal Club, IIT Guwahati. Special thanks to Dr. M. C. Kumar, Dr. Sunando Patra and Srimoy Bhattacharya for some very useful physics discussions related to this work. I am grateful to Mr. Basab Purkayastha and Mr. Hemanta Medhi for their help to resolve the technical issues on many occasions.

I am grateful to my friends and colleagues, specially, Kamal Jyoti Nath, Kamal Dutta, Shibananda Sahoo, Subhasish Behera, Deepanjali Goswami, Dr. V. Prasad, Dr. Satendra Kumar, Dr. Deepanwita Dutta and Dr. Biswajit Karmakar.

My sincere thanks extend to IIT Guwahati and SERC, DST (India), for providing financial assistance during this course of work. A part of this work had been supported by a SERC, DST (India) project SR/S2/HEP-41/2009.

Acronyms

ATLAS	:	A Toroidal LHC Apparatus
(B-L)SSM	:	B-L Supersymmetric Standard Model
BP	:	banchmark points
BR	:	branching ratio
BSM	:	beyond the Standard Model
CEDM	:	chromo electric dipole moment
CL	:	confidence limit
CMS	:	Compact Muon Solenoid
CPC	:	CP-conserving
CPV	:	CP-violating
DM	:	dark matter
ED	:	extra dimension
EDM	:	electric dipole moment
EW	:	electroweak
EWSB	:	electroweak symmetry breaking
FCNC	:	flavor changing neutral current
GeV	:	Giga electron Volt
GGF	:	gluon gluon fusion
GUT	:	Grand Unified Theory
h.c.	:	Hermitian Conjugate

HO	:	higher order
LEP	:	Large Electron-Positron Collider
LHC	:	Large Hadron Collider
LO	:	leading order
MSSM	:	Minimal Supersymmetric Standard Model
NMSSM	:	Next-to-Minimal Supersymmetric Model
NNLO	:	next-to-next leading order
NP	:	new physics
NWA	:	narrow width approximation
QCD	:	quantum chromodynamics
QED	:	quantum electrodynamics
SM	:	Standard Model
SSB	:	spontaneous symmetry breaking
SUSY	:	Supersymmetry
TeV	:	Tera electron Volt
2HDM	:	2 Higgs Doublet Model
VEV	:	vacuum expectation value
VBF	:	vector bosons fusion

Abstract

In 2012, the ATLAS and CMS collaborations independently observed a new Higgs-like particle with a mass $M_h \sim 125$ GeV and properties similar to that predicted by the Standard Model (SM) at the Large Hadron Collider (LHC). So far, although the measurements indicate that this Higgs-like boson is compatible with the SM hypothesis, however due to large uncertainties in some of the Higgs detection channels, one still has the possibility of testing this new particle as being a candidate for some beyond the SM (BSM) physics scenarios, for example, the Minimal Supersymmetric Standard Model (MSSM), in the CP-conserving version (CPC-MSSM). We evaluate the modifications of the CPC-MSSM results when CP-violating (CPV) phases are turned on explicitly, leading to the CP-violating MSSM (CPV-MSSM). We investigate the role of the CPV phases in (some of) the soft Supersymmetry (SUSY) breaking terms on both the mass of the lightest Higgs boson h_1, and the rates for some of the gluon gluon fusion (GGF) processes like, $gg \to h_1 \to \gamma\gamma$, $gg \to h_1 \to ZZ^* \to 4l$, $gg \to h_1 \to W^+W^- \to l\nu l\nu$, and the vector boson fusion (VBF) processes like, $qq \to h_1 \to b\bar{b}$ and $qq \to h_1 \to \tau^+\tau^-$, at the LHC, considering the impact of stringent flavor constraints as well as the constraints coming from electric dipole moment (EDM) measurements. We find that it is possible to have a Higgs mass of about 125 GeV with relatively small $\tan\beta$, large A_t and a light stop, which is consistent with the current SUSY particle searches at the LHC. We obtain that the imaginary part of the top and bottom Yukawa couplings can take very small but non-zero values even after satisfying all the recent updates from both the ATLAS and CMS collaborations within 1-2σ uncertainties which might be an interesting signature to look for at the future runs of the LHC. Our study shows that the CPV-MSSM provides a potential solution to the recent LHC Higgs data, in fact offering very little in the way of distinction between these two SUSY models (CPC-MSSM and CPV-MSSM) at the 7 and 8

TeV run of the LHC. Improvement in different Higgs coupling measurements is necessary in order to test the possibility of probing any small dependence on these CPV phases in the MSSM Higgs sector.

In the Next-to-Minimal Supersymmetric Standard Model (NMSSM), it is possible for either one of the additional singlet-like scalar and pseudoscalar Higgs bosons to be almost degenerate in mass with the 125 GeV SM-like Higgs state. In the real NMSSM (rNMSSM), when the mass difference between two scalar states is comparable to their individual total decay widths, the quantum mechanical interference, due to the relevant diagonal as well as off-diagonal terms in the propagator matrix, between them can become sizable. This possibility invalidates usage of the narrow width approximation (NWA) to compute the cross section for the production of a di-photon pair with a given invariant mass via resonant Higgs boson(s) in the gluon fusion process at the LHC. When, motivated by the baryon asymmetry of the universe, CPV phases are explicitly invoked in the Higgs sector of the NMSSM, all the interaction eigenstates mix to give five CP-indefinite physical Higgs bosons. In this scenario, the interference effects due the off-diagonal terms in the Higgs mass matrix that mix the pseudoscalar-like state with the SM-like one can also become significant, when these two are sufficiently mass-degenerate. We perform a detailed analysis, in both the real and complex NMSSM, of these interference effects, when the full propagator matrix is taken into account, in the production of a photon pair with an invariant mass near 125 GeV through gluon fusion. We find that these effects can account for up to $\sim 40\%$ of the total cross section for certain model parameter configurations. We also investigate how such mutually interfering states contributing to the 125 GeV signal observed at the LHC can be distinguished from a single resonance.

In the NMSSM, it is possible to have strong mass degeneracies between the new singlet-like scalar and the heavy doublet-like scalar, as well as between the singlet-like and doublet-like pseudoscalar Higgs states. When the difference in masses of such states is comparable to their widths, the quantum mechanical interference between their propagators can become significant. We study these effects by taking into account the full Higgs boson propagator matrix in the calculation of the production process of $\tau^+\tau^-$ pairs in gluon fusion at the LHC. We find that, while these interference effects are sizable, they are not resolvable in terms of the distributions of differential cross sections, owing to poor detector resolution of the $\tau^+\tau^-$ invariant mass. They are, however, identifiable via the inclusive cross

sections, which are subject to significant variations with respect to the standard approaches, wherein the propagating Higgs bosons are treated independently from one another. We quantify these effects for several representative benchmark points (BPs), extracted from a large set of points, obtained by numerical scanning of the NMSSM parameter space, that satisfy the most stringent experimental constraints currently available.

List of publications included in the thesis

1. A. Chakraborty, **B. Das**, J. L. Diaz-Cruz, D. K. Ghosh, S. Moretti and P. Poulose; "125 GeV Higgs signal at the LHC in the CP-volating MSSM"; Phys.Rev. D90 (2014) no.5, 055005; arXiv:1301.2745 [hep-ph].

2. **B. Das**, S. Moretti, S. Munir and P. Poulose; "Two Higgs bosons near 125 GeV in the NMSSM: beyond the narrow width approximation"; Eur.Phys.J. C77 (2017) no.8, 544; arXiv:1704.02941 [hep-ph].

3. **B. Das**, S. Moretti, S. Munir and P. Poulose; "Quantum interference amongst heavy NMSSM Higgs bosons"; Phys.Rev. D98 (2018) no.5, 055020; arXiv:1804.10393 [hep-ph].

Contents

List of Figures

List of Tables

Preface

The thesis describes my research activities carried out during the course of my Ph.D. studies. The main objective in the thesis is the BSM phenomenology at the particle colliders, especially the LHC. A detailed phenomenological study has been performed on the rich and extended Higgs sector of widely popular SUSY models, namely, the MSSM and the NMSSM, with a special focuss to their CP-nature.

Chapter 1 provides an introduction and motivation of the thesis and a brief discussion on the SM as well as its drawbacks. A discussion on the standard mechanism of electroweak symmetry breaking (EWSB), that is the Higgs mechanism, is presented in detail. Next, a detailed discussion on the theoretical framework of the MSSM is presented along with its solutions to the SM and its potential drawbacks followed by a brief discussion on the NMSSM. The CP-nature of the Higgs sector of these models is given a special attention here and it proivdes an elaborate discussion on the correlation between the CPV phases of the complex SUSY parameters with the EDMs of elementary particles as well as atomic EDMs.

Chapter 2 presents our investigation on the promising LHC signatures and discovery potentials of the MSSM Higgs sector and the CPV signatures in some of the most prominent Higgs discovery channels like, $gg \to h_1 \to \gamma\gamma$, $gg \to h_1 \to WW^*$ and $gg \to h_1 \to ZZ^*$. Other channels associated with VBF processes, like, $qq \to h_1 \to b\bar{b}$ and $qq \to h_1 \to \tau^+\tau^-$ are also studied here.

Chapter 3 is devoted to the study of the NMSSM Higgs sector (which includes an extra scalar field in addition to the two scalar doublets of the MSSM) in the light of SM-like resonance discovered at the LHC, as the NMSSM opens further possibilities in the Higgs as well as other sectors, at the same time resolving few flaws of the MSSM, like the famous $\mu-$problem. In the NMSSM, it is possible for anyone of the additional singlet-like scalar and pseudoscalar Higgs bosons to be almost degenerate in mass with the 125 GeV SM-like Higgs state. A detailed

analysis, in both the real and complex NMSSM, of the quantum mechanical interference effects which become significant in case of strong mass-degeneracies, is presented here, when the full propagator matrix is taken into account instead of usual NWA approach, in the production of a photon pair with an invariant mass near 125 GeV through gluon fusion. Also an investigation on how such mutually interfering states contributing to the 125 GeV signal can be distinguished from a single resonance is performed here.

Chapter 4 deals with the possibility of having strong mass degeneracies between the new singlet-like scalar and the heavy doublet-like scalar, as well as between the singlet-like and doublet-like pseudoscalar Higgs states in the context of the NMSSM. The analysis is performed by taking into account the full Higgs boson propagator matrix in the calculation of cross sections for the production of a $\tau^+\tau^-$ pair in the gluon fusion at the LHC.

Chapter 5 provides an over all summary and conclusions of the thesis.

Chapter 1

Introduction

The observation of a new particle by the ATLAS and CMS experiments in 2012 with properties consistent with the Higgs boson predicted by the SM [1, 2] was a major turning point in particle physics, establishing the Higgs mechanism as a correct way to understand the dynamics of EWSB. The discovery of this SM-like Higgs boson has put the focus of particle physics phenomenology on the nuances of the Higgs sector. Coupled with the issues like the stability of the scalar mass against large quantum corrections, absence of a dark matter (DM) candidate, non-zero neutrino masses, matter-antimatter asymmetry observed in the universe, a need for new ideas, classified as BSM scenarios emerged. Typically, BSM scenarios involve introducing additional particle spectrum and additional interactions. In many cases, these could involve additional gauge symmetries as well. Some popular ideas in this direction are the Left-Right Symmetric Models, $U(1)$ extensions of the SM, Grand Unified Theories (GUTs), etc, extending the gauge symmetry; Two (Three) Higgs Doublet Models (2(3)HDMs), Higgs Triplet Models, etc, extending the Higgs sector of the SM; models with heavy neutrinos, additional vector-like fermions, etc, extending the fermionic sector. Many of these scenarios can present a candidate for DM, with suitable arrangements like the presence of discrete Z_2 symmetries. In an entirely new direction, scenarios considering more than three spatial dimensions have become very attractive in the recent past. Such models explain the gauge hierarchy problem by bringing down the scale at which gravity becomes comparable in strength to other interactions to the TeV level with the help of fields in higher dimensional space-time. The idea of SUSY introduces a new class of invariant transformations. Unlike the gauge symmetry, SUSY involves space-time transformation and relates the $\frac{1}{2}-$integer spin fields to the integer spin

fields. This can be introduced along with any gauge field theory. BSM scenarios generally introduce new particles, exotic to the SM, with masses possibly in the TeV range – an energy regime within the reach of the LHC, which makes the BSM scenarios phenomenologically interesting.

SUSY models are the most popular and intensely studied BSMs, which have a class of new particles, as they relate bosonic and fermionic degrees of freedom, making the phenomenology interesting, rich and well-motivated, while at the same time addressing the issues like the stability of Higgs mass and providing a natural DM candidate. In order to explain the LHC Higgs data, several studies have been performed within different SUSY models, like the MSSM [3–6], the NMSSM [7, 8], the B-L Supersymmetric Standard Model ((B–L)SSM) [9]. These models can have a SM-like Higgs boson with mass around 125 GeV and also accommodate potential slight disagreement between the data and the SM predictions in different decay channels of the Higgs boson observed at the LHC. However, in the CPC-MSSM, such solutions indicate the presence of relatively heavy stop and large $\tan\beta$ (ratio of the vacuum expectation values of the two scalar doublets), which are increasingly constrained by LHC measurements. On the other hand, as shown in chapter 2 of this thesis, the CPV-MSSM or the complex MSSM (cMSSM), where all the parameters in the Higgs and sfermion sectors are assumed to be complex, could provide a viable solution with relatively lighter stop and smaller $\tan\beta$, at the same time satisfying stringent flavor as well as EDM constraints (see ref. [10]). However, the recent LHC Run 2 data severely constrain the MSSM parameter space by excluding $\tan\beta$ above 9 in the $\tau^+\tau^-$ final state [11]. Besides this, the MSSM is also foiled by issues like the presence of the Higgsino mass parameter μ, which is phenomenologically required to be at the electroweak (EW) scale but has no theoretical ground to be so, known as the $\mu-$problem [12].

The NMSSM was proposed to take care of this so-called $\mu-$problem by introducing a new singlet superfield [13, 14]. The presence of this field leads to two additional neutral mass eigenstates in the NMSSM compared to the MSSM. When all the parameters in the Higgs and sfermion sectors are assumed to be real and hence CP-conserving, one of these two additional states is a scalar and the other a pseudoscalar. With three scalars, H_1, H_2, H_3, and two pseudoscalars, A_1, A_2 (H's and A's are in ascending order of their masses), in total, the real NMSSM (rNMSSM) or CP-conserving NMSSM (CPC-NMSSM) provides some novel possibilities for collider phenomenology like presence of a light pseudoscalar state. The extended

Higgs sector of the NMSSM gives rise to unique phenomenological possibilities, which are hindered or experimentally ruled out in the MSSM. For example, in the CPC-NMSSM either of the two lightest CP-even Higgs bosons, H_1 or H_2, can be the 125 GeV SM-like Higgs boson, H_{obs}, observed at the LHC. The scenario with H_2 identified as the H_{obs} is realized in a particular parameter space region of the NMSSM, where the tree-level mass of H_2 is maximal. Thus H_2 can gain a mass near 125 GeV without requiring large radiative corrections from supersymmetric sectors, unlike the case of MSSM.

An alternate possibility is that in multi Higgs models like the MSSM and the NMSSM, the observed peak near 125 GeV can actually be due to two or more Higgs resonances, which cannot be resolved individually by experiments, in contrast to the SM, where a single Higgs doublet field is involved in the EWSB, and as a consequence, one physical scalar Higgs boson is viable. In the CPC-MSSM, the possibility of two scalars both lying near 125 GeV is ruled out by the fact that such a mass for one of the scalars generally requires the other scalar to be essentially decoupled, and hence much heavier or lighter. In the CPC-NMSSM though, it is still a plausible scenario, as discussed in ref. [15–18] for two scalar mass-degenerate resonances, and in ref. [19] for a scalar and a pseudoscalar both having masses near 125 GeV.

Moreover, CP violation can be invoked in the NMSSM Higgs sector at the tree-level by assuming the Higgs self-couplings λ and κ to be complex, unlike the MSSM, where CP violation enters via Higgs-sfermion couplings at one-loop level [20–22]. CP violation, being one of the main conditions for baryogenesis [23], can lead to the observed matter-antimatter asymmetry in the universe. In the SM, CP violation based on the Cabibbo-Kobayashi-Maskawa (CKM) matrix [24] is too small to explain quantitatively the baryon asymmetry. These facts motivate to study, particularly those models which include additional sources of CP violation. Although the corresponding CPV phases are tightly constrained by fermionic and atomic EDMs [25–27], these constraints can be relaxed under certain conditions [21, 28]. Beyond the Born approximation, the phases of the complex higgsino mass parameter μ, and the SUSY breaking Higgs-sfermion couplings A_f also induce CP violation in the Higgs sector, as in the case of MSSM. In the presence of the complex phases, the five neutral Higgs bosons are CP-indefinite states, due to the mixing between the scalar and pseudoscalar interaction eigenstates. CPV phases can therefore influence the phenomenology of the NMSSM Higgs bosons by, e.g.,

modifying their mass spectrum as well as the production and decay rates [29], similar to the MSSM [10, 30, 31]. In addition, like in the case of CPC-NMSSM, in the CP-violating NMSSM (CPV-NMSSM) also, mass-degenerate states can arise.

The specific case of two mass-degenerate Higgs resonances near 125 GeV in the CPV-NMSSM or the complex NMSSM (cNMSSM) was considered in a recent study [32], which shows that the two mass-degenerate Higgs bosons near 125 GeV can give a better-fit to the LHC data, compared to a single resonance in the NMSSM, with non-zero CPV phases improving the situation. In all these previous analyses of this scenario in the NMSSM, it was assumed that each of the two resonant Higgs bosons are produced on-shell and decay subsequently into the observed channels, assuming the narrow width approximation (NWA). In chapter 3, we study the effects of the possible mixing at the propagator level, where, H_i is produced, but propagates to H_j (where $i \neq j$) through mixing facilitated by quantum mechanical corrections, before decaying into two photons [33].

In the MSSM, in principle, either of the H_1 and H_2 could be the Higgs boson, H_{obs}, observed at the LHC. However, the model's parameter space region where H_2 has a mass near 125 GeV and almost SM-like couplings to EW gauge bosons is very tightly constrained by experimental data [34, 35]. Alternatively, the condition on H_1 to be a candidate for H_{obs}, while a phenomenologically much more favored scenario, pushes m_{H_2} and m_A upwards into the so-called decoupling regime, where they are nearly mass-degenerate. Thus, if a bump appears in the experimental data near a certain large invariant mass of a fermion-antifermion or photon pair above the SM expectation, it could very well be due to these two states combined, unless their mass difference is large enough to enable the experiments to resolve them individually. A formidable difference in the statistical significance of the peaks observed in the fermionic channels versus the W^+W^- and ZZ^* channels could also be interpreted as a hint of the (H_2, A) mass-degeneracy. However, if the Higgs sector of the MSSM is CP-violating, the two heavy mass-degenerate states could mutually interfere quantum mechanically. This interference could significantly alter the cross section expected for a given SM final state that these Higgs bosons decay into [36–38].

In the NMSSM, there exists an extra scalar, H_s, and an extra pseudoscalar, A_s, in the Higgs sector. The masses of these two new Higgs states are essentially free model parameters and either of them could very well lie near 125 GeV, along with the MSSM-like H_1. The scenario with m_{H_s} near m_{H_1} is in fact well-motivated by

naturalness considerations, since the doublet-singlet mixing can enhance the tree-level mass of H_1 appreciably [7, 8, 39]. The potentially strong interference effects in the scenario where these Higgs bosons are too close in mass for the peaks to be individually identifiable, given the current di-photon mass resolution at the LHC, have therefore been analyzed in chapter 3 of the thesis (see ref. [33]). Finally, in the next chapter we consider the alternative scenarios wherein one (or possibly even both) of H_s and A_s could be mass-degenerate with the heavier H_2 and A instead of H_1. Our main purpose here is to investigate the phenomenological implications of such a scenario, which is a viable one in general extended Higgs sector, without delving into its theoretical motivations in the specific model considered here (see [40]).

The thesis is organized in five chapters. In the remaining part of this chapter, we present a brief overview of the SM and its main drawbacks. After that, we briefly revisit the MSSM and the NMSSM, and their advantages over the SM, with a particular emphasis on the CP-nature of the Higgs bosons. It is followed by a dedicated discussion on atomic and sub-atomic EDMs, and their effects on non-trivial CPV phases in the MSSM. Chapter 2 is based on our investigation on the viability of CPV-MSSM solutions in the light of LHC Higgs data (Run 2). Chapter 3 presents our analysis, in both real and complex NMSSM, of the quantum mechanical interference effects in case of strong mass-degeneracy between two Higgs bosons near 125 GeV. In chapter 4, we revisit the case of strong mass-degeneracy between the singlet-like scalar and the heavy doublet-like scalar, as well as between the singlet-like and doublet-like pseudoscalar Higgs states in the NMSSM. Finally we draw our conclusions in chapter 5. Some explicit calculations and expressions on topics like, convolution, Higgs self-energies and mass matrix elements etc, are presented in the Appendices.

1.1 The Standard Model

The SM is a quantum field theory of three fundamental interactions of nature, namely, strong, weak and electromagnetic (EM) interactions. It is a gauge theory based on the symmetry group $SU(3)_c \times SU(2)_L \times U(1)_Y$. Here $SU(3)_c$ is the gauge group of the quantum chromodynamics (QCD) with c representing the color. $SU(2)_L \times U(1)_Y$ is related to the EW interaction with L indicating that this transformation applies to left handed fields only and Y is the hypercharge. The

EW symmetry is broken down to $U(1)_{\rm em}$ symmetry. It results in three massive vector bosons $W^{\pm}$ and Z, while photon (γ) is the massless gauge boson associated with the unbroken $U(1)_{\rm em}$ symmetry. Photon is responsible for EM interactions and $W^{\pm}$ and Z correspond to weak interactions. There are eight gluons which mediate strong interactions.

The fermionic fields in the SM can be broadly classified into two categories: leptons and quarks. The leptons are further categorized into two types: charged leptons and neutrinos (the neutral ones). There are three charged leptons: electron (e), muon (μ), tau (τ); and three neutrinos: electron neutrino (ν_e), muon neutrino (ν_μ), tau neutrino (ν_τ). All the charged leptons have same electric charge (Q $= -1$ for leptons, Q $= 1$ for antileptons), whereas neutrinos have zero electric charge. On the other hand, there are three up-type quarks (with Q $= 2/3$, for up-type antiquarks Q $= -2/3$): up (u), charm (c), top (t); and three types of down-type quarks (with Q $= -1/3$, for down-type antiquarks Q $= 1/3$): down (d), strange (s), bottom (b). The left-handed and right-handed fermions belong to different representations in the SM. Left-handed fermions are $\rm SU(2)_L$ doublets, whereas right-handed fermions are $\rm SU(2)_L$ singlets. These are summarized in Tab. 1.1.

Generation	Lepton	Quark
1st Generation	$\begin{pmatrix}\nu_e\\ e\end{pmatrix}_L;\ e_R$	$\begin{pmatrix}u\\ d\end{pmatrix}_L;\ u_R, d_R$
2nd Generation	$\begin{pmatrix}\nu_\mu\\ \mu\end{pmatrix}_L;\ \mu_R$	$\begin{pmatrix}c\\ s\end{pmatrix}_L;\ c_R, s_R$
3rd Generation	$\begin{pmatrix}\nu_\tau\\ \tau\end{pmatrix}_L;\ \tau_R$	$\begin{pmatrix}t\\ b\end{pmatrix}_L;\ t_R, b_R$

TABLE 1.1: The fermionic field contents in the SM. The subscripts L, R stands for the left-handed and right-handed particles.

1.1.1 Electroweak symmetry breaking: the Higgs mechanism

Breaking of EW symmetry $SU(2)_L \times U(1)_Y$ down to $U(1)_{\rm em}$ symmetry takes place within the SM in presence of a scalar field Φ which transforms as a doublet under $SU(2)_L$ carrying hypercharge, $Y = 1$. The EW part of the SM Lagrangian

invariant under $SU(2)_L \times U(1)_Y$ gauge symmetry is given by

$$\mathcal{L}_{\rm EW} = \mathcal{L}_{\text{kin, gauge}} + \mathcal{L}_{\text{kin, matter}}, \tag{1.1}$$

with

$$\begin{aligned} \mathcal{L}_{\text{kin, gauge}} &= -\frac{1}{4}W^a_{\mu\nu}W^{a\mu\nu} - \frac{1}{4}B_{\mu\nu}B^{\mu\nu}\,, \\ W^a_{\mu\nu} &= \partial_\mu W^a_\nu - \partial_\nu W^a_\mu + g_2\xi^{abc}W^b_\mu W^c_\nu\,, \\ B_{\mu\nu} &= \partial_\mu B_\nu - \partial_\nu B_\mu\,; \end{aligned} \tag{1.2}$$

and

$$\begin{aligned} \mathcal{L}_{\text{kin, matter}} &= \overline{\Psi}_L i\gamma^\mu D_\mu \Psi_L + \overline{\Psi}_R i\gamma^\mu(\partial_\mu + ig_1\frac{Y}{2}B_\mu)\Psi_R\,, \\ D_\mu &= \partial_\mu + \frac{1}{2}ig_2\tau^a W^a_\mu + \frac{1}{2}ig_1 Y B_\mu\,; \end{aligned} \tag{1.3}$$

where $\mathcal{L}_{\text{kin, gauge}}$ represents the normalized kinetic part of the Lagrangian involving the gauge fields ($W^{a=1,2,3}_\mu$ for $SU(2)_L$ and B_μ for $U(1)_Y$) and $\mathcal{L}_{\text{kin, matter}}$ corresponds to the kinetic part of the Lagrangian involving the fermionic fields. g_1 and g_2 are the $U(1)_Y$ and $SU(2)_L$ coupling constants, respectively. Ψ_R and Ψ_L stand for fermionic right-handed and left-handed fields, respectively.

Higgs mechanism: Here we briefly describe how the Higgs mechanism is employed to generate masses for elementary particles. In the SM, one needs to generate the masses for the three gauge bosons, $W^\pm$ and Z. At the same time photon should remain massless, so that QED must be preserved as an exact symmetry. In order to break the EW symmetry spontaneously, a complex $SU(2)_L$ scalar doublet field (i.e. the Higgs field)

$$\Phi = \begin{pmatrix} \phi^+ \\ \phi^0 \end{pmatrix} \qquad \text{with hypercharge} \;\; Y = 1 \tag{1.4}$$

is introduced. The part the SM Lagrangian, involving the scalar or the Higgs field can be written as

$$\mathcal{L}_{\rm scalar} = (D_\mu\Phi)^\dagger(D^\mu\Phi) - V(\Phi) \;\; \text{with} \;\; V(\Phi) = \mu^2\Phi^\dagger\Phi + \lambda(\Phi^\dagger\Phi)^2\,. \tag{1.5}$$

$V(\Phi)$ in the above expression of the scalar Lagrangian is responsible for the spontaneous symmetry breaking (SSB) of $SU(2)_L \times U(1)_Y \to U(1)_{\rm em}$. For a choice

with $\mu^2 < 0$ and $\lambda > 0$, the minimum energy configuration of Φ, obtained by minimizing the potential, is given by $|\Phi^\dagger\Phi| = -\frac{\mu^2}{2\lambda} \equiv \frac{v^2}{2}$. The vacuum expectation value (VEV) should be chosen in such a way that it preserves $U(1)_{\rm em}$ symmetry. The neutral component of the scalar field acquires a non-zero VEV, v. The usual choice is

$$\langle\Phi\rangle = \frac{1}{\sqrt{2}}\begin{pmatrix} 0 \\ v+h \end{pmatrix}, \tag{1.6}$$

where h is the physical Higgs field. The choice of this new ground state *spontaneously* breaks the $SU(2)_L \times U(1)_Y$ symmetry to $U(1)_{\rm em}$, while maintaining the renormalizability and unitarity of the theory. As the $U(1)_Y$ gauge symmetry remains unbroken in this transformation, the associated gauge boson, the photon, remains massless. However, three of the degrees of freedom of the scalar doublet (corresponding to the would be Goldstone bosons) are *eaten by* or transformed into the longitudinal polarization components of the weak-isospin triplet of $W^\pm$ and Z bosons, giving them masses of $m_W = \frac{vg_2}{2}$ and $m_Z = \frac{v}{2}\sqrt{g_1^2+g_2^2}$, respectively. The mass eigenstates are expressed in terms of the gauge eigenstates as

$$\begin{aligned} W_\mu^\pm &= \frac{1}{\sqrt{2}}(W_\mu^1 \mp iW_\mu^2)\,, \\ Z_\mu &= W_\mu^3\cos\theta_W - B_\mu\sin\theta_W\,, \\ A_\mu &= W_\mu^3\sin\theta_W - B_\mu\cos\theta_W\,, \end{aligned} \tag{1.7}$$

where A_μ is the gauge field of the EM interaction (the photon), and θ_W is the Weinberg mixing angle or weak mixing angle. The remaining degree of freedom of the scalar field Φ corresponds to a massive neutral scalar particle, the Higgs boson h, with a mass $m_h = \sqrt{2v^2\lambda}$.

Interestingly, the same Higgs field provides masses to the fermions (leptons and quarks, except neutrinos) through the Yukawa interaction term in the Lagrangian which is given by

$$\mathcal{L}_{\rm Yukawa} = -g_l\overline{L}\Phi e_R - g_d\overline{Q}_L\Phi d_R - g_u\overline{Q}_L\widetilde{\Phi}u_R + \text{h.c.}\,, \tag{1.8}$$

where $\widetilde{\Phi} = i\tau_2\Phi^*$ with τ_2 being the Pauli spin matrix, and L, Q_L represent the left-handed lepton and quark doublets respectively; e_R, d_R, u_R denote the right-handed charged leptons, down-type and up-type quarks, respectively. g_l, g_d, g_u are the complex Yukawa couplings for the charged leptons, down-type and up-type quarks, respectively. From this interaction, when Φ gets VEV, masses for charged

lepton, down-type and up-type quarks can be obtained as

$$m_e = \frac{g_e v}{\sqrt{2}}, \qquad m_u = \frac{g_u v}{\sqrt{2}}, \qquad m_d = \frac{g_d v}{\sqrt{2}}. \tag{1.9}$$

The couplings of the Higgs boson with the fermions are fixed in terms of the mass of the fermion and the VEV as

$$\begin{aligned} g_{\bar{e}eh} &= \frac{\sqrt{2}m_e}{v}, \quad g_{\bar{u}uh} = \frac{\sqrt{2}m_u}{v}, \quad g_{\bar{d}dh} = \frac{\sqrt{2}m_d}{v}, \\ g_{\bar{\mu}\mu h} &= \frac{\sqrt{2}m_\mu}{v}, \quad g_{\bar{c}ch} = \frac{\sqrt{2}m_c}{v}, \quad g_{\bar{s}sh} = \frac{\sqrt{2}m_s}{v}, \\ g_{\bar{\tau}\tau h} &= \frac{\sqrt{2}m_\tau}{v}, \quad g_{\bar{t}th} = \frac{\sqrt{2}m_t}{v}, \quad g_{\bar{b}bh} = \frac{\sqrt{2}m_b}{v}. \end{aligned} \tag{1.10}$$

Similarly, the self-couplings of the Higgs boson derived from the scalar Lagrangian, given in Eq. 1.5, are

$$g_{hhh} = \frac{m_h^2}{2v}, \qquad g_{hhhh} = \frac{m_h^2}{8v^2} \tag{1.11}$$

The Higgs couplings with the gauge bosons arises through the covariant kinetic term of the scalar field $(D_\mu \Phi)^\dagger (D^\mu \Phi)$, which are given by

$$\begin{aligned} g_{hWW} &= \frac{2m_W^2}{v}, & g_{hZZ} &= \frac{2m_Z^2}{v} \\ g_{hhWW} &= \frac{2m_W^2}{v^2}, & g_{hhZZ} &= \frac{2m_Z^2}{v^2} \end{aligned} \tag{1.12}$$

Cabibbo-Kobayashi-Maskawa matrix: One can diagonalize the Yukawa complex coupling matrices associated with the quark mass matrices using the transformations

$$\begin{aligned} u_{L_i} &= V_{u_{ij}} u'_{L_j}, & d_{L_i} &= V_{d_{ij}} d'_{L_j}, \\ u_{R_i} &= W_{u_{ij}} u'_{R_j}, & d_{R_i} &= W_{d_{ij}} d'_{R_j}. \end{aligned} \tag{1.13}$$

Here u_{L_i}, d_{L_i} (u_{R_i}, d_{R_i}) and u'_{L_i}, d'_{L_i} (u'_{R_i}, d'_{R_i}) are the fields in the interaction and mass bases, respectively. $V_{u_{ij}}$ ($W_{u_{ij}}$) and $V_{d_{ij}}$ ($W_{d_{ij}}$) are 3×3 unitary matrices, with i, j being the fermion family indices. The charged current interaction between quarks and the $W^\pm$ bosons (followed from the first term in the first expression of

Eq. 1.3) can be written as

$$-\frac{g_2}{\sqrt{2}}(\bar{u}_L \;\; \bar{c}_L \;\; \bar{t}_L)\gamma^\mu W^+_\mu \begin{pmatrix} d_L \\ s_L \\ b_L \end{pmatrix} = -\frac{g_2}{\sqrt{2}}(\bar{u}'_L \;\; \bar{c}'_L \;\; \bar{t}'_L)\gamma^\mu W^+_\mu (V_u^\dagger V_d) \begin{pmatrix} d'_L \\ s'_L \\ b'_L \end{pmatrix} , \quad (1.14)$$

where the matrix $V_u^\dagger V_d$ is known as the Cabibbo-Kobayashi-Maskawa (CKM) matrix, $V_{\rm CKM}$, [24, 41]. It can be parameterized in terms of three mixing angles and a CP phase as [42]

$$V_{\rm CKM} = \begin{pmatrix} c_{12}c_{13} & s_{12}c_{13} & s_{13}e^{-i\delta} \\ -s_{12}c_{23} - c_{12}s_{13}s_{23}e^{i\delta} & c_{12}c_{23} - s_{12}s_{13}s_{23}e^{i\delta} & c_{13}s_{23} \\ s_{12}s_{23} - c_{12}s_{13}c_{23}e^{i\delta} & c_{12}s_{23} - s_{12}s_{13}c_{23}e^{i\delta} & c_{13}c_{23} \end{pmatrix} . \quad (1.15)$$

In the SM, the CKM matrix is the only source of flavor violation. In the charged current interaction, the flavor violation occurs at the tree-level, but there are no tree-level flavor changing neutral currents (FCNC). Although at loop level there can be FCNCs, but they are very much suppressed. The CKM matrix elements have been measured very precisely in various flavor changing transitions, and are given by [43]

$$V_{\rm CKM} = \begin{pmatrix} 0.97446 \pm 0.00010 & 0.22452 \pm 0.00044 & 0.00365 \pm 0.00012 \\ 0.22438 \pm 0.00044 & 0.97359^{+0.00010}_{-0.00011} & 0.04214 \pm 0.00076 \\ 0.00896^{+0.00024}_{-0.00023} & 0.04133 \pm 0.00074 & 0.999105 \pm 0.000032 \end{pmatrix} \quad (1.16)$$

Note that the off-diagonal (flavor violating) elements are smaller as compared to the diagonal (flavor conserving) ones, which are essentially of $\mathcal{O}(1)$.

SM parameters: In addition to the Yukawa couplings, the SM contains four free parameters: two of them come from the Higgs potential (μ^2, λ); the other two are the gauge couplings constants (g_1, g_2). Using the relation,

$$g_2 \sin\theta_W = g_1 \cos\theta_W = e \, , \quad (1.17)$$

one can express g_1 and g_2 in terms of the fine structure constant α ($= e^2/16\pi^2$) and the Weinberg angle ($\sin\theta_W$). Using the relation $m_h = \sqrt{-2\mu^2} = \sqrt{2v^2\lambda}$ one can eliminate μ^2 in terms of m_h, and λ in terms of v ($v^2 = 1/\sqrt{2}G_F$) and m_h, where G_F is the Fermi coupling constant.

The following three parameters are measured very precisely: [43]

$$\begin{aligned} \alpha(m_Z) &= 1/128.962\,, \\ \sin^2\theta_W(m_Z) &= 0.23126(5)\,, \\ G_F &= 1.1663787(7)\times 10^{-5}\ \text{GeV}^{-2}\,. \end{aligned} \tag{1.18}$$

1.1.2 Discovery of Higgs boson at the LHC and its current status

As discussed before, to generate masses for the SM particles through the Higgs mechanism, a new particle, the Higgs boson, was introduced. In the SM, prior to its discovery at CERN, the mass of Higgs boson ($m_h = \sqrt{2v^2\lambda}$) was an unknown parameter. The Higgs mass was constrained by a global-fit to EW precision data from LEP. At 95% confidence limit (CL) it was given as [44, 45]

$$114.4\ \text{GeV} \ < \ m_h \ < \ 144.0\ \text{GeV}\,. \tag{1.19}$$

The Higgs boson was discovered in 2012 by both the CMS and ATLAS experiments at the LHC. The combined measurement of its mass by the ATLAS and CMS collaborations on 7 and 8 TeV datasets[1] is given by 125.09±0.21(stat.)±0.11(syst.) GeV [47], which is indeed within the bound from the EW precision data (Eq. 1.19). Its spin and parity J^P are measured to be 0^+ [46]. In a given channel, the signal strength variable μ is defined as

$$\mu = \frac{(\sigma \times \text{BR})_{\text{Exp}}}{(\sigma \times \text{BR})_{\text{SM}}}\,, \tag{1.20}$$

where σ is the production cross section and BR is the branching ratio for a given final state of the Higgs boson. The combined analysis on two separate datasets (5 fb^{-1} at 7 TeV and 20 fb^{-1} at 8 TeV) by the ATLAS and CMS on five production processes (ggF, VBF, WH, ZH and ttH) and five decay channels ($H \to ZZ$, $H \to WW$, $H \to \gamma\gamma$, $H \to bb$ and $H \to \tau\tau$) leads to the global-fit value of μ, which is found to be 1.09 ± 0.11 [48], and is consistent with the corresponding SM value 1. The measured values of the signal strengths in various production and

[1] here we do not quote the results on the 13 TeV dataset, since the combined results by two experiments is not available yet. However, we note that CMS has published the result on Higgs mass at 13 TeV [49].

decay modes, tested by the ATLAS, in Run 2 at 13 TeV are shown in the left panel of Fig. 1.1 [50].

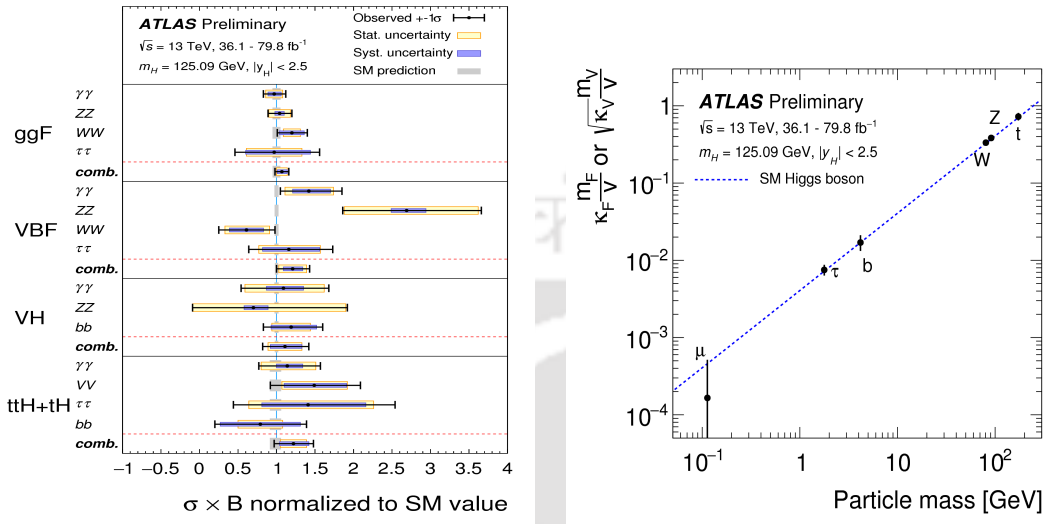

FIGURE 1.1: Left: the signal strength parameter μ in various channels. Right: Higgs couplings to fermions and bosons. These plots are taken from [48].

In the right panel of Fig. 1.1 [51], the Higgs couplings to fermions and gauge bosons are presented. These measurements were performed by the ALTAS collaboration. Combined measurements of Higgs boson production cross sections, branching fractions and couplings are presented in $\gamma\gamma$, ZZ^*, W^+W^-, $\tau^+\tau^-$, $\mu^+\mu^-$ and $b\bar{b}$ decay channels at $\sqrt{s} = 13$ GeV and 80 fb^{-1} luminosity. In this analysis, gluon gluon fusion, vector boson fusion and the associated production with vector bosons or top quarks, are considered. Clearly, the couplings follow a straight line pattern as expected in the SM (see Eq. 1.8 & 1.10). This indicates that the observed Higgs boson is indeed a SM-like Higgs, however, due to uncertainties in some of its detection modes, there is still room for new physics (NP). We shall see that there are sufficient reasons to look beyond the SM, even if the properties of the Higgs boson matches exactly with that predicted by the SM, as we shall discuss below. Thus, it is important to see how compatible are the extensions of the SM with these Higgs measurements. One of the main objectives of this thesis work is to understand where do the supersymmetric models, like the MSSM and the NMSSM, stand in this picture. We investigate such issues: like the compatibility of these supersymmetric models with a SM-like Higgs boson as observed at the LHC; or in case of some discrepancies with the SM expectations, how much the models under study could be accommodating as far as those discrepancies are concerned.

1.1.3 Drawbacks of the SM

Despite the fact that the SM is a remarkably successful theory, obeying stringent experimental constraints till date, it is generally considered as a low energy approximation of a more fundamental theory of nature, since there are many experimental and theoretical facts indicating that the SM is not a complete theory. This section briefly presents some of such flaws of the SM that motivate to look for BSM physics. Below, some of the important observational evidences that are not addressed in the SM are briefly discussed.

Dark Matter and dark energy: There is ample evidence from observations like the rotation curve of galaxies, that luminous matter in the universe accounts for only a small fraction of the total matter-energy density. The unknown matter content of the universe is called the dark matter which accounts for about 27% of the total matter-energy density of the observable universe, while the ordinary matter accounts for only about 5%, and the rest constitutes the unknown form of energy, the so-called dark energy, which is considered to be responsible for the acceleration of the expansion of the universe.

Matter-antimatter asymmetry: It is well observed that the universe is made up of protons, neutrons and electrons. According to astrophysical observations, the density of protons and neutrons constitute the bulk of visible matter, as the baryon content of the universe. These observations do not show any large antimatter-dominated region in the observable universe. At the same time, according to the SM, matter is created in particle-antiparticle pairs during the beginning of the universe. The SM does not propose a way to reach the presently observed baryon-dominated universe starting from such a symmetric situation.

Neutrino Mass: Neutrinos, initially thought to be massless have now been shown to have non-zero masses. The SM cannot construct a renormalizable mass term for the neutrinos. Thus, in order to have massive neutrinos one must either extend the particle content or abandon gauge invariance and/or renormalizability of the model.

Apart from the above-mentioned experimental issues, the SM suffers from several theoretical issues as well. First of all, the SM does not incorporate the gravity, which is one of four fundamental forces of nature. This is one of the main reasons why the SM is considered to be a manifestation of a more fundamental theory at

low energy. Another important theoretical shortcoming of the SM appears in the fermion sector. Even though the model generates the fermion masses through the Higgs mechanism, the Yukawa couplings are taken as free parameters so that the hierarchy patterns of the fermion generations remain unexplained. These features appearing in the fermion sector could be consequences of some higher symmetries, but the source of the mass hierarchy as well as the number of the generations are not understood in the context of the SM. In the following we discuss one of the most prominent theoretical flaws of the SM Higgs sector known as the hierarchy problem that appears when the quantum corrections to the Higgs mass are taken into account.

Hierarchy problem: The fact that gravity is much weaker than all other forces implies the existence of two vastly different scales of energy: $\Lambda_{\text{Planck}} \sim 10^{19}\ GeV$ where gravity gets stronger, and the electroweak scale: $\Lambda_{\text{EW}} \sim \mathcal{O}(100\ GeV)$. If the SM is a complete theory, describing the strong and EW interactions and holds all the way up to the Planck scale, then this leads to a difficult situation in the computation of mass of the Higgs boson. The Higgs boson mass is measured to be about 125 GeV. On the other hand, unlike gauge boson masses, the scalar particle mass is not protected by any symmetry. Thus, it is observed that the quantum corrections involving higher order fermionic loops are quadratically divergent. The physical Higgs mass m_h can be defined as

$$m_h^2 = m_0^2 + \Delta m_{\text{rad}}^2 \,, \tag{1.21}$$

where m_0 denotes bare mass (parameter appearing in the Lagrangian) and Δm_{rad}^2 is the radiative correction to the Higgs mass. The fermionic loop contribution to the Higgs mass reads [52]

$$\Delta m_{rad}^2 = -\frac{g_f^2}{8\pi^2}\left[\Lambda^2 - 3m_f^2\ \ln(\tfrac{\Lambda}{m_f})\right] \,, \tag{1.22}$$

which is quadratically divergent to the scale Λ, where NP is believed to exist. The dominant contribution comes from the top quark in the loop since it has the largest Yukawa coupling to the Higgs boson. If the SM is a complete theory, i.e., valid all the way up to the Planck scale ($\Lambda = \Lambda_{\text{Planck}}$), then it implies that in order to obtain a physical Higgs mass $m_h \sim \Lambda_{\text{EW}}$, m_0 must be of the order Λ_{Planck}. Since, the ratio of square of EW scale to that of Planck scale is very small ($\mathcal{O}(10^{-34})$), the cancellation must be extremely precise.

In the absence of a symmetry, that impedes the sensitivity of Higgs mass to quantum corrections, a light fundamental scalar field seems to be highly unnatural. The hierarchy problem itself provides strong evidence for the existence of BSM scenarios. In an attempt to stabilize and explain the EW scale, BSM scenarios almost inevitably introduce new particles, which in turn cause conflicts with constraints from EW precision data. Such conflicts can be avoided by

- making new particles heavy or suppressing their couplings to the SM particles;
- or introducing new symmetries that forbid new particles to contribute to SM processes at tree-level.

SUSY is a very popular BSM candidate, fulfilling the above requirements. Moreover, it is a testable theory at the collider experiments. In the following sections, we briefly review two well-motivated SUSY models, namely, the MSSM and the NMSSM.

1.2 Basic Supersymmetry and the MSSM

SUSY can cure some of the drawbacks of the SM [53]. SUSY is a spacetime symmetry which relates fermions to bosons and vice versa, as the SUSY operator $\mathcal{Q}$ acts like

$$\mathcal{Q}|\text{fermion}\rangle = |\text{boson}\rangle, \qquad \mathcal{Q}|\text{boson}\rangle = |\text{fermion}\rangle\,. \tag{1.23}$$

The transformations of $\mathcal{Q}$ define non-trivial extensions of the Poincare group [54, 55]. The transformed particle states into each other are called *superpartners*. They are assigned to *supermultiplets*, which are the multiplets of SUSY algebra. Except for spin, the superpartners have same quantum numbers and equal masses, provided SUSY is an unbroken symmetry. Since superpartners are not observed yet, they must be heavier than the currently achievable energies at colliders, hinting for broken SUSY. Phenomenologically, one way to achieve this is through SUSY breaking terms, which do not spoil renormalizability of the Lagrangian. Such terms are generically called *soft SUSY breaking* terms.

Gravity could be accomoddated within SUSY if it is a local symmetry [56]. SUSY could provide a DM candidate, that is the lightest neutralino and is called the

lightest supersymmetric particle (LSP), if the baryon and lepton numbers are conserved [57, 58]. The superpartners modify the running of the gauge coupling constants such that they converse at a higher energy scale $M_{\text{GUT}} \sim 10^{16}$ GeV [59, 60]. Most importantly, SUSY can resolve the hierarchy problem [61] as described in the previous section. The SM loop contributions to the square of the Higgs boson mass, which cause quadratically divergent radiative corrections, are compensated by the corresponding SUSY contributions as indicated in Fig. 1.2. If SUSY is an unbroken symmetry, the net radiative correction to the Higgs mass becomes zero. The addition of soft SUSY breaking terms leads to logarithmically divergent terms, however cancelling the dangerous quadratically divergent terms. This cancellation stabilizes the hierarchy between the GUT and the EW scales without requiring much fine-tuning to the mass of Higgs boson.

Thus, SUSY must to be broken resulting in heavier superpartners than their corresponding SM particles. Broken SUSY can only unify the gauge couplings and resolve the hierarchy problem if the superpartners are not much heavier. This can be achieved by adding soft SUSY breaking terms to the Lagrangian, and the effective Lagrangian can be schematically written as

$$\mathcal{L}_{\text{eff}} = \mathcal{L}_{\text{SUSY}} + \mathcal{L}_{\text{soft}} \,. \tag{1.24}$$

$\mathcal{L}_{\text{SUSY}}$ denotes the gauge and Yukawa parts preserving SUSY, and the SUSY breaking term $\mathcal{L}_{\text{soft}}$ contains mass terms and coupling parameters with positive mass dimensions. The associated mass scale of superpartners M_{soft} contributes to the radiative corrections to m_h^2. If this contribution is small enough in order to not reintroduce large fine-tuning, the masses of the superpartners should not differ from each other by more than one order of magnitude. Hence, the masses of the lightest superpartners should be in TeV range.

FIGURE 1.2: One-loop corrections to m_h^2. Contributions from Dirac fermions (left) generate quadratically divergent terms in the expression of m_h^2 which are cancelled by contributions from scalar fermions (right) in supersymmetric models.

1.2.1 The MSSM

The MSSM is the simplest supersymmetric extension of the SM. Below we briefly discuss the gauge symmetries, the particle content and the $R-$parity conservation associated to the MSSM. The superpotential and the Lagrangian are also presented.

The gauge group: The gauge group associated to the MSSM is the same as that of the SM, which is $SU(3)_c \times SU(2)_L \times U(1)_Y$. Each spin -1 gauge field gets a spin$-\frac{1}{2}$ superpartner, which gives eight gluinos corresponding to $SU(3)_c$, three winos corresponding to $SU(2)_L$ and a bino corresponding to $U(1)_Y$ as shown in Tab. 1.2.

Supermultiplets	Superpartners	Spin-$\frac{1}{2}$	Spin-1	$(\mathrm{SU(3)}_C, SU(2)_L, U(1)_Y$
$\widehat{G}_a$ $(a = 1, ..., 8)$	gluinos, gluons	$\widetilde{G}_a$	G_a^μ	(8,1,0)
$\widehat{W}_a$ $(a = 1, 2, 3)$	winos, W bosons	$\widetilde{W}_a$	W_a^μ	(1,3,0)
$\widehat{B}$	bino, B boson	$\widetilde{B}$	B^μ	(1,1,0)

TABLE 1.2: Gauge supermultiplets and superpartners in the MSSM and their quantum numbers [62, 63].

The particle content: The SM fermions are assigned to chiral supermultiplets as the left- and right-handed fermions transform differently under $SU(2)_L$. Atleast two complex scalar Higgs doublets, H_u and H_d, are required which give masses to the up-type and down-type fermions separately. The two spin -0 Higgs doublets together with their superpartners, the spin$-\frac{1}{2}$ higgsinos, form two chiral supermultiplets. The fermion and Higgs supermultiplets are shown in Tab. 1.3.

Supermultiplets	Superpartners	Spin-0	Spin-$\frac{1}{2}$	$(\mathrm{SU(3)_C, SU(2)_L, U(1)_Y})$
$\widehat{Q}$	squarks, quarks	$(\widetilde{u}_L\ \widetilde{d}_L)$	$(u_L\ d_L)$	(3,2,$\frac{1}{3}$)
$\widehat{u}^c$	(1^{st} family)	$\widetilde{u}_R^*$	$u_R^\dagger$	(3,1,$-\frac{4}{3}$)
$\widehat{d}^c$		$\widetilde{d}_R^*$	$d_R^\dagger$	(3,1,$\frac{2}{3}$)
$\widehat{L}$	sleptons, leptons	$(\widetilde{\nu}_L\ \widetilde{e}_L)$	$(\nu_L\ e_L)$	(1,2,-1)
$\widehat{e}^c$	(1^{st} family)	$\widetilde{e}_R^*$	$e_R^\dagger$	(1,1,2)
$\widehat{H}_u$	Higgs, higgsinos	$(H_u^+\ H_u^0)$	$(\widetilde{H}_u^+\ \widetilde{H}_u^0)$	(1,2,1)
$\widehat{H}_d$		$(H_d^0\ H_d^-)$	$(\widetilde{H}_d^0\ \widetilde{H}_d^-)$	(1,2,-1)

TABLE 1.3: The MSSM chiral supermultiplets and superpartners and their quantum numbers. Only the first generation is presented here [62].

$R-$parity conservation: Generally SUSY models violate baryon and lepton number conservations resulting into unstable proton with a decay life-time shorter than the experimental measurement. Thus, $R-$parity is introduced in order to conserve the baryon and lepton numbers, which is given as

$$P_R = (-1)^{2s+3B+L} \,. \tag{1.25}$$

L and B are the lepton and baryon quantum numbers and s is the spin quantum number. Accordingly, the SM particles have $P_R = +1$ and their superpartners have $P_R = -1$. With conserved $R-$parity, the LSP is stable providing a good candidate for the DM of the universe.

The MSSM superpotential: The MSSM superpotential can be given as [63]

$$\begin{aligned} W_{\text{MSSM}} &= u^{cia}(g_u)^j_i Q_{ja\alpha}(H_u)_\beta \epsilon^{\alpha\beta} + d^{cia}(g_d)^j_i Q_{ja\alpha}(H_d)_\beta \epsilon^{\alpha\beta} \\ &+ e^{cia}(g_e)^j_i L_{ja\alpha}(H_d)_\beta \epsilon^{\alpha\beta} + \mu(H_u)_\alpha (H_d)_\beta \epsilon^{\alpha\beta} \,, \end{aligned} \tag{1.26}$$

with generation indices $i, j = 1, 2, 3$; the color index $a = 1, 2, 3$; the weak isospin $\alpha, \beta = 1, 2$ and the fully antisymmetric tensor $\epsilon^{\alpha\beta}$. $H_{u,d}$, Q, L, u^c, d^c, e^c are the chiral supermultiplets as given in Tab. 1.3 (here we drop the operator sign of the superfields for simplicity). $g_{u,d,e}$ are the Yukawa coupling constants. The last term in Eq. 1.26 is the so-called $\mu - term$ which is the supersymmetric Higgs mass term with the Higgs mass parameter μ.

The MSSM Lagrangian reads

$$\mathcal{L}_{\text{MSSM}} = \mathcal{L}_{\text{chiral}} + \mathcal{L}_{\text{gauge}} \,, \tag{1.27}$$

where

$$\begin{aligned} \mathcal{L}_{\text{chiral}} &= -D^\mu \phi^{*i} D_\mu \phi_i + i\psi^{\dagger i}(-1)\tau^\mu D_\mu \psi_i \\ &- \frac{1}{2}\left(W^{ij}\psi_i\psi_j + W^*_{ij}\psi^{\dagger i}\psi^{\dagger j}\right) - W^i W^*_i \,, \end{aligned} \tag{1.28}$$

with the complex scalar fields ϕ_i, left–handed Weyl fermion fields ψ_j, the Pauli spin matrices τ^μ, and the total derivatives

$$W^i = \frac{\delta W}{\delta \phi_i} \,, \qquad W^{ij} = \frac{\delta^2 W}{\delta \phi_i \delta \phi_j} \,, \tag{1.29}$$

of the superpotential W.

The Lagrangian for the gauge fields (G_a, W_a, B) can be written as

$$\mathcal{L}_{\text{gauge}} = -\frac{1}{4}F^a_{\mu\nu}F^{\mu\nu a} + i\lambda^{\dagger a}\bar{\tau}^\mu D_\mu \lambda^a + \frac{1}{2}g^2(\phi^* T^a \phi)^2\,, \tag{1.30}$$

with the field strength tensor

$$F^a_{\mu\nu} = \partial_\mu A^a_\nu - \partial_\nu A^a_\mu + g f^{abc} A^b_\mu A^c_\nu\,, \tag{1.31}$$

and the covariant derivative

$$D_\mu \lambda^a = \partial_\mu A^a + g f^{abc} A^b_\mu \lambda^c\,, \tag{1.32}$$

of the two-component Weyl gaugino fields λ^a, with the massless gauge boson fields A^a_μ, and the structure constant f^{abc}. In Eq. 1.30, T^a are the generators of the gauge groups and g is the respective coupling constant. For the three MSSM gauge supermultiplets, the index a runs over $1, ..., 8$ for the $SU(3)_c$ gauge group, $a = 1, 2, 3$ for the $SU(2)_L$ gauge group and $a = 1$ for $U(1)_Y$.

Minimal soft SUSY breaking: For the MSSM to be a viable model, SUSY has to be softly broken as discussed above. The specific mechanism of SUSY breaking is not known so far. Instead, the effects of spontaneous SUSY breaking are parameterized by adding by hand the most general soft SUSY breaking terms to the MSSM Lagrangian

$$\begin{aligned}
\mathcal{L}^{\text{MSSM}}_{\text{soft}} &= -\frac{1}{2}\left(M_3 \widetilde{G}^a \widetilde{G}_a + M_2 \widetilde{W}^b \widetilde{W}_b + M_1 \widetilde{B}\widetilde{B} + \text{c.c.}\right) \\
&- \left(\widetilde{\bar{u}} a_u \widetilde{Q} H_u - \widetilde{\bar{d}} a_d \widetilde{Q} H_d - \widetilde{\bar{e}} a_e \widetilde{L} H_d + \text{c.c.}\right) \\
&- \widetilde{Q}^\dagger m^2_Q \widetilde{Q} - \widetilde{L}^\dagger m^2_L \widetilde{L} - \widetilde{\bar{u}} m^2_{\bar{u}} \widetilde{\bar{u}}^\dagger - \widetilde{\bar{d}} m^2_{\bar{d}} \widetilde{\bar{d}}^\dagger - \widetilde{\bar{e}} m^2_{\bar{e}} \widetilde{\bar{e}}^\dagger \\
&- m^2_{H_u} H^*_u H_u - m^2_{H_d} H^*_d H_d - (B_\mu H_u H_d + \text{c.c.})\,,
\end{aligned} \tag{1.33}$$

with the indices $a = 1, ..., 8$ and $b = 1, 2, 3$. $M_{1,2,3}$ are the bino, wino and gluino mass terms, $a_{u,d,e}$ are complex 3×3 matrices in family space which correspond to the Yukawa matrices $g_{u,d,e}$ of the superpotential such that the matrix elements are given by $a^{ij}_{u,d,l} = A^{ij}_{u,d,l} g^{ij}_{u,d,l}$, with the trilinear Higgs-sfermion couplings $A^{ij}_{u,d,l}$. $m^2_{Q,L,\bar{u},\bar{d},\bar{e}}$ are 3×3 matrices in family space for squarks and sleptons. The last line in Eq. 1.33 contains the Higgs mass-square parameters $m^2_{H_u}$ and $m^2_{H_d}$, the Higgs

mixing parameter μ, and the SUSY breaking bilinear Higgs coupling term B, for the two Higgs doublets H_u and H_d. The soft SUSY breaking terms in Eq. 1.33 introduce more than 100 free parameters, in addition to the 19 free parameters of the SM. Without restrictions on any of these parameters, the model is called the unconstrained MSSM.

Gauge and mass eigenstates: The superpartner states presented in Tab. 1.2 & 1.3 are the gauge eigenstates, and may not be necessarily the physical states. SUSY breaking and EW effects induce mixing between the EW gauginos and higgsinos and, also among sfermions and Higgs bosons to form the mass eigenstates, which are given in Tab. 1.4.

Particles	Spin	P_R	Gauge eigenstates	Mass eigenstates
Higgs bosons	0	+1	$H_u^0, H_d^0, H_u^+, H_d^-$	$h, H, A, H^\pm$
squarks	0	-1	$\widetilde{u}_L, \widetilde{u}_R, \widetilde{d}_L, \widetilde{d}_R$	$\widetilde{u}_1, \widetilde{u}_2, \widetilde{d}_1, \widetilde{d}_2$
sleptons	0	-1	$\widetilde{e}_L, \widetilde{e}_R, \widetilde{\nu}_e$	$\widetilde{e}_1, \widetilde{e}_2, \widetilde{\nu}_e$
neutralinos	1/2	-1	$\widetilde{B}^0, \widetilde{W}^0, \widetilde{H}_1^0, \widetilde{H}_2^0$	$\widetilde{\chi}_1^0, \widetilde{\chi}_2^0, \widetilde{\chi}_3^0, \widetilde{\chi}_4^0$
charginos	1/2	-1	$\widetilde{W}^\pm, \widetilde{H}_u^+, \widetilde{H}_d^-$	$\widetilde{\chi}_1^\pm, \widetilde{\chi}_2^\pm$
gluino	1/2	-1	$\widetilde{G}$	$\widetilde{G}$
goldstino	1/2	-1	$\widetilde{g}$	$\widetilde{g}$

TABLE 1.4: The gauge and mass eigenstates of MSSM [62]. Spin and $R-$parity quantum numbers are also listed.

The MSSM Higgs sector: Here two Higgs doublets are necessary for EWSB. In the SM, chiral anomalies which spoil the renormalizability of the theory are cancelled because the sum of hypercharges (Y) and isospin (I^3) quantum numbers of the left-handed fermions, i.e. of the electric charges in each generation is zero, $\mathrm{Tr}[Y_f] = \mathrm{Tr}[Q_f] = 0$. In the MSSM, the Higgs fields are the members of chiral supermultiplets in which their fermionic superpartners are weak isodoublets with $Y = \pm 1$. If there is only one doublet, then $\mathrm{Tr}[Y_f] = \mathrm{Tr}[Q_f] \neq 0$ and chiral anomalies will not be cancelled out. Thus, to preserve these cancellations, two chiral Higgs supermultiplets are required with $Y = \pm 1$.

Secondly, the generation of masses for up-type and down-type fermions separately. In the SM, this is achieved by Yukawa couplings of the field ϕ and its conjugate. In a supersymmetric theory, the superpotential is only a function of the superfields and not of their conjugates (see Eq. 1.26). Therefore, two separate scalar fields

with hypercharges $Y = \pm 1$ are required to provide masses separately to the up-type and down-type fermions. With the two Higgs doublets

$$H_u = \begin{pmatrix} H_u^+ \\ H_u^0 \end{pmatrix}, \qquad H_d = \begin{pmatrix} H_d^0 \\ H_d^- \end{pmatrix}, \tag{1.34}$$

the corresponding scalar Higgs potential is given by

$$\begin{aligned} V_H &= \left(|\mu|^2 + m_{H_u}^2\right)\left(|H_u^0|^2 + |H_u^+|^2\right) + \left(|\mu|^2 + m_{H_d}^2\right)\left(|H_d^0|^2 + |H_d^-|^2\right) \\ &+ \left[B_\mu\left(H_u^+ H_d^- - H_u^0 H_d^0\right) + \text{h.c.}\right] \\ &+ \frac{1}{8}\left(g_1^2 + g_2^2\right)\left(|H_u^0|^2 + |H_u^+|^2 - |H_d^0|^2 - |H_d^-|^2\right)^2 \\ &+ \frac{1}{2} g_2^2 |H_u^+ H_d^{0*} + H_u^0 H_d^{-*}|^2 , \end{aligned} \tag{1.35}$$

where terms proportional to $|\mu|^2$ come from the last term in the superpotential in Eq. 1.26 and terms proportional to g_1^2 and g_2^2 come from the last term in the gauge part of the MSSM Lagrangian given in Eq. 1.30. The terms proportional to $m_{H_u}^2$, $m_{H_d}^2$ and B_μ correspond to the fourth line of the soft SUSY breaking Lagrangian in Eq. 1.33. Additional terms in the complete scalar potential involving sfermion fields are not included here because they do not contribute to EWSB. The minimum of the potential V_H needs to break $SU(2)_L \times U(1)_Y$ symmetry while preserving $U(1)_{\text{em}}$. This is achieved by choosing the VEV of H_u^+ to be zero which requires the VEV of H_u^- to be zero as well. The scalar potential is bounded from below if

$$2B_\mu < 2|\mu|^2 + m_{H_u}^2 + m_{H_d}^2 . \tag{1.36}$$

To break the EW symmetry, a linear combination of H_u^0 and H_d^0 has to acquire a negative value of the mass-square parameter, which requires

$$(B_\mu)^2 > \left(|\mu|^2 + m_{H_u}^2\right)\left(|\mu|^2 + m_{H_d}^2\right) . \tag{1.37}$$

Both conditions can only be satisfied simultaneously if $m_{H_u}^2 \neq m_{H_d}^2$, which means that the EW symmetry can only be broken if SUSY is broken.

In models with minimal Supergravity [64, 65] or in gauge mediated SUSY breaking models [66, 67], $m_{H_u}^2 = m_{H_d}^2$ is satisfied at tree-level at high energy scales. But heavy fermion and sfermion contributions to the running of $m_{H_{u,d}}^2$ break this mass

degeneracy at the EW scale. This mechanism is called radiative EW symmetry breaking [68] and provides a mechanism for the EW phase transition.

The VEVs of the two Higgs doublets,

$$v_u = \langle H_u \rangle \,, \qquad v_d = \langle H_d \rangle \,, \tag{1.38}$$

are chosen to be real and positive and their ratio is written as

$$\tan\beta = \frac{v_u}{v_d} \,. \tag{1.39}$$

The two complex scalar doublets in Eq. 1.34 have eight real degrees of freedom. The mass eigenstates of the Higgs fields (see Tab. 1.4) are obtained from rotations,

$$\begin{aligned} \begin{pmatrix} H_u^0 \\ H_d^0 \end{pmatrix} &= \begin{pmatrix} v_u \\ v_d \end{pmatrix} + \frac{1}{\sqrt{2}} \begin{pmatrix} \cos\alpha & \sin\alpha \\ \sin\alpha & \cos\alpha \end{pmatrix} \begin{pmatrix} h \\ H \end{pmatrix} \\ &+ \frac{i}{\sqrt{2}} \begin{pmatrix} \sin\beta & \cos\beta \\ \cos\beta & \sin\beta \end{pmatrix} \begin{pmatrix} G \\ A \end{pmatrix} , \end{aligned} \tag{1.40}$$

and

$$\begin{pmatrix} H_u^+ \\ H_d^{-*} \end{pmatrix} = \begin{pmatrix} \sin\beta & \cos\beta \\ \cos\beta & \sin\beta \end{pmatrix} \begin{pmatrix} G^+ \\ H^+ \end{pmatrix} , \tag{1.41}$$

with the angles α and β chosen such that the quadratic part of the scalar potential is transformed into diagonal mass terms. The scalars G^+ and H^+ have electric charge $+1$, their conjugates $G^- = G^{+*}$ and $H^- = H^{+*}$ have charge -1. The scalars h and H are electrically neutral and CP-even while the scalars A and G are neutral and CP-odd. As in the SM, the massless neutral and charged Goldstone bosons $G, G^\pm$ become the longitudinal modes of the massive gauge bosons, Z and $W^\pm$, after a suitable gauge transformation. The masses of the MSSM Higgs bosons are then given by [63]

$$\begin{aligned} m_A^2 &= \frac{2B_\mu}{\sin 2\beta} = 2|\mu|^2 + m_{H_u}^2 + m_{H_d}^2 \,, \\ m_{h,H}^2 &= \frac{1}{2}\left(m_A^2 + m_Z^2 \mp 4 m_Z^2 m_A^2 \sin^2 2\beta \sqrt{\left(m_A^2 - m_Z^2\right)^2} \right) , \\ m_{H^\pm}^2 &= m_A^2 + m_W^2 \,. \end{aligned} \tag{1.42}$$

At tree-level, the mixing angle α is given by

$$\alpha = \frac{1}{2}\tan^{-1}\left(\tan 2\beta \frac{m_A^2 + m_Z^2}{m_A^2 - m_Z^2}\right), \quad -\frac{\pi}{2} < \alpha < 0\,. \tag{1.43}$$

As can be seen from Eq. 1.42, the masses of A, H and $H^{\pm}$ can have arbitrary values, but the mass of h is bounded from above. At tree-level, m_h is constrained as

$$m_h < m_Z |\cos 2\beta|\,, \tag{1.44}$$

but radiative corrections, in particular from top quark and squark contributions, can weaken this bound notably.

Theoretical constraints on the MSSM Higgs sector: In the MSSM, $\tan\beta$ is a free parameter. The couplings of the pseudoscalar and charged MSSM Higgs bosons, as well as the coupling of the $h(H)$ boson for small (large) values of m_A, to up-type and down-type fermions are proportional to $\cot\beta$ and $\tan\beta$, respectively, as can be seen from Tab. 1.5 using Eq. 1.43. The requirement that the couplings should remain in the perturbative regime puts constraints on $\tan\beta$. In the most general MSSM scenarios, the resulting bound is rather loose, $\tan\beta \lesssim 150$, but in models with universal boundary conditions at the GUT scale, perturbation theory breaks down unless $\tan\beta$ is within the range of $0.5 \leq \tan\beta \leq \frac{m_t}{m_b} \simeq 60$ [69] for $M_{\text{SUSY}} \sim 1$ TeV.

ϕ	CP	$g_{\phi\bar{u}u}$	$g_{\phi\bar{d}d}$	$g_{\phi VV}$
SM h	even	1	1	1
h	even	$\cos\alpha/\sin\beta$	$-\sin\alpha/\cos\beta$	$\sin(\beta-\alpha)$
H	even	$\sin\alpha/\sin\beta$	$\cos\alpha/\cos\beta$	$\cos(\beta-\alpha)$
A	odd	$\cot\beta$	$\tan\beta$	0

TABLE 1.5: Couplings of the neutral MSSM Higgs bosons to up-type and down-type fermions and to gauge bosons relative to the couplings of the SM Higgs boson

1.3 The NMSSM

The NMSSM is the simplest extension of the MSSM (for review on the NMSSM, see ref. [7, 8]). In the NMSSM an additional chiral superfield, $\widehat{S}$, which is a

singlet under all gauge groups, is added to the MSSM with a modified NMSSM superpotential. The singlet superfield adds a CP-even and a CP-odd Higgs fields to the theory. The fermionic component of $\widehat{S}$ appears as an additional neutralino (as compared to the four neutralinos in the MSSM).

1.3.1 Motivation

In the NMSSM two shortcomings of the MSSM are addressed directly: it solves the $\mu-$problem [12, 14, 70–73] and increases the upper bound for the mass of the lightest, doublet-like Higgs field compared to the MSSM.

The $\mu-$problem: The MSSM superpotential (Eq. 1.26) contains the $\mu-$term ($\widehat{\mu}\widehat{H}_u H_d$) that has no analogue in the SM. Since it is made of superfields, it influences not only the neutralino sector (where the $\mu-$term provides mass for higgsino) but more importantly also the scalar potential of the Lagrangian, that has changed significantly compared to the SM because of the presence of the two Higgs doublets. Now one would like to find the minimum of the scalar potential (Eq. 1.35) and make sure that it is (a) bounded from below and (b) has non-zero VEV. The potential minimization conditions, $\partial V_H/\partial H_u^0 = 0$ and $\partial V_H/\partial H_d^0 = 0$, lead to

$$\begin{aligned} \sin 2\beta &= \frac{2B_\mu}{m_{H_u}^2 + m_{H_d}^2 + 2|\mu|^2}\,, \\ m_Z^2 &= \frac{|m_{H_d}^2 - m_{H_u}^2|}{\sqrt{1-\sin^2 2\beta}} - m_{H_u}^2 - m_{H_d}^2 - 2|\mu|^2\,, \end{aligned} \tag{1.45}$$

where $\tan\beta$ has been defined in Eq. 1.39. Eq. 1.45 shows that in order to achieve EWSB, the parameters $m_{H_u}^2, m_{H_d}^2, B_\mu$, μ must be within an order of magnitude or two of the mass of the Z boson. However, μ is the parameter of the superpotential, linked to the SUSY nature of the Lagrangian and as such it has no knowledge about the SUSY breaking scale which governs the values of the soft SUSY breaking parameters $m_{H_u}^2, m_{H_d}^2, B_\mu$. In fact, the natural value of μ should be either 0 or something close to the Planck or GUT scale. That the parameter μ must have value close to the EW and SUSY breaking scales against its naturally expected value is called the $\mu-$problem.

From the NMSSM superpotential trilinear term $\lambda\widehat{S}\widehat{H}_u\widehat{H}_d$, an effective $\mu-$term, $\mu_{\text{eff}}\widehat{H}_u\widehat{H}_d$ may be generated dynamically with the acquisition of VEV by $\widehat{S}$, i.e., $\langle\widehat{S}\rangle = s$. The VEV s, must be of the order of the SUSY breaking scale M_{SUSY},

in order to resolve the $\mu-$problem. This can be done by introducing negative soft mass-squares or soft trilinear couplings of $\mathcal{O}(M^2_{\rm SUSY})$, such that the only scale of the theory is the SUSY breaking scale.

Higher tree-level scalar mass: The upper bound on the tree-level mass, $m_h^{\rm tree}$, of the lightest CP-even Higgs doublet field is lifted in the NMSSM compared to the MSSM by the new Higgs self-coupling parameter λ,

$$\left(m_h^{\rm tree}\right)^2 < m_Z^2 \cos^2 2\beta + \lambda^2 v^2 \sin^2 2\beta \,, \tag{1.46}$$

where $v^2 = v_u^2 + v_d^2$. In the NMSSM, the magnitude of higher order corrections necessary to lift the mass of the SM-like Higgs to its measured value is therefore reduced compared to the MSSM.

1.3.2 The generalized NMSSM

The most general, $R-$parity and CP-conserving version of the NMSSM, the generalized NMSSM (GNMSSM), features the Higgs sector superpotential [7]

$$W_{\rm GNMSSM} = W_{\rm MSSM}^{\rm Yukawa} + \left(\mu + \lambda \widehat{S}\right) \widehat{H}_u \widehat{H}_d + \xi_F \widehat{S} + \frac{\mu' \widehat{S}^2}{2} + \frac{\kappa \widehat{S}^3}{3} \,, \tag{1.47}$$

where $W_{\rm MSSM}^{\rm Yukawa}$ represents the first three terms in Eq. 1.26. The GNMSSM soft Lagrangian can be written as

$$\begin{aligned}
\mathcal{L}_{\rm soft}^{\rm GNMSSM} &= -\frac{1}{2}\left(M_3 \widetilde{G}^a \widetilde{G}_a + M_2 \widetilde{W}^b \widetilde{W}_b + M_1 \widetilde{B}\widetilde{B} + \text{h.c.}\right) \\
&- \left(\widetilde{\overline{u}} a_u \widetilde{Q} H_u - \widetilde{\overline{d}} a_d \widetilde{Q} H_d - \widetilde{\overline{e}} a_e \widetilde{L} H_d + \text{h.c.}\right) \\
&- \widetilde{Q}^\dagger m_Q^2 \widetilde{Q} - \widetilde{L}^\dagger m_L^2 \widetilde{L} - \widetilde{\overline{u}} m_{\overline{u}}^2 \widetilde{\overline{u}}^\dagger - \widetilde{\overline{d}} m_{\overline{d}}^2 \widetilde{\overline{d}}^\dagger - \widetilde{\overline{e}} m_{\overline{e}}^2 \widetilde{\overline{e}}^\dagger \\
&- \left(\lambda A_\lambda H_u H_d S + \frac{\kappa A_\kappa S^3}{3} + B_\mu H_u H_d B'_{\mu'} S^2 + \xi_S S + \text{h.c.}\right) \\
&- m_{H_u}^2 |H_u|^2 - m_{H_d}^2 |H_d|^2 - m_S^2 |S|^2 \,.
\end{aligned} \tag{1.48}$$

Finally, the NMSSM gauge group is the same as in the MSSM and in the SM. Note that the signs of some of the Lagrangian parameters have no physical meaning, due to the possibility of field redefinition $\phi \to -\phi$. One finds that keeping λ, v_u, v_d and the Yukawa couplings positive, κ, s and the dimensionful parameters may have both signs [7].

1.3.3 The Z_3 invariant NMSSM

In order to solve the $\mu-$problem, the most common exercise is to impose a symmetry, called the Z_3 symmetry, corresponding to the transformation

$$\widehat{\Phi} \to e^{2\pi i/3}\widehat{\Phi}\,, \quad \widehat{V} \to \widehat{V}\,, \tag{1.49}$$

which implies a phase multiplication for all chiral superfields $\widehat{\Phi}$, while the vector superfields $\widehat{V}$ are unchanged[2]. The Z_3-symmetry requires

$$\mu = \mu' = \xi_F = \xi_S = B_\mu = B'_{\mu'} = 0\,. \tag{1.50}$$

This results in the so-called the Z_3-invariant NMSSM, with the scale invariant superpotential

$$W_{Z_3\ \mathrm{NMSSM}} \supset \lambda\widehat{S}\widehat{H}_u\widehat{H}_d + \frac{\kappa\widehat{S}^3}{3}\,. \tag{1.51}$$

As mentioned earlier, an effective $\mu-$term in the scalar potential may dynamically be generated by the VEV of $\widehat{S}$, triggered by means of SUSY breaking

$$\mu_{\mathrm{eff}} = \lambda\langle\widehat{S}\rangle = \lambda s\,. \tag{1.52}$$

The dimensional parameters A_λ and A_κ appear in the Lagrangian of the Higgs sector soft terms

$$\mathcal{L}^{Z_3\ \mathrm{NMSSM}}_{\mathrm{soft}} \supset -\lambda A_\lambda H_u H_d S - \frac{\kappa A_\kappa S^3}{3}\,. \tag{1.53}$$

From now on we shall refer to the Z_3 invariant NMSSM simply as the NMSSM. From Eq. 1.51 & 1.53 the scalar potential can be written as

$$\begin{aligned} V_H^{\mathrm{NMSSM}} &= |\lambda(H_u^+H_d^- - H_u^0H_d^0) + \kappa S|^2 \\ &+ \left(m_{H_u}^2 + |\mu+\lambda S|^2\right)\left(|H_u^0|^2 + |H_u^+|^2\right) \\ &+ \left(m_{H_d}^2 + |\mu+\lambda S|^2\right)\left(|H_d^0|^2 + |H_d^-|^2\right) \\ &+ \frac{g_1^2+g_2^2}{8}\left(|H_u^0|^2 + |H_u^+|^2 - |H_d^0|^2 - |H_d^-|^2\right)^2 + \frac{g_2^2}{2}|H_u^+H_d^{0*} + H_u^0H_d^{-*}|^2 \\ &+ m_S^2|S|^2 + \left(\lambda A_\lambda(H_u^+H_d^- - H_u^0H_d^0)S + \frac{\kappa A_\kappa S^3}{3} + \mathrm{h.c.}\right)\,. \end{aligned} \tag{1.54}$$

[2]In the GNMSSM the $\mu-$term may be removed by the redefinition $s \to s - \mu/\lambda$.

In the potential (Eq. 1.54), the singlet S appears in bilinear terms together with the MSSM Higgs doublets H_u, H_d and therefore mixes with them due to EWSB. The scalar and pseudoscalar components of S mix with those of H_u^0, H_d^0 resulting in three CP-even neutral physical Higgs states (H_1, H_2, H_3) and two CP-odd neutral states (A_1, A_2).

1.3.4 Masses of Higgs bosons, gauginos, higgsinos and sfermions

The superpartner fields of the SM particles as obtained directly from the superfields are not observable. They can mix and have to be expressed in the mass basis. In the following the mass matrices for the superpartner fields are given in the conventions of ref. [74, 75].

Higgs masses: The Higgs potential V_H (Eq. 1.54), contains all terms in the Lagrangian that emerge from terms proportional to arbitrary powers of Higgs fields. In terms of their VEVs, the Higgs doublets and the singlet can be represented as

$$H_u = \begin{pmatrix} H_u^+ \\ \frac{1}{\sqrt{2}}(v_u + H_{uR} + iH_{uI}) \end{pmatrix}, \quad H_d = \begin{pmatrix} \frac{1}{\sqrt{2}}(v_d + H_{dR} + iH_{dI}) \\ H_d^- \end{pmatrix}$$
$$S = \frac{1}{\sqrt{2}}(s + S_R + iS_I). \tag{1.55}$$

Rearranging V_H by powers of the fields leads to

$$\begin{aligned} V_H &= \ldots - T_{H_{uR}} H_{uR} - T_{H_{dR}} H_{dR} - T_{S_R} S_R \\ &+ \frac{1}{2} \begin{pmatrix} H_{uR} & H_{dR} & S_R \end{pmatrix} \mathbf{M}_H \begin{pmatrix} H_{uR} \\ H_{dR} \\ S_R \end{pmatrix} + \frac{1}{2} \begin{pmatrix} H_{uI} & H_{dI} & S_I \end{pmatrix} \mathbf{M}_A \begin{pmatrix} H_{uI} \\ H_{dI} \\ S_I \end{pmatrix} \\ &+ \begin{pmatrix} H_u^+ & H_d^- \end{pmatrix} \mathbf{M}_{H^\pm} \begin{pmatrix} H_u^+ \\ H_d^- \end{pmatrix} + \ldots . \end{aligned} \tag{1.56}$$

$T_{H_{uR}}, T_{H_{dR}}, T_{S_R}$ are the tadpole coefficients and $\mathbf{M}_H, \mathbf{M}_A, \mathbf{M}_{H^\pm}$ are the Higgs mass matrices (see App. A for detail). In Eq. 1.56 the Higgs potential is given in the interaction basis. A unitary transformation has to be applied in order to obtain physical fields in the mass basis. For the CP-conserving case (where all the model parameters are real) the mixing into mass eigenstates can be described at lowest

order by the unitary transformations

$$\begin{pmatrix} H_1 \\ H_2 \\ H_3 \end{pmatrix} = \mathcal{R}_H \begin{pmatrix} H_{uR} \\ H_{dR} \\ S_R \end{pmatrix}, \quad \begin{pmatrix} A_1 \\ A_2 \\ G^0 \end{pmatrix} = \mathcal{R}_A \begin{pmatrix} H_{uI} \\ H_{dI} \\ S_I \end{pmatrix},$$
$$\begin{pmatrix} H^\pm \\ G^\pm \end{pmatrix} = \mathcal{R}_{H^\pm} \begin{pmatrix} H_u^+ \\ H_d^- \end{pmatrix}. \tag{1.57}$$

The new fields correspond to the five neutral Higgs bosons $H_{1,2,3}$ and $A_{1,2}$, the charged Higgs pair $H^\pm$ and the Goldstone bosons G^0 and $G^\pm$. For the interaction fields the Higgs mass matrices are not diagonal. They are diagonalized at tree-level by the matrices $\mathcal{R}_H, \mathcal{R}_A, \mathcal{R}_{H^\pm}$,

$$\begin{aligned} \mathcal{R}_H \mathbf{M}_H \mathcal{R}_H^\dagger &= \text{diag}\left(m_{H_1}^2,\ m_{H_3}^2, m_{H_3}^2\right), \\ \mathcal{R}_A \mathbf{M}_A \mathcal{R}_A^\dagger &= \text{diag}\left(m_{A_1}^2,\ m_{A_2}^2,\ 0\right), \\ \mathcal{R}_{H^\pm} \mathbf{M}_{H^\pm} \mathcal{R}_{H^\pm}^\dagger &= \text{diag}\left(m_{H^\pm}^2,\ 0\right). \end{aligned} \tag{1.58}$$

Charginos: Charginos are mixed states of the charged higgsino and winos. They acquire a Dirac mass term. The mass matrix for the fields in the interaction basis reads

$$\mathbf{X} = \begin{pmatrix} M_2 & \sqrt{2} m_W \sin\beta \\ \sqrt{2} m_W \cos\beta & \mu_{\text{eff}} \end{pmatrix}. \tag{1.59}$$

It can be diagonalized by a biunitary transformation

$$\mathbf{X}^{(\text{diag})} = \mathbf{U}_{\widetilde{\chi}^+}^* \mathbf{X} \mathbf{V}_{\widetilde{\chi}^-}^\dagger = \text{diag}\left(m_{\widetilde{\chi}_1^\pm},\ m_{\widetilde{\chi}_2^\pm}\right). \tag{1.60}$$

A numerical singular value decomposition on $\mathbf{X}$ yields numerical results for the positive and real singular values, which can be identified with the two chargino masses. The decomposition also yields results for the matrices $\mathbf{U}$ and $\mathbf{V}$.

Neutralinos: The superpartner fields of the singlet mix with the other neutral gauginos and higgsinos. Thus there are five neutralinos in the NMSSM. Their

mass matrix in the interaction basis reads

$$\mathbf{Y} = \begin{pmatrix} M_1 & 0 & -m_Z s_W \cos\beta & m_Z s_W \sin\beta & 0 \\ 0 & M_2 & m_Z c_W \cos\beta & -m_Z c_W \sin\beta & 0 \\ -m_Z s_W \cos\beta & m_Z c_W \cos\beta & 0 & -\mu_{\text{eff}} & \lambda v_u \\ m_Z s_W \sin\beta & -m_Z c_W \sin\beta & -\mu_{\text{eff}} & 0 & \lambda v_d \\ 0 & 0 & \lambda v_u & \lambda v_d & -\sqrt{2}\kappa s \end{pmatrix}. \tag{1.61}$$

It can be diagonalized by a unitary transformation

$$\mathbf{Y}^{(\text{diag})} = \mathbf{N}^*_{\widetilde{\chi}^0} \mathbf{Y} \mathbf{N}^\dagger_{\widetilde{\chi}^0} = \text{diag}\left(m_{\widetilde{\chi}^0_1},\ m_{\widetilde{\chi}^0_2},\ m_{\widetilde{\chi}^0_3},\ m_{\widetilde{\chi}^0_4},\ m_{\widetilde{\chi}^0_5}\right). \tag{1.62}$$

Since $\mathbf{Y}$ is hermitian, it can be diagonalized with only one unitary matrix $\mathbf{N}$. The numerical values for the mixing matrix and the neutralino masses are obtained by performing a numerical singular value decomposition on $\mathbf{Y}$.

Sfermions: The sfermions are mixtures of the superpartners of the right-handed and left-handed SM fermions. The mass matrix for the fields in the interaction basis reads

$$\mathbf{M}_{\widetilde{f}} = \begin{pmatrix} m^2_{\widetilde{f}_L} + m_f^2 + m_Z^2 \cos 2\beta (I_3^f - Q_f s_W^2) & m_f X_f \\ m_f X_f & m^2_{\widetilde{f}} + m_f^2 + m_Z^2 \cos 2\beta Q_f s_W^2 \end{pmatrix} \tag{1.63}$$

with $(f, \widetilde{f}, \widetilde{f}_L) \in \{(u, \widetilde{u}, \widetilde{Q}), (d, \widetilde{d}, \widetilde{Q}), (e, \widetilde{e}, \widetilde{L})\}$ and $X_f = (A_f - \mu_{\text{eff}} t_f\beta)$, where $t_f\beta = \tan\beta$ for sleptons and down-type squarks and $t_f\beta = \cot\beta$ for up-type squarks. I_f^3 and Q_f denote the weak isospin and electric charge of the corresponding SM fermion.

It can be diagonalized by a unitary 2×2 matrix $\mathbf{U}_{\widetilde{f}}$ given by

$$\mathbf{M}^{(\text{diag})}_{\widetilde{f}} = \mathbf{U}_{\widetilde{f}} \mathbf{M}_{\widetilde{f}} \mathbf{U}^\dagger_{\widetilde{f}} = \text{diag}\left(m^2_{\widetilde{f}_1},\ m^2_{\widetilde{f}_2}\right). \tag{1.64}$$

The mixing matrix is parameterized by the mixing angle $\theta_{\widetilde{f}}$,

$$\mathbf{U}_{\widetilde{f}} = \begin{pmatrix} \cos\theta_{\widetilde{f}} & \sin\theta_{\widetilde{f}} \\ -\sin\theta_{\widetilde{f}} & \cos\theta_{\widetilde{f}} \end{pmatrix}, \tag{1.65}$$

which depends on the mass hierarchy between the two stop masses. The elements of the mixing matrix elements fulfill the relation

$$\left(\mathbf{U}_{\tilde{f}}\right)_{11}\left(\mathbf{U}_{\tilde{f}}\right)_{12} = \frac{m_f X_f}{m^2_{\tilde{f}_1} - m^2_{\tilde{f}_2}}\,. \tag{1.66}$$

1.3.5 MSSM-limit

The MSSM can be obtained as a limit of the NMSSM for

$$\lambda \to 0\,,\ \kappa \to 0\,,\ \mu_{\text{eff}} = \text{const.}\,,\ \frac{\lambda}{\kappa} = \text{const.} \tag{1.67}$$

If κ maintains a finite value in this limit, the singlet and singlino sector decouples from the remaining fields. The result is the MSSM with a self-interacting singlet and singlino sector.

In the following section we briefly discuss various atomic and subatomic EDMs and their measurements associated with the CPV phases of the Higgs sector of the MSSM and the NMSSM, as the EDM measurements play a crucial role in our study.

1.4 The EDM measurements

Searches for the EDMs of molecules, atoms, nucleons and nuclei provide strong probes to CP violation both in the SM and BSM scenarios. The EDMs depend upon the scale of physics from the long atomic and molecular scales to the short distance at or beyond the Fermi level.

The existence of EDM of an elementary particle or a quantum system does not require flavor changing interactions. The situation is more complex in the SM due to the participation of the three generations of quarks and thus flavor changing interactions at higher orders. As a result, the EDMs of light quarks and leptons generated by CP violation are highly suppressed. The individual quark EDM or chromo EDM (CEDM) vanishes at two-loop level [76, 77]. The lowest order contribution to the neutron EDM (d_{n}), then arises not from the individual CEDM, but from hadronic interactions at two-loop level. The CPC interaction appears at tree-level, while the CPV interaction is generated at one-loop level that contains a

sum over all three flavors of positively charged quarks. The electron EDM (d_e) first appears at four-loop level, which is suppressed by several orders of magnitude with respect to d_n. The null results for the neutron and mercury ($d_{Hg^{199}}$) EDMs imply that $\bar{\theta}$ ($\bar{\theta}$: vacuum angle, θ: the 4-D QCD θ term) is tiny ($\bar{\theta} \lesssim 10^{-10}$). Within the SM as well as in BSM scenarios, CPV radiative corrections to the quark masses (or the Yukawa interactions) could introduce unacceptedly large magnitude for $\bar{\theta}$. If a given CPV scenario does not suppress these contributions, the constraints on the CPV source can be quite severe.

EDMs of composite systems reflect few or many body dynamics as well as the fundamental sources of CP violation. In heavier neutral systems, the shielding effect, i.e., the shielding of the EDMs of protons in nucleus by those of the electrons, is important. The transmission of CP violation through a nucleus into an atom must overcome this shielding and its effectiveness in doing so is expressed by a nuclear Schiff moment. The primary fact of the EDMs of neutral atoms is expressed by the Schiff theorem [78], which states that in the limit of a point like nucleus and non-relativistic electrons, any nuclear EDM is completely screened by the atomic electrons, so that the net atomic EDM is zero. In real systems, finite nuclear size essentially reduces the moments by $\mathcal{O}(R^2_{nucl}/R^2_{atom})$ with respect to the unscreened nuclear EDM. In diamagnetic atoms, this suppression is mitigated by the relativistic electrons and can be further mitigated by the nuclear octupole deformation. In paramagnetic atoms, relativistic electrons can lead to a large enhancement to the atomic EDM.

The atom associated with Hg^{199} nucleus has the best limit on its EDM for years (for Hg^{199} see ref. [79] and for Ra^{225} see ref. [80]). Hg is a soft nucleus in which a single mean field exists, the dominance of which underlies all of the results obtained so far, is probably insufficient. The Schiff moment calculation for Hg is thus challenging in nature. If a BSM is generated only by the six dimensional CEDM operators, then the corresponding effect on the Hg atom would be dominated by the induced neutron and proton EDMs. The Schiff moments in nuclei with asymmetric shapes could be enhanced by two or three orders of magnitude. Radium (Ra) is octupole deformed and, has favorable atomic physics and has spin $\frac{1}{2}$, making the nuclear orientation insensitive to quadrapole fields. Thus Ra is more favorable for experiments. The thallium (Tl^{205}) EDM (d_{Tl}) has by far the strongest dependence on d_e [81–84].

Any new source of CP violation generally induces contribution to the QCD and the vacuum angle ($\bar{\theta}_{\rm BSM}$). In the MSSM, such contributions arise at one-loop level via correlations to the quark propagators. Given the already severe bounds on $\bar{\theta}$, such contributions to $\bar{\theta}_{\rm BSM}$ by themselves imply stringent limits on the CPV phases in absence of a mechanism to alleviate them. Possibilities include invoking a new symmetry such as flavor symmetry, that yields a vanishing one-loop result.

Secondly, non-observation of atomic, molecular and neutron EDMs generally imply that any new CPV phase ($\phi_{\rm CPV}$) must be quite small if the BSM mass scale (Λ) is of sub-TeV order. Conversely, allowing $\sin\phi_{\rm CPV} \sim 1$ implies $\Lambda \geq$ few TeV. In order to allow sub-TeV mass scale and $\mathcal{O}(1)$ CPV phases, while respecting present constraints, one must either invoke cancellations between different contributions [85] or mechanisms that suppress the one-loop EDMs. In the case of the MSSM, taking the sfermions to have multi-TeV masses can result in the leading contribution arising at two-loop level and involving the EW gaugino-Higgs/Higgsino sector with sub-TeV masses [86, 87]. Given the suppression of an additional loop factor, the resulting dependence on the CPV phases weaken and the present constraints are generally less severe.

CP violation in SUSY theories generally leads to one-loop EDMs that exceed present experimental bounds, assuming that the superpartner masses lie below 1 TeV, leading to the so called *SUSY-CP problem*. The SUSY mechanism for solving the hierarchy problem leads one to expect sub-TeV scale superpartner masses, implying $|\sin\phi_{\rm CPV}| \lesssim 0.01-0.1$. On the other hand, one might naturally expect $\sin\phi_{\rm CPV} \sim \mathcal{O}(1)$. The possible solutions to the SUSY-CP problem are listed below.

• Heavy sfermions: This leads to a suppression of one-loop EDMs and allowing for $\mathcal{O}(1)$ phases [86, 87]. Null results for superpartner searches at the LHC may point out to the split SUSY scenario [88], as the generic mass bounds on the gluinos and first and second generations squarks are now at TeV scale. The EW gauge bosons and Higgsino may still be relatively light, thereby allowing for a viable baryogenesis mechanism.

• Cancellation: It is proposed in ref. [85] that contributions to EDMs from different CPV phases may cancel, leading to a suppression that again allows for $\mathcal{O}(1)$ CPV phases and light superpartners.

It is particularly notable that the limit on $d_{\rm Hg}$ places severe constraint on ϕ_3 while generating a strong correlation between this phase and $\phi_{u,d}$, both of which enter the CEDM operators at one-loop level. In contrast, limits on $d_{\rm n,Tl}$ have a relatively stronger impact on ϕ_2, though at present, the latter constraint is not strongly correlated with any of the other phases. Any global analysis for EDM search results, should take into account the rather sizable hadronic and nuclear uncertainties associated with the sources of CP violation.

The direct observation of the EDM of a charged particle is very difficult, due to the presence of hugely dominating monopole contributions, i.e., its charge. Therefore the most sensitive measurements, at least so far, come from the neutral systems, especially, neutrons and atoms/molecules. For reviews on EDMs see ref. [82, 89–92]. For recent analyses within SUSY models see ref. [80, 90, 93–99].

In paramagnetic atoms, i.e., atoms with non-vanishing total angular momentum, relativistic effects are important, and these are largely enhanced for atoms with a large proton number [100], scaling at least like d $\sim Z^3$. This implies sensitivity mainly to $d_{\rm e}$, but also the electron-nucleon interactions are enhanced. At present, the most constraining measurements from this class, performed with Tl atom and ytterbium fluoride (YbF) molecule [84, 101], allow for model independent determination of $d_{\rm e}$, which improves significantly, using in addition, the information from the Hg system.

In diamagnetic atoms, i.e., atoms with vanishing total angular momentum, the finite size of the nucleus is the main source of violation of the Schiff theorem. The dominant contribution to the corresponding EDM comes from its nuclear Schiff moment which can be expressed in terms of nucleon EDMs and pion-nucleon interactions [78]. Although the contributions from the nucleon EDMs are present as well, which are dominated by the pion-nucleon interactions. All the necessary calculations are very involved and the wide range of results indicates that the related theoretical uncertainties are large [80, 92, 93]. For Hg at some stage, all the interactions show problems and the differences between the calculations are not well understood [79]. In absence of errors, the problems might arise from the fact that Hg^{199} is a soft nucleus [79]. For direct limit on $d_{\rm n}$ refer [102–104]. The corresponding calculations, however show a high sensitivity to the higher oder effects, the correction to the previous estimate [105] amounts to $\sim$ 200% and change in sign. In the light of these situations, an upper limit on $d_{\rm e}$ from Hg atom is not so meaningful until the theoretical situations improve.

System	Present limit at 95% CL on absolute value
$\lvert d_{\rm Tl}\rvert$	9.0×10^{-25} e cm (90% CL) [27]
$\lvert d_{\rm n}\rvert$	3.3×10^{-26} e cm (95% CL) [102, 103]
$\lvert d_{\rm e}\rvert$	8.7×10^{-29} e cm (90% CL) [27, 83, 84, 101, 106]
$\lvert d_{\rm Hg}\rvert$	7.4×10^{-30} e cm (95% CL) [27, 107]

TABLE 1.6: Summary table for current limits on some particular EDMs.

There remains an $\mathcal{O}(1)$ theoretical uncertainty with $d_{\rm n,Hg}$. For $d_{\rm n}$, the uncertainty arises from hadronic physics, while for $d_{\rm Hg}$, the source of uncertainty is associated with (a) atomic effects in extracting the nuclear Schiff moment from $d_{\rm Hg}$, (b) nuclear effects going into extracting T- and P-odd pion-nucleom couplings $\bar{g}_{\pi NN}$, from the Schiff moment and (c) the hadronic effects in computing the $\bar{g}_{\pi NN}$ in terms of quark CEDM operator, Weinberg three gluon operator and the CPV four fermion operator. A primary impact of the new result on $d_{\rm Hg}$ is to impose more stringent constraint on the relative phase ϕ_3 between the gluino soft SUSY breaking mass and the μ parameter, while generating a strong correlation between this phase and the soft SUSY breaking trilinear couplings involving first generation of sfermions. The limits on $d_{\rm n,Tl}$ have a stronger impact on the relative phase ϕ_2 between the wino soft mass parameter and μ, than the $d_{\rm Hg}$ bound, but at present there does not exist any strong correlation between ϕ_2 and the other phases.

In particular, the CPV phases include the phases $\phi_{1,2,3}$ of the gaugino masses $M_{1,2,3}$ and the phases $\phi_{u,d,e}$, $\phi_{c,s,\mu}$, $\phi_{t,b,\tau}$ of the sfermion trilinear couplings $A_{u,d,e}$, $A_{c,s,\mu}$, $A_{t,b,\tau}$, respectively. These phases play different roles in generating various CP-odd operators, including the electron EDM $d_{\rm e}$, quark EDM $d_{\rm q}$ and chromo EDM $\widetilde{d}_{\rm q}$, the Weinberg three gluon operator d^{3G} and the four fermion operator $C_{ff'}$. These CP-odd operators are responsible for the EDMs of the neutron, as well the Tl and Hg atoms. In particular, in the MSSM, $d_{\rm Tl}$ is dominated by $d_{\rm e}$, possibly by the four fermion operator $C_{ff'}$, if $\tan\beta > 30$ [108]. The neutron EDM, mainly stems from the EDM and CEDM operators of u and d quarks, $d_{\rm u,d}$ and $\widetilde{d}_{\rm u,d}$, and from the three gluon operator d^{3G}. The Hg EDM is generated primarily by the CEDM operators $\widetilde{d}_{\rm u,d}$ [89].

ϕ_3 induces EDMs of n, Tl and Hg. Since it does not induce electron EDM, its contribution to $d_{\rm Tl}$ is highly suppressed. ϕ_3 could induce $d_{\rm Tl}$ sizably by generating $\widetilde{d}_{\rm u,d}$ at two-loop level. However, the most stringent constraint comes from the

current $d_{\rm n}$ bound. The constraint on ϕ_3 from $d_{\rm n}$ depends on tanβ and relevant mass scale and M_3. The current bound on $d_{\rm Tl}$ is in general weaker than that of n and Hg in constraining ϕ_t, and does not put any constraint on ϕ_b. The relative strengths of the $d_{\rm n,Hg}$ bounds on ϕ_t and ϕ_b depends upon tanβ. At small tanβ, $d_{\rm n}$ constraint is stronger than that of Hg, while at large tanβ, $d_{\rm Hg}$ becomes more dominant. ϕ_t and ϕ_b are rather loosely bounded and can reach $\frac{\pi}{2}$ for a few hundred GeV mass scale, while ϕ_τ phase is not constrained by the current EDM bounds at all. Similarly, the CPV phases related to the second generation of sfermions $\phi_{c,s,\mu}$, are essentially unconstrained by the experimental EDM limits.

Chapter 2

125 GeV Higgs boson in the CP-violating MSSM

This chapter is devoted to our investigation on the role of CPV phases in some of the soft SUSY terms on both the mass of the lightest Higgs boson h_1 (which is considered here to be the observed one at the LHC), and the rates for the processes $gg \to h_1 \to \gamma\gamma$, $gg \to h_1 \to ZZ^* \to 4l$, $gg \to h_1 \to W^+W^- \to l\nu l\nu$, $qq \to h_1 \to b\bar{b}$ and $qq \to h_1 \to \tau^+\tau^-$, at the LHC in the context of the MSSM. We consider the impact of constraints coming from b-physics observables and sparticle masses as well as EDM measurements on our model parameter space.

2.1 Introduction

The experimental observation of the SM Higgs boson and the determination of its properties were among the main motivations of the LHC. Both the ATLAS and CMS collaborations reported a Higgs boson discovery with the new particle having mass around 125 GeV [109–112]. It is also evident from the LHC data that the signals observed in different production and decay channels seem to follow the SM predictions. However, primarily due to the presence of large experimental uncertainties, there could be some deviations in some of the individual channels from the SM expectations. According to the recent updates on LHC results, CMS results are consistent with the SM expectations within 1σ uncertainty in all channels, except for a slight tension in the case of W^+W^- decay mode [113–118]. On the other hand, a slight excess still persists in the case of ATLAS observations

in most of the channels [119–125]. While not incompatible with statistical fluctuations, it is also possible that such deviations could signal the presence of BSM physics. For instance, one can explain these results in models with an extended Higgs sector like those embedded in SUSY [52, 62, 63, 126].

SUSY is one of the most popular extensions of the SM, with motivations that include: (i) the solution to the hierarchy and naturalness problems in the SM, (ii) the unification of the SM gauge couplings at some high scale close to the Planck scale, (iii) the provision for a dark DM candidate (provided $R-$parity is conserved), (iv) being a natural ingredient of String theories.

The MSSM, the simplest realization of SUSY, however predicts the maximum tree-level value of the lightest Higgs mass to be $M_{h_1} \leq M_Z$. Significant radiative corrections are needed in order to push M_{h_1} beyond the LEP bound $M_h > 114$ GeV (h denotes the SM-like Higgs boson). However, making the Higgs mass close to 125 GeV requires the inclusion of sizable top/stop loop corrections, which depend quadratically on the top quark mass and logarithmically on the stop masses, combined with a large value of $\tan\beta$, the ratio of the VEVs of the two Higgs doublets pertaining to the MSSM. Several studies have already been performed in the context of different SUSY models, including the MSSM [3–6, 34, 127–142] (also the constrained version [143]), the NMSSM [144] and the ((B–L)SSM) [9]. All of these scenarios predict a SM-like Higgs boson with mass around 125 GeV and also offer solutions explaining the potential slight disagreement between the data and the SM predictions in different decay channels.

Another route to follow in order to obtain similar results is to consider the possibility of having non-zero values of CPV phases in (some of) the soft SUSY parameters that can substantially modify the Higgs boson phenomenology at colliders by affecting mass spectrum and production cross sections and/or decay widths. This motivated an avalanche of phenomenological studies in the CPV-MSSM framework [30, 31, 36, 145–172]. In the presence of CPV complex parameters, the top and bottom squark couplings to the Higgs boson are modified substantially in a large domain of the MSSM parameter space [173–177]. The CPV phases in the MSSM are constrained by the EDM measurements. At the same time, the non-zero phases, satisfying the EDM constraints, may be allowed under certain conditions, as explained in the following sections, and in some details in refs. [97, 98, 178–182].

The MSSM Higgs potential is CP invariant at tree-level. Several studies have been performed to explore scenarios that break the CP invariance of the Higgs potential spontaneously [183]. However, these possibilities are now almost ruled out by various experiments [184]. Instead, CP violation can be induced explicitly in the MSSM Higgs sector. This can be achieved by introducing complex parameters that break CP invariance in the sfermion and chargino/neutralino sectors. Many parameters like the Higgsino mass parameter μ, the soft SUSY breaking gaugino masses M_1, M_2, M_3, and the soft trilinear couplings A_f, of the Higgs boson to the (massive) sfermions of flavor f, could in principle be complex. In general, each of these phases can be independent of each other. The CPV effects are then carried into the Higgs sector through the interactions of the two Higgs doublets with the sfermions and/or charginos/neutralinos.

In this chapter, we study the possibilities to have the Higgs signals with mass around 125 GeV in the context of the CPV-MSSM, which are in agreement with the aforementioned LHC data as well as other experimental constraints. We look for parameter configurations of the model for which there exists agreement with both the Higgs mass and the rates into the channels observed by the LHC. We investigate the dependence of the feasible CPV-MSSM signals on the couplings of the Higgs boson to both the relevant particle and sparticle states entering the model spectrum, as well as upon the masses of the latter, thereby aiming at a general understanding of the role of the complex phases. While scanning the CPV-MSSM parameter space, we also take into account the constraints coming from the flavor sector and the EDM measurements.

The chapter is structured as follows. In the next section we give a brief introduction to the Higgs sector of the CPV-MSSM. In Sec. 2.3 we discuss the relevant experimental constraints coming from the SUSY particle searches, flavor sector and EDM measurements. In Sec. 2.4 we investigate the possible numerical values of the parameters after performing scans of the CPV-MSSM parameter space against available experimental constraints. In Sec. 2.5 we present our results on Higgs production and decay processes in connection with the LHC Higgs data. Finally, we conclude in Sec. 2.6.

2.2 A light Higgs in the CPV-MSSM

In the MSSM, non-zero phases of μ, M_i $(i = 1, 2, 3)$ and/or A_f, $(f = t, b, \tau)$ can induce CP violation in the Higgs sector radiatively, via the interactions of the Higgs bosons with the sfermions and gauginos. These interactions lead to modifications of the Higgs masses as well as the Higgs couplings, breaking the CP invariance of the tree-level scalar potential. Presence of CP violation in the Higgs sector leads to scalar-pseudoscalar mixing, resulting in CP-mixed physical Higgs states. In the following we describe this mixing schematically and explicitly present the dependence of mixing on different complex parameters. The gauge eigenstates of the MSSM Higgs doublets are given by

$$\widehat{H}_u = \begin{pmatrix} h_u^+ \\ h_u^0 + i a_u^0 \end{pmatrix}, \qquad \widehat{H}_d = \begin{pmatrix} h_d^0 + i a_d^0 \\ h_d^- \end{pmatrix}, \tag{2.1}$$

with

$$\langle \widehat{H}_u \rangle = \frac{1}{\sqrt{2}} \begin{pmatrix} 0 \\ v_u \end{pmatrix}, \qquad \langle \widehat{H}_d \rangle = \frac{1}{\sqrt{2}} \begin{pmatrix} v_d \\ 0 \end{pmatrix},$$

where h_i^0/a_i^0, $(i \equiv u, d)$ are the scalar/pseudoscalar components of the two Higgs doublets.

In the presence of CPV phases in the scalar potential, the mass matrix for the neutral Higgs bosons enters in the Lagrangian through the general form

$$\mathcal{L}_{\text{mass}} = \begin{pmatrix} a_u^0 & a_d^0 \,\big|\, h_u^0 & h_d^0 \end{pmatrix} \left(\begin{array}{c|c} \mathcal{M}_P^2 & \mathcal{M}_{SP}^2 \\ \hline [\mathcal{M}_{SP}^2]^T & \mathcal{M}_S^2 \end{array}\right) \begin{pmatrix} a_u^0 \\ a_d^0 \\ \hline h_u^0 \\ h_d^0 \end{pmatrix}. \tag{2.2}$$

This 4×4 mass matrix is divided into 2×2 blocks with $\mathcal{M}_P^2$ and $\mathcal{M}_S^2$ representing the mixing between the pseudoscalar and scalar states, respectively, and the off-diagonal block, $\mathcal{M}_{SP}^2$, representing the mixing between the scalar-pseudoscalar states. Note that $\mathcal{M}_{SP}^2$ is absent in the CPC-MSSM and is generated in the CPV-MSSM through one-loop corrections [20–22, 74, 185–189]. The 2×2 matrix $\mathcal{M}_{SP}^2$ can be given as [21, 185]:

$$\mathcal{M}_{\text{SP}}^2 \sim \mathcal{O}\left(\frac{m_t^4 \mid \mu \mid\mid A_t \mid}{32\pi^2 v^2 M_{\text{SUSY}}^2}\right) \sin\Phi_{\text{CP}} \begin{pmatrix} 6 & \frac{|A_t|^2}{M_{\text{SUSY}}^2} \\ \frac{|\mu|^2}{\tan\beta M_{\text{SUSY}}^2} & \frac{\sin 2\Phi_{\text{CP}} |A_t||\mu|}{\sin\Phi_{\text{CP}} M_{\text{SUSY}}^2} \end{pmatrix} \tag{2.3}$$

where $\Phi_{\rm CP} = {\rm Arg}(A_t\mu)$, $v = 246$ GeV and the mass scale $M_{\rm SUSY}$ is defined by

$$M^2_{\rm SUSY} = \frac{m^2_{\tilde{t}_1} + m^2_{\tilde{t}_2}}{2} \ , \tag{2.4}$$

with $m_{\tilde{t}_1}$ and $m_{\tilde{t}_2}$ being the stop masses.

One can easily estimate the degree of CP violation in the Higgs sector by considering the dominant one(s) of these contributions. For example, sizable scalar-pseudoscalar mixing is possible for a large CPV phase $\Phi_{\rm CP}$, $|\mu|$ and $|A_t| > M_{\rm SUSY}$. Apart from a massless Goldstone boson G^0, which does not mix further with the other neutral states, the 4×4 mass matrix effectively reduces to a 3×3 Higgs mass-squared matrix $\mathcal{M}^2_{ij}$, in the basis (A, h^0_u, h^0_d), where A is the appropriate eigenstate of $\mathcal{M}^2_P$. The 3×3 symmetric matrix $\mathcal{M}^2_{ij}$ can be diagonalized by an orthogonal matrix $\mathcal{O}$, i.e., $M^2_i\delta_{ij} = O_{ik}\mathcal{M}^2_{kl}O_{jl}$, leading to physical states, $h_i = O_{ji}\ \phi_j$, where $\phi_j \equiv (A, h^0_u, h^0_d)$. The physical mass eigenstates h_1, h_2 and h_3 are considered in ascending order of mass ($M_{h_1} < M_{h_2} < M_{h_3}$). Moreover, as A is no longer a physical state, the charged Higgs boson mass $M_{H^\pm}$ is a more appropriate parameter for the description of the CPV-MSSM Higgs sector instead of M_A often used in the CPC-MSSM. Hence, the tree-level Higgs masses in the CPV-MSSM can be conveniently expressed in terms of $\tan\beta$ and $M_{H^\pm}$.

Radiative corrections enhance the Higgs mass significantly via the top quark Yukawa coupling, the third generation top squark mass parameters M_{Q_3}, M_{U_3} and the trilinear coupling A_t, while the bottom squark sector has a somewhat subdued effect. At the same time though, flavor physics observations from the b-quark sector often serve as stringent constraints on Higgs phenomenology and we therefore include the sbottom sector parameters M_{D_3} and the trilinear coupling A_b along with the above mentioned top squark parameters. The stau sector, in principle, can play a significant role in the Higgs to di-photon decay mode. To take this into account, we include the parameters M_{L_3}, M_{E_3} and A_τ corresponding to the stau sector in our parameter space scan.

Coming to the first two generations of soft masses, it is well known that they have very little impact on the Higgs sector of the MSSM. At the same time, their phases $\phi_{A_{e/\mu}}$, $\phi_{A_{u/d}}$ can provide significant contributions to the atomic EDMs. These can however be drastically reduced either by assuming these phases to be sufficiently small or by taking the first and second generation squarks and sleptons sufficiently heavy. Thus, in our study, we consider the hierarchy factor between the first two

and third generation soft masses to be 20. Nonetheless, sizable contributions to the EDMs are always possible from Higgs-mediated two-loop diagrams [190–192]. Therefore, in order to ascertain whether the regions of parameter space of interest are potentially compatible with the EDM constraints, we calculate the EDMs of thallium, mercury, electron and neutron and compare their values with the current experimental bounds [27, 78, 80, 83, 84, 92, 97, 101–104, 106]. In fact, in general, it has been shown in ref. [97] that the constraints from the EDMs are highly dependent upon the combinations of different phases of soft SUSY breaking parameters as different loop diagrams can interfere either destructively or constructively so as to either suppress or enhance, respectively, individual contributions to the EDMs. In the case of $d_{\rm Hg}$, the experimental limits put severe constraint on ϕ_3, due to the strong correlation between this phase and $\phi_{A_{u,d}}$, both of which enter the EDM operators at one-loop level. In contrast, $d_{\rm n}$ and $d_{\rm Tl}$ limits have a relatively stronger impact on ϕ_2 though, presently, the latter constraint is not strongly correlated with any of the other phases. A detailed analysis of the impact of the EDM data on the Higgs sector of the CPV-MSSM, considering all the three Higgs bosons and all CPV phases, is complicated and beyond the scope of this study. Nevertheless, herein we take a straightforward approach and present our results after compliance with the available EDM constraints. In the following section we present our numerical analysis and discuss the CPV-MSSM parameter space respecting these constraints along with all other experimental restrictions including those from the flavor and sfermion sectors.

2.3 Current experimental constraints

As explained in Sec. 2.2, the non-trivial CPV phases modify the Higgs mass significantly by introducing mixing between the scalar and pseudoscalar Higgs states. CPV phases can also affect the Higgs couplings with the gauge bosons and fermions, altering significantly their tree-level values. For example, in a situation with maximal CP violation, known as CPX scenario [162, 188, 193, 194], one can have the lightest Higgs boson which is almost CP-odd with a highly suppressed coupling to a pair of W's or Z's [21, 185].

The combined measurement of the Higgs boson mass in pp collisions at 7 and 8 TeV centre of mass (CM) energy with the ATLAS and CMS experiments is $125.09 \pm 0.21(\text{stat.}) \pm 0.11(\text{syst.})$ GeV [47]. Thus, considering the 1σ uncertainty band

around the best fit value, we primarily demand that the lightest Higgs boson mass (M_{h_1}) should always lie in the range of 124.0−126.0 GeV, while scanning the CPV-MSSM parameter space. Besides this, we also enforce the following constraints to select the final allowed parameter space points for our further analyses.

We impose 95% CL[1] lower bounds on the masses of sparticles, listed by the Particle Data Group (PDG) [195], as follows:

$$\begin{aligned} &M_{\widetilde{\chi}_1^0} > 46 \text{ GeV}, \quad M_{\widetilde{\chi}_2^0} > 62.4 \text{ GeV}, \quad M_{\widetilde{\chi}_1^\pm} > 94 \text{ GeV}, \\ &M_{\widetilde{t}_1} > 240 \text{ GeV}, \quad M_{\widetilde{b}_1} > 600 \text{ GeV}, \quad M_{\widetilde{g}} > 1150 \text{ GeV}. \end{aligned} \tag{2.5}$$

It is well known that flavor observables play a crucial role in determining the viable regions of the SUSY parameter space. Several rare b-decays, which are helicity suppressed in the SM, can acquire substantial contribution from different SUSY particles present in the model and these corrections may come with same or opposite sign with the SM expectations. To take into account the stringent constraints on the SUSY parameter space coming from the flavor sector, we consider several low energy processes like the purely leptonic decays $B_s \to \mu^+\mu^-$ and $B_d \to \tau^+\tau^-$, the radiative decay $B \to X_s\gamma$. The $B_s \to \mu^+\mu^-$ decay is a flavor changing neutral current (FCNC) process which occurs at loop levels in both the SM and the MSSM. In the SM, it is helicity suppressed by the muon mass, which results in tiny SM expectation for the BR of the order of 10^{-9} [196]. For large values of $\tan\beta$, order of magnitude enhancements of BR($B_s \to \mu^+\mu^-$) are possible in the MSSM. For detail see ref. [197–199] and the references therein. In the MSSM, the dominant contribution mainly comes from the Higgs penguin diagrams with the exchange of the heavy scalars present in the flavor changing b→s couplings. Besides, there are also contributions from the charged Higgs and gluino exchange diagrams which may interfere constructively or destructively with the Higgs diagrams and the SM expectations depending upon the sign of the μ and A_t terms. Due to its strong dependence on $\tan\beta$, MSSM parameter space with large $\tan\beta$ is now tightly constrained by the current experimental results on BR($B_s \to \mu^+\mu^-$) [200, 201]. The experimental measurement by the LHCb for BR($B_s \to \mu^+\mu^-$) is $(3.0 \pm 0.6^{+0.3}_{-0.2}) \times 10^{-9}$ [202], and in our analysis we consider the 3σ error band

[1]In our analysis, we consider 3σ bound for almost all the experimental constraints. But, for the sparticle masses, we find 95% CL limit from the Particle Data Group [195]. However, the updated results on different sparticle masses, which are available in the literature but not included in the PDG database yet, do not change our results substantially.

around the central value,

$$1.11 \times 10^{-9} < \text{BR}(B_s \to \mu^+\mu^-) < 5.01 \times 10^{-9}. \tag{2.6}$$

Let us now consider another important b-observable, i.e., BR($B \to X_s\gamma$). In the SM, it comes from the $t - W$ loop [203] and, in the MSSM, the dominant contribution comes from the $t - H^\pm$ and $\tilde{t}_{1,2} - \tilde{\chi}^\pm_{1,2}$ loops [204], where the former have the same sign with the SM $t - W$ loop. The chargino loop contribution is proportional to the product $A_t\mu \tan\beta$. Depending on the sign of $A_t\mu$, there might be cancellation or enhancement between the above two loop contributions within the MSSM [205]. Here, we choose positive A_t and positive μ and so we expect some cancellations between these different SUSY corrections for large values of $\tan\beta$. Considering the large uncertainty in the measurement, here we assume 3σ uncertainty around the experimental value of BR($B \to X_s\gamma$) $= (3.32 \pm 0.16) \times 10^{-4}$ [206] which leads to

$$2.84 \times 10^{-4} < \text{BR}(B \to X_s\gamma) < 3.80 \times 10^{-4}. \tag{2.7}$$

Apart from the above-mentioned two flavor constraints, which play a significant role in the present study, there exist other flavor constraints with subdued influences. The mass differences measured in the $B_0 - \bar{B}_0$ mixing, ΔM_{B_d} and ΔM_{B_s}, are equally sensitive to the new physics contributions. For both these two observables, at large $\tan\beta$, non-negligible contribution comes from the most dominant double scalar penguin diagrams [207, 208]. The experimental and the SM values for the mass differences in the B_d system are $\Delta M^{\text{Exp}}_{B_d} = 0.510 \pm 0.004$ ps^{-1} [209, 210] and $\Delta M^{\text{SM}}_{B_d} = 0.502 \pm 0.006$ ps^{-1} [211], respectively. On the other hand, for the B_s system they are, $\Delta M^{\text{Exp}}_{B_s} = 17.768 \pm 0.024$ ps^{-1} [209, 212] and $\Delta M^{\text{SM}}_{B_s} = 17.3 \pm 2.6$ ps^{-1} [213], respectively. The SUSY contributions to the $B^0_d - \bar{B}^0_d$ and $B^0_s - \bar{B}^0_s$ mass differences are usually denoted as $\Delta M^{\text{SUSY}}_{B_d}$ and $\Delta M^{\text{SUSY}}_{B_s}$, respectively, and calculated by subtracting the SM prediction from the experimentally measured quantity i.e. $\Delta M^{\text{SUSY}}_{B_d} = \Delta M^{\text{Exp}}_{B_d} - \Delta M^{\text{SM}}_{B_d}$ [214, 215]. Note that the theoretical uncertainty associated to ΔM_{B_s} dominates the experimental uncertainties, unlike ΔM_{B_d} where both theoretical and experimental errors are relatively small. In rest of our analysis, we therefore, consider only ΔM_{B_d} mass difference[2] and allow the SUSY contribution $\Delta M^{\text{SUSY}}_{B_d}$ lie within the 3σ error band drawn around the

[2]We check that if we consider the ΔM_{B_s} mass difference after satisfying Eq. 2.8 and allow even 1σ uncertainty in $\Delta M^{\text{SUSY}}_{B_s}$ estimation, we loose only $\sim$1% points.

experimental best-fit number. We also consider the ratio of the experimentally measured BR($B_u \to \tau\nu$) to its SM value, $R_{B_u\to\tau\nu} = \frac{\mathrm{BR}^{\mathrm{Exp}}(B_u\to\tau\nu)}{\mathrm{BR}^{\mathrm{SM}}(B_u\to\tau\nu)} = 1.21 \pm 0.30$ [199, 216]. Besides, we further check whether our results are consistent with the experimental result on the BR($B_d \to \tau^+\tau^-$) available in the PDG [195].

Finally, we consider the measurement of direct CP asymmetry, $A_{\mathrm{CP}}(B \to X_s\gamma)$, associated with the $B \to X_s\gamma$ decay with its present limit 0.015 ± 0.020 [195]. In summary, the experimental limits used, corresponding to 3σ uncertainty, (except BR($B_d \to \tau^+\tau^-$) which is given at 95% CL in the PDG) are the following:

$$\begin{aligned} 0.31 < R_{B_u\to\tau\nu} < 2.1, \quad \mathrm{BR}(B_d \to \tau^+\tau^-) < 2.1 \times 10^{-3}, \\ -0.045 < A_{\mathrm{CP}}(B \to X_s\gamma) < 0.075, \quad -0.0136 < \Delta M_{B_d}^{\mathrm{SUSY}} < 0.0296 \text{ ps}^{-1}. \end{aligned} \tag{2.8}$$

All these constraints are imposed on the points satisfying the primary selection criterion on the Higgs boson mass.

Furthermore, we investigate the effect of the EDM constraints on the parameter space. As already discussed, atomic EDMs receive contributions from electron as well as quark EDMs. In a quantum field theory, like the CPV-MSSM being discussed here, the presence of CPV phases induces EDMs for elementary particles like the electrons and quarks. How these contributions present themselves at the atomic level is a complex phenomenon, which depends on the nature of the atom or molecule being studied and on the theoretical model being considered. In the case of diamagnetic systems like Hg, the dominant contribution comes from the CEDMs, while the effect of d_{e} is sub-dominant. It is known that these atomic EDMs receive large theoretical (hadronic and nuclear) uncertainties. Besides, while the EDM of Hg is one of the best known experimentally, theoretical calculations using different techniques do not quite agree with each other, for reasons those are not fully understood [92]. Thus, the upper bounds on d_{e} obtained from these results should be considered with caution [83, 103]. In contrast, in the case of paramagnetic systems like Tl and YbF, the atomic EDMs depend on d_{e} and another term arising from electron-nucleon interactions, therefore the d_{e} extracted from these systems are more reliable. Traditionally, while extracting d_{e} from these systems, it is assumed that only the single unpaired electron would contribute to their EDMs. Besides, there are also direct measurements on d_{n} [102, 104], which receives contributions from the CEDMs arising in several BSM models. Similar to

the atomic case, these results too receive large theoretical uncertainties. We list the current bounds on $d_{\rm n}$ and $d_{\rm Tl}$ in Tab. 2.1.

System	Present limit on absolute value
$\lvert d_{\rm n}\rvert$	3.3×10^{-26} e cm (95% CL) [102, 104]
$\lvert d_{\rm Tl}\rvert$	9.0×10^{-25} e cm (90% CL) [84, 97]

TABLE 2.1: Summary table for the current experimental limits on $d_{\rm n}$ and $d_{\rm Tl}$.

The lower bound on $d_{\rm Hg}$ at 95% CL is [27]

$$|d_{\rm Hg}| < 3.1 \times 10^{-29} \text{ e cm.} \tag{2.9}$$

At present, the most stringent model independent limits on $d_{\rm e}$ stem from the searches for the EDMs of YbF and Tl, with upper limits of 1.05×10^{-27} e cm [101] and 1.6×10^{-27} e cm [84] at 90% CL, respectively. An improved analysis including the effect of electron-nucleon interaction and combining the results from Tl, YbF and Hg is available in ref. [83]. While considering the $d_{\rm e}$ constraints coming from these experiments, we adopt the result of this analysis with $d_{\rm e}$ given at 95% CL [83] as

$$|d_{\rm e}| < 1.4 \times 10^{-27} \text{ e cm.} \tag{2.10}$$

However, the Advanced Cold Molecule Electron (ACME) EDM Collaboration [106] recently put a strong limit on $d_{\rm e}$ which is lowered by one order of magnitude compared to the previous measurements. The experimental bound at 90% CL is[3]

$$|d_{\rm e}| < 8.7 \times 10^{-29} \text{ e cm.} \tag{2.11}$$

More recently, the limit on the permanent EDM of Hg at 95% CL is further reduced from the former limit by one order of magnitude [107]

$$|d_{\rm Hg}| < 7.4 \times 10^{-30} \text{ e cm.} \tag{2.12}$$

[3]Note that there are certain observables for which 90% or 95% CL data are available in the literature. We consider those at the same CL at which they are available. For example, the sparticle mass bounds in the PDG are given at 95% CL, while some of the EDM results are available either at 90% CL or at 95% CL.

In the next section, we first discuss the details of our CPV-MSSM parameter space scans and then show the impact of these constraints on the scanned parameter space.

2.4 Impact of the constraints on the parameter space

Here we explore the CPV-MSSM parameter space in order to estimate the regions which respect all the above mentioned experimental constraints. The scans were performed using the publicly available numerical package `CPsuperH-v2.3` [217]. We consider two separate scans with different sets of input parameters.[4] The choice of the first set of input parameters was aimed at maximizing the effect of CP violation in the MSSM, while the second set was with a view at searching for solutions within the CPV-MSSM compatible with the LHC and other experimental results.

2.4.1 Scan 1: with maximum CPV phases

The first scan considered the following values of the input parameters:

$$\begin{aligned} 1 < \tan\beta < 60, \quad & 100 \text{ GeV} < M_{H^\pm} < 300 \text{ GeV}, \\ 50 \text{ GeV} < |M_1| < 500 \text{ GeV}, \quad & 100 \text{ GeV} < |M_2| < 1000 \text{ GeV}, \\ 500 \text{ GeV} < A_t = A_b = A_\tau < 3000 \text{ GeV}, \quad & 500 \text{ GeV} < |\mu| < 2000 \text{ GeV}, \\ 500 \text{ GeV} < M_{Q3}, M_{U3} < 2000 \text{ GeV}, \quad & 500 \text{ GeV} < M_{D3} < 2000 \text{ GeV}, \\ 100 \text{ GeV} < M_{L3}, M_{E3} < 2000 \text{ GeV}. & \end{aligned} \tag{2.13}$$

The 100 GeV lower limit for M_2 is taken from model independent chargino searches with LEP-2, while the lower limit on $\tan\beta$ is close to the LEP-2 Higgs search exclusion limit. In ref. [150, 151], it was shown that there is a transition point at $M_{H^\pm} \sim 150$ GeV (for some specific choices of the model parameters) above which

[4]The reader may note that the first set of the parameter space scanning was planned and performed when preliminary results of the LHC were available. However, the second scan is performed keeping in mind the latest results of the LHC and the recent electron EDM measurement by the ACME collaboration.

the lightest Higgs mass state h_1, is almost a pure scalar state and thus there would be no CP violation through the scalar and pseudoscalar mixing. So, in our first scan (Scan 1), we set the upper limit on $M_{H^\pm}$ at 300 GeV in accordance with the above observation. However, we will see in Sec. 2.4.2, interesting phenomenology appears when we relax this upper limit on the $H^\pm$ mass. In order to have maximum CP violation, the three phases $\phi_{A_{\tilde{f}}}$ $(f = t, b, \tau)$ and ϕ_3 are fixed at 90°, while all other phases are set to zero. Trilinear couplings of the first and second sfermion families $(A_e, A_\mu, A_u, A_d, A_c, A_s)$ are less relevant for our analysis, hence we have set them to zero. Both the CMS and ATLAS collaborations have already excluded gluino masses less than 1.1 TeV for different possible final states in the context of the Constrained-MSSM (CMSSM) [218, 219]. Note that, the CMSSM bound can not be directly applied here as the bound is expected to change in the context of the CPV-MSSM due to modifications in the different decay/branching ratios. Here, we fix the magnitude of the gluino mass parameter M_3 at 1.2 TeV just to reduce the number of free parameters.

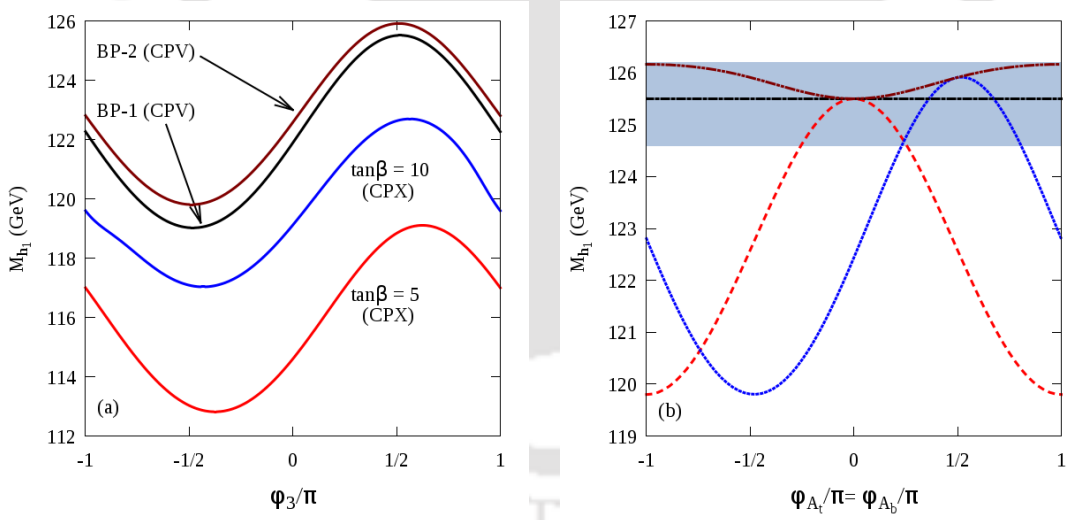

FIGURE 2.1: In panel (a) we show the dependence of M_{h_1} upon ϕ_3 for two BPs from our scan (upper two curves) against two benchmark points in the CPX scenario (lower two curves), keeping $\phi_{A_{\tilde{t}}} = \phi_{A_{\tilde{b}}} = \pi/2$. While in panel (b) the red (dotted), blue (small-dash dotted) and brown (long-dash dotted) curves correspond to $\phi_3 = 0$, $\phi_3 = \pi/2$, and $\phi_3 = \phi_{A_{\tilde{t}}} = \phi_{A_{\tilde{b}}}$, respectively, corresponding to BP-2. The horizontal solid curve in panel (b) represents the value of M_{h_1} in the CPC-MSSM and the shaded region corresponds to the 1σ range of the observed Higgs boson mass 125.3 ± 0.4 (stat.) ± 0.5 (syst.) GeV from the CMS Run 1 data [111].

We now begin our discussion on the numerical analyses by defining some benchmark points (BPs). In Fig. 2.1(a), we display the variation of the lightest Higgs boson mass (M_{h_1}) as a function of the phase ϕ_3, while keeping $\phi_{A_f} = \pi/2$ ($f = t, b, \tau$). The upper two curves represent two characteristic BPs (BP-1 & BP-2, see Tab. 2.2) obtained from Scan 1 represented by Eq. 2.13, whereas the lower two curves represent the CPX scenario [162, 188, 193, 194]. In Fig. 2.1(b), we present a similar variation of M_{h_1} with different combinations of CPV phases for BP-2. From Fig. 2.1, it is clear that the mass of the Higgs boson crucially depends on the CPV phases. In particular, notice that the radiative corrections to the lightest Higgs boson mass strongly depend on the stop mixing parameter $X_t = A_t - \mu \cot\beta$. Now, in our case, μ is real while A_t is a complex quantity. Hence, for different choice of phases, X_t can change, resulting in significant variations of the Higgs mass.

BP	M_1	M_2	M_3	$\tan\beta$	$M_{H^\pm}$	M_{Q3}	M_{D3}	M_{L3}	A_t	μ	M_{h_1}
1	496.7	356.1	1200	7.7	268.6	758.2	889.3	125.6	2458.0	796.6	125.5
2	469.7	456.8	1200	9.4	294.2	1371.8	704.5	1221.6	2621.7	1179.2	125.9

TABLE 2.2: Two BPs obtained after performing a random scan over the CPV-MSSM parameter space using `CPsuperH-v2.3`. In addition to the parameters relevant to describe the Higgs sector, we have also presented the mass of the lightest neutral Higgs boson. We have fixed the CPV phases to 90°. All masses, A_t and μ are expressed in units of GeV.

In Tab. 2.2, we have listed the details of BP-1 and BP-2, where the last column gives the mass of the lightest neutral Higgs boson. These two points are illustrative of the fact that it is always possible to have the lightest Higgs boson mass around 125 GeV when one includes the sizable corrections coming from the CPV phases into the MSSM results.

Before proceeding to analyze some LHC observables, it is important to take a look at the CPV-MSSM parameters and the particle spectrum after constraints are enforced upon the points obtained in the random scan with Eq. 2.13. In Fig. 2.2 (left) and (right) we have shown the allowed region in the $\tan\beta - M_{H^\pm}$ and $M_{h_1} - M_{h_2}$ planes, respectively. The brick red points are allowed by the set of constraints mentioned in Eq. 2.5 to Eq. 2.8, while the black dots represent points, which in addition to those constraints, also satisfy the electron EDM constraint given in Eq. 2.10. We find that once we impose the d_e constraint as given in Eq. 2.10, the allowed parameter space shrinks to the region depicted by the black dots, still with sufficient regions in the parameter space surviving all the constraints.

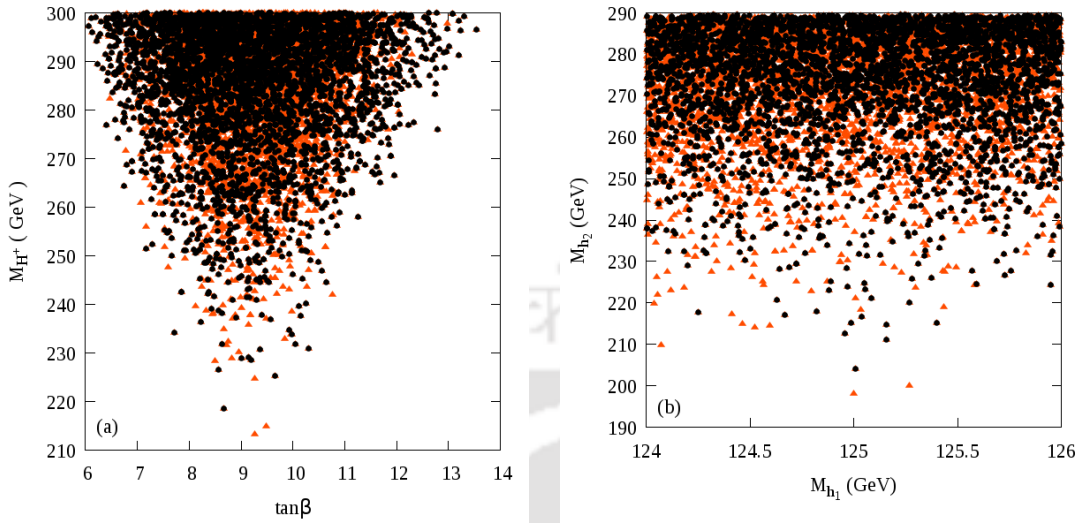

FIGURE 2.2: Constraints on the (left) $\tan\beta - M_{H^\pm}$ plane and (right) $M_{h_1} - M_{h_2}$ plane obtained after scanning the CPV-MSSM parameter space randomly. The brick red/grey triangles are allowed by the set of constraints mentioned in Eq. 2.5 to Eq. 2.8, while black points represent points which in addition to those constraints also satisfy the d_e constraint given in Eq. 2.10.

From Fig. 2.2 (left) one can conclude that the current limit on BR($B_s \to \mu^+\mu^-$) prefers low to medium values of $\tan\beta \sim 6 - 13$ and a somewhat heavy charged Higgs mass $M_{H^\pm} \gtrsim 200$ GeV (brick red points). In the CPC-MSSM, one has BR($B_s \to \mu^+\mu^-$) $\propto \tan^6\beta/M_A^4$, where M_A is the pseudoscalar Higgs boson mass. Now, in the case of the CPV-MSSM, as A is no longer a physical state, the charged Higgs boson mass is a more appropriate parameter for the description of the CPV-MSSM. Thus, in order to satisfy the current limit on BR($B_s \to \mu^+\mu^-$), one requires a heavier $H^\pm$ and a lower $\tan\beta$. Fig. 2.2 (right) shows that when the lightest Higgs boson is SM-like, the second lightest Higgs boson can have mass around 200–300 GeV. This mass window may be accessible at the 14 TeV LHC run via $gg \to h_2 \to h_1 Z$, followed by $h_1 \to b\bar{b}$ and $Z \to \nu\bar{\nu}$ or $\ell^+\ell^-$, as the analysis is very similar to the one performed in the case of the heavy Higgs boson searches at the LHC in the CPC-MSSM [63].

We further proceed to check how the most updated d_e and d_{Hg} measurements affect the CPV-MSSM parameter space. We find that, the latest bound on d_e, quoted in Eq. 2.11, completely rules out the parameter space region corresponding to Eq. 2.13. However, we shall see that relaxing the CPV phases from their maximal values (90^o), and with more appropriate choices of the parameters, one can satisfy

the latest $d_{\rm e}$ bound along with other EDM constraints (mentioned in Tab. 2.1) including the recent $d_{\rm Hg}$ bound (Eq. 2.12), and the low energy experimental bounds. Without moving further with the results corresponding to this set of parameters (Eq. 2.13), we now proceed to a new scan with a modified parameter set, in order to satisfy all the constraints discussed before including the stringent electron and Mercury EDM bounds.

2.4.2 Scan 2: allowing CPV phases to vary within $0^o - 90^o$

Moving away from the maximal CPV scenario (where ϕ_3 and ϕ_{A_f} are fixed to 90^o), sample test scans varying the magnitude of M_3 and the CPV phases (ϕ_3, ϕ_{A_t}, ϕ_{A_b} and ϕ_{A_τ}) between $0^o - 90^o$, were performed to optimize the parameter ranges suitable to accommodate all the experimental constraints coming from the flavor sector and the EDM measurements. After a dedicated analysis using those sample data sets, we fix the ranges (upper and lower limits) of the CPV parameters and then proceed to scan the CPV-MSSM parameter space for larger statistics. In our second scan (Scan 2), we choose an extended $M_{H^\pm}$ range by setting the upper limit to 1000 GeV, which was fixed at 300 GeV in our first scan, in order to avoid the loss of significant amount of parameter space due to the 300 GeV upper bound on $M_{H^\pm}$. Similarly for $\tan\beta$ we now choose the range to be from 1 to 30, as our first scan has already discarded regions with very large values of $\tan\beta$.

We consider the following set of parameters in our final scan and vary them randomly within the specified ranges:

$$\begin{aligned}
1 < \tan\beta < 30, \qquad & 250 \text{ GeV} < M_{H^\pm} < 1000 \text{ GeV}, \\
50 \text{ GeV} < |M_1| < 500 \text{ GeV}, \qquad & 100 \text{ GeV} < |M_2| < 1000 \text{ GeV}, \\
800 \text{ GeV} < |M_3| < 2000 \text{ GeV}, \qquad & 500 \text{ GeV} < |\mu| < 1000 \text{ GeV}, \\
1500 \text{ GeV} < A_t < 3000 \text{ GeV}, \qquad & 500 \text{ GeV} < A_b, A_\tau < 3000 \text{ GeV}, \\
500 \text{ GeV} < M_{\rm Q3} < 1500 \text{ GeV}, \qquad & 1000 \text{ GeV} < M_{\rm U3} < 3000 \text{ GeV}, \\
500 \text{ GeV} < M_{\rm D3} < 2000 \text{ GeV}, \qquad & 100 \text{ GeV} < M_{\rm L3},\ M_{\rm E3} < 2000 \text{ GeV}, \\
0^o < \phi_3, \phi_{A_t}, \phi_{A_b}, \phi_{A_\tau} < 90^o. & \qquad (2.14)
\end{aligned}$$

We take the 800 GeV lower limit on M_3 to satisfy the experimental lower bound on the gluino mass [195]. We would like to remind our reader that the lower bound

on the gluino mass is applicable for the CPC-MSSM and will change in the CPV-MSSM due to the significant modifications in different BRs. However, from the current LHC results, we expect that the gluino mass bound would be in the TeV regime, and so we choose 800 GeV as the lower limit. The ranges for μ, A_t, M_{Q3} and M_{U3} are set consulting sample test scans which favor relatively large values of A_t and small values of μ. We allow the CPV phases $(\phi_3, \phi_{A_t}, \phi_{A_b}, \phi_{A_\tau})$ to vary between 0^o to 90^o independently and randomly. Other remaining parameters in this second scan (Scan 2) are identical to those of the previous one (Scan 1).

With these new set of CPV-MSSM parameter ranges, we scan the parameter space for around 10^7 points and impose all the experimental constraints starting from Eq. 2.5 to Eq. 2.8 and the latest bounds on $d_{\rm e}$ (Eq. 2.11), $d_{\rm Hg}$ (Eq. 2.12), $d_{\rm Tl}$ and $d_{\rm n}$ (Tab. 2.1), after the primary selection criterion on the Higgs boson mass. In Fig. 2.3 (left) and (right), we present the allowed region in the $\tan\beta - M_{H^\pm}$ and $M_{h_1} - M_{h_2}$ planes, respectively, for the parameter ranges mentioned in Eq. 2.14. Clearly, larger $M_{H^\pm}$ values can accommodate larger $\tan\beta$, possibly even going beyond 30, satisfying all the constraints. From Fig. 2.3 (left) we can see that values of $\tan\beta$ smaller than around 5 are not allowed. In order to understand which constraint disallows $\tan\beta$ below 5, we plot the points allowed by the different set of constraints, where yellow dots are the points without any experimental bound, the blue dots are the points which obey only the Higgs mass bound, the red dots are the points which obey the constraints starting from Eq. 2.5 to Eq. 2.8 and the latest bounds on $d_{\rm e}$ (Eq. 2.11), $d_{\rm Tl}$ and $d_{\rm n}$ (Tab. 2.1) along with the previous $d_{\rm Hg}$ bound (Eq. 2.9), and the black points are allowed by all the experimental constraints starting from Eq. 2.5 to Eq. 2.8 and the latest bounds on $d_{\rm e}$ (Eq. 2.11), $d_{\rm Hg}$ (Eq. 2.12), $d_{\rm Tl}$ and $d_{\rm n}$ (Tab. 2.1). It is clear that the Higgs mass bound itself puts a upper limit of $\tan\beta \lesssim 5$. Here we would like to mention that, this pattern is consistent with the CPC-MSSM, see ref. [220]. Fig. 2.3 (right) says that the second lightest Higgs boson (h_2) can be as heavy as the $H^\pm$, with a preference for heavier masses.

In Fig. 2.4 we plot the allowed points in the (left) $\phi_{A_t} - \phi_3$ and (right) $\phi_{A_t} - \phi_{A_b}$ planes. Most of the allowed points fall in the region with relatively smaller values of ϕ_{A_t} and ϕ_3, even though there are some points with large phase values as well. We note that there were no surviving points from the first scan (corresponding to Eq. 2.13) with $\phi_{A_t} = \phi_{A_b} = \phi_{A_\tau} = \phi_3$ fixed at 90^o. In the present scan the large $M_{H^\pm}$ values make it possible to evade the experimental constraints for large values

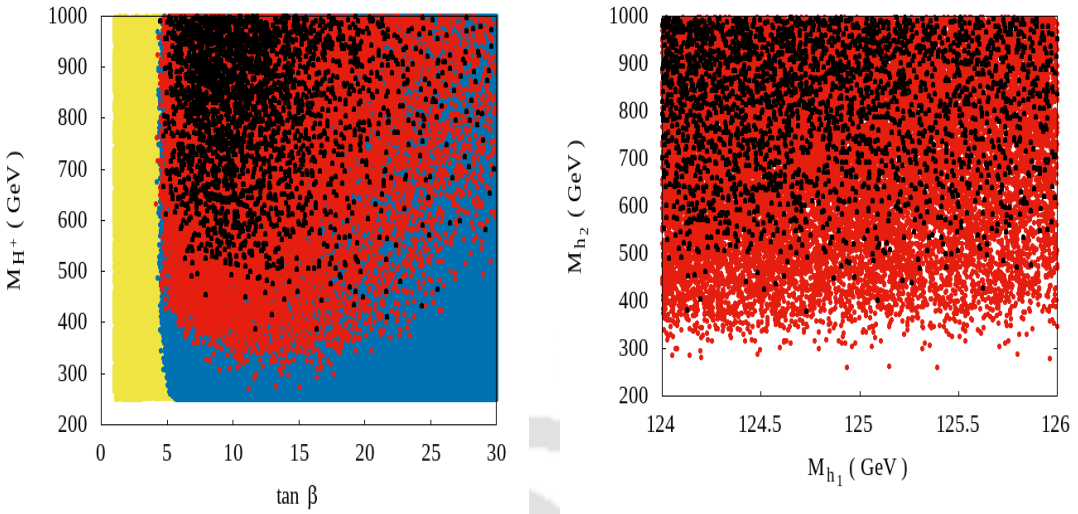

FIGURE 2.3: Constraints on the (left) $\tan\beta - M_{H^\pm}$ and (right) $M_{h_1} - M_{h_2}$ plane, respectively, obtained after scanning the CPV-MSSM parameter space randomly, for the input parameters mentioned in Eq. 2.14. The yellow region is without any experimental constraint, the blue region is allowed only by the primary Higgs mass bound, the red region is allowed by the constraints from Eq. 2.5 to Eq. 2.8 and the latest bounds on $d_{\rm e}$ (Eq. 2.11), $d_{\rm Tl}$ and $d_{\rm n}$ (Tab. 2.1), along with the previous $d_{\rm Hg}$ bound (Eq. 2.9), and the black region is allowed by the set of constraints mentioned in Eq. 2.5 to Eq. 2.8 and also the latest $d_{\rm e}$ (Eq. 2.11), $d_{\rm Hg}$ (Eq. 2.12), $d_{\rm Tl}$, $d_{\rm n}$ (Tab. 2.1) constraints.

of the CPV phases. Fig. 2.4 (right) clearly shows that ϕ_{A_b} has negligible effect. A similar result is obtained also for ϕ_{A_τ}, which is not presented here.

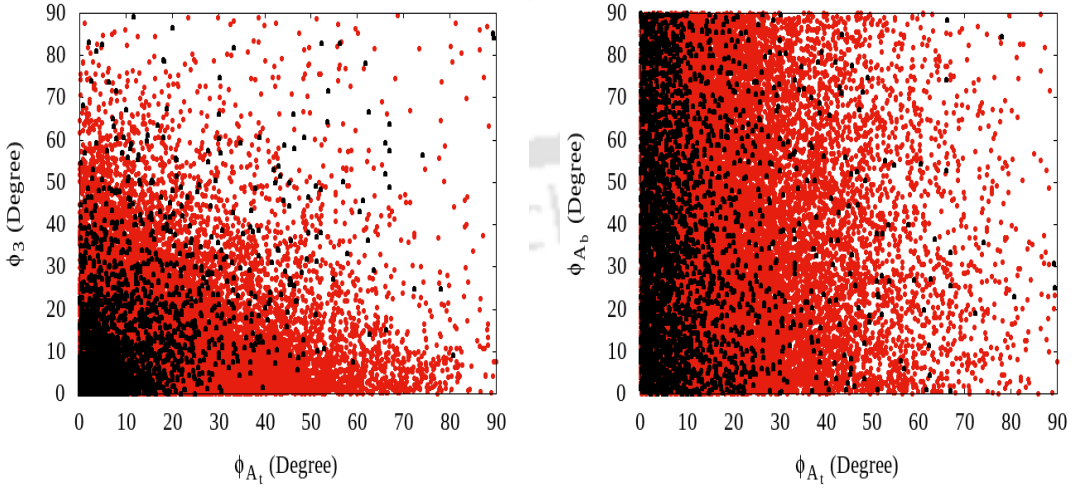

FIGURE 2.4: Correlation of ϕ_{A_t} with (left) ϕ_3 and (right) ϕ_{A_b}. The red and black color codes are same as in Fig. 2.3.

Fig. 2.5 (left) and (right) summarize the spectrum of some relevant particles in

the context of the CPV-MSSM under the same conditions as previously explained, with the same red and black color codes as in Fig. 2.3. Fig. 2.5 (left) shows, in particular, that the lightest chargino and neutralino masses could be as high as 900 GeV and 500 GeV respectively, while Fig. 2.5 (right) says that the lightest stop and stau masses could be as low as 600 GeV (for the black dots) and 100 GeV respectively, satisfying all the present experimental bounds.

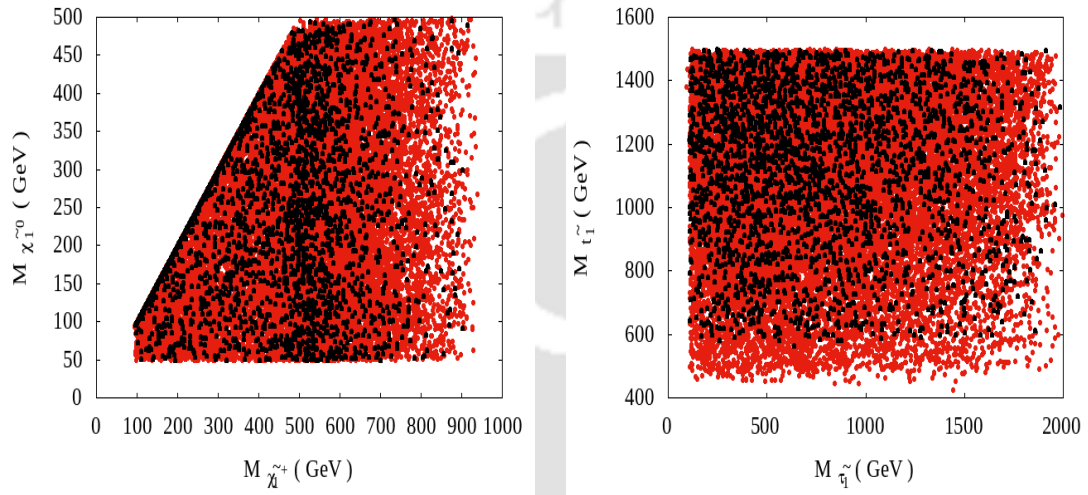

FIGURE 2.5: (left) $M_{\widetilde{\chi}_1^\pm} - M_{\widetilde{\chi}_1^0}$ and (right) $M_{\tilde{\tau}_1} - M_{\tilde{t}_1}$ planes after imposing all our selection criteria. The color codes are same as in Fig. 2.3.

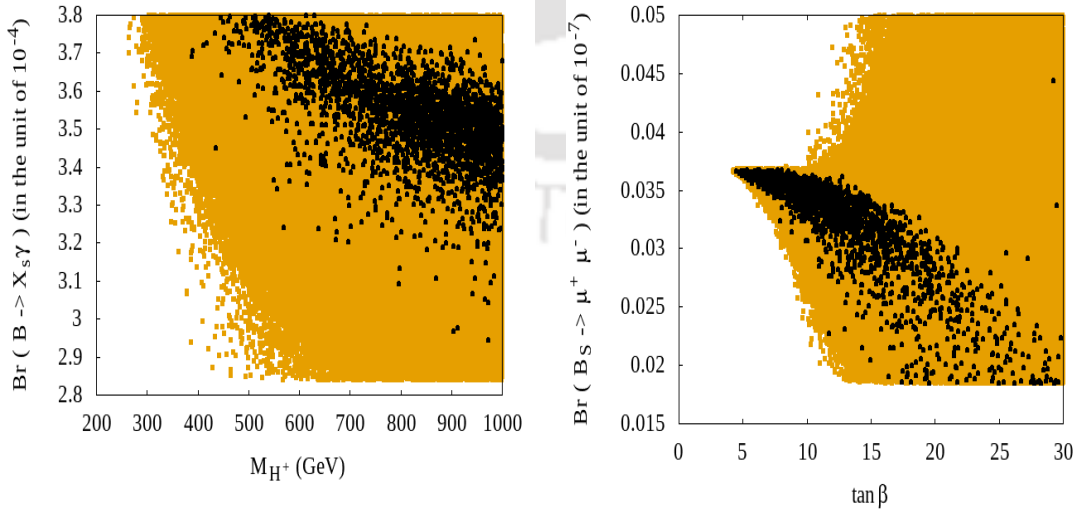

FIGURE 2.6: Variation of BR($B \to X_s\gamma$) with the charged Higgs mass (left) and the correlation between BR($B_s \to \mu^+\mu^-$) and $\tan\beta$ (right). The black points satisfy all the constraints, while the orange points correspond to the points satisfying all of the constraints except the EDM ones.

To study the constraints coming from the flavor sector, in Fig. 2.6 (left) we show the dependence of BR($B \to X_s\gamma$) on the charged Higgs boson mass, with and without the imposition of the EDM constraints. Similar kind of correlation can be seen in Fig. 2.6 (right), where we plot the variation of BR($B_s \to \mu^+\mu^-$) with $\tan\beta$. The black color code is the usual one which represents the points satisfying all the constraints, while the orange points satisfy all the experimental bounds starting from Eq. 2.5 to Eq. 2.8, except the EDM constraints. We have already discussed in Sec. 2.3 that significant amount of SUSY contribution may come from the charged Higgs loop and the chargino loop in $b \to s\gamma$ decay, and cancellation between the SUSY contribution and the SM value may occur, resulting in enhancement/suppression in the decay width. On the other hand, the SUSY contribution to the flavor changing $b \to s$ couplings, present in the BR($\mathrm{B_s} \to \mu^+\mu^-$) decay, strongly depends on $\tan\beta$. From both Fig. 2.6 (left) and Fig. 2.6 (right), we find that the recent electron and mercury EDM measurements affect the CPV-MSSM parameter space significantly the region with large $\tan\beta$. The generic SUSY contribution to the electron EDM comes from charginos, neutralinos at the one-loop level and from neutral Higgses at the two-loop level. One can significantly reduce the one-loop contributions by making the first two generations of sfermions very heavy (around 5–10 TeV). However, the Higgsino contribution is always present and it strongly depends on the Higgs boson coupling with the down-type fermions which grows with $\tan\beta$. Thus, we find that the imposition of the current d_e bound strongly discards the large $\tan\beta$ regime and thereby affect both the rare b-decays $B \to X_s\gamma$ and $B_s \to \mu^+\mu^-$ significantly. Apart from the $\tan\beta$ effect, non-trivial effects coming from the different loops associated with the different SUSY particles also play crucial role in accepting/discarding the parameter space points.

In Fig. 2.7 (left), we show the correlation in the $\Delta M_{B_d}^{\mathrm{SUSY}}$ - $\Delta M_{B_s}^{\mathrm{SUSY}}$ plane where these quantities measure the SUSY contributions to the $B_d^0 - \bar{B}_d^0$ and $B_s^0 - \bar{B}_s^0$ mass differences, respectively. From the figure, it is clear that all the points, which survive the Higgs mass cut and the low energy flavor data, are well within the experimental 3σ limit. This figure also justifies our choice of neglecting the $\Delta M_{B_s}^{\mathrm{SUSY}}$ cut as a selection criterion. However, with reduced theoretical uncertainty, this constraint will play a significant role in the CPV-MSSM parameter space. Finally, in Fig. 2.7 (right) we show the variation of the electron EDM with ϕ_{A_t}. We find that the current experimental electron and mercury EDM limits mostly favor smaller values of the CPV phases, though few parameter points may

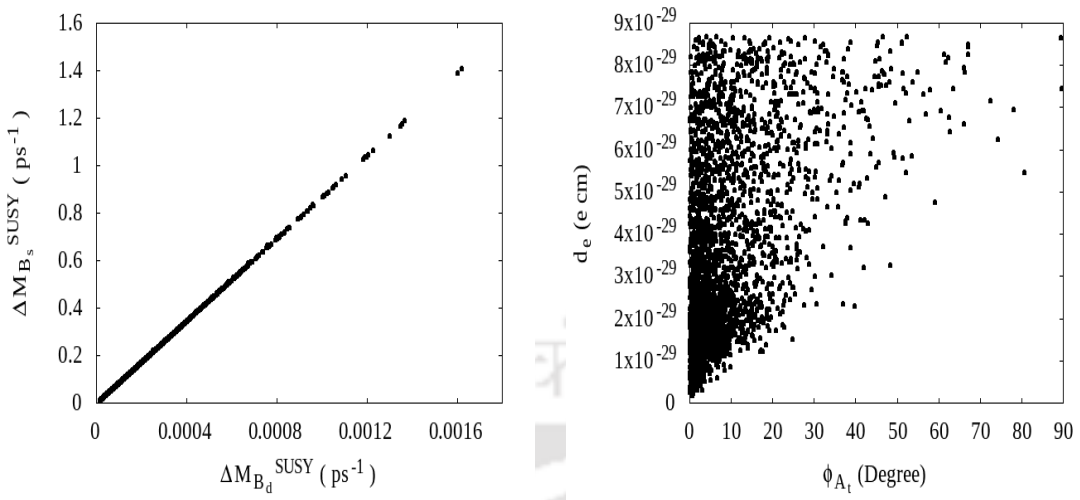

FIGURE 2.7: The left panel displays the correlation in the $\Delta M_{B_d}^{\rm SUSY}$ - $\Delta M_{B_s}^{\rm SUSY}$ plane, while the right panel shows the impact of the CPV phase ϕ_{A_t} on the electron EDM. The color code is same as in Fig. 2.3.

signal large phase values. We also find similar kind of behavior for all other EDMs against the relevant CPV phases.

2.5 Results for the LHC Higgs signals

Here we present the compatibility of the selected parameter space regions with the LHC measurements specific to the discovered Higgs boson. As Scan 1 is found to be incompatible with the EDM bounds, we focus our attention on Scan 2. The results presented in this section are, therefore, those from Scan 2, unless explicitly mentioned.

At the LHC, the Higgs boson is dominantly produced via gluon gluon fusion (GGF), which at the lowest order occurs at one-loop level, with the Higgs boson subsequently decaying into $\gamma\gamma$ or $ZZ^* \to 4\ell$ or $W^+W^- \to \ell\nu\ell\nu$[5]. Now, the leading contribution of Higgs boson decays into ZZ^* is via a tree-level process, whereas the Higgs decays into the di-photon final state via a one-loop process at leading order. This one-loop decay process potentially contains SUSY particles like stop, sbottom, stau, charginos and charged Higgs bosons in addition to the SM particles (top, bottom and charged gauge bosons). Conversely, in the GGF production

[5]We neglect here the consideration of the $\tau^+\tau^-$ and $b\bar{b}$ decay modes from GGF, as corresponding experimental errors are still very large.

mode only colored particles (top, bottom, stop and sbottom) contribute to the loop. Assuming the narrow width approximation (NWA)[6] and neglecting higher order QCD corrections at production level[7], we define the Higgs boson event ratios as follows:

$$R_{XX} \;=\; \frac{\Gamma(h_1 \to gg)^{\rm CPV-MSSM}}{\Gamma(h \to gg)^{\rm SM}} \times \frac{{\rm BR}(h_1 \to XX)^{\rm CPV-MSSM}}{{\rm BR}(h \to XX)^{\rm SM}}, \qquad (2.15)$$

where, $XX = \gamma\gamma$ or ZZ^* or W^+W^- and h_1 is the lightest Higgs boson in the CPV-MSSM, while in the SM case it is marked as h.

Turning our attention to the study of effects specifically due to the CPV phases, notice that CPV effects enter into Eq. 2.15 through higher order corrections in the definition of the physical h_1 mass as well as through lowest order terms via the $h_1\tilde{f}\tilde{f}^*$ couplings, where $\tilde{f}$ refers to any possible sfermion. In fact, as emphasized in refs. [145–151], the most significant CPV effects are induced by the latter, since the former is responsible for mass shifts between models which are within current experimental uncertainties in the determination of the resonant Higgs mass.

In order to appreciate such specific CPV effects in our analysis, we find it convenient to study the ratio of the bottom/top Yukawa coupling for the h_1 state of the CPV-MSSM relative to SM values for the h_1 boson, which can be written as ($q = b, t$):

$$\frac{y_q^{\rm CPV-MSSM}}{y_q^{\rm SM}} = R_{q-S} + i\gamma_5 R_{q-PS}. \qquad (2.16)$$

Here R_{q-S} and R_{q-PS} denote the scalar and pseudoscalar part of the Higgs Yukawa coupling, respectively. The full expressions for these terms can be found in the `CPsuperH` manual [217]. When $R_{\gamma\gamma}$ is plotted as a function of the b-quark couplings, R_{b-S} and R_{b-PS}, as shown in Fig. 2.8 (top left) and (top right), one finds that there are solutions to the LHC Higgs data with both positive and negative values of R_{b-S}, which is typical of the CPV-MSSM, unlike the case of the CPC-MSSM, which only allows for positive values. A similar behavior is obtained for the dependence on the t-quark couplings, as shown in Fig. 2.8 (bottom left) and (bottom right). Further, if one recalls that the coupling of the top quark to h_1 is

[6] Which is justified by the fact that in all the models (SM, CPC-MSSM and CPV-MSSM) considered here, the Higgs width is always several orders of magnitude smaller than the Higgs mass.

[7] Which would induce a different finite term inside the QCD k-factor in the SM with respect to the CPC-MSSM (and CPV-MSSM as well), though with differences generally too small to be of relevance here.

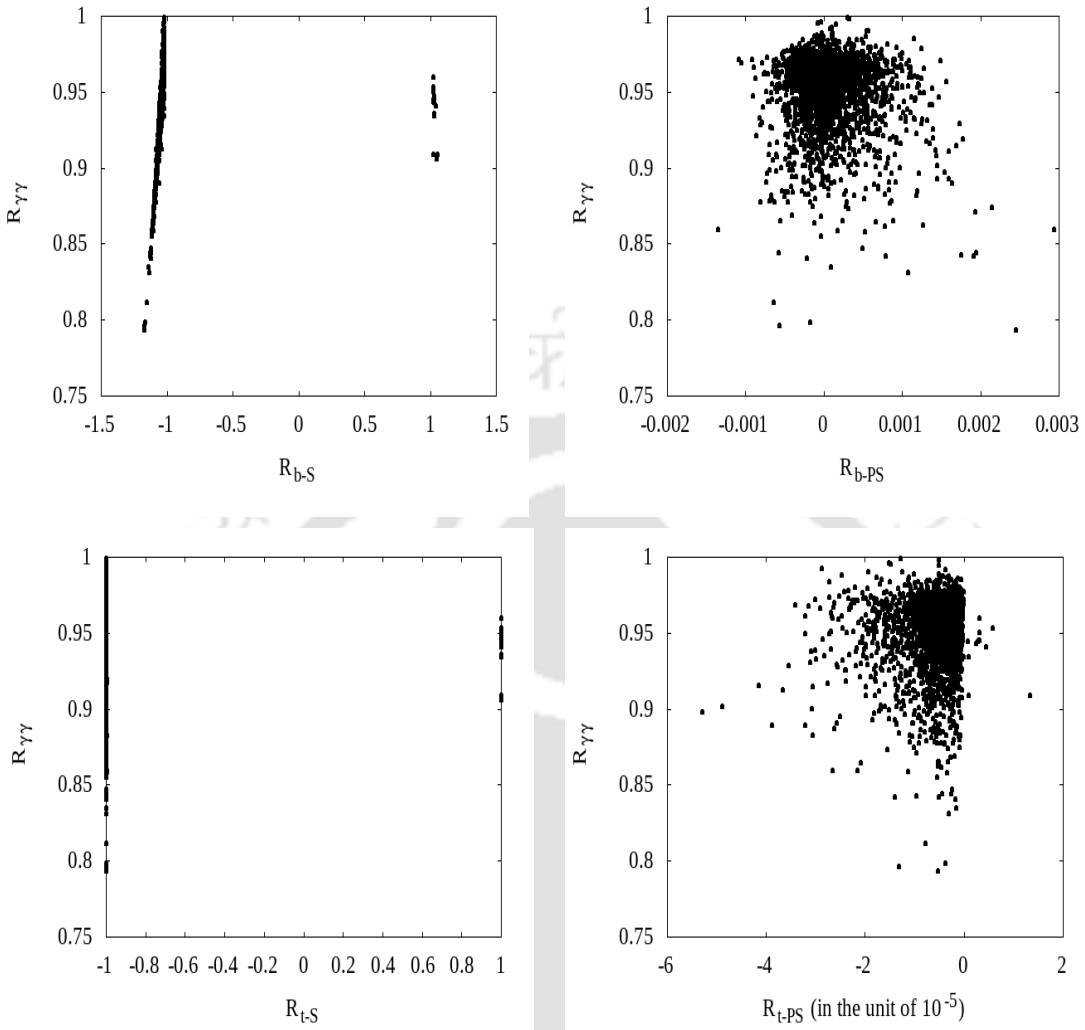

FIGURE 2.8: Variation of $R_{\gamma\gamma}$ with the scalar and pseudoscalar part of the ratio of the b-quark ((top left) & (top right)) and t-quark ((bottom left) & (bottom right)) Yukawa couplings defined in Eq. 2.16 in the CPV-MSSM. The black color code is same as in Fig. 2.3.

inversely proportional to sinβ (relative to the SM case) and that we have varied tanβ from 1 to 30 (which implies sin$\beta \sim 1$), it is not surprising to see that R_{t-S} remains around unity. Needless to say, by definition, R_{b-PS} and R_{t-PS} are zero in the CPC-MSSM, whereas both of them are non-zero in the CPV-MSSM, although their absolute values are much smaller than those for R_{b-S} and R_{t-S}, respectively.

We now proceed to study correlations among the different signal strength variables as mentioned above. According to the CMS collaboration (Run 2 data at 13 TeV and 35.9 fb^{-1}), the signal strengths or event ratios for the $\gamma\gamma$, ZZ^* and W^+W^- channels are $1.16^{+0.15}_{-0.14}$ [221], $1.05^{+0.19}_{-0.17}$ [222] and $1.28^{+0.18}_{-0.17}$ [223], respectively. We plot our results against the corresponding CMS results using 1σ (green patch) and 2σ (yellow patch) error bands around the experimental best-fit values (red dots).

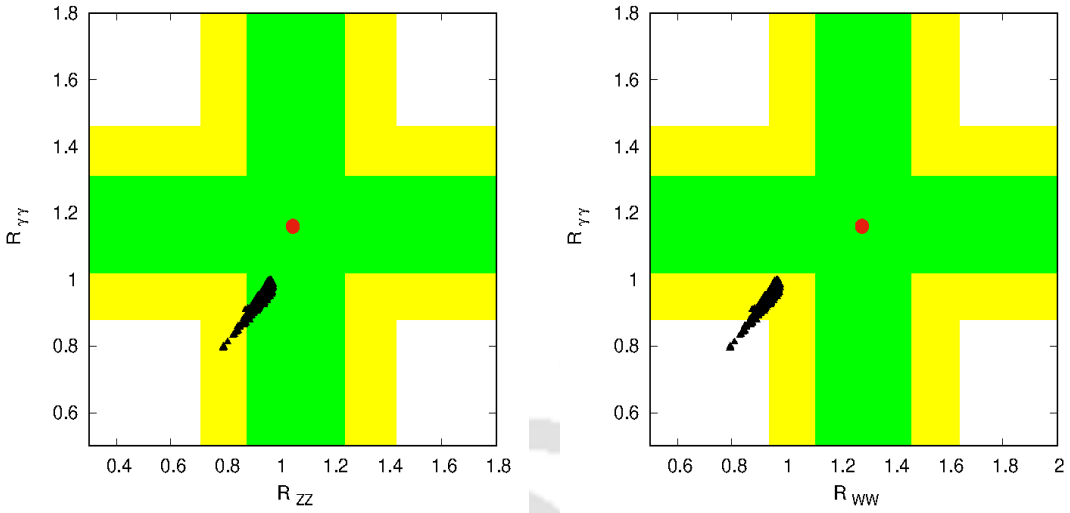

FIGURE 2.9: Correlation of $R_{\gamma\gamma}$ with (left) R_{ZZ} and (right) R_{WW}, when the Higgs boson is produced via GGF, in comparison to the latest CMS (Run 2) data along with the error bands (the yellow and green patches are the 2σ and 1σ uncertainty levels, respectively, around the experimental best-fit values, represented by the red dot marks). The black color scheme is same as in Fig. 2.3.

We first study the correlation of $R_{\gamma\gamma}$ with R_{ZZ} and R_{WW} when the Higgs is produced via GGF channel. It is evident from Fig. 2.9 that our results for $R_{\gamma\gamma}$ and R_{WW} are compatible with the Run 2 Higgs data as collected by the CMS collaboration within 2σ uncertainty band. Similarly, for R_{ZZ} our result is compatible within 1σ error band compared to the CMS result. The observation of the $h_1 \to b\bar{b}$ and $h_1 \to \tau^+\tau^-$ decays using GGF production mode are considered nearly impossible due to overshadow of QCD di-jet events. Hence, to discuss signal strength variables associated with the bottoms and taus, we assume the Higgs production via vector boson fusion (VBF), as both CMS and ATLAS observed some sensitivity in these channels [116, 117, 122, 123]. In this case, the definition of the corresponding event ratios will be modified to (here, $V = W/Z$):

$$R_{YY} = \frac{\Gamma(h_1 \to VV)^{\rm CPV-MSSM}}{\Gamma(h \to VV)^{\rm SM}} \frac{{\rm Br}(h_1 \to YY)^{\rm CPV-MSSM}}{{\rm Br}(h \to YY)^{\rm SM}}, \qquad (2.17)$$

where $YY = b\bar{b},\ \tau^+\tau^-$.

The CMS collaboration results (Run 2) on these decay channels are $R_{bb} = 1.06^{+0.31}_{-0.29}$ [224] and $R_{\tau\tau} = 1.09^{+0.27}_{-0.26}$ [225], respectively. In Fig. 2.10 we display the scatter plots in the (a) $R_{bb} - R_{\gamma\gamma}$ plane and (b) $R_{\tau\tau} - R_{\gamma\gamma}$ plane, with the CMS results. The color scheme is same as earlier. We note that the QCD and SUSY QCD corrections to M_b (Δ_b) play important roles in modifying the total decay width

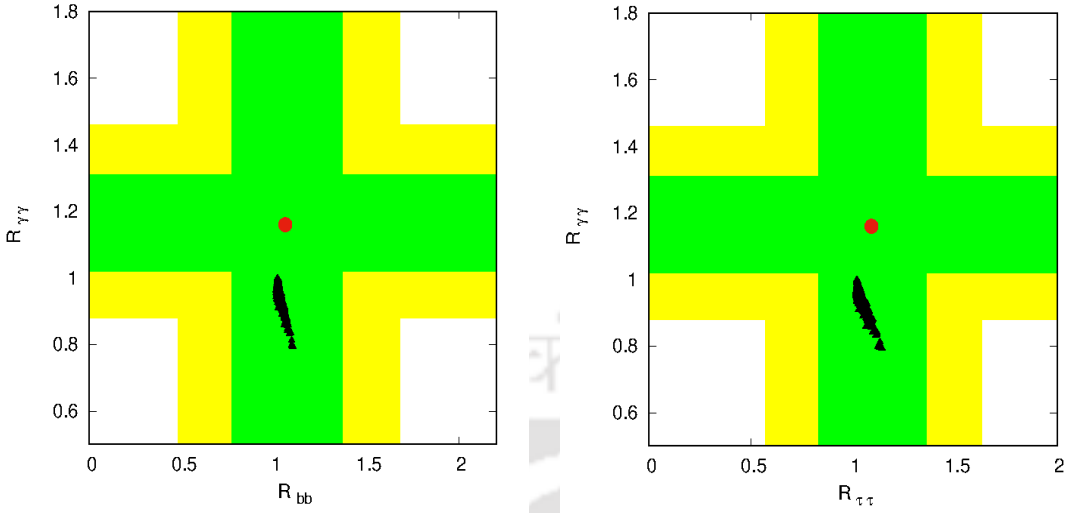

FIGURE 2.10: (left) R_{bb} vs $R_{\gamma\gamma}$ and (right) $R_{\tau\tau}$ vs $R_{\gamma\gamma}$ with the best-fit corresponding CMS values (Red dots). The yellow and green patches are the 2σ and 1σ uncertainty bands, respectively. The black color scheme is same as in Fig. 2.3.

as well as the relevant BRs of the Higgs boson [34, 226, 227]. This primarily changes the $h_1 \to b\bar{b}$ coupling values which are reduced for large Δ_b[8]. In general, a reduction (enhancement) of the $h_1 \to b\bar{b}$ coupling decreases (increases) the total decay width of the Higgs boson. This in turn enhances (reduces) the BRs to modes like $h_1 \to \gamma\gamma$ thereby increasing (decreasing) $R_{\gamma\gamma}$ [34]. This is evident in Fig. 2.10 (left) that shows an anti-correlation between the values of $R_{\gamma\gamma}$ and $R_{b\bar{b}}$. A similar kind of anti-correlation exists in Fig. 2.10 (right) where we show the variation in the $R_{\tau\tau} - R_{\gamma\gamma}$ plane. The red dot marks represent the experimental best-fit values (CMS Run 2) for R_{bb} and $R_{\tau\tau}$ [118], with 1σ and 2σ error levels (green and yellow patches, respectively).

The updated ATLAS results (Run 2 at 13 TeV and 36.1 fb^{-1}) for the signal strengths of the aforementioned channels are: $R_{\gamma\gamma} = 0.99^{+0.15}_{-0.14}$ [50], $R_{ZZ} = 1.28^{+0.21}_{-0.19}$ [228], $R_{WW} = 1.21^{+0.22}_{-0.21}$ [229], $R_{bb} = 0.90^{+0.28}_{-0.26}$ [230] and $R_{\tau\tau} = 1.09^{+0.36}_{-0.30}$ [231]. We present and compare our results with those from the ATLAS in Fig. 2.11 and Fig. 2.12. From the plots it is clear that our $R_{\gamma\gamma}$ is consistent within the 1σ region, R_{ZZ} and R_{WW} are within the 2σ band, whereas R_{bb} and $R_{\tau\tau}$ are within the 1σ error band, about the best-fit experimental values from the ATLAS.

Before we end this section, we would like to comment on the phenomenological implications of the presence of non-zero pseudoscalar Higgs Yukawa couplings.

[8]Notice that Δ_b is typically positive for this analysis with positive μ [227].

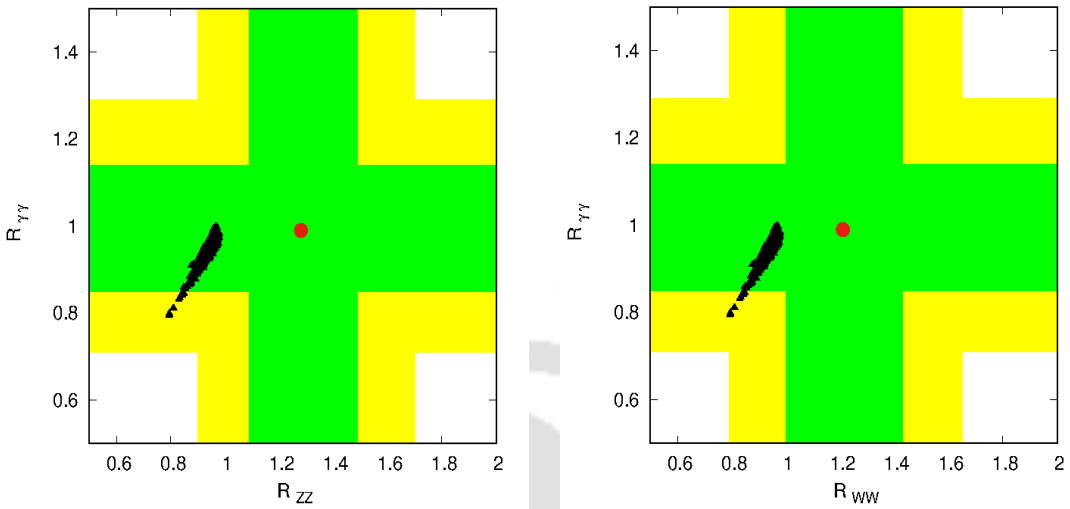

FIGURE 2.11: Results on $R_{\gamma\gamma}$, R_{ZZ} and R_{WW}, presented with the corresponding ATLAS results in (left) $R_{ZZ} - R_{\gamma\gamma}$ and (right) $R_{WW} - R_{\gamma\gamma}$ planes. The red dots are the best-fit experimental values. The green and yellow patches are 1σ and 2σ uncertainty levels, and the color scheme is same as before.

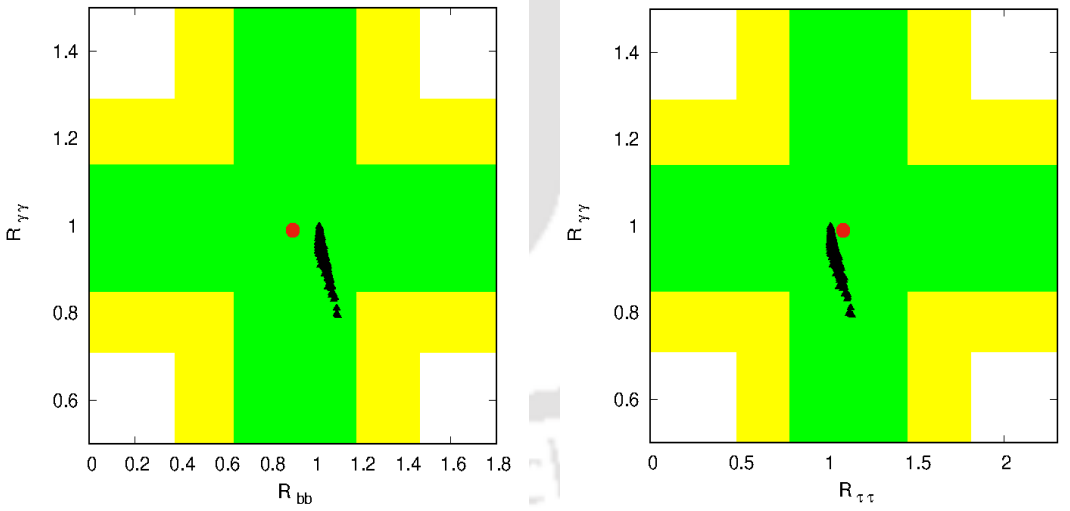

FIGURE 2.12: Results on R_{bb} and $R_{\tau\tau}$ presented with the corresponding ATLAS results in (left) $R_{bb} - R_{\gamma\gamma}$ and (right) $R_{\tau\tau} - R_{\gamma\gamma}$ plane. The green and yellow patches are 1σ and 2σ error bands and the red dots represent the best-fit ATLAS values for R_{bb}, $R_{\tau\tau}$ and $R_{\gamma\gamma}$.

Note that, the possibility of being a pure CP-odd state for the observed Higgs particle has now been mostly ruled out [232, 233], however the option of being a CP-mixed state is still an open issue [234–237]. A non-zero pseudoscalar Higgs Yukawa coupling would affect several production and decay modes of the observed Higgs boson. For example, the gluon fusion process crucially depends on the Higgs

couplings with the top and bottom quarks, while the decay of the Higgs to a pair of photons mostly involves the top quark coupling. A global analysis involving all the Higgs couplings and the available LHC results have been performed with and without the current EDM constraints [236–238]. According to ref. [236, 237], the current data cannot rule out the possibility of non-zero pseudoscalar Higgs couplings, in fact it gives equally good fits compared to the CPC case. However, when current EDM bounds are considered, the Higgs pseudoscalar couplings are restricted to approximately 10^{-2} [238]. Note that, from Fig. 2.8 (left) and (right), it is evident that our findings are in good agreement with the results obtained from a dedicated global fit. The measurement of the CP properties of the Higgs boson at the LHC mostly rely on its couplings to massive vector bosons. It has been shown in ref. [239] that the gluon fusion process could be sensitive enough at the 14 TeV run of the LHC to study the CP properties of the Higgs boson. In fact, the presence of non-trivial CPV Higgs couplings would have important implications in the electroweak (EW) baryogenesis [240].

2.6 Conclusions

The discovery of a Higgs-like resonance with a mass close to 125 GeV by both the multi-purpose experimental collaborations ATLAS and CMS operating at the LHC created a great interest in understanding the ultimate means adopted by nature for mass generation. The precise determination of its spin, CP properties and couplings to the SM fermions and gauge bosons are highly crucial to knowing the exact dynamics of EWSB. Although the measurements done so far indicate that this Higgs-like boson is compatible with the SM hypothesis, however due to significant uncertainties in some of the Higgs detection channels, one still has the possibility of testing this object as being a candidate of some BSM physics.

With this motivation in mind, we scan the CPV-MSSM parameter space in order to accommodate the 125 GeV Higgs boson with signal strengths (or event rates) consistent with the LHC data and all other available experimental bounds till date. It is well known that any new source of CP violation (above and beyond what is embedded in the SM) would lead to additional contributions to various EDMs. Therefore, while scanning the CPV-MSSM parameter space, we also enforce different EDM constraints, namely the electron, neutron, mercury and thallium EDMs. In addition, we vary the CPV phases of the gaugino mass

parameter M_3, and the trilinear couplings A_t, A_b, A_τ from 0^o to 90^o. Note that we set other CPV phases like ϕ_1 (phase of M_1), ϕ_2 (phase of M_2), phases of the first two generations of fermions to zero since these variables affect the Higgs sector negligibly. We further impose several low energy constraints, mainly coming from the different heavy flavor physics processes.

We perform two separate parameter space scans: (a) with the CPV phases setting to their maximal value (90^o) and (b) varying these phases from 0^o to 90^o. For both these two scans, other parameters vary randomly within some specified ranges. We see that maximal phase scenario (case (a)) is ruled out by the current EDM measurements, specially updated electron EDM measurement. However, we find significant amount of parameter space points, in case (b), satisfying all the constraints including EDMs. As expected, we see that relatively smaller values (c.f. Fig. 2.7 (right)) of these CPV phases are favored by the EDM constraints. We also calculate the signal strengths of the Higgs boson in the gluon gluon fusion processes like, $gg \to h_1 \to \gamma\gamma$, $gg \to h_1 \to ZZ^* \to 4\ell$, $gg \to h_1 \to W^+W^- \to \ell\nu\ell\nu$, and the vector boson fusion processes like, $qq \to h_1 \to b\bar{b}$ and $qq \to h_1 \to \tau^+\tau^-$ ($V \equiv W^\pm, Z$), and find that over a large expanse of parameter space of the CPV-MSSM, our results are compatible within $1\sigma/2\sigma$ uncertainty levels with the ATLAS and CMS Run 2 data.

We find some interesting results in terms of some of the observables of the CPV-MSSM. The couplings of the Higgs boson with the bottom quark and top quark are very important to claim the discovery of the observed particle as the SM Higgs boson. We find that the imaginary part of the top and bottom Yukawa couplings can take very small but non-zero values even after satisfying all the recent updates from both the CMS and ATLAS collaborations (in terms of the signal strength variable μ, or R in our case) within $1\sigma - 2\sigma$ uncertainty. Moreover, we also find an interesting result from the correlation plots of the different signal strength variables. We do not find any significant excess in the $\gamma\gamma$, ZZ^* and W^+W^- decay modes (in both Scan 1 and Scan 2), but we do see excess of events over the SM predictions for both the $b\bar{b}$ and $\tau^+\tau^-$ decay modes, when the Higgs boson is produced via vector boson fusion. The suppression in the di-photon decay mode with simultaneous enhancement in $b\bar{b}$ and $\tau^+\tau^-$ decay modes with respect to the SM prediction and presence of non-zero imaginary parts of the top and bottom Yukawa couplings, could be an interesting signature of this model. We briefly discuss the phenomenological implications of the presence of such non-zero

pseudoscalar Higgs couplings. In addition to that, we also find that it is possible to have a Higgs mass near 125 GeV with relatively small $\tan\beta$, large A_t and a light stop, which is consistent with the current supersymmetric searches at the LHC.

Altogether then, these findings point to the fact that the CPV-MSSM provides a viable solution to the updated LHC Higgs data, in fact offering very little in the way of distinction between the two SUSY models (CPC-MSSM and CPV-MSSM) at the LHC Run 2. Improvement in different Higgs coupling measurements is necessary in order to test the possibility of probing the mild dependence of these CPV phases in the Higgs sector of the minimal SUSY realization.

Chapter 3

NMSSM light Higgs sector

This chapter accounts our detailed analysis of quantum mechanical interference effects due to the presence of one or more additional Higgs states being almost degenerate in mass with the SM-like Higgs state, in both the real and complex NMSSM. Here we consider the production of a photon pair with an invariant mass near 125 GeV through gluon fusion. We also investigate how such mutually interfering states contributing to the 125 GeV signal observed at the LHC can potentially be distinguished from a single resonance.

3.1 Introduction

Although, SUSY is considered to be a good BSM candidate, its minimal manifestation, the MSSM, is getting increasingly constrained by the LHC measurements of the Higgs boson properties, besides becoming more and more fine-tuned in explaining null searches for its own direct signatures, i.e., sparticle states. The presence of an extra singlet scalar superfield in the NMSSM, not only solves the so-called $\mu-$problem in the MSSM, but also leads to two additional neutral Higgs mass eigenstates in the NMSSM, as discussed in chapter 1. With all the parameters in the Higgs and sfermion sectors assumed to be real and hence CP-conserving, and with five neutral Higgs bosons in total (three scalar and two pseudoscalar), the rNMSSM or the CPC-NMSSM provides some unique possibilities for collider phenomenology.

In multi-Higgs models like the MSSM and NMSSM, the observed boson near 125 GeV can in principle be explained in terms of a single Higgs resonance or, alternatively, two or more Higgs resonances that cannot be individually resolved by the experiment as yet. In the MSSM, the possibility of the two scalars both lying near 125 GeV is ruled out by the fact that such a mass for one of the scalars generally necessitates the other scalar to be essentially decoupled, and hence much heavier or lighter [63]. In the rNMSSM, in contrast, it is still a plausible scenario, as discussed in ref. [15–18, 241]. The alternate possibility of a pair of scalar and pseudoscalar near 125 GeV has also been studied in ref. [19].

In the NMSSM, in order to address the baryonic asymmetry of the universe, CP violation can be invoked directly and explicitly in the Higgs sector at the tree-level, unlike in the MSSM, where it is only radiatively induced into the Higgs sector beyond the Born approximation. This is done by taking the Higgs sector trilinear couplings to be complex parameters, hence we refer to this version of the model as the cNMSSM or the CPV-NMSSM here. For non-zero CPV phases of these parameters, instead of the distinct CP-even and CP-odd Higgs bosons, the model contains five CP-indefinite neutral states. This CP mixing in the Higgs sector can get additional contributions from the complex Higgs-sfermion-sfermion couplings as well as the phases in the the neutralino-chargino sector, as in the CPV-MSSM. Consequently, depending on the sizes of these phases, the mass spectrum and production/decay rates of the Higgs states can get considerably modified compared to the CPC case [29], similarly to the MSSM [10, 30, 31, 36, 145, 146, 151, 166, 167, 171, 242]. The phenomenology of a single CPV Higgs boson near 125 GeV in the cNMSSM has been studied for a variety of possible underlying scenarios in ref. [29, 243, 244]. The specific case of two mass-degenerate Higgs resonances near 125 GeV within the cNMSSM has also been considered in ref. [32], where it was shown that these can give a better fit to the LHC Run 1 data, performed using the program `HiggsSignals` [245], compared to a single resonance.

In all the above-mentioned analyses of two ~ 125 GeV Higgs bosons in the NMSSM, it was assumed that each of them is produced on-shell and decays subsequently into any of the observed final states. However, for very strong mass degeneracy, it is possible that the two Higgs states produced in gluon fusion oscillate into each other before they decay. This could be perceived as being facilitated through quantum corrections at the propagator level with two different mass eigenstates at the two ends. Such effects, coming into play beyond a Breit-Wigner (BW) resonance,

in general contexts as well as in specific scenarios like the CPC-MSSM, have been considered in some studies [37, 38, 246, 247]. The specific case of the CPV-MSSM with one-loop effects in the full propagator was treated in ref. [36, 149–151].

The purpose of the present work is to explore this possibility of quantum mechanical interference between two Higgs states near 125 GeV in both the real and complex NMSSM. We shall demonstrate here that the inclusion of such effects enhances the span of the model solutions to the LHC observation. We shall then investigate possible ways to identify signatures of such a coupled system of Higgs bosons through a shape study of the profile of the resonance in the invariant mass distribution of the di-photon decay products. The analysis is carried out by first performing numerical scans of the model parameter space to identify specific BPs where two of the Higgs bosons are nearly degenerate in mass around 125 GeV, within the uncertainty allowed by present LHC measurements. For these BPs, we then calculate the cross section for the production of a di-photon pair with invariant mass near 125 GeV via Higgs resonance(s) in the gluon fusion process at the LHC, using a Monte Carlo (MC) integration code developed in-house. This cross section is calculated assuming three different approaches: (i) for two individual Higgs bosons without any mutual interference at the propagator level; (ii) only the diagonal interference terms in the propagator matrix; (iii) the full Higgs propagator matrix in the amplitude. A comparison of these three cross sections shows significant effects of interference, with the full propagator case deviating by up to about 40% compared to the sum of the two individual Higgs boson contributions, along with a hint of a distortion in the line-shape of the differential distribution.

The chapter is organized as follows. In the next section we briefly revisit the Higgs sector of the NMSSM. In Sec. 3.3 we derive the analytical expression for the cross section that includes the full Higgs propagator matrix. In Sec. 3.4 we provide details of our methodology for the numerical analysis. In Sec. 3.5 we discuss our results and finally in Sec. 3.6 we draw our conclusions.

3.2 The NMSSM Higgs sector

The NMSSM is defined by the superpotential

$$W_{\rm NMSSM} = h_u\, \widehat{Q}\cdot\widehat{H}_u\, \widehat{U}^c_R + h_d\, \widehat{H}_d\cdot\widehat{Q}\, \widehat{D}^c_R + h_e\, \widehat{H}_d\cdot\widehat{L}\, \widehat{E}^c_R + \lambda\widehat{S}\widehat{H}_u\cdot\widehat{H}_d + \frac{\kappa}{3}\, \widehat{S}^3\,, \quad (3.1)$$

where h_u, h_d and h_e are the quark and lepton Yukawa coupling constants, $\widehat{Q}$ and $\widehat{L}$ are the left-handed quark and lepton doublet superfields, $\widehat{U}$, $\widehat{D}$ and $\widehat{E}$ are the right-handed up-type, down-type and electron-type singlet superfields, respectively, and the charge conjugation is denoted by the superscript c. Furthermore, $\widehat{H}_u$ and $\widehat{H}_d$ in the above superpotential are $\mathrm{SU(2)_L}$ Higgs doublet superfields with opposite hypercharge, $Y = \pm 1$, as in the MSSM, and $\widehat{S}$ is a Higgs singlet superfield. Here, λ and κ are dimensionless trilinear coupling constants. The fourth term on the right hand side of Eq. 3.1 replaces the higgsino mass term, $\mu \widehat{H}_u \widehat{H}_d$, present in the MSSM superpotential. The Higgs singlet superfield acquires a non-zero VEV, s, which is naturally of the order of the SUSY breaking scale M_{SUSY} (where $M^2_{\mathrm{SUSY}} = \frac{m^2_{\tilde{t}_1} + m^2_{\tilde{t}_2}}{2}$, $m_{\tilde{t}_1}$ and $m_{\tilde{t}_2}$ are the physical masses of the two stops), thus solving the μ-problem of the MSSM by generating an effective μ-term,

$$\mu_{\mathrm{eff}} \equiv \lambda \langle \widehat{S} \rangle = \lambda s \,. \tag{3.2}$$

The absence of a $\mu \widehat{H}_u \widehat{H}_d$ term, however, results in a $\mathrm{U(1)_{PQ}}$ symmetry, which is explicitly broken here by the last term in Eq. 3.1, thus introducing instead a discrete Z_3 symmetry and making the NMSSM superpotential scale-invariant as well.

The Higgs potential, derived from the above superpotential, is given as

$$\begin{aligned} V_H &= \left|\lambda \left(H_u^+ H_d^- - H_u^0 H_d^0\right) + \kappa S^2\right|^2 + \left(m^2_{H_u} + |\mu + \lambda S|^2\right) \left(|H_u^0|^2 + |H_u^+|^2\right) \\ &+ \left(m^2_{H_d} + |\mu + \lambda S|^2\right) \left(|H_d^0|^2 + |H_d^-|^2\right) + \frac{g^2}{4} \left(|H_u^0|^2 + |H_u^+|^2 - |H_d^0|^2 - |H_d^-|^2\right)^2 \\ &+ \frac{g_2^2}{2} |H_u^+ H_d^{0*} + H_u^0 H_d^{-*}|^2 + m_S^2 |S|^2 \\ &+ \left[\lambda A_\lambda \left(H_u^+ H_d^- - H_u^0 H_d^0\right) S + \frac{1}{3} \kappa A_\kappa S^3 + \mathrm{h.c.}\right], \end{aligned} \tag{3.3}$$

where g_1 and g_2 are the $\mathrm{U(1)_Y}$ and $\mathrm{SU(2)_L}$ gauge coupling constants, respectively, and $g^2 = \frac{g_1^2 + g_2^2}{2}$. Here, A_λ and A_κ are soft SUSY breaking Higgs trilinear couplings, while m_{H_d}, m_{H_u} and m_S denote the soft Higgs masses. The fields H_d, H_u and S are expanded about their respective VEVs, v_d, v_u and s, as

$$H_d^0 = \begin{pmatrix} \frac{1}{\sqrt{2}}(v_d + H_{dR} + i H_{dI}) \\ H_d^- \end{pmatrix}, \quad H_u^0 = e^{i\phi_u} \begin{pmatrix} H_u^+ \\ \frac{1}{\sqrt{2}}(v_u + H_{uR} + i H_{uI}) \end{pmatrix},$$
$$S^0 = \frac{e^{i\phi_s}}{\sqrt{2}}(s + S_R + i S_I). \tag{3.4}$$

For correct EWSB, V_H, rewritten in terms of these expanded fields, should have a minimum at non-vanishing v_d, v_u and s, implying

$$\left\langle \frac{\delta V_H}{\delta \theta} \right\rangle = 0 \quad \text{for} \quad \theta = H_{dR}, H_{uR}, S_R, H_{dI}, H_{uI}, S_I \,, \tag{3.5}$$

which leads to six *tadpole conditions* (refer App. B)

Taking the second derivative of V_H at the vacuum yields the tree-level 6×6 neutral Higgs mass matrix-squared, $\mathbf{M}_0^2$, in the basis $\mathrm{H}^T = (H_{dR}, H_{uR}, S_R, H_{dI}, H_{uI}, S_I)$. It can be expressed in the general form

$$\mathbf{M}_0^2 = \left(\begin{array}{c|c} \mathbf{M}_S^2 & \mathbf{M}_{SP}^2 \\ \hline (\mathbf{M}_{SP}^2)^T & \mathbf{M}_P^2 \end{array}\right) , \tag{3.6}$$

where the 3×3 block $\mathbf{M}_S^2$ corresponds to the CP-even interaction states (H_{dR}, H_{uR}, S_R), the 3×3 block $\mathbf{M}_P^2$ to the CP-odd states (H_{dI}, H_{uI}, S_I) while $\mathbf{M}_{SP}^2$ is responsible for mixing between the CP-even and CP-odd states. For the explicit expressions of the entries in $\mathbf{M}_0^2$ matrix given in Eq. 3.6, see App. B.

In the rNMSSM, where all the Higgs trilinear coupling parameters are real, $\mathbf{M}_{SP}^2$ is a null matrix. One can therefore simply rotate only the submatrix $\mathbf{M}_P^2$ to isolate the Nambu-Goldstone boson field, G, which can then be dropped to yield a 5×5 mass matrix $\mathbf{M}_0'^2$. This mass matrix receives higher order corrections, $\Delta\mathbf{M}^2$, from various sectors of the model, and thus gets modified as

$$\mathbf{M}_H^2 = \mathbf{M}_0'^2 + \Delta\mathbf{M}^2 \,. \tag{3.7}$$

The most dominant of these corrections can be found in ref. [7, 248]. Some further two-loop corrections have been calculated in ref. [249, 250]. After the inclusion of these corrections, the submatrices $\mathbf{M}_S^2$ and $\mathbf{M}_P^2$ are separately diagonalized to obtain the three CP-even mass eigenstates, $H_{1,2,3}$ (with $m_{H_1} < m_{H_2} < m_{H_3}$), and the two CP-odd physical Higgs bosons, $A_{1,2}$ (with $m_{A_1} < m_{A_2}$).

On the other hand, one can also invoke CP violation explicitly by assuming $\lambda \equiv |\lambda| e^{i\phi_\lambda}$, $\kappa \equiv |\kappa| e^{i\phi_\kappa}$, $A_\lambda \equiv |A_\lambda| e^{i\phi_{A_\lambda}}$ and $A_\kappa \equiv |A_\kappa| e^{i\phi_{A_\kappa}}$. This leads to non-zero entries in the $\mathbf{M}_{SP}^2$ submatrix, implying that the CP-even and CP-odd interaction eigenstates also mix. In the cNMSSM, the G state is first separated out through

a rotation of the entire $\mathbf{M}_0^2$ by $\mathcal{R}^G$,

$$(H_{dR}, H_{uR}, S_R, H_I, S_I, G)^T = \mathcal{R}^G \, (H_{dR}, H_{uR}, S_R, H_{dI}, H_{uI}, S_I)^T \ , \tag{3.8}$$

and dropped before calculating the higher order corrections to the resulting $\mathbf{M}_0'^2$. The complete expressions for the tree-level $\mathbf{M}_0'^2$ and the dominant one-loop contributions to $\Delta\mathbf{M}^2$ from the (s)quark and gauge sectors in the cNMSSM were studied in ref. [251–254] in the renormalization group equations-improved effective potential approach. The corrections from the gaugino sector were included in ref. [244] and, more inclusively, in ref. [255]. In the Feynman diagrammatic approach, the complete one-loop Higgs mass matrix was derived in ref. [243] and the $\mathcal{O}(\alpha_t\alpha_s)$ contributions to it were calculated recently in ref. [256].

The physical Higgs mass eigenstates of the cNMSSM are then obtained from the interaction states through another rotation by $\mathcal{R}^H$,

$$(H_1, H_2, H_3, H_4, H_5)^T = \mathcal{R}^H \, (H_{dR}, H_{uR}, S_R, H_I, S_I)^T \ , \tag{3.9}$$

resulting in the diagonalized square-mass matrix,

$$\text{diag}\left(m_{H_1}^2, m_{H_2}^2, m_{H_3}^2, m_{H_4}^2, m_{H_5}^2\right) = \mathcal{R}^H \left[\mathcal{R}^G \mathcal{M}_H^2 \big(\mathcal{R}^G\big)^T\right] \big(\mathcal{R}^H\big)^T \ . \tag{3.10}$$

Here H_1, H_2, H_3, H_4 and H_5 are the five neutral CP-indefinite Higgs bosons, ordered in terms of increasing mass.

Note here that only the physical phase combination $\phi_\lambda - \phi_\kappa + \phi_u - 2\phi_s$ appears in the cNMSSM Higgs sector at the tree-level, as the other possible phase combinations involving ϕ_{A_λ} and ϕ_{A_κ} are determined by it, up to a twofold ambiguity, through the tadpole conditions. Beyond this level, the CPV phases of the gaugino mass parameters, $M_{1,2,3}$, and of the soft trilinear couplings, $A_{\tilde{f}}$, of the Higgs boson to the sfermions also get radiatively induced into this sector.

3.3 Di-photon production via gluon fusion

We now turn our attention to the process under study, i.e., di-photon production from gluon fusion via Higgs states at the LHC. The squared-amplitude for the $gg \to H \to \gamma\gamma$ process, with H collectively denoting the five neutral CP-indefinite

Higgs bosons, can be written as [257]

$$\mid \mathcal{M} \mid^2 = \sum_{\lambda,\sigma=\pm} \mathcal{M}_{P\lambda}\mathcal{M}^*_{P\lambda} \mid D_H(\hat{s}) \mid^2 \mathcal{M}_{D\sigma}\mathcal{M}^*_{D\sigma}\,, \tag{3.11}$$

where $\lambda, \sigma = \pm 1$ are the gluon and photon helicities, respectively, and $D_H(\hat{s})$ is the Higgs boson propagator, with $\hat{s}$ being the squared CM energy of the incoming gluons. The amplitude for the production part is given as

$$\mathcal{M}_{P\lambda} = \sum_{i=1-5} \mathcal{M}_{P_i\lambda} = \sum_{i=1-5} \frac{\alpha_s m^2_{H_i}}{4\pi v}\Big\{S^g_i(m_{H_i}) + i\lambda P^g_i(m_{H_i})\Big\}\,, \tag{3.12}$$

where the scalar and pseudoscalar form factors are [258]

$$\begin{aligned} S^g_i(m_{H_i}) &= 2\sum_q g^S_{H_iqq}\tau_q\{1+(1-\tau_q)f(\tau_q)\} - \sum_{\tilde{q}} \frac{m^2_Z\tau_{\tilde{q}}}{m^2_{\tilde{q}}} g_{H_i\tilde{q}\tilde{q}}\{1-\tau_{\tilde{q}}f(\tau_{\tilde{q}})\}, \\ P^g_i(m_{H_i}) &= 2\sum_q g^P_{H_iqq}\tau_q f(\tau_q)\,, \end{aligned} \tag{3.13}$$

with $\tau_x = 4m^2_x/m^2_{H_i}$ $(x = q, \tilde{q})$ and the loop functions being

$$\begin{aligned} f(\tau) &= \arcsin^2(1/\sqrt{\tau}),\ \tau \geq 1, \\ f(\tau) &= -\frac{1}{4}\left\{\ln\left(\frac{1+\sqrt{1-\tau}}{1-\sqrt{1-\tau}}\right) - i\pi\right\}^2,\ \tau < 1. \end{aligned} \tag{3.14}$$

Note that $g^{S,P}_{H_iqq}$ and $g^S_{H_i\tilde{q}\tilde{q}}$ in Eq. 3.13 are the couplings of H_i to quarks q and squarks $\tilde{q}$, respectively, which depend on the elements of the Higgs mixing matrix, $\mathcal{R}^H$, noted in Eq. 3.10 above. The exact forms of these couplings can be found in ref. [254].

The amplitude for the decay part is given as

$$\mathcal{M}_{D\sigma} = \sum_{i=1-5} \mathcal{M}_{D_i\sigma} = \sum_{i=1-5} \frac{\alpha_{em} m^2_{H_i}}{4\pi v}\Big\{S^\gamma_i(m_{H_i}) + i\sigma P^\gamma_i(m_{H)i})\Big\}\,, \tag{3.15}$$

with the form factors being

$$
\begin{aligned}
S_i^{\gamma}(m_{H_i}) &= 2\sum_f N_{cf} e_q^2 g^S_{H_i qq} \tau_q \{1 + (1-\tau_q) f(\tau_q)\} - \sum_{\tilde{f}} N_{cf} e_{\tilde{q}}^2 \frac{M_Z^2}{M_{\tilde{q}}^2} g_{H_i \tilde{q}\tilde{q}} \tau_{\tilde{q}} \{1 - \tau_{\tilde{q}} f(\tau_{\tilde{q}})\} \\
&- g_{H_i WW} \{2 + 3\tau_W + 3\tau_W (2-\tau_W) f(\tau_W)\} \\
&- \frac{M_Z^2}{2M_{H^\pm}^2} g_{H_i H^+ H^-} \tau_{H^\pm} \{1 - \tau_{H^\pm} f(\tau_{H^\pm})\} \\
&+ 2 \sum_{\tilde{\chi}^\pm_{j=1,2}} \frac{M_W}{M_{\tilde{\chi}_j^\pm}} g^S_{H_i \tilde{\chi}_j^+ \tilde{\chi}_j^-} \tau_{\tilde{\chi}_j^\pm} \{1 + (1 - \tau_{\tilde{\chi}_j^\pm}) f(\tau_{\tilde{\chi}_j^\pm})\}\,, \\
P_i^{\gamma}(m_{H_i}) &= 2\sum_f N_{cf} e_q^2 g^P_{H_i qq} \tau_q f(\tau_q) + 2 \sum_{\tilde{\chi}^\pm_{j=1,2}} \frac{M_W}{M_{\tilde{\chi}_j^\pm}} g^P_{H_i \tilde{\chi}_j^+ \tilde{\chi}_j^-} \tau_{\tilde{\chi}_j^\pm} f(\tau_{\tilde{\chi}_j^\pm})\,,
\end{aligned}
\tag{3.16}
$$

where $N_{cf} = 3, 1$ is the color factor for (s)quarks and charged (s)leptons, respectively, with e_f being the corresponding electric charge. $g_{H_i WW}$, $g_{H_i H^+ H^-}$ and $g_{H_i \tilde{\chi}_j^+ \tilde{\chi}_j^-}$ are the Higgs to W boson coupling, Higgs self coupling and Higgs to chargino coupling, respectively. Finally, the full propagator in Eq. 3.11 is a 5×5 matrix[1], given as

$$
D_H(\hat{s}) = \hat{s} \begin{pmatrix}
\mathrm{m}_{11} & i\mathfrak{Im}\hat{\Pi}_{12}(\hat{s}) & i\mathfrak{Im}\hat{\Pi}_{13}(\hat{s}) & i\mathfrak{Im}\hat{\Pi}_{14}(\hat{s}) & i\mathfrak{Im}\hat{\Pi}_{15}(\hat{s}) \\
i\mathfrak{Im}\hat{\Pi}_{21}(\hat{s}) & \mathrm{m}_{22} & i\mathfrak{Im}\hat{\Pi}_{23}(\hat{s}) & i\mathfrak{Im}\hat{\Pi}_{24}(\hat{s}) & i\mathfrak{Im}\hat{\Pi}_{25}(\hat{s}) \\
i\mathfrak{Im}\hat{\Pi}_{31}(\hat{s}) & i\mathfrak{Im}\hat{\Pi}_{32}(\hat{s}) & \mathrm{m}_{33} & i\mathfrak{Im}\hat{\Pi}_{34}(\hat{s}) & i\mathfrak{Im}\hat{\Pi}_{35}(\hat{s}) \\
i\mathfrak{Im}\hat{\Pi}_{41}(\hat{s}) & i\mathfrak{Im}\hat{\Pi}_{42}(\hat{s}) & i\mathfrak{Im}\hat{\Pi}_{43}(\hat{s}) & \mathrm{m}_{44} & i\mathfrak{Im}\hat{\Pi}_{45}(\hat{s}) \\
i\mathfrak{Im}\hat{\Pi}_{51}(\hat{s}) & i\mathfrak{Im}\hat{\Pi}_{52}(\hat{s}) & i\mathfrak{Im}\hat{\Pi}_{53}(\hat{s}) & i\mathfrak{Im}\hat{\Pi}_{54}(\hat{s}) & \mathrm{m}_{55}
\end{pmatrix}^{-1},
\tag{3.17}
$$

where $\mathrm{m}_{ii} \equiv \hat{s} - m_{H_i}^2 + i\mathfrak{Im}\hat{\Pi}_{ii}(\hat{s})$, with $\mathfrak{Im}\hat{\Pi}_{ij}(\hat{s})$ being the absorptive parts of the Higgs self-energies, for $i,\ j = 1-5$. The diagonal absorptive parts are equivalent to the widths of the corresponding Higgs states. The explicit expressions for $\mathfrak{Im}\hat{\Pi}_{ij}(\hat{s})$ are given in App. C. Note that in our numerical analysis we shall only focus on H_1 and H_2 having masses very close to 125 GeV. This implies that essentially the propagator matrix elements with $i,\ j = 1,\ 2$ are the only ones that contribute to the production of the di-photon pair with invariant mass near 125 GeV, assuming that the remaining three Higgs bosons are relatively heavy. Moreover, in the case of the rNMSSM, since the CP-even-odd mixing terms in the Higgs mass matrix vanish, it is sufficient for our purpose to consider only the 3×3 propagator matrix corresponding to the CP-even states instead of the complete one above.

[1] Assuming negligible off-resonance self-energy transitions of any of the five Higgs bosons to the Goldstone boson, G.

When the splitting between the Higgs boson masses is much larger than the sizes of the absorptive parts in Eq. 4.8, NWA can be applied to the i-th Higgs boson propagator as

$$|D_{ii}(\hat{s})|^2 = \left|\frac{1}{\hat{s} - m_{H_i}^2 + i m_{H_i}\Gamma_{H_i}}\right|^2 \to \frac{\pi}{m_{H_i}\Gamma_{H_i}}\delta(\hat{s} - m_{H_i}^2)\,, \tag{3.18}$$

so that the partonic cross section becomes

$$\hat{\sigma}(gg \to H \to \gamma\gamma) = \frac{1}{1024\pi\hat{s}} \sum_{i=1-5} \left(\sum_{\lambda=\pm} |\mathcal{M}_{P_i\lambda}|^2 \times \frac{\pi}{m_{H_i}\Gamma_{H_i}}\delta(\hat{s} - m_{H_i}^2) \times \sum_{\sigma=\pm} |\mathcal{M}_{D_i\sigma}|^2 \right). \tag{3.19}$$

The total cross-section for the process $pp \to H \to \gamma\gamma$ is then written as

$$\begin{aligned} \sigma_{pp}^{\gamma\gamma} &= \int_0^1 dx_2 \int_0^1 dx_1 \;\; \hat{\sigma}(gg \to H \to \gamma\gamma) \;\; g(x_1)g(x_2) \\ &= \int_0^1 dx_2 \int_0^1 dx_1 \frac{g(x_1)g(x_2)}{1024\pi\hat{s}} \sum_{i=1-5} \left(\sum_{\lambda=\pm} |\mathcal{M}_{P_i\lambda}|^2 \frac{\pi}{m_{H_i}\Gamma_{H_i}}\delta(\hat{s} - m_{H_i}^2) \sum_{\sigma=\pm} |\mathcal{M}_{D_i\sigma}|^2 \right), \end{aligned} \tag{3.20}$$

where $g(x_1)$ and $g(x_2)$ are the Parton Distribution Functions (PDFs) of the two gluons. By substituting x_2 in the above equation as

$$\hat{s} = x_1 x_2 s \implies x_1 x_2 = \frac{\hat{s}}{s} \equiv \tau \implies x_2 = \frac{\tau}{x_1} \implies dx_2 = \frac{d\tau}{x_1}\,, \tag{3.21}$$

where s is the total CM energy of the pp system, and performing the integration over $d\tau$, one gets

$$\sigma_{pp}^{\gamma\gamma} = \int_{\frac{m_{H_i}^2}{s}}^1 dx_1 \, \frac{1}{1024 s m_{H_i}^3 \Gamma_{H_i}} \sum_{i=1-5} \left(\sum_{\lambda=\pm} |\mathcal{M}_{P_i\lambda}|^2 \sum_{\sigma=\pm} |\mathcal{M}_{D_i\sigma}|^2 \right) \frac{g(x_1) g\left(\frac{m_{H_i}^2}{s\, x_1}\right)}{x_1}\,. \tag{3.22}$$

In contrast, when two (or more) Higgs bosons of the model are almost degenerate in mass near a given $\hat{s}$, the sizes of the corresponding absorptive parts can become comparable to their mass difference. As a result, the i-th Higgs state can undergo resonant transition to the j-th state through quantum corrections, as shown in Fig. 3.1. In such a scenario, the NWA is no longer valid, and the total cross

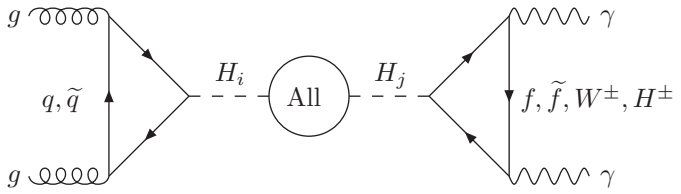

FIGURE 3.1: Illustration of the effect of mixing in the propagator induced by quantum corrections.

section is given as

$$\sigma_{pp}^{\gamma\gamma} = \int_0^1 d\tau \int_\tau^1 \frac{dx_1}{x_1} \frac{g(x_1)g(\tau/x_1)}{1024\pi\hat{s}^3} \sum_{i,j=1-5} \left\{ \sum_{\lambda=\pm} |\mathcal{M}_{P_i\lambda}|^2 |D_{ij}(\hat{s})|^2 \sum_{\sigma=\pm} \left|\mathcal{M}_{D_j\sigma}\right|^2 \right\}, \tag{3.23}$$

where $|D_{ij}(\hat{s})|^2$ is given by Eq. 3.17. From the above equation, one obtains the differential cross section (recall that $\tau = \frac{\hat{s}}{s}$) as

$$\frac{d\sigma_{pp}^{\gamma\gamma}}{d\sqrt{\hat{s}}} = \int_\tau^1 \frac{2\sqrt{\hat{s}}}{s} \frac{dx_1}{x_1} \frac{g(x_1)g(\hat{s}/sx_1)}{1024\pi\hat{s}^3} \sum_{i,j=1-5} \left\{ \sum_{\lambda=\pm} |\mathcal{M}_{P_i\lambda}|^2 |D_{ij}(\hat{s})|^2 \sum_{\sigma=\pm} \left|\mathcal{M}_{D_j\sigma}\right|^2 \right\}. \tag{3.24}$$

3.4 Numerical analysis

We first performed numerical scanning of the NMSSM parameter space, requiring H_1 and H_2 to lie within the 123 GeV − 127 GeV range[2]. Our first scan was performed in the framework of the rNMSSM, wherein sufficient mass degeneracy near 125 GeV between the two lightest scalars can generally be obtained for large values of the couplings λ and κ and a relatively small $\tan\beta$, which results in maximal mixing between the doublet- and singlet-like states, as noted in some earlier studies [15, 16, 241]. In the rNMSSM, while it is also possible for A_1 to lie near 125 GeV [19], it does not mix with the SM-like H_1 when the coupling parameters are all real. Therefore, the corresponding off-diagonal absorptive parts in the propagator matrix given in Eq. 3.17 are zero. When complex phases are turned on, all the Higgs states become CP-indefinite, and any of the off-diagonal terms in

[2]The extended range of Higgs boson masses around the actual measured experimental value of ∼ 125 GeV is to allow for up to ±2 GeV uncertainty from unknown higher order corrections in their model prediction.

Parameter	Scanned range
M_0 (GeV)	800 – 2000
$M_{1/2}$ (GeV)	100 – 500
A_0 (GeV)	−3000 – 0
$\tan\beta$	2 – 8
λ	0.58 – 0.7
κ	0.3 – 0.6
μ_{eff} (GeV)	100 – 200
A_λ (GeV)	200 – 1000
A_κ (GeV)	−300 – 0

TABLE 3.1: NMSSM parameters and their scanned ranges.

the full 5×5 propagator matrix can be non-zero and contribute to the interference effects. Therefore, either one of the scalar singlet-like and pseudoscalar singlet-like states can have strong mass-degeneracy with the 125 GeV SM-like state and interfere with it.

As stated earlier, at tree-level, only the phase combination $\phi_\lambda - \phi_\kappa + \phi_u - 2\phi_s$ appears in the Higgs sector of the cNMSSM. Furthermore, several studies [243, 253, 254] have shown that, out of all the individual phases, including those appearing beyond the Born approximation, the phase ϕ_κ is virtually unconstrained by the measurements of the fermionic EDMs. Therefore, after setting all the other phases to 0°, we further performed two separate cNMSSM parameter space scans, with the value of ϕ_κ fixed to 3° in one and to 10° in the other. In Tab. 3.1 we list the scanned ranges of the free parameters of the model, which assume the following universality conditions

$$M_0 \equiv M_{Q_{1,2,3}} = M_{U_{1,2,3}} = M_{D_{1,2,3}} = M_{L_{1,2,3}} = M_{E_{1,2,3}}\,,$$
$$M_{1/2} \equiv 2M_1 = M_2 = \frac{1}{3}M_3\,, \quad A_0 \equiv A_{\tilde{t}} = A_{\tilde{b}} = A_{\tilde{\tau}}\,,$$

where $M_{Q_{1,2,3}}$, $M_{U_{1,2,3}}$, $M_{D_{1,2,3}}$, $M_{L_{1,2,3}}$ and $M_{E_{1,2,3}}$ are the soft sfermion masses, $M_{1,2,3}$ those of the gauginos and $A_{\tilde{t},\tilde{b},\tilde{\tau}}$ are the soft trilinear couplings. These ranges are consistent across the three scans (one in the rNMSSM and two in the cNMSSM with ϕ_κ fixed at 3° and 10°) and correspond to the parameter space region that was noted to yield maximally mass-degenerate H_1 and H_2 in a previous study [32]. Note that for larger values of ϕ_κ it gets increasingly difficult to obtain both H_1 and H_2 near 125 GeV in the cNMSSM.

For each input point generated by the scanning algorithm, the masses as well as

BRs of the Higgs bosons were calculated with the public code `NMSSMCALC-v2.00` [258]. The Supersymmetric Les Houches Accord [259, 260] output file produced by `NMSSMCALC` for a scanned point was then passed to `HiggsBounds-v4.3.1` [261–264] to check for the consistency of each Higgs boson with the direct Higgs search results from LEP, Tevatron and LHC. We further made sure that a point only got through the scan if it satisfied the limits from measurements of the EDMs, computed intrinsically by `NMSSMCALC`. Finally, the CMS and ATLAS collaborations have performed measurements of the total width of the observed Higgs boson $h_{\rm obs}$, by analyzing its off-shell production and subsequent decays in the ZZ^* and W^+W^- channels [265–267]. The most recent observed 95% CL upper limit for the two channels combined is 13 MeV. Therefore, we also require each of the H_1 and H_2 in a given scan to satisfy this constraint, unless stated otherwise. Considering the fact that this limit is obtained with the assumption of a single Higgs boson produced on-shell, we may relax this criterion in our analysis, which goes beyond the NWA or BW resonance [268, 269].

Next, from the points collected in each scan, we selected BPs satisfying certain specific criteria, which will be explained later. In order to perform the numerical calculation of the cross sections for these BPs, we implemented the expressions given in Eqs. 3.23 and Eq. 3.24 in a locally developed `fortran` program. This code is linked to the `LAPACK` package [270] for propagator matrix inversion, as well as to a locally modified version of the `VEGAS` routine [271] to perform the 2-dimensional numerical integration. As a test of reliability of our results for a given model point, we calculated the leading order (LO) cross section in the NWA for each of the five Higgs bosons with our code, and compared it to the gluon fusion production cross section obtained from publicly available `SusHi-v1.6.0` [272–274], multiplied by its di-photon BRs obtained from `NMSSMCALC` in the rNMSSM case. This exercise is summarized in Tab. 3.2, which shows that the two results agreed within 5% or better. Note that the various Higgs boson couplings for a given parameter space point, needed for the calculation of the absorptive parts of the propagator matrix as well as of the production and decay form factors with our code, were calculated with a customized version of `NMSSMCALC`, since `NMSSMCALC` does not provide the Higgs couplings as its default output.

Note that our program calculates the total cross section only at LO, since implementation of higher order (HO) corrections is a highly involved task going beyond the scope of this work, which is aimed at comparing the effects of including the full

BP	Higgs	Mass	$\sigma(pp \to H_i)$ (SusHi)	BR($H_i \to \gamma\gamma$) (NMSSMCALC)	$\sigma\times$BR	$\sigma_{\rm NWA}(pp \to H_i \to \gamma\gamma)$ (Our code)
1	A_1	124.75	0.095	1.11×10^{-5}	1.06×10^{-6}	1.06×10^{-6}
	H_1	125.24	10.997	2.29×10^{-5}	2.52×10^{-4}	2.48×10^{-4}
	H_2	142.67	1.395	1.12×10^{-4}	1.56×10^{-4}	1.57×10^{-4}
	A_2	221.50	4.861	6.02×10^{-6}	2.92×10^{-5}	2.93×10^{-5}
	H_3	232.38	2.782	2.31×10^{-6}	6.42×10^{-6}	6.28×10^{-6}
2	A_1	126.73	0.0001	6.59×10^{-1}	7.25×10^{-5}	7.21×10^{-5}
	H_1	126.76	12.69	2.34×10^{-3}	2.97×10^{-2}	2.96×10^{-2}
	H_2	258.62	0.228	9.28×10^{-6}	2.12×10^{-6}	2.07×10^{-6}
	A_2	443.28	1.427	1.72×10^{-5}	2.46×10^{-5}	2.43×10^{-5}
	H_3	455.68	0.526	1.68×10^{-5}	8.81×10^{-6}	8.75×10^{-6}
3	A_1	126.65	0.261	4.70×10^{-5}	1.23×10^{-5}	1.24×10^{-5}
	H_1	126.69	13.18	1.30×10^{-3}	1.71×10^{-2}	1.70×10^{-2}
	H_2	306.80	0.478	2.83×10^{-7}	1.35×10^{-7}	1.32×10^{-7}
	A_2	365.59	4.270	2.05×10^{-5}	8.75×10^{-5}	8.68×10^{-5}
	H_3	389.65	0.696	1.38×10^{-5}	9.59×10^{-6}	9.43×10^{-6}

TABLE 3.2: The LO cross sections for three sample points at 14 TeV, selected from our rNMSSM parameter space scan, calculated with public tools (SusHi and NMSSMCALC), and our code assuming the NWA. Masses are in GeV and cross sections are in pb. The quantity in the 6-th column is the LO Higgs production cross section given by SusHi, times the Higgs to di-photon BRs given by NMSSMCALC

propagator against the simplest approach of two separate BWs on the total cross section. In fact, since these HO corrections apply only to the production process, they should have exactly the same impact in both approaches, hence including their effect is simply tantamount to rescaling the cross section by a k-factor (defined as $k_{\rm HO} \equiv \sigma_{\rm HO}/\sigma_{\rm LO}$, with HO implying the perturbative order at which the cross section is to be evaluated), which can be obtained from a dedicated public tool. For a few test points corresponding to the rNMSSM, using SusHi, we thus also estimated the next-to-next-to-LO (NNLO) factor, $k_{\rm NNLO}$, by calculating the gluon fusion cross section at both LO and NNLO in QCD. We found this $k_{\rm NNLO}$ to always lie very close to 3 for both H_1 and H_2. However, since SusHi is not yet compatible with the cNMSSM, the k-factor cannot be estimated exactly for the points corresponding to the cNMSSM. Therefore, for an approximate evaluation of the NNLO cross section in our discussion below, we multiply the LO cross section obtained with our code for a given point, both in the real and the complex NMSSM, with a constant $k_{\rm NNLO} = 3$. In fact, for an almost decoupled SUSY sector, as is generally the case here, the k-factor is indeed a constant for a SM-like 125 GeV Higgs boson, which can be obtained from, e.g., [275].

Finally, we use the CT10 [276] PDF set for gluons in our cross section calculation, with renormalization/factorization scale set to the $h_{\rm obs}$ mass, i.e., 125 GeV. We have, however, verified that the gross features of our analysis are independent of the choice of PDF set for a fixed set of model input parameters. In Tab. 3.3, we compare the values of $\sigma_{\rm NWA}(pp \to H_i \to \gamma\gamma)$, calculated with our code using the CT10 and CT10W PDF sets for the three sample points presented in Tab. 3.2.

BP	Higgs	Mass	$\sigma_{\rm NWA}(pp \to H_i \to \gamma\gamma)$ (CT10)	$\sigma_{\rm NWA}(pp \to H_i \to \gamma\gamma)$ (CT10W)
1	A_1	124.75	1.06×10^{-6}	1.07×10^{-6}
	H_1	125.24	2.48×10^{-4}	2.54×10^{-4}
	H_2	142.67	1.57×10^{-4}	1.59×10^{-4}
	A_2	221.50	2.93×10^{-5}	2.96×10^{-5}
	H_3	232.38	6.28×10^{-6}	6.35×10^{-6}
2	A_1	126.73	7.21×10^{-5}	7.24×10^{-5}
	H_1	126.76	2.96×10^{-2}	2.99×10^{-2}
	H_2	258.62	2.07×10^{-6}	2.09×10^{-6}
	A_2	443.28	2.43×10^{-5}	2.46×10^{-5}
	H_3	455.68	8.75×10^{-6}	8.79×10^{-6}
3	A_1	126.65	1.24×10^{-5}	1.27×10^{-5}
	H_1	126.69	1.70×10^{-2}	1.74×10^{-2}
	H_2	306.80	1.32×10^{-7}	1.39×10^{-7}
	A_2	365.59	8.68×10^{-5}	8.81×10^{-5}
	H_3	389.65	9.43×10^{-6}	9.45×10^{-6}

TABLE 3.3: Comparison between the LO cross sections calculated with our code for three sample points, given in Tab. 3.2, using CT10 and CT10W PDF sets.

3.5 Results and discussion

In Fig. 3.2 we show those points obtained from our three scans (one for the rNMSSM and two for the cNMSSM with ϕ_κ fixed at 3° and 10°) for which $\Delta m \equiv m_{H_2} - m_{H_1}$ is smaller than one (or both) of the widths, Γ_{H_1} and Γ_{H_2}, of the two lightest Higgs bosons. The top panel corresponds to the rNMSSM while the bottom panels to the cNMSSM with $\phi_\kappa = 3°$ (left) and $\phi_\kappa = 10°$ (right). We note in the figure that, given the parameter space in Tab. 3.1, for the vast majority of points, Γ_{H_1} and Γ_{H_2} tend to lie within 3–4 MeV of each other in the rNMSSM. For $\phi_\kappa = 3°$, the size of splitting between Γ_{H_1} and Γ_{H_2} can range from very small to fairly large across the points collected. However, for $\phi_\kappa = 10°$, no

points appear along the diagonal for $\Gamma_{H_1/H_2} > 6\,\text{MeV}$ in the bottom right frame, as the splitting between these two widths starts growing beyond this value.

From each of these scans we selected a few BPs to study the cross section for the production of a di-photon pair with an invariant mass, $\mathcal{M}_{\gamma\gamma}$, near 125 GeV via resonant Higgs boson(s) in gluon fusion at the LHC with $\sqrt{s} = 14\,\text{TeV}$. More specifically, we studied the distributions, with respect to the partonic CM energy $\sqrt{\hat{s}}$ (which is the same as $\mathcal{M}_{\gamma\gamma}$ at LO), of the differential cross section, calculated such that:

• Case 1: the m_{11} and m_{22} terms in the propagator matrix (Eq. 3.17), each contribute alternatively to two amplitudes, which are squared and then summed, implying two independent Higgs states.

• Case 2: both m_{11} and m_{22} contribute to the amplitude which is then squared, thus allowing for interference between H_1 and H_2 but without any mixing effects.

• Case 3: besides m_{11} and m_{22}, the off-diagonal terms $i\Im\text{m}\hat{\Pi}_{12}$ and $i\Im\text{m}\hat{\Pi}_{21}$ also contribute to the amplitude before squaring, leading to additional interference effects arising from the mixing of the two Higgs states.

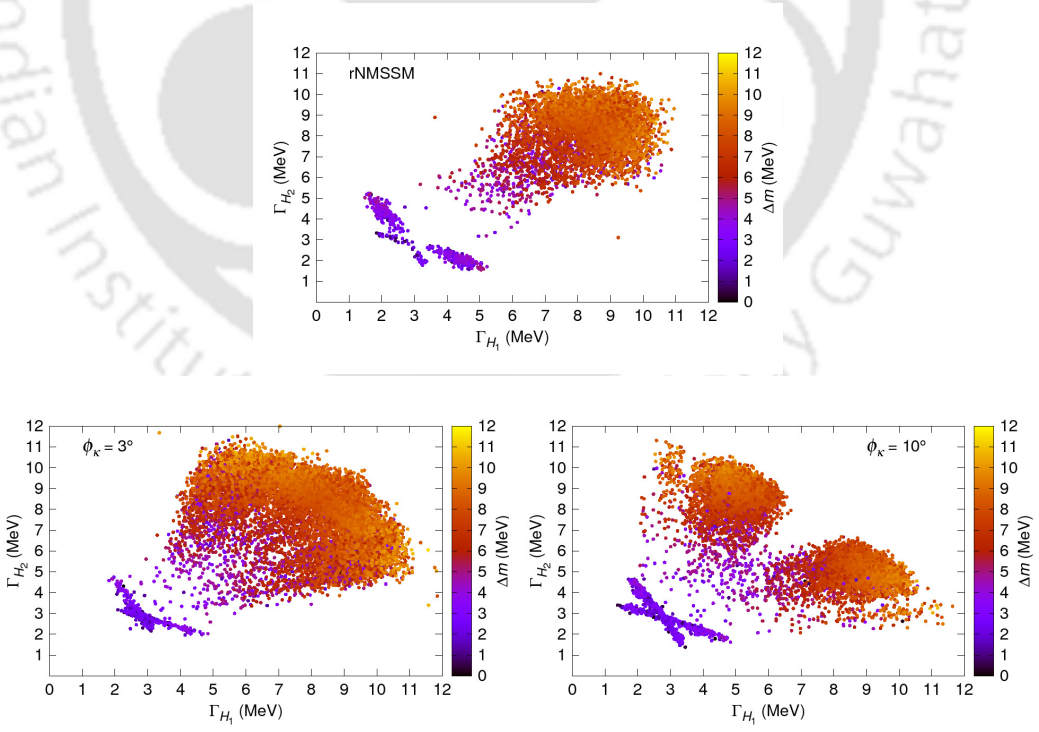

FIGURE 3.2: Points obtained from the parameter scans of the rNMSSM (top) and of the cNMSSM with $\phi_\kappa = 3°$ (bottom left) and with $\phi_\kappa = 10°$ (bottom right). For all the points shown, Δm (color map) is always smaller than Γ_{H_1} (x-axis) and/or Γ_{H_2} (y-axis).

The distributions obtained for the Cases 1, 2 and 3 (color-coded in red, green and blue, respectively) are plotted in Fig. 3.3 for each of the three selected BPs corresponding to the rNMSSM, with the integrated cross section for each curve are also given in the legend. For these distributions, a $\mathcal{M}_{\gamma\gamma}$ bin width of 2 MeV has been considered. As noted above, $\Gamma_{H_1} \sim \Gamma_{H_2}$ for most of the points in the rNMSSM. Therefore, in order to illustrate the dependence of the interference effects on the mass difference and relative widths of the two Higgs bosons, we selected BP1 such that $\Delta m \sim \Gamma_{H_1/H_2}$, BP2 such that $\Delta m < \Gamma_{H_1/H_2}$ and BP3 with $\Delta m \ll \Gamma_{H_1/H_2}$. As can be seen going from the top panel to the bottom right one in Fig. 3.3, the interference effects are always positive and grow larger as Δm decreases compared to Γ_{H_1/H_2}, as expected. Also, the interference effects due to the mixing terms in the propagator matrix (Case 3) are notably larger than those due only to the diagonal terms (Case 2) for each of the three BPs. The deviation in the total cross section with the full propagator matrix compared to the Case 1 for BP3 at an inclusive level is about 40%, clearly indicating that the interference effects can be quite sizable. Note that although BP3 represents maximal enhancement of these effects among all the points collected in our scans, it is possible that they can be even slightly larger for certain other parameter combinations in the vicinity of this BP. Note also that the total integrated cross section (obtained at NNLO in QCD, as mentioned earlier for the $pp \to h_{\rm obs} \to \gamma\gamma$ channel) is generally consistent with the fiducial one, as estimated for the SM-like Higgs boson near 125 GeV [277], or measured by the ATLAS and CMS collaborations for $h_{\rm obs}$ at $\sqrt{s} = 13$ TeV.[3]

The values of the input parameters for all the selected BPs can be found in Tab. 3.4, and the masses and widths of H_1 and H_2 as well as the total cross sections corresponding to the three cases (as mentioned above) for each of the BPs are given in Tab. 3.5.

The enhancement in the interference effects for a larger difference between Δm and $\Gamma_{H_1} \sim \Gamma_{H_2}$ is further confirmed by the distributions shown in the top panels of Fig. 3.4 for BP4 and BP5, in the cNMSSM with $\phi_\kappa = 3°$. For both these BPs, the interference is again constructive, as in the rNMSSM. It is, however, also possible for the interference to be destructive in this scenario. This is the case for BP6, shown in the bottom left panel of the figure, for which the cumulative cross

[3]Note that a considerable discrepancy exists between the ATLAS measurement, which reads 55 ± 10 fb [50], and the CMS one, 84 ± 13 fb [278], besides a fairly large error in each of these itself. This renders an accurate estimation of the total cross section of little significance here and justifies our use of an approximate constant NNLO k-factor.

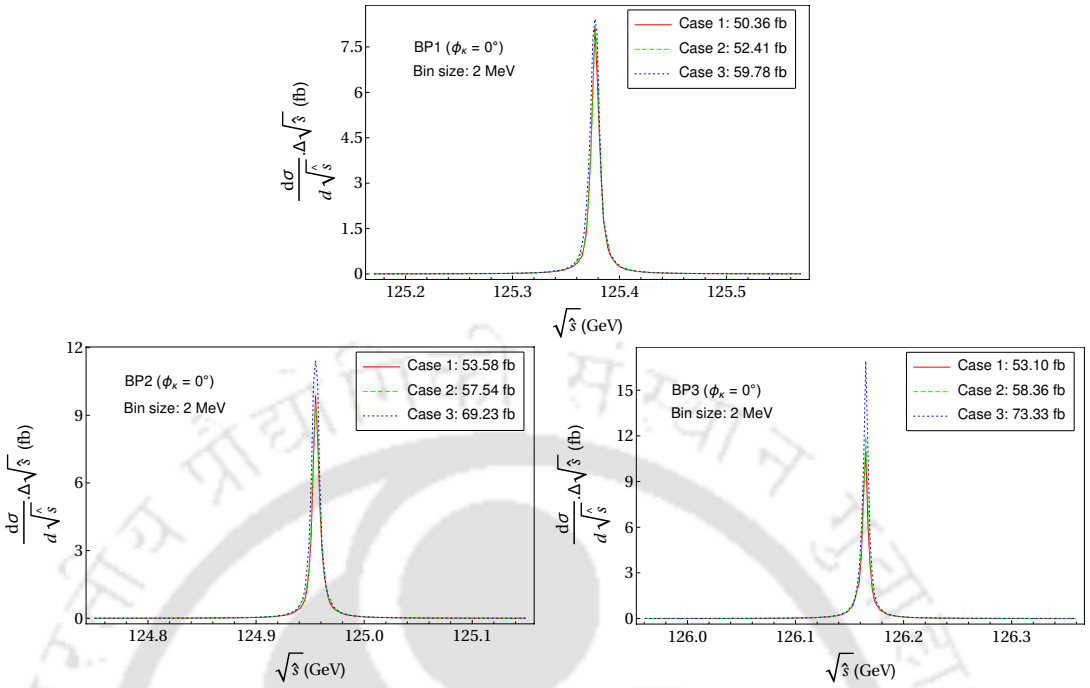

FIGURE 3.3: Distribution of the differential cross section as a function of the di-photon invariant mass (assumed equal to $\sqrt{\hat{s}}$) for the three benchmark points in the rNMSSM. The red, green and blue curves correspond to the Cases 1, 2 and 3, respectively, discussed in the text.

BP	ϕ_κ	M_0	$M_{1/2}$	A_0	$\tan\beta$	λ	κ	A_λ	A_κ	μ_{eff}
1		1380.9	458.51	−2946.2	4.39	0.6970	0.4594	423.23	−5.271	113.60
2	0°	1598.3	471.51	−2875.0	4.34	0.6907	0.4823	402.53	−17.117	110.86
3		1498.2	379.87	−2822.4	3.91	0.6969	0.4538	385.05	−16.566	117.92
4		1366.6	426.35	−2694.3	3.92	0.6878	0.4657	361.11	−13.780	112.79
5	3°	1476.6	363.81	−2969.1	4.67	0.6725	0.4304	485.87	−35.335	120.41
6		1427.1	249.93	−2918.1	4.53	0.6852	0.3360	610.69	−26.038	147.10
7		1350.2	23.24	−2727.6	4.50	0.6630	0.3053	618.04	−13.900	148.83
8		1270.6	176.67	−2218.0	3.96	0.6781	0.4501	538.70	−263.98	168.65
9		1491.9	167.11	−2728.0	5.22	0.6920	0.4599	797.56	−291.36	175.84
10	10°	1378.0	173.35	−2291.7	3.99	0.6877	0.4483	564.66	−266.73	172.87
11		1416.6	170.40	−2741.2	4.45	0.6684	0.3853	687.11	−221.00	177.72
12		1429.0	168.46	−2821.6	4.71	0.6562	0.4303	689.40	−276.65	173.02

TABLE 3.4: Values of the input parameters for all the selected BPs. All dimensionful parameters are in units of GeV.

section is smaller for Case 2 compared to Case 1. Turning on the mixing terms in the propagator matrix further contributes negatively to lower the cross section, although the overall effect is hardly per cent level for this particular parameter space point.

For BPs 4–6 above, the H_1 and H_2 are scalar-like, which is the case for almost all the points obtained in the scan for this scenario. We note here that the singlet-like

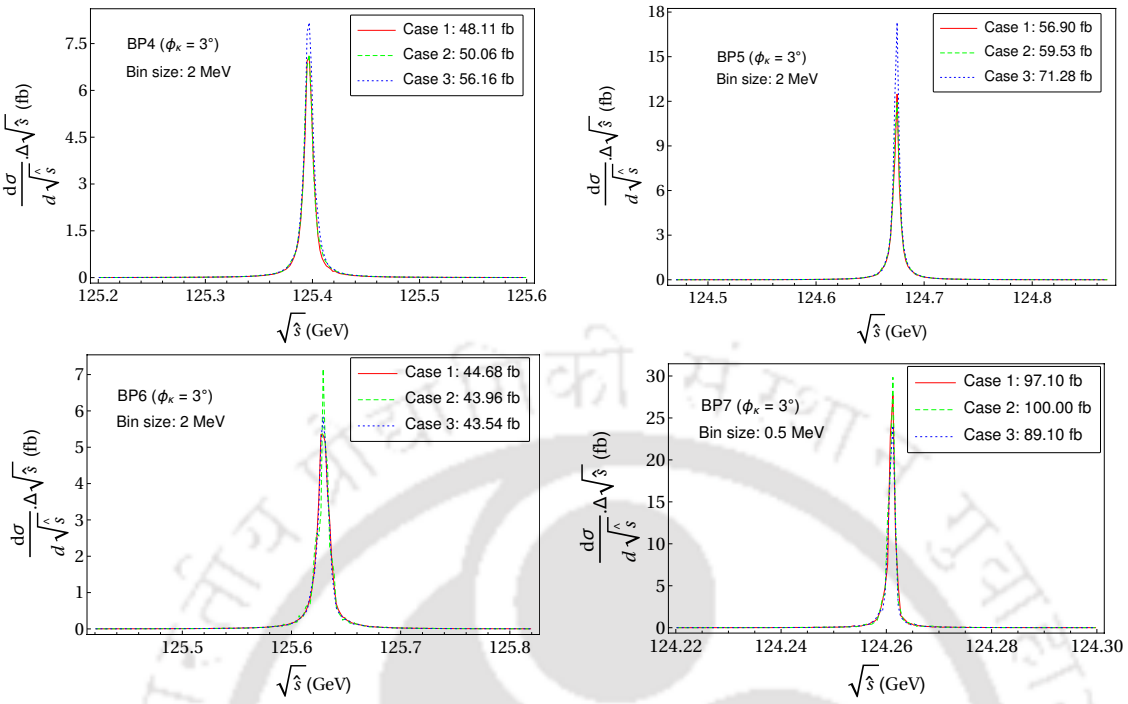

FIGURE 3.4: As in Fig. 3.3, for the BPs corresponding to the cNMSSM with $\phi_\kappa = 3°$.

BP	m_{H_1} (GeV)	m_{H_2} (GeV)	Δm_H (MeV)	Γ_{H_1} (MeV)	Γ_{H_2} (MeV)	$\sigma_{pp}^{\gamma\gamma}$ (fb) Case 1	Case 2	Case 3
1	125.3688	125.3782	9.4	10.7	9.7	50.36	52.41	59.78
2	124.9498	124.9562	6.4	10.1	9.1	53.58	57.54	69.23
3	126.1641	126.1667	2.6	10.1	9.3	53.10	58.36	73.33
4	125.3960	125.4052	9.2	9.6	9.5	48.11	50.06	56.16
5	124.6742	124.6757	1.5	9.1	8.4	56.90	59.53	71.28
6	125.6285	125.6393	10.8	11.1	5.9	44.68	43.96	43.54
7	124.2607	124.2625	1.8	2.5	2.3	97.10	100.00	89.10
8	124.9873	124.9968	9.5	10.3	3.0	46.94	48.38	48.89
9	124.9669	124.9742	7.3	10.6	3.0	45.22	46.54	47.31
10	125.1874	125.1924	5.0	10.3	2.9	46.56	49.55	50.62
11	125.1826	125.1828	2.0	10.1	2.6	50.14	51.42	52.22
12	124.7542	124.7604	6.2	10.3	2.7	47.96	47.12	49.03

TABLE 3.5: The masses and total widths of H_1 and H_2 in the selected BPs. Also listed for each BP is the cross section for the $pp \to H \to \gamma\gamma$ process calculated in the three different ways considered.

Higgs boson near 125 GeV is classified as scalar (pseudoscalar)-like if its coupling to the gauge bosons are significantly larger(smaller) than those of the singlet-like H_3, which itself also lies fairly close in mass[4]. While one of the main reasons

[4]Evidently, both H_1 and H_2 cannot be singlet-like, since in that case both of them will have highly reduced couplings to the SM particles and resultantly the di-photon production

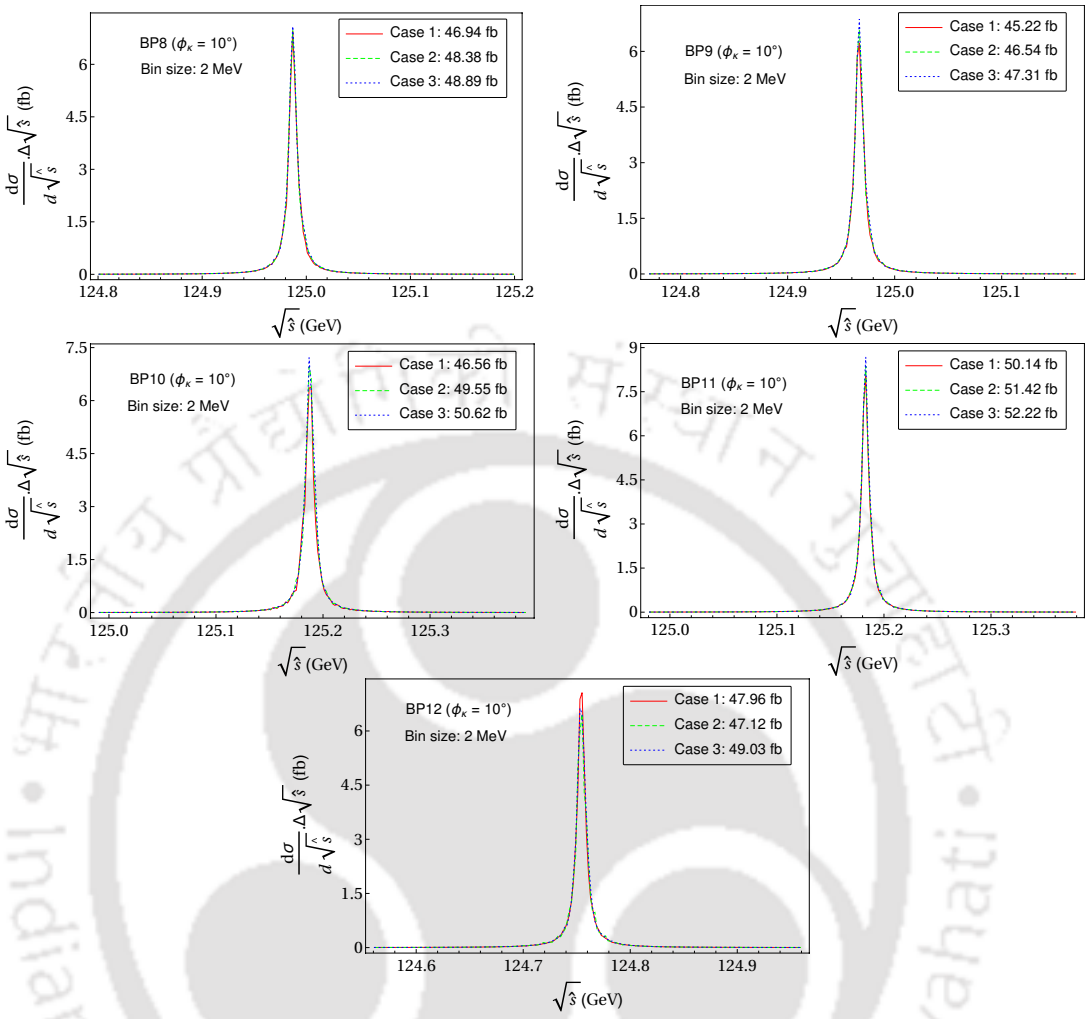

FIGURE 3.5: As in Fig. 3.3, for the BPs corresponding to the cNMSSM with $\phi_\kappa = 10°$.

for considering the cNMSSM was to explore the possibility of interference of a $\sim 125\,\text{GeV}$ pseudoscalar-like Higgs boson with the SM-like one, only a handful of such points were found by our scan, wherein the widths of the H_1 and H_2 are always relatively small.

BP7 in Fig. 3.4 illustrates the scenario with a pseudoscalar-like H_2, with its total width, as well as that of the SM-like H_1, being smaller than 3 MeV. An intriguing feature of this BP is that, while the overall interference effect is positive for Case 2, enhancing the cross section compared to Case 1, and it becomes negative when the complete propagator matrix is included. The destructive interference here is much stronger than in BP6, and has the desirable consequence of bringing the

cross section will be extremely suppressed. Moreover, H_3 in such a scenario ought to have SM-like couplings and would therefore be ruled out by the collider limits tested against using `HiggsBounds`.

total cross section down to a level consistent with the LHC measurements noted earlier. The reason why the cross section for Case 1 for this point is considerably higher than that seen for the other BPs so far can be ascribed to the fact that the H_1 is much more SM-like here compared to the points where the scalar-like H_2 gets closer in mass to it owing to large singlet-doublet mixing.

In Fig. 3.5 we display the distributions for the five BPs selected from the cNMSSM scenario with $\phi_\kappa = 10°$. As noted from the corresponding scatter plot above, this value of ϕ_κ allows for a much larger splitting between Γ_{H_1} and Γ_{H_2}, compared particularly to the rNMSSM case. This makes it possible to test the impact of interference when Δm, instead of being smaller than both the widths, lies somewhere in between them. Thus, for each of these points $\Gamma_{H_1} < 3\,\text{MeV}$ and $\Gamma_{H_2} > 10\,\text{MeV}$, with Δm varying from about 9.5 MeV for BP8 to 2 MeV for BP11. While the behavior of the interference is similar to what has been observed earlier, i.e., it grows larger as the gap between Δm and Γ_{H_2} increases, its overall size remains comparatively small, reaching about 9% for BP10, for which Δm is only slightly larger than Γ_{H_1}. However, when Δm is lowered below Γ_{H_1} also, as in BP11, the interference effects get reduced instead of continuing to grow. BP12 is another example of mutually opposite contributions to the interference effects from the diagonal and off-diagonal elements of the Higgs propagator matrix. As opposed to BP7 though, here the negative interference comes from the diagonal elements in the propagator matrix, while the mixing effects contribute positively to again raise the cross section slightly for Case 3.

However, note that a bin width of 2 MeV is about three orders of magnitude smaller than the current experimental $\mathcal{M}_{\gamma\gamma}$ resolution of around 1 GeV [48]. Evidently, any differences between their shapes corresponding to each of the three cases for a given BP with a smaller bin size, which could be crucial for distinguishing them and hence unraveling the interference effects, would not appear with a realistic bin width of 1 GeV. It is nevertheless interesting to study whether these differences persist to some extent once the differential distributions are convolved with a Gaussian distribution emulating detector effects. We perform the convolution using the `ListConvolve` function in `Mathematica` [279] by supplying the differential distribution data for a point as a list, as well as specifying the mean and width of the Gaussian function. A brief discussion on the convolution technique adopted here is provided in App D.

In the top frames of Fig. 3.6 we display the result of the convolution of the distributions corresponding to Cases 1 and 3 for BP10 with a Gaussian of width (resolution) 1 GeV, which is also used as the size of the $\mathcal{M}_{\gamma\gamma}$ bins for first reproducing these distributions with our MC integrator. We use two prospective integrated luminosities at the LHC: 300 fb^{-1} (left), which is expected by the end of the machine runs in standard configuration; and 1000 fb^{-1} (right), foreseen for the High-Luminosity (HL) LHC option [280][5]. It is worth appreciating in Fig. 3.6 that there exists some marginal scope at the LHC to distinguish at the differential level the simplistic scenario generally assumed (Case 1) and the one rigorously predicted (Case 3), as the difference in the heights of the red and blue curves is not constant for all the bins in $\sqrt{\hat{s}}$. However, evidently this requires knowledge of additional model inputs (e.g., the Higgs boson couplings) as such difference could also be generated by a different point in the parameter space. This difference is even more pronounced in the bottom panels of the figure, which correspond to the convolution with a Gaussian of resolution 300 MeV (clearly an unrealistic value at present, yet potentially within the reach of an upgraded detector). In fact, the histograms referring to these two predictions could eventually be statistically separable, again though, with the aforementioned caveat that one ought to have established additional model parameters elsewhere.

The difficulty to separate Cases 1 and 3 for BP10 (as it would be for all other BPs) with present machine and detector conditions at the LHC is ultimately related to the enforcement of the $\Gamma_{H_1/H_2} < 13$ MeV constraint from off-shell Higgs measurements in our selection of the BPs. We therefore consider a test point (TP), where this constraint is dismissed and only the milder $\Gamma_{h_{\text{obs}}} < 41$ MeV constraint, as obtained from a global fit to the on-shell Higgs boson signal strength measurements [281], is imposed. This is all the more important in light of the fact that some critiques have been drawn about the model-independence of such a measurement, see, e.g., [282] and [283], or its stability against theoretical uncertainties [284, 285][6]. The top right frame of Fig. 3.7 shows the convolved distributions of Cases 1 and 3 for TP1 with a Gaussian of 1 GeV width, illustrating again the fact that also in this case there exists some scope in separating the Cases 1 and 3, even for current di-photon mass resolutions, so long that sufficient luminosity

[5]The higher luminosity only serves to reduce the sizes of the error bars in the figure, which refer only to the statistical errors here.

[6]Recall also that the mentioned experimental measurement of the (off-shell) SM-like Higgs width suffers from a small signal yield and large backgrounds.

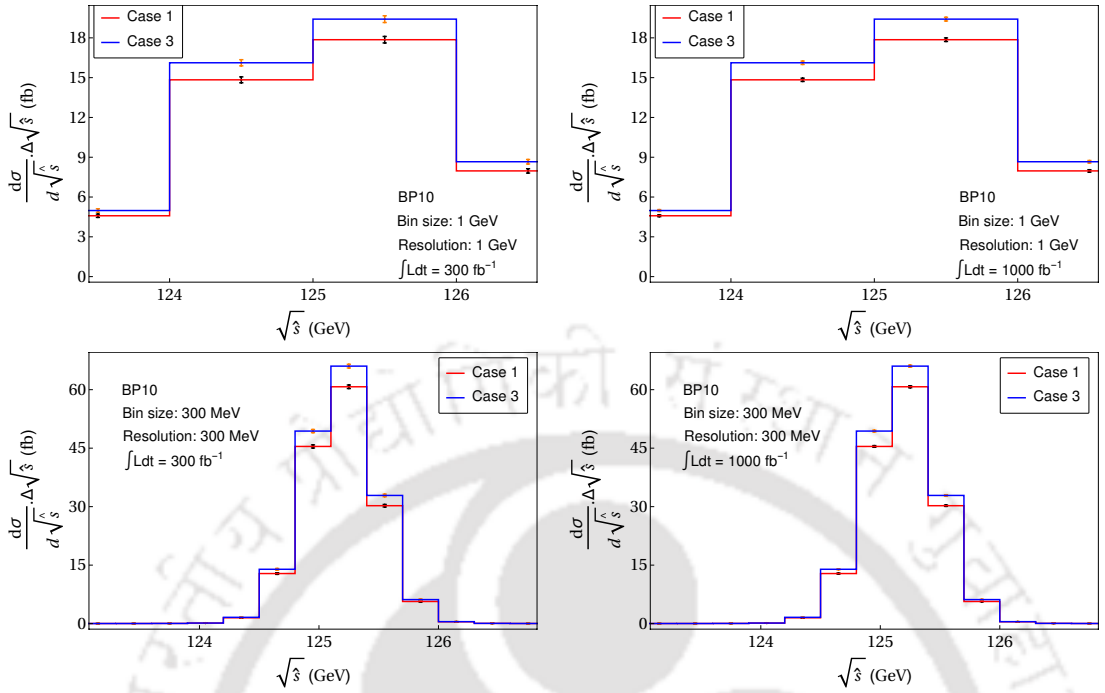

FIGURE 3.6: Convolution of the distributions 1 and 3 for BP10 with Gaussians of width 1 GeV (top) and 300 MeV (bottom). An integrated luminosity of 300 fb^{-1} is assumed in the left panels and of 1000 fb^{-1} in the right panels.

is accrued. The bottom frames of the figure illustrate that this scope gets further enriched if the mass resolution is improved to 300 MeV.

In fact, one could ignore constraints on the total width altogether in order to estimate the minimal mass splitting that could be potentially detectable. While this exercise may appear academic (i.e., to dismiss a crucial experimental constraint), it is worth noting that the current procedures adopted to extract the Higgs boson properties inevitably work with the underlying assumption that only one resonance is produced around 125 GeV. This implies that the allowed intrinsic widths of a pairs of degenerate Higgs states need not relate directly to the currently fitted value.

In Fig. 3.8 and Fig. 3.9 we thus display the distributions of Cases 1 and 3 for two more TPs, 2 and 3, respectively, convolved, again, with Gaussians of 1 GeV and 300 MeV widths for two prospective integrated luminosities. In both these TPs, Γ_{H_1} is very wide, $\mathcal{O}(100)$ MeV, while Γ_{H_2} is of $\mathcal{O}(100)$ MeV, as seen in Tab. 3.6 [7]. But since $\Gamma_{H_1} - \Delta m$ is only about 70 MeV for TP2, while it is larger than half of Γ_{H_1} for TP3, the interference effects are highly enhanced for the latter (about 46%) compared to the former ($\sim$ 30%). These figures more effectively bring home

[7]The input parameters for the three TPs are provided in Tab. 3.7.

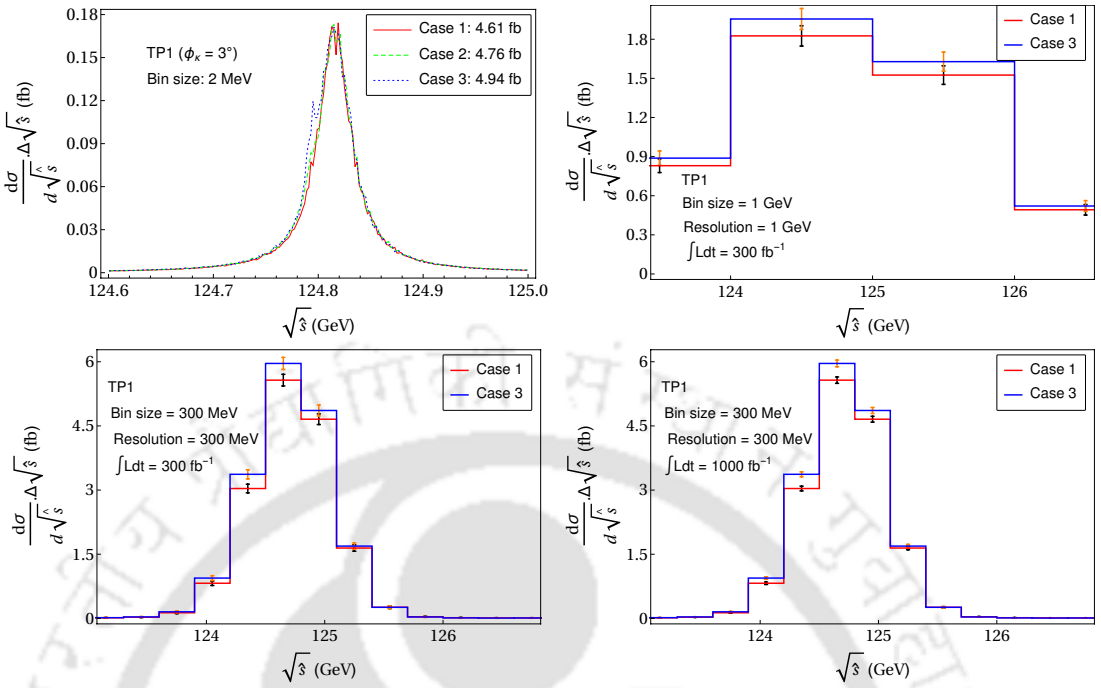

FIGURE 3.7: Top: The differential distributions for TP1 without convolution (left) and after convolution with a Gaussian of width 1 GeV for an integrated luminosity of 300 fb^{-1} (right). Bottom: TP1 distributions after convolution with a Gaussian of width 300 MeV for an integrated luminosity of 300 fb^{-1} (left) and 1000 fb^{-1} (right).

TP	m_{H_1} (GeV)	m_{H_2} (GeV)	Δm_H (MeV)	Γ_{H_1} (MeV)	Γ_{H_2} (MeV)	$\sigma_{pp}^{\gamma\gamma}$ (fb) Case 1	Case 2	Case 3
1	124.7928	124.8158	23	10.8	38.3	4.61	4.76	4.94
2	123.8696	124.1991	329.5	400.2	73.5	0.353	0.385	0.458
3	123.4590	123.7876	328.6	704.9	39.2	1.09	1.45	1.58

TABLE 3.6: Higgs boson masses and widths as well as the $pp \to H \to \gamma\gamma$ cross sections corresponding to the three Cases for the three selected TPs.

the point that a very large Γ_{H_1} (as noticeable in the top left frames) does not impact significantly the quality of the fit to what, in the end, looks like a single object shape (as visible in the other three frames). Though, clearly, the difference between the Cases 1 and 3 is much more pronounced here than for TP1 (and all the BPs). This difference may potentially be established experimentally within the next few years, more likely so the wider (one of) the Higgs states.

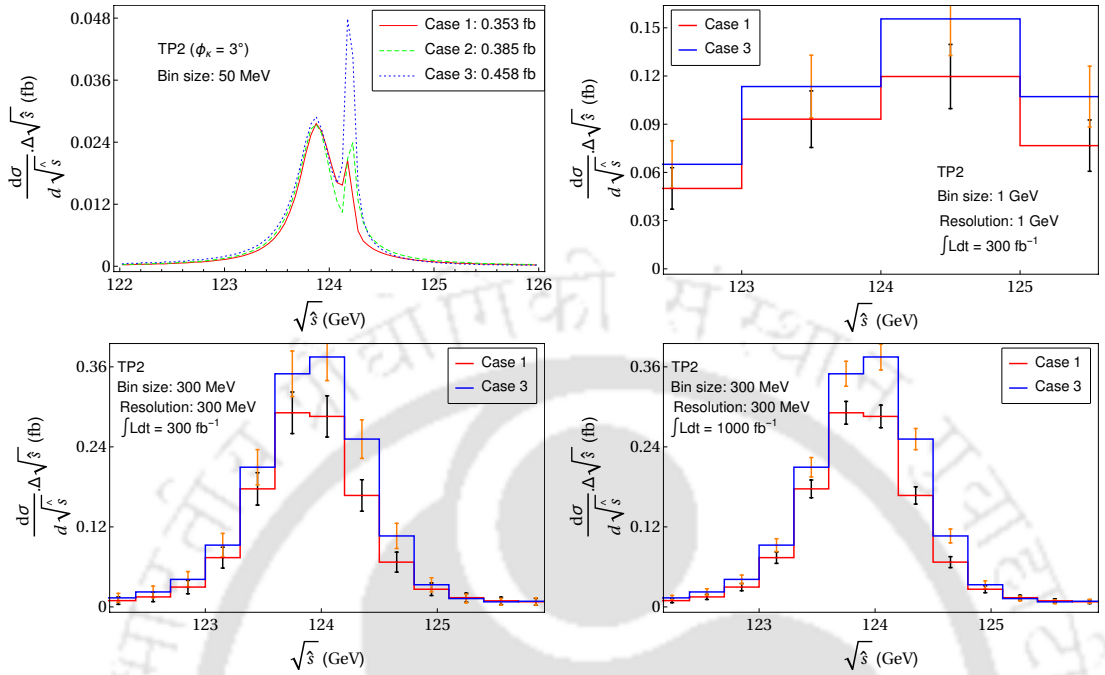

FIGURE 3.8: As in Fig. 3.7, for the TP2.

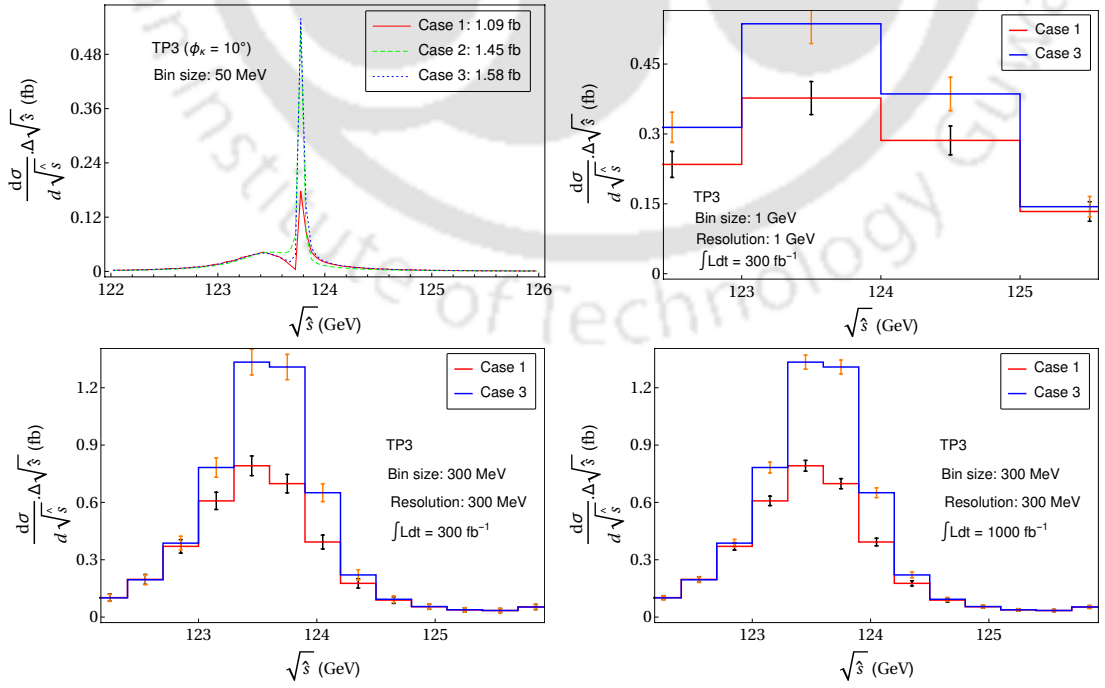

FIGURE 3.9: As in Fig. 3.7, for the TP3.

TP	ϕ_κ	M_0	$M_{1/2}$	A_0	$\tan\beta$	λ	κ	A_λ	A_κ	μ_{eff}
1	3°	1438.0	255.53	-2859.2	4.80	0.6935	0.3287	653.21	-6.399	145.77
2		1405.7	154.63	-2706.5	5.63	0.6861	0.4602	546.59	1.555	108.58
3	10°	1895.2	115.14	-835.20	1.76	0.6524	0.5752	74.865	-120.70	105.95

TABLE 3.7: Values of the input parameters for the three TPs considered. All dimensionful parameters are in units of GeV.

3.6 Conclusions

In summary, we have scrutinized in detail the proton-proton to di-photon process, through which a 125 GeV resonance consistent with the SM Higgs boson has been discovered at the LHC. Indeed, this is the signature for which the Higgs mass resolution is highest amongst all those accessible at the CERN colliders. Measurements of its cross section, at both the inclusive and exclusive level, however, do not exclude the possibility of non-SM explanations. Amongst these, particularly intriguing are those invoking two Higgs bosons produced via gluon fusion, with such a small mass difference that they cannot be resolved by the current experimental apparata. This scenario can emerge only in non-minimal realizations of SUSY, such as the NMSSM, wherein (unlike the MSSM) two coexisting Higgs bosons can contribute to the 125 GeV signal (in $\gamma\gamma$ as well as other final states). In this case, an accurate treatment is required for the propagation of the two states, which not only goes beyond the NWA but also allows for full interference between these. Hence, we have studied the quantitative impact of interference between two Higgs states near 125 GeV, with and without mixing effects, relative to the simplistic approach where the two resonant objects are treated independently of each other. For a full treatment, including the possibility of complex couplings as well, we have considered both real and complex NMSSM.

Our analysis involved scanning the parameter space of the model for finding possible solutions consistent not only with the LHC exclusion limits on the additional Higgs bosons but also with the constraints from EDM measurements. These scans further collected only model solutions yielding two Higgs bosons with masses lying within the uncertainty of the measurements of the 125 GeV resonance. This was followed by a dedicated computation, performed with the help of a locally developed MC tool, producing both integrated and differential cross sections for the full process $pp(gg) \to H_1, H_2 \to \gamma\gamma$. We have found that the aforementioned interference effects can be sizable, with some of the selected BPs providing a difference of around 40% in inclusive rates between the standard approach consisting

in treating the two resonances as separate BW functions, and the full propagator including all non-trivial quantum effects.

We then considered the possibility of a shape analysis of the emerging profile, which could reveal the presence of multiple resonances, assuming realistic, current and prospective, di-photon mass resolutions of the LHC detectors. This revealed some long term potential to see the difference between the generally exploited simplistic case of assuming two separate resonances and the one where the two nearly mass-degenerate states interfere due to the inclusion of the complete propagator matrix in the amplitude calculation. These differences are in fact more visible with a smaller di-photon mass resolution and a larger data sample, both of which can only be achieved with upgraded detectors and/or machine. Finally, in attempting to distinguish the two approaches, we have also noted a tension in the underlying dynamics. Any distortion effect of a single BW shape can only be exploited when the mass difference is sufficiently larger than the assumed width of the bins (which should naturally be consistent with the available experimental mass resolution) in the distribution of the differential cross section. However, a larger mass difference leads to smaller interference effects.

Chapter 4

NMSSM heavy Higgs sector

This chapter focuses on the scenarios with strong mass-degeneracy between the singlet-like scalar and the heavy doublet-like scalar, as well as between the singlet-like and doublet-like pseudoscalar Higgs states, in the context of the NMSSM. When the difference in the masses of such states is comparable to their decay widths, the quantum mechanical interference between their propagators can become significant. We study these effects by taking into account the full Higgs boson propagator matrix in the calculation of the production of a $\tau^+\tau^-$pair in gluon fusion at the LHC.

4.1 Introduction

SUSY predicts the existence of at least two Higgs doublets of opposite hypercharge, which are necessary to cancel chiral anomalies, unlike the SM, where only one Higgs doublet is sufficient. In the MSSM, after EWSB, the two doublets result in three physical neutral Higgs states, two scalars (h and H, with $m_h < m_H$) and a pseudoscalar (A), as well as a charged Higgs pair ($H^\pm$). In principle, either h or H could be the Higgs boson, $h_{\rm obs}$, observed at the LHC [1, 2]. However, the model's parameter space region where H has a mass near 125 GeV and SM-like couplings to the EW gauge bosons is very tightly constrained by experimental data [34, 35]. Alternatively, the condition on h to be a candidate for $h_{\rm obs}$, while a phenomenologically much more favored scenario, pushes m_H and m_A upwards into the so-called decoupling regime [63], wherein they are nearly identical in mass.

Thus, if a bump appears in the experimental data near a certain (large) invariant mass of a fermion-antifermion or photon pair above the SM expectation, it could very well be due to these two states combined, unless their mass difference is large enough to enable the experiment to resolve them individually. A formidable difference in the statistical significance of the peaks observed in the fermionic channels versus the W^+W^- and ZZ^* channels could also be interpreted as a hint of the (H, A) mass-degeneracy. However, if the MSSM Higgs sector is CP-violating, the two heavy mass-degenerate states could mutually interfere quantum mechanically. This interference could significantly alter the anticipated cross section for a given SM final state that these Higgs bosons decay into [36–38].

In the NMSSM, there exists an extra scalar, h_s, and an extra pseudoscalar, a_s, in the Higgs sector. The masses of these two new Higgs bosons are essentially free model parameters, and either of them could very well lie near 125 GeV, along with the MSSM-like h. The scenario with m_{h_s} near m_h is in fact well-motivated by naturalness considerations, since the doublet-singlet mixing can enhance the tree-level mass of h appreciably [7, 8, 39]. The potentially strong effects of interference in the scenario where these Higgs bosons are too close in mass for the peaks to be individually distinguishable, given the current di-photon mass resolution at the LHC, have therefore been analyzed in the previous chapter. In this work, we consider the alternative scenarios wherein one (or possibly even both) of h_s and a_s could be mass-degenerate with the heavier H and A, instead of h. Here our main purpose is to investigate the phenomenological implications of such a scenario, which is a viable one in general extended Higgs sectors, without delving into its theoretical motivations in the specific model considered.

For our analysis, we first perform numerical scans of the NMSSM parameter space to identify regions where $m_{h_s} \approx m_H$ ($\approx m_A$) or $m_{a_s} \approx m_A$ ($\approx m_H$). We then quantify the impact of quantum interference on the process where nearly mass-degenerate Higgs bosons are produced in gluon fusion at the 14 TeV LHC and decay into $\tau^+\tau^-$ pairs. This is done by comparing the cross section obtained by including the full Higgs propagator matrix in the expression for amplitude and the one obtained by assuming two (or more) individual BW Higgs propagators with nearly equal masses. We restrict our analysis to the CPC-NMSSM Higgs sector here, such that the scalar and pseudoscalar interaction eigenstates do not mix. Hence, the off-diagonal elements in the Higgs propagator matrix contribute to the interference effects only when the two mass-degenerate states have the same

CP-properties. Furthermore, while we explored the di-photon final state in the previous chapter pertaining to 125 GeV Higgs bosons in a similar context [33], it cannot be employed here. This is because the cross section, which is already phase-space suppressed, gets further depleted considerably due to the extremely small partial decay widths, and consequently BRs of the heavy Higgs states into photon pairs.

During numerical scan, each randomly generated parameter space point is tested against the most crucial and recent experimental constraints, including those from the LHC, from b-physics measurements and DM searches. Among those passing all the constraints, we then identify a few BPs and carry out the cross section comparison noted above for them, using a MC integration tool developed in-house. We find that, as concluded by the previous studies in the MSSM [38, 286], the interference is (almost) always negative and can result in a sizable reduction in cross section for the considered process. However, the heavy Higgs boson masses for the filtered points, collected in our parameter space scan, are always quite large (> 800 GeV). As a result, the effects of interference on the shape of the distribution of the differential cross section may not be detectable even with an integrated luminosity of 3000 fb^{-1} at the LHC, given the low $\tau^+\tau^-$ invariant mass resolution.

The chapter is organized as follows. In the next section we briefly revisit the Higgs sector of the NMSSM and the analytical expression for the cross section that includes the full Higgs propagator matrix. In section 4.3 we discuss our methodology for the parameter space scan. We present the results of our comparative numerical analysis of cross sections in section 4.4 and our conclusions in section 4.5.

4.2 The $\tau^+\tau^-$ signal from heavy NMSSM Higgs bosons at the LHC

4.2.1 The NMSSM Higgs sector

The Higgs potential of the Z_3 invariant NMSSM is written in terms of the two $\mathrm{SU(2)_L}$ doublets H_u and H_d, with $Y = \pm 1$, and the singlet S as

$$\begin{aligned} V_H &= \left|\lambda\left(H_u^+ H_d^- - H_u^0 H_d^0\right) + \kappa S^2\right|^2 + \left(m_{H_u}^2 + |\mu + \lambda S|^2\right)\left(|H_u^0|^2 + |H_u^+|^2\right) \\ &+ \left(m_{H_d}^2 + |\mu + \lambda S|^2\right)\left(|H_d^0|^2 + |H_d^-|^2\right) + \frac{g^2}{4}\left(|H_u^0|^2 + |H_u^+|^2 - |H_d^0|^2 - |H_d^-|^2\right)^2 \\ &+ \frac{g_2^2}{2}|H_u^+ H_d^{0*} + H_u^0 H_d^{-*}|^2 + m_S^2|S|^2 \\ &+ \left[\lambda A_\lambda\left(H_u^+ H_d^- - H_u^0 H_d^0\right) S + \frac{1}{3}\kappa A_\kappa S^3 + \text{h.c.}\right], \end{aligned} \tag{4.1}$$

Here λ and κ are dimensionless Higgs trilinear couplings and A_λ and A_κ are their respective soft SUSY breaking counterparts, m_{H_d}, m_{H_u} and m_S are the soft Higgs masses, and g_1 and g_2 are the $U(1)_Y$ and $SU(2)_L$ gauge coupling constants, respectively, with $g^2 = \frac{g_1^2+g_2^2}{2}$.

By taking the second derivative of V_H after developing the fields H_d, H_u and S about their respective VEVs, v_d, v_u and s, as

$$H_d^0 = \begin{pmatrix} \frac{1}{\sqrt{2}}(v_d + H_{dR} + iH_{dI}) \\ H_d^- \end{pmatrix}, \quad H_u^0 = e^{i\phi_u}\begin{pmatrix} H_u^+ \\ \frac{1}{\sqrt{2}}(v_u + H_{uR} + iH_{uI}) \end{pmatrix},$$
$$S^0 = \frac{e^{i\phi_s}}{\sqrt{2}}(s + S_R + iS_I), \tag{4.2}$$

one obtains the tree-level 5×5 neutral Higgs mass-squared matrix in the $\mathrm{H}^T \equiv (H_{dR}, H_{uR}, S_R, H_I, S_I)$ basis, from which the would be Goldstone boson G, has been rotated away. In the CPC limit, where all the Higgs sector coupling parameters are real, after the inclusion of the higher order corrections, this mass matrix

can be expressed in the form

$$\mathbf{M}_H^2 = \left(\begin{array}{c|c} \mathbf{M}_S^2 & \mathbf{0} \\ \hline \mathbf{0} & \mathbf{M}_P^2 \end{array}\right), \tag{4.3}$$

where the 3×3 submatrix $\mathbf{M}_S^2$ corresponds to the CP-even states and the 2×2 submatrix $\mathbf{M}_P^2$ to the CP-odd states, while all the CP-mixed terms vanish. The explicit entries to the CP-even and CP-odd blocks, i.e, $\mathbf{M}_S^2$ and $\mathbf{M}_P^2$, respectively, can be found in App. B. The CP-even and CP-odd Higgs mass eigenstates can be obtained from the interaction states through the rotations

$$(h_s, h, H)^T = \mathcal{R}^H \, (H_{dR}, H_{uR}, S_R)^T \quad \text{and} \quad (a_s, A)^T = \mathcal{R}^A \, (H_I, S_I)^T \,, \tag{4.4}$$

respectively, where $\mathcal{R}^H$ and $\mathcal{R}^A$ are orthogonal matrices, which are used to diagonalize $\mathbf{M}_S^2$ and $\mathbf{M}_P^2$ blocks of the Higgs mass matrix $\mathbf{M}_H^2$, respectively.

Note that, here we have chosen a slightly different notation from the previous chapter in order to denote the physical Higgs states, for reasons which will be clear in the subsequent sections. Throughout our analysis, we identify the lighter doublet-like scalar h as the 125 GeV $h_{\rm obs}$, so that H is always heavier than 125 GeV. We disregard the alternative possibility of H playing the role of the $h_{\rm obs}$. The mass of the singlet-like h_s (a_s) can be smaller or larger than m_h and/or $m_H (m_A)$.

4.2.2 Gluon fusion production of Higgs bosons

The differential cross section for the process $pp \to H \to \tau^+\tau^-$ (with H collectively denoting the five neutral Higgs bosons of the model, and assuming vanishing contribution from processes other than gluon fusion) can be written as

$$\frac{d\sigma_{pp\to\tau^+\tau^-}}{d\sqrt{\hat{s}}} = \int_\tau^1 \frac{2\sqrt{\hat{s}}}{s} \frac{dx_1}{x_1} \frac{g(x_1)g(\hat{\tau}x_1)}{1024\pi\hat{s}} \mathcal{A}^2_{gg\to\tau^+\tau^-} \,, \tag{4.5}$$

where $g(x_1)$ and $g(x_2)$ are the PDFs of the two incoming gluons having squared CM energy $\hat{s}$, and $\tau = \hat{s}/s$, with s being the squared CM energy of the pp system. In the limit of negligible non-factorizable loop contributions, the amplitude-squared

in the above equation can be cast into the most general form

$$\mathcal{A}^2_{gg\to H\to\tau^+\tau^-} = \Big| \sum_{i,j=1-5} \sum_{\lambda,\sigma=\pm} \mathcal{M}_{P_i\lambda} D_{ij} \mathcal{M}_{D_j\sigma} \Big|^2 , \tag{4.6}$$

where $\lambda = \pm 1$ and $\sigma = \pm 1$ are the helicities of the incoming gluons and outgoing $\tau^\pm$, respectively. The expressions for the production amplitude $\mathcal{M}_{P_i\lambda}$, can be found in Eq. 3.12 to Eq. 3.14 in the previous chapter.

The amplitude for the decay part is given as

$$\mathcal{M}_{D_i\sigma} = \frac{\sqrt{2\hat{s}\beta_\tau}\, m_\tau}{v} \Big(\beta_\tau S_i^\tau + i\sigma P_i^\tau \Big) , \tag{4.7}$$

where $S_i^\tau = \mathcal{R}^H_{H_{dR}i}/\cos\beta$, $P_i^\tau = -\mathcal{R}^A_{H_I i}(\sin\beta/\cos\beta)$, and $\beta_\tau = \sqrt{1-4\frac{m_\tau^2}{\hat{s}}}$.

In principle, for calculating the differential cross section, given in Eq. 4.5, one should include in $\mathcal{A}^2_{gg\to H\to\tau^+\tau^-}$ the full NMSSM Higgs boson propagator matrix which is given in Eq. 3.17. In absence of CPV phases, the CP-mixing elements will be zero and the propagator matrix in Eq. 3.17 takes the form

$$D_{ij} = \begin{pmatrix} \mathrm{M}_{11} & i\Im\mathrm{m}\hat{\Pi}_{12}(\hat{s}) & i\Im\mathrm{m}\hat{\Pi}_{13}(\hat{s}) & 0 & 0 \\ i\Im\mathrm{m}\hat{\Pi}_{21}(\hat{s}) & \mathrm{M}_{22} & i\Im\mathrm{m}\hat{\Pi}_{23}(\hat{s}) & 0 & 0 \\ i\Im\mathrm{m}\hat{\Pi}_{31}(\hat{s}) & i\Im\mathrm{m}\hat{\Pi}_{32}(\hat{s}) & \mathrm{M}_{33} & 0 & 0 \\ 0 & 0 & 0 & \mathrm{M}_{44} & i\Im\mathrm{m}\hat{\Pi}_{45}(\hat{s}) \\ 0 & 0 & 0 & i\Im\mathrm{m}\hat{\Pi}_{54}(\hat{s}) & \mathrm{M}_{55} \end{pmatrix}^{-1} . \tag{4.8}$$

Note that the pre-factor $\hat{s}$ in Eq. 3.17 is absorbed in the phase space factor in Eq. 4.5. The total cross section can then be obtained by integrating Eq. 4.5 over $\sqrt{\hat{s}}$. In general, however, the off-diagonal absorptive terms in the propagator are assumed to be negligible compared to all m_{H_i}. In that case, the amplitudes due to all H_i can be summed *incoherently* as

$$\mathcal{A}^2_{gg\to H\to\tau^+\tau^-} = \sum_{i=1-5} \sum_{\lambda,\sigma=\pm} \Big| \mathcal{M}_{P_i\lambda} \frac{1}{\hat{s} - m^2_{H_i} + i\Im\mathrm{m}\hat{\Pi}_{ii}(\hat{s})} \mathcal{M}_{D_i\sigma} \Big|^2 . \tag{4.9}$$

In fact, if a given Higgs boson's width, Γ_{H_i}, defined through $i\Im\mathrm{m}\hat{\Pi}_{ii} \equiv i m_{H_i}\Gamma_i$ from the corresponding diagonal term M_{ii} in Eq. 4.8, is additionally much smaller than m_{H_i}, one can further apply the NWA (see Eq. 3.18 to Eq. 3.22 in the previous chapter). In the following, we define the total cross section for $\tau^+\tau^-$ production

calculated using the NWA as

$$\sigma_{H_1 \ldots H_n} = \sum_{H_i = H_1, \ldots, H_n} \sigma(gg \to H_i) \times \mathrm{BR}(H_i \to \tau^+ \tau^-)\,, \tag{4.10}$$

for all mass-degenerate H_i. This is the most commonly adopted approach, and we aim to examine to what extent this cross section might differ from the one obtained by the incoherent summing of amplitudes with individual BW propagators, as in Eq. 4.9, which we refer to as σ_{BW}. We then assess the further impact of the interference effects, by calculating the cross section, σ_{Int}, calculated using the complete amplitude expression given in Eq. 4.6, along with the propagator matrix given in Eq 4.8.

4.3 Parameter space scan and favored regions

In order to find solutions with nearly mass-degenerate (h_s, H) and/or (a_s, A) pairs that also satisfy all known experimental constraints, we first performed numerical scanning of the NMSSM parameter space. As the model contains a large number of free parameters at the EW scale, we fixed the soft masses of the sfermions as $M_{Q_{1,2,3}} = M_{U_{1,2,3}} = M_{D_{1,2,3}} = 3\,\mathrm{TeV}$ and $M_{L_{1,2,3}} = M_{E_{1,2,3}} = 2\,\mathrm{TeV}$, and of the gauginos as $2M_1 = M_2 = \frac{1}{3}M_3 = 1\,\mathrm{TeV}$, since variations in these parameters are not expected to have a significant influence on the overall findings of our particular case study. Note also that the parameters A_λ and A_κ appearing in the potential in Eq. 4.1 can be traded for the pseudoscalar masses mP ($\sim m_{a_s}$) and mA as inputs. As in the previous case discussed in chapter 3, we assume universal trilinear couplings of the charged sfermions: $A_0 \equiv A_{\tilde{u},\tilde{c},\tilde{t}} = A_{\tilde{d},\tilde{s},\tilde{b}} = A_{\tilde{e},\tilde{\mu},\tilde{\tau}}$. The ranges of input parameters, used for the wide-ranged initial scan, are given in the second column of Tab. 4.1. We calculate the Higgs mass spectra and BRs for all the randomly scanned points using `NMSSMTools-v5.3.0` [287–289].

As for the experimental constraints, a scanned input point was rejected if it did not predict m_h lying within the $123 - 127\,\mathrm{GeV}$ bracket (thus allowing for up to $\pm 2\,\mathrm{GeV}$ uncertainty in the theoretical prediction of its mass, given the experimental measurement of $125.09 \pm 0.21(\mathrm{stat.}) \pm 0.11(\mathrm{syst.})\,\mathrm{GeV}$ [47]). In addition, we required the neutralino DM relic abundance, calculated by `NMSSMTools` via an interface to `MicrOmegas` [290, 291], to satisfy $\Omega_{\tilde{\chi}_1^0} h^2 \leq 0.131$.This difference of the upper limit enforced on $\Omega_{\tilde{\chi}_1^0} h^2$ from the actual PLANCK measurement of

Parameter	Initial wide scanned range	Narrow range for scenario 1	Narrow range for scenario 2 with	
			$m_{h_s} < m_h$	$m_{h_s} > m_h$
A_0 (GeV)	-5000 – -1000	-5000 – -3800	-5000 – -3800	-5000 – -1000
$\tan\beta$	2 – 50	12 – 17	2 – 15	6 –17
λ	0.001 – 0.7	0.001 – 0.02	0.01 – 0.7	0.01 – 0.3
κ	0.001 – 0.7	0.001 – 0.04	0.01 – 0.7	0.01 – 0.7
$\mu_{\rm eff}$ (GeV)	100 – 1000	100 – 300	100 – 250	100 – 400
mA (GeV)	125 – 1000	860 – 1000	870 – 1000	880 – 1000
mP (GeV)	10 – 1000	10 – 1000	880 – 1000	890 – 1000

TABLE 4.1: Wide and narrowed-down (for a given scenario) scanned ranges of the seven NMSSM parameters considered free in this study. mA and mP denote the diagonal doublet and singlet CP-odd mass matrix elements, respectively.

$\Omega_{\rm DM} = 0.1199 \pm 0.0027$ [292] is to accommodate up to a +10% possible error in its theoretical calculation. A point was also discarded during the scan if the spin-independent $\widetilde{\chi}_1^0$-proton scattering cross section, $\sigma_p^{\rm SI}$ (which is written out in the `NMSSMTools` output, like the b-physics observables), did not satisfy the 95% CL limits from the XENON1T direct detection experiment [293]. The points collected in the scan were further filtered by the requirement on the most constraining of these observables to lie within 2σ of their latest measurements, which read

- BR$(B \to X_s\gamma) = (3.32 \pm 0.16) \times 10^{-4}$ [206],
- BR$(B_u \to \tau^\pm\nu_\tau) = (1.06 \pm 0.19) \times 10^{-4}$ [206],
- BR$(B_s \to \mu^+\mu^-) = (3.0 \pm 0.6^{+0.3}_{-0.2}) \times 10^{-9}$ [202].

The successful points were then run through `HiggsBounds-v4.3.1` [261, 262, 264] to test each of the additional NMSSM Higgs bosons against the exclusion bounds from LEP, TeVatron and LHC. These points were further subjected to the 95% CL exclusion limits from the combined analysis of $\widetilde{\chi}_1^0\widetilde{\chi}_1^0 \to b\bar{b}$ annihilation in dwarf spheroidal galaxies performed by the Fermi-LAT and MAGIC collaborations [294], which are currently the strongest of the DM indirect detection bounds. We calculated the the signal strengths, μ_X, of h in the decay channels, $X = \gamma\gamma$, ZZ^*, W^+W^-, $\tau^+\tau^-$, $b\bar{b}$, for each point using the public program `HiggsSignals-v1.4.0` [245]. Since the discovery of $h_{\rm obs}$, the CMS and ATLAS collaborations have frequently updated the measurements of μ_X independently from each other, and released their combined results based on the $\sqrt{s} = 7$ and 8 TeV data for each of the above-mentioned channel in [48]. However, no such combined result for the $\sqrt{s} = 13$ TeV data has been published so far. While the

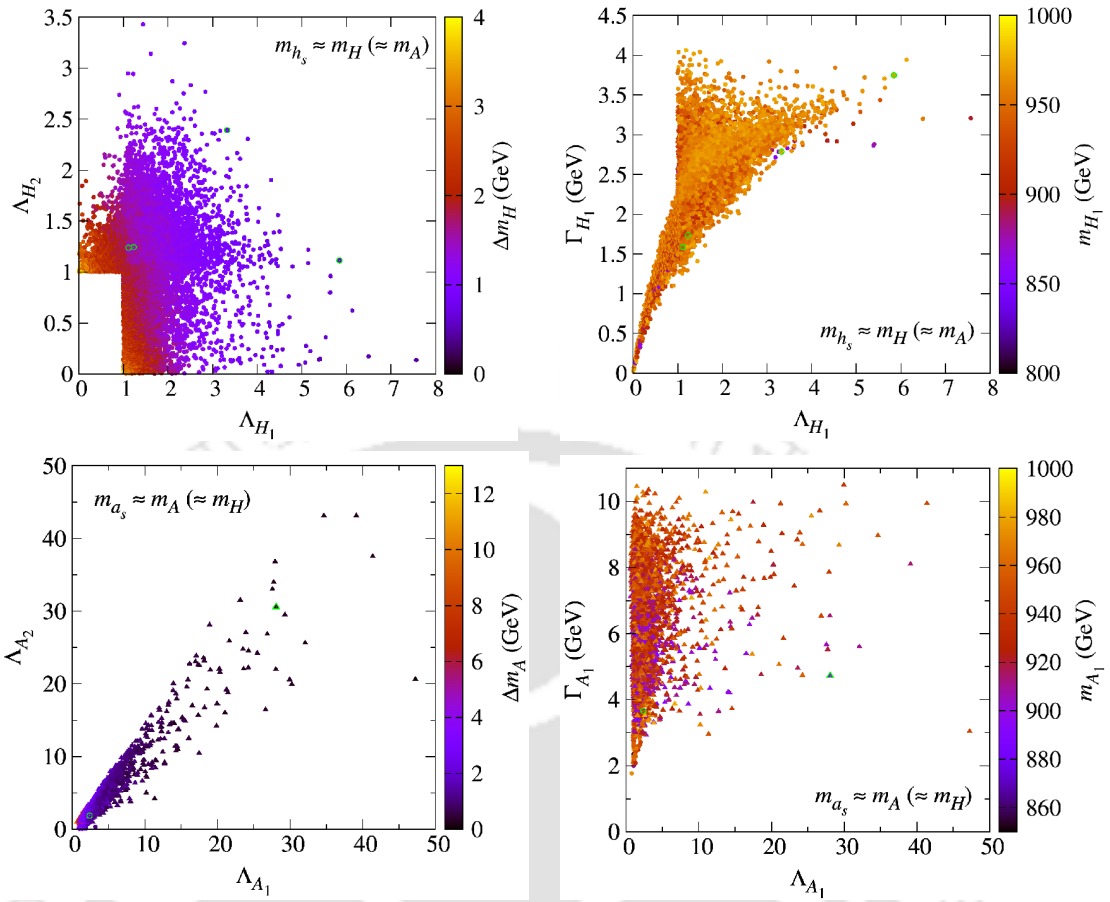

FIGURE 4.1: Λ_{X_i} for variuos Δm_X (left), and Γ_{X_i} for various m_{X_1} (right), for the points corresponding to scenario-1 (top) and scenario-2 (bottom), obtained from the parameter space scans of the NMSSM. See text for details.

measurements by the two collaborations have generally been in agreement with each other, there are also non-negligible differences in at least one of the channels (see, e.g., [295] and [50, 228]). Since these results have increasingly favored the SM predictions, instead of choosing any one of the two results from ATLAS and CMS collaborations, or performing fits to both, which would be beyond the scope of this study, we simply enforced the SM value, $\mu_X = 1 \pm 0.34$ at 1σ for each X on all points.

Finally, it has previously been established in the literature [246, 286] that the interference effects between two Higgs states grow as the mass-splitting between them drops off compared to their widths. We therefore define

$$\Lambda_{X_i} = \frac{\Gamma_{X_i}}{\Delta m_X}, \quad \text{with} \quad \Delta m_X = m_{X_2} - m_{X_1}\,, \tag{4.11}$$

with $i = 1$ implying the lighter and $i = 2$ the heavier of the two nearly mass-degenerate scalars ($X = H$) or pseudoscalars ($X = A$), and retained only the points for which $\Lambda_{X_1} > 1$ or $\Lambda_{X_2} > 1$. These points were then split into two categories,

- scenario-1: $m_{h_s} \approx m_H$,
- scenario-2: $m_{a_s} \approx m_A$.

Note, however, that for a vast majority of the points satisfying the aforementioned filters, the doublet-like H and A were found to be highly mass-degenerate and thus lying in the decoupling regime of the MSSM. This is understandable, in particular in scenario-1, since the requirement for h_s to have a mass close to that of H forces h to be almost entirely doublet-like, with maximal tree-level mass and SM-like couplings. Furthermore, for all the points the lightest neutralino turned out to be a pure higgsino, with the difference in its mass from that of the next-to-lightest neutralino always lying within $10 - 13\,\text{GeV}$. A recent ATLAS search [296] has ruled out such a DM for a mass up to $\sim 145\,\text{GeV}$ (which effectively translates into $\mu_{\text{eff}} \geq 145\,\text{GeV}$). We therefore removed all the points with $m_{\widetilde{\chi}_1^0} < 145\,\text{GeV}$ from the scanned set. We point out here that the limits from a CMS search [297] which could also be of relevance here have already been incorporated in `NMSSMTools-v5.3.0`, so that each scanned point was intrinsically tested against them.

The points in scenario-2 can be further divided into two distinct sets, one with h_s lighter than h and the other with h_s heavier than h. In order to find more solutions with a possibly enhanced mass-degeneracy in a given scenario, we performed secondary scans for narrowed-down parameters ranges. The ranges of the input parameters for the points corresponding to the two scenarios are given in columns 3–5 of Tab 4.1. All the constraints and conditions noted above were applied to the points collected in these scans.

In the top left panel of Fig. 4.1, we show Λ_{H_i} for the final set of points belonging to scenario-1 (where H_1, and likewise H_2, can be either one of h_s or H). We see that Γ_{H_1} can be up to 8 times larger than Δm_H, as illustrated by the color map. According to the top right panel, the maximum width of H_1 for these points is about $4.5\,\text{GeV}$ (while that of H_2, not shown here, is much smaller, as can be deduced from the overall smaller Λ_{H_2} in the left panel). We point out again the anti-correlation between Λ_{H_1} and Λ_{H_2}, so that $\Lambda_{H_2} > 1$ whenever $\Lambda_{H_1} < 1$, and

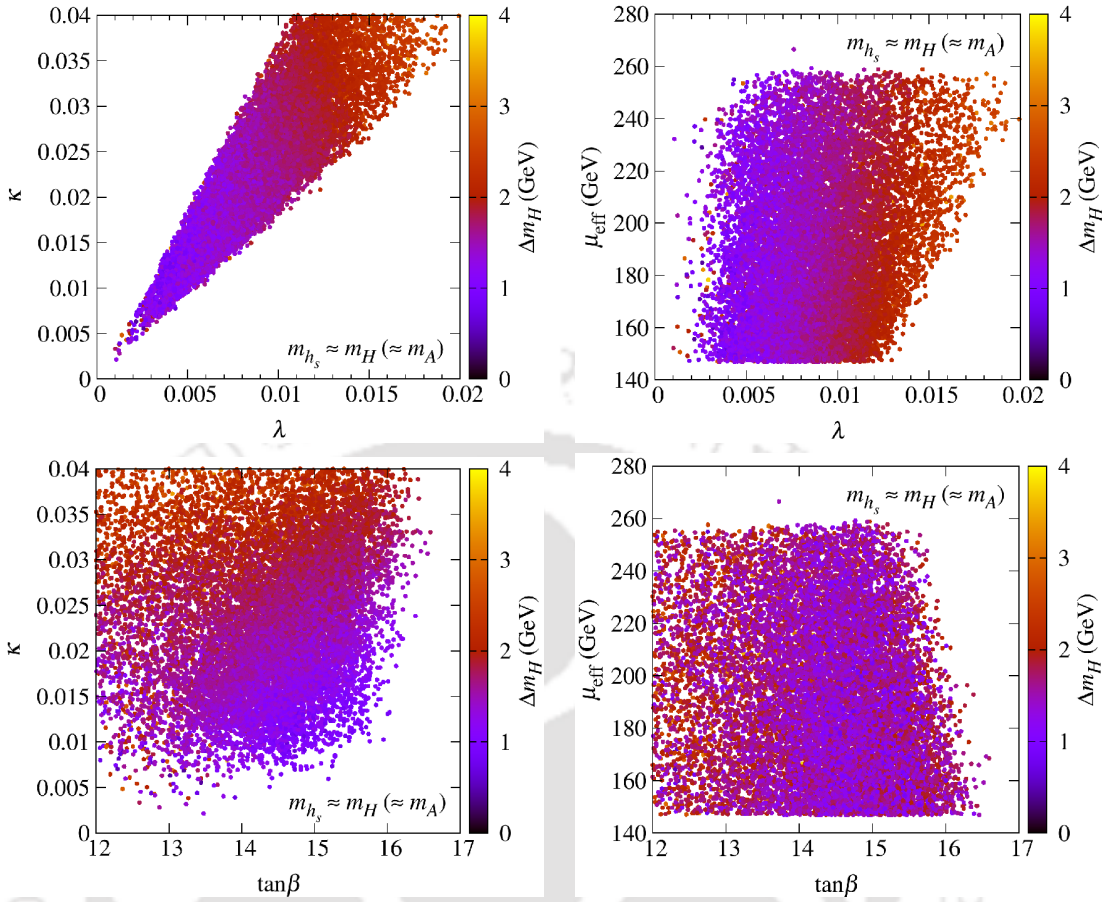

FIGURE 4.2: Distributions of the input parameters, showing the correlations among them that lead to a strong mass-degeneracy between h_s and H, for the points corresponding to scenario-1 obtained from the numerical scans.

vice versa. In the bottom left panel of Fig. 4.1, which similarly shows Λ_{A_i} for scenario-2, one notices Γ_{A_1} being as much as 50 times larger than Δm_A. Hence, one notices that, while among the former case Λ_{A_2} never exceeds Λ_{A_1}, there are a few of the latter points for which both Λ_{A_1}, $\Lambda_{A_1} \sim 40$. The bottom right panel illustrates that in the $m_{h_s} > m_h$ case large values of Λ_{A_1} are a consequence of large values ($\sim 10\,\text{GeV}$) of the A_1 width. In the $m_{h_s} < m_h$ case, in contrast, Γ_{A_1} stays low generally (between $2 - 4\,\text{GeV}$), and large Λ_{A_1} results mainly from the fact that Δm_A can reach values lower than in the $m_{h_s} > m_h$ case, according to the color map in the bottom left panel. The points encircled in green in Fig. 4.1 are the BPs we identified for our cross section analysis, to be explained in the next section.

We now briefly discuss the parameter combinations that lead to strong mass-degeneracies between Higgs bosons in the two scenarios. Fig. 4.2 corresponds to scenario-1, and shows that a smaller Δm_H favors lower values of both λ and κ

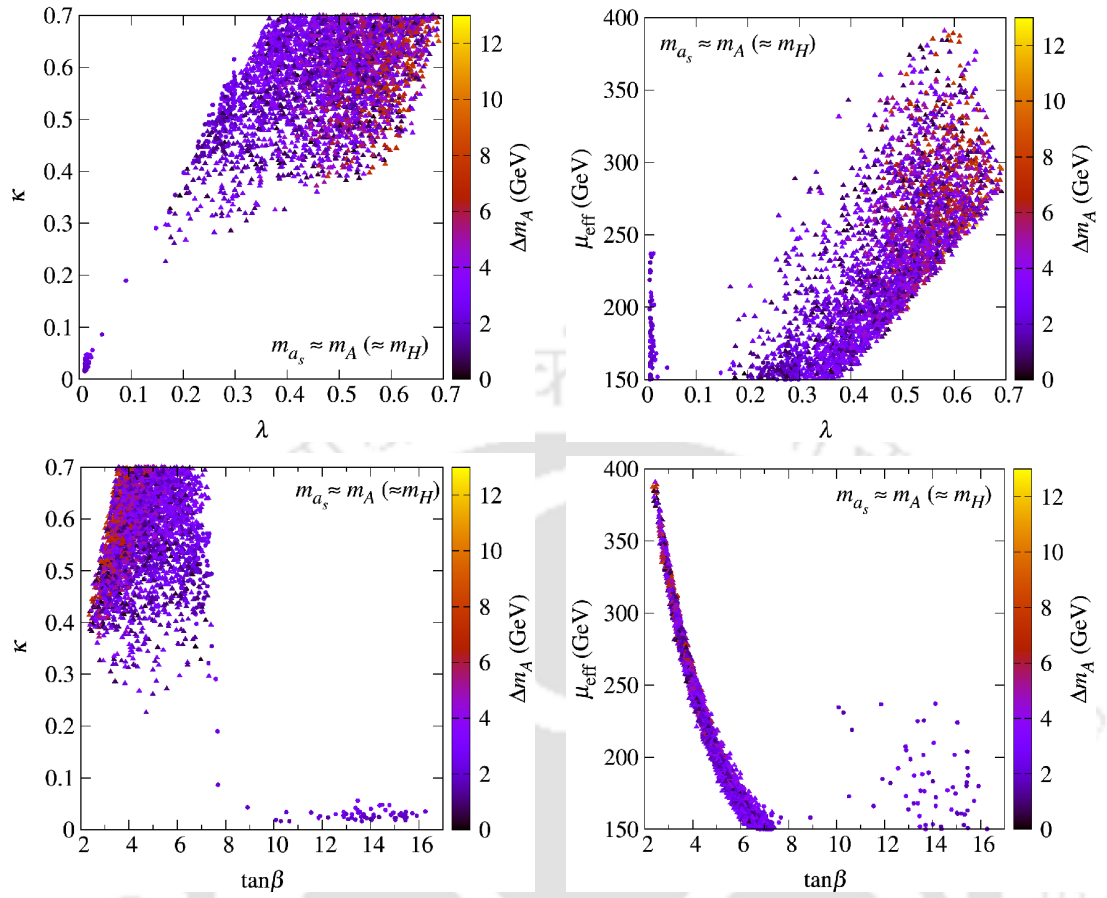

FIGURE 4.3: Distributions of the input parameters, showing the correlations among them that lead to a strong mass-degeneracy between a_s and A, for the points corresponding to scenario-2 obtained from the numerical scans.

but larger values of $\tan\beta$ (within the considered range). The reason is that the mass-degeneracy condition in this scenario effectively implies the decoupling of h_s from h too. The smaller values of λ essential for that in turn put a virtual cut-off on $\mu_{\rm eff} \equiv \lambda v_s$ of about 250 GeV, below which it can vary relatively freely.

Scenario-2 shows a much stronger dependence on the correlations between the input parameters, as seen in Fig. 4.3. In particular, the parameter space regions with smaller Δm_A are rather distinct for the $m_{h_s} < m_h$ and $m_{h_s} > m_h$ cases. Recall that the $m_{h_s} < m_h$ case forces the model into the 'natural' limit, so that both h and h_s are states with a large singlet-doublet mixing, made possible by larger λ and κ, and smaller $\tan\beta$. Such values of these parameters, with some fine tuning, allow $\mu_{\rm eff}$ to reach up to ~ 400 GeV. Note, however, that in the $m_{h_s} > m_h$ case also it is possible for h_s to be a highly mixed state lying very close in mass to the h, and for such points the parameter values can be similar to the ones in the $m_{h_s} < m_h$ case. Generally though, the parameter combinations in the $m_{h_s} > m_h$

case follow a somewhat similar trend to that seen for scenario-1, with relatively small (large) λ and κ ($\tan\beta$), and $\mu_{\rm eff}$ restricted to below 250 GeV.

4.4 Cross section analysis

As noted earlier, we selected some BPs from the two scenarios to study the impact of quantum interference between the Higgs bosons on the cross section for the $pp \to \tau^+\tau^-$ process at the LHC with $\sqrt{s} = 14$ TeV. The calculation of the cross sections $\sigma_{\rm BW}$ and $\sigma_{\rm Int}$ defined in Sec. 4.2.2 was carried out using a `Fortran` program developed in-house, which performs Higgs propagator matrix inversion and numerical integration through interfaces with the `LAPACK` package [270] and a locally modified version of the `VEGAS` routine [271], respectively. The Higgs boson masses and couplings for a given NMSSM parameter space point, which the program takes as inputs for the calculation of the propagator matrix as well as the form factors for Higgs boson production via gluon fusion, were written out by a suitably modified version of `NMSSMTools`.

For comparison, we also calculated $\sigma_{H_1 \ldots H_n}$ by multiplying the $\sigma(gg \to H_i)$ obtained from the public code `SusHi-v1.6.0` [272–274] with BR($H_i \to \tau^+\tau^-$) given by `NMSSMTools`. We note here that we required `SusHi` to evaluate these $\sigma(gg \to H_i)$ at the Next-to-Next-to-Leading Order (NNLO) in QCD, while our program calculates the production process only at the Leading Order (LO).[1] For a more accurate comparison, we therefore estimated the $k_{\rm NNLO}$ factor by obtaining also the LO $\sigma(gg \to H_i)$ from `SusHi` for each H_i in a given BP and multiplied our LO amplitude-squared with it before summing over all H_i's to obtain the total $\sigma_{\rm BW}$. In the case of $\sigma_{\rm Int}$ though, since the contribution due to every H_i is not computed separately, we simply multiply the total amplitude-squared with an average of the $k_{\rm NNLO}$ factors for the (three) Higgs bosons near a given $\tau^+\tau^-$ invariant mass (or, equivalently, $\sqrt{\hat{s}}$). For all the cross sections, the `CT10` [276] PDF sets were used for gluons and the default values of the SM input parameters inside `NMSSMTools` were retained, except for the t-quark mass, which was fixed to 172.5 GeV.

[1] Including higher order (HO) corrections for the production process is a highly involved task, which would be beyond the scope of this work. Their inclusion is, however, tantamount to rescaling the cross section for a given H_i by a 'k factor', which is defined as $k_{\rm HO} \equiv \sigma_{\rm HO}/\sigma_{\rm LO}$, with HO implying the perturbative order at which the cross section is to be evaluated. In this particular case study, $k_{\rm NNLO}$ varies between $2-3$ in the mass range under consideration.

BP	1	2	3	4	5	6
A_0 (GeV)	-4624.6	-4516.5	-4371.9	-4574.8	-4967.9	-4518.8
$\tan\beta$	13.90	13.84	15.14	15.84	6.42	5.65
λ	0.0045	0.0034	0.0035	0.0041	0.2965	0.3948
κ	0.0092	0.0068	0.0112	0.0141	0.5486	0.6197
$\mu_{\rm eff}$ (GeV)	217.34	217.73	150.50	152.63	151.21	172.92
mA (GeV)	926.92	904.00	994.13	998.86	898.56	902.80
mP (GeV)	72.37	698.12	189.83	626.85	919.23	931.95
m_h (GeV)	124.13	124.16	123.84	124.23	123.04	124.21
m_{h_s} (GeV)	889.98	893.37	970.47	973.01	191.07	107.13
m_H (GeV)	891.39	894.86	971.11	973.85	895.73	900.11
m_{a_s} (GeV)	72.36	218.19	189.83	626.84	893.97	896.63
m_A (GeV)	891.21	894.63	970.87	973.61	892.45	896.46
Δm_H (GeV)	1.41	1.49	0.64	0.84		
Δm_A (GeV)					1.53	0.17
Γ_h (MeV)	4.11	4.11	4.04	4.08	4.09	2.90
Γ_{h_s} (GeV)	1.75	1.93	0.71	2.01		
Γ_H (GeV)	1.73	1.92	3.75	2.79	3.65	4.84
Γ_{a_s} (GeV)					2.86	5.14
Γ_A (GeV)	3.53	3.87	4.49	4.82	3.65	4.72
BR($h \to \tau^+\tau^-$)	0.069	0.069	0.069	0.068	0.071	0.061
BR($h_s \to \tau^+\tau^-$)	0.103	0.102	0.103	0.106	0.005	0.091
BR($H \to \tau^+\tau^-$)	0.102	0.100	0.100	0.105	0.021	0.012
BR($a_s \to \tau^+\tau^-$)	0.087	0.012	0.010	0.002	10^{-5}	10^{-7}
BR($A \to \tau^+\tau^-$)	0.101	0.101	0.103	0.105	0.021	0.013
σ_{h_sHA} (fb)	0.547	0.537	0.334	0.322		
σ_{Ha_sA} (fb)					0.364	0.267
$\sigma_{\rm BW}$ (fb)	0.637	0.584	0.354	0.351	0.445	0.314
$\Delta\sigma_{\rm BW}$ (%)	16	9	6	9	22	17
$\sigma_{\rm Int}$ (fb)	0.565	0.514	0.314	0.286	0.445	0.314
$\Delta\sigma_{\rm Int}$ (%)	−11	−12	−11	−19	0	0

TABLE 4.2: Masses and decay widths of the Higgs bosons, and the cross sections obtained using the three approaches discussed in the text, for the six selected benchmark points. BPs 1–4 correspond to scenario-1 and BPs 5 and 6 to scenario-2. Blank space in front of a quantity implies that it is not relevant for the given BP.

The values of the input parameters, the masses and widths of the Higgs bosons, as well as the total cross sections calculated using each of the approaches explained above are given in Tab. 4.2 for all the selected BPs. BP1–BP4 correspond to scenario-1, and the first one of these has been selected such that m_{h_s} and m_H lie very close to their lowest observed values, in order to minimize phase-space suppression of the cross section, while also requiring $\Lambda_{H_{1,2}} > 1$. However, these

masses are still close to 900 GeV and thus, while the $\sigma_{H_1...H_n}$ for this BP is the highest among all, it nevertheless stays just below 1 fb. Also noted down in the table is the quantity $\Delta\sigma_{\rm BW} \equiv \frac{\sigma_{\rm BW}-\sigma_{H1...H_n}}{\sigma_{H1...H_n}} \times 100$ and its value for BP1 indicates that the total cross section assuming BW propagators is enhanced by about 16% over the one obtained using the NWA. $\Delta\sigma_{\rm Int} \equiv \frac{\sigma_{\rm Int}-\sigma_{\rm BW}}{\sigma_{\rm BW}} \times 100$ in the last row of the table similarly quantifies the impact of including the full propagator matrix in the amplitude. We note that $\sigma_{\rm Int}$ is 11% smaller than $\sigma_{\rm BW}$, implying that the interference between the h_s and H propagators is destructive, reducing the total cross section somewhat, although it is still significantly larger than σ_{h_sHA} (i.e, $\sigma_{H1...H_n}$, defined in Eq. 4.10, calculated assuming the NWA for $H_1, ..., H_n = h_s$, H, A).

For all the points with m_{h_s} and m_H similar to those for BP1, $\Lambda_{H_{1,2}}$ stays very close to 1. Larger values of these ratios are typically obtained for higher masses, and BP2 was selected such that it has the former slightly increased, while the latter are still below 900 GeV. Even this slight increase in mass reduces each cross section by a few percent compared to the BP1 case, while enhancing the interference effects only marginally. The interference for this BP, and in fact also for the other two BPs for scenario-1, is again destructive. The selection criteria for BP3 were maximal Λ_{H_1} only, while for BP4 maximal $\Lambda_{H_{1,2}}$, with their respective m_{h_s} and m_H being very similar. This effectively implies that for BP3 one has $\Gamma_{H_2}(=\Gamma_{h_s})$ considerably smaller than $\Gamma_{H_1}(=\Gamma_H)$, while for BP4 both these widths are much closer in size. This difference leads to a clear rise in the magnitude of interference for BP4, which leads to a $\Delta\sigma_{\rm Int}$ of 19%, compared to the BP3, for which the increase in the cross section is 11%, similar to BPs 1 and 2. $\Delta\sigma_{\rm BW}$ for BPs 3 and 4 are also considerably smaller than for BP1, despite a large hike in m_{h_s} and m_H, as is the respective absolute value of each type of the cross section itself. Note that $\mu_{\rm eff}$ for both these high-mass BPs lies just above the effective exclusion limit from ATLAS discussed earlier, and could thus be within the reach of subsequent analyses at the LHC in the near future. BR($H_i \to \tau^+\tau^-$), with $H_i = h_s$, H, A, for BP1 to BP4 is $\sim 10\%$.

BP5 belongs to the $m_{h_s} > m_h$ case and BP6 to the $m_{h_s} < m_h$ case in scenario-2. For BP5 one finds that Γ_{a_s} is somewhat smaller than Γ_A, while for BP6 the two widths are much closer in magnitude. Furthermore, $\sigma_{\rm BW}$ shows an enhancement of about 22% over σ_{Ha_sA} for BP5, but $\sigma_{\rm Int}$ is same as $\sigma_{\rm BW}$, implying negligible interference between the a_s and A propagators. This is also the case for BP6,

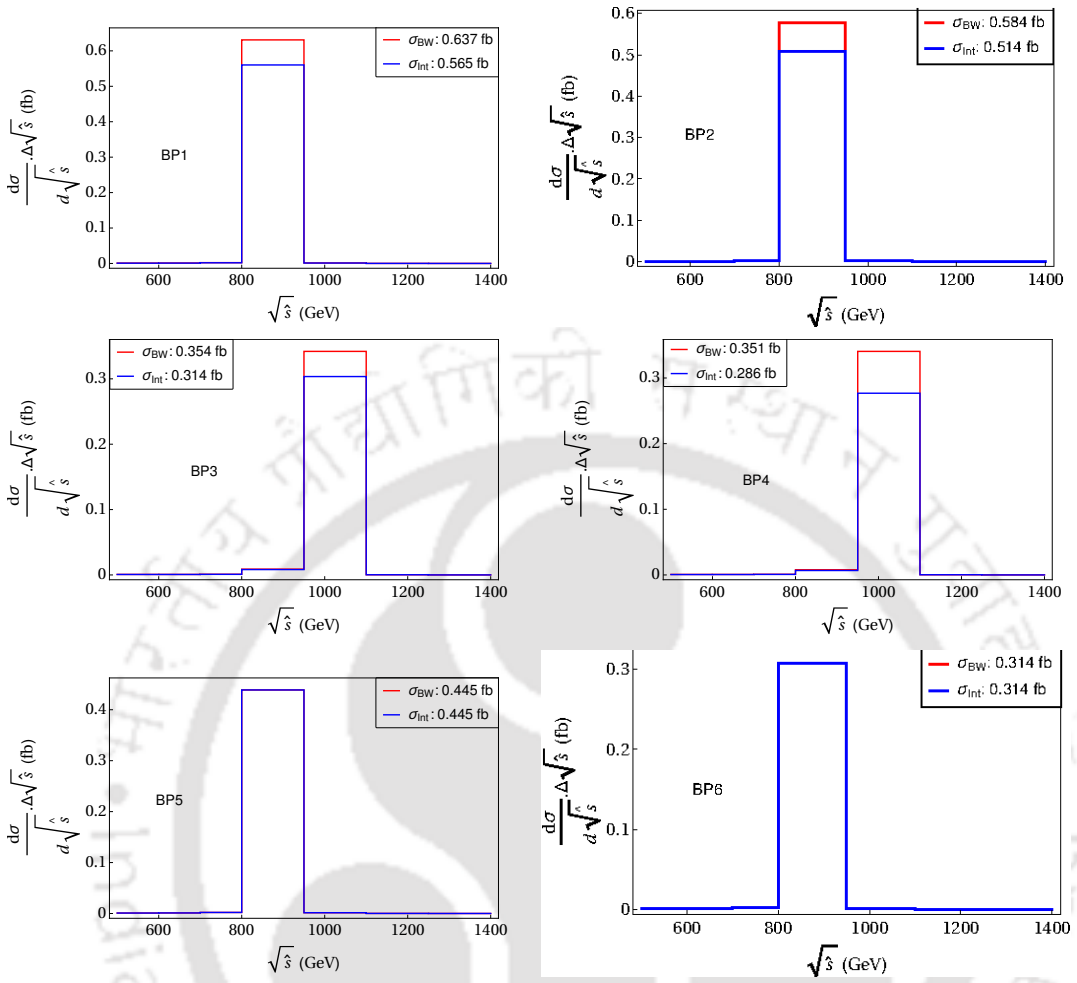

FIGURE 4.4: Distributions of the differential cross sections with respect to $\sqrt{\hat{s}}$ for the six selected BPs. The blue lines correspond to the amplitude containing the full Higgs propagator matrix, and the red lines to the one assuming individual BW propagators.

despite Λ_{a_s} and Λ_A both being very large owing to the very small mass splitting between a_s and A. $\sigma_{h_s HA}$ for BP6 is sizably smaller than for BP5, which is a consequence of the relatively small BR($A \to \tau^+\tau^-$), even though the respective pseudoscalar masses are only about 4 GeV larger. Notice that for both of these BPs, even though Γ_{a_s} are of order 1 GeV, the $\tau^+\tau^-$ partial decay widths, and hence the BR($a_s \to \tau^+\tau^-$), are extremely small, resulting in vanishing interference effects.

Moving on, the differential cross sections $\sigma_{\rm BW}$ and $\sigma_{\rm Int}$ with respect to $\sqrt{\hat{s}}$, which corresponds to the invariant mass of the tau pair, are computed to examine if the interference effects can make observable impact in the shape analysis that may be performed at the HL-LHC. For this we employ a binning template closely replicating the one used by the ATLAS collaboration in the searches for heavy

resonances in the $\tau^+\tau^-$ decay channel [298], based on an expected detector mass resolution of $\sim 15-20\%$ of $M_{\tau^+\tau^-}$. Our template thus assumes bins of width 50 GeV, 100 GeV and 150 GeV for $\sqrt{\hat{s}} = 0-500$ GeV, $500-800$ GeV and $800-1400$ GeV, respectively. The differential distributions are shown in Fig. 4.4 for all the six BPs, with the red lines corresponding to $\sigma_{\rm BW}$ and the blue ones to $\sigma_{\rm Int}$. Since the mass-degenerate Higgs bosons in both the scenarios investigated are always heavier than 800 GeV and the remaining two Higgs bosons typically much lighter, these distributions have a lower cut-off at $\sqrt{\hat{s}} = 500$ GeV. In fact, for these distributions we included only H_i with $i = 3-5$ in the calculation of the two differential cross sections.

Importantly though, the two differential distributions do not reveal much beyond what can be inferred from the total cross sections, owing to the poor $M_{\tau^+\tau^-}$ resolution at the LHC. We noticed earlier that Δm_H in scenario-1 never exceeds 4 GeV, and even this maximum value is about 1/38 of the adopted widths of the bins around $\sqrt{\hat{s}} = 1$ TeV, despite $\sim 0.15 \times M_{\tau^+\tau^-}$ itself being on the conservative side of the expected detector resolution. Thus, the red boxes in each of the first four panels of Fig. 4.4 rise higher than the blue ones (recall that the interference is always destructive) only in the bins within which the three mass-degenerate Higgs bosons lie. In the remaining bins, the boxes in the two histograms almost entirely overlap. Evidently, for BP5 and BP6 from scenario-2, a complete overlapping of the two lines occurs even in the bin containing the three heavy Higgs bosons (so that the red lines, plotted first, are entirely invisible behind the blue ones), since no interference effects appear there.

Finally, we took the distributions for the differential $\sigma_{\rm BW}$ and $\sigma_{\rm Int}$ for the four BPs of scenario-1 and convolved them with a Gaussian of 150 GeV width. The purpose of this exercise is to emulate the detector effect of smearing the cross sections over a few adjacent bins, to see whether the resulting distributions can be visually distinguishable from each other, despite the poor mass resolution. Fig. 4.5 shows these convolved distributions. We note that the convolution spreads out the differences in the heights of the red and blue boxes to the bins around the ones containing the resonant Higgs masses. However, the shapes of these convolved distributions for $\sigma_{\rm Int}$ do not show any peculiar features. They could very well be the distributions of the differential $\sigma_{\rm BW}$ for slightly different parameter space points, with the peaks arising from a single heavy Higgs resonance or even from nearly mass-degenerate H and A (with the underlying model being simply the

MSSM). Therefore, even with an integrated luminosity as large as 3000 fb^{-1} (as assumed in this figure, in order to reduce the sizes of the error bars, which account for the statistical error only), the LHC will not be able to exploit the interference effects in order to identify two Higgs resonances with highly identical masses.

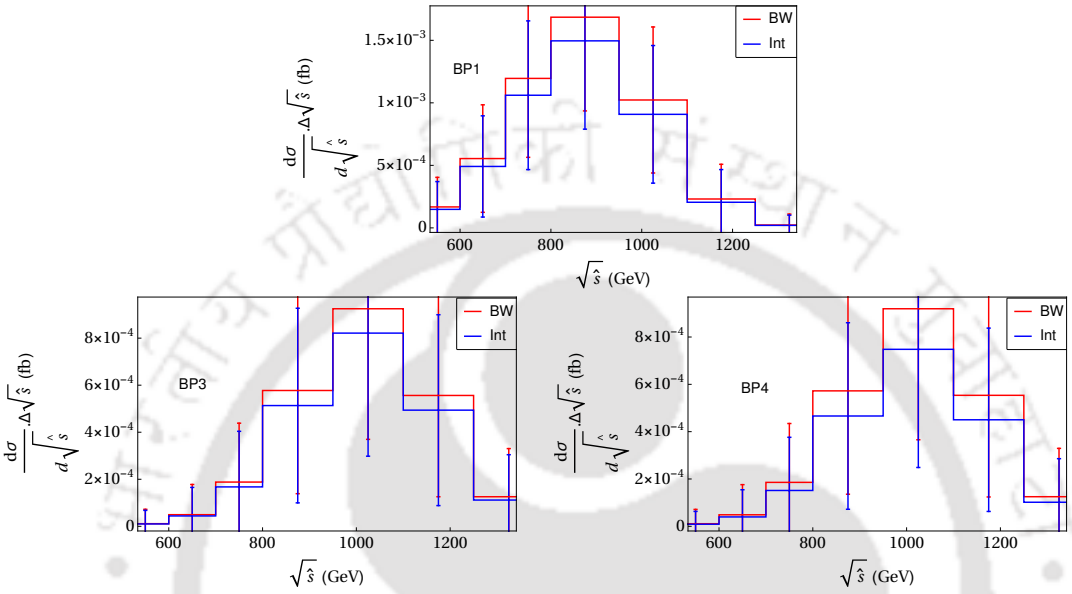

FIGURE 4.5: Distributions of the differential cross sections for three selected BPs from scenario-1, after convolution with Gaussians of width 150 GeV. The color convention for the lines is the same as in Fig. 4.4, and the error bars on them correspond to an assumed integrated luminosity of 3000 fb^{-1}.

4.5 Conclusions

The commonly adopted approach of calculating the cross section for a given $2 \to 2$ process by factorizing it into the production and decay parts, assuming a narrow width(s) of the mediator(s), by construction cannot account for the possible quantum interference among the propagators of several mass-degenerate states. In this chapter, we have considered the specific example of the NMSSM, wherein nearly identical-mass pairs of CP-even or CP-odd Higgs bosons are viable over large regions of the parameter space. These regions were found by numerical scanning of broad ranges of the model parameters, while imposing the most important experimental constraints, including those from the LHC pertaining to the Higgs, exotic and flavor sectors as well as those from the DM searches.

By analyzing six illustrative benchmark points from the scanned set, we have highlighted the importance of taking the interference effects into account. This was

done by including the full propagator matrix in the calculation of the cross section for the process of production of $\tau^+\tau^-$ in gluon fusion at the 14 TeV LHC. We have shown that this cross section can deviate considerably from the one obtained by employing the NWA, and even from the one obtained assuming BW propagators, an approach most experimental searches are based on. This deviation, in fact, implies a reduction in the cross section in the case of two mass-degenerate CP-even Higgs bosons, as the interference is always destructive. In the case of CP-odd states, on the other hand, no interference effects appear. We have also reasserted the fact that the smaller the mass-splitting between two nearby Higgs bosons compared to the sum of their widths, the larger the interference effects.

The reason for considering the $\tau^+\tau^-$ decay channel of the Higgs bosons is that the $\gamma\gamma$ channel, while cleaner, has a prohibitively small decay rate for Higgs bosons with masses close to 1 TeV.[2] The BR for the $\tau^+\tau^-$ is significantly larger, but the price to pay is a poor experimental resolution. As a result of this, we have concluded that the LHC will not be able to disentangle the two resonances, even if they have a mass splitting of a few GeV and the integrated luminosity is as large as 3000 fb^{-1}. Alternative Higgs boson production and decay modes that might be more suitable for this purpose are therefore the subject of a future study. However, this study has clearly brought out the importance of including the quantum interference effects in the case of closely degenerate resonances. With the effects between 10% and 20% in the degenerate scalar cases considered, ignoring such effects would result in misinterpretation of the model parameter region.

[2]For W^+W^- and ZZ channels, the corresponding BRs are smaller by three order of magnitude as compared to $\tau^+\tau^-$ mode.

Chapter 5

Summary and conclusions

The discovery of the 125 GeV Higgs boson at the LHC, establishing the Higgs mechanism as the way to achieve electroweak symmetry breaking, has opened an era of detailed studies of the Higgs sector. Although the measurements so far are compatible with the SM expectations, there are unsettled issues like the hierarchy problem, presence of dark matter and dark energy, non-zero neutrino masses, matter-antimatter asymmetry, to which SM has no answer. Many new models, classified as beyond the Standard Models, have been proposed to address these issues. SUSY models, multiple Higgs doublet models, and models with extra dimensions are some popular formalisms in the BSM scenario. These models typically introduce new interactions and particles that are absent in the SM, with masses possibly in the TeV range − an energy regime within the reach of the LHC. This possibility to explore their signatures at the LHC makes their phenomenological study interesting, and into some extent essential.

SUSY models are the most popular and most intensely studied BSM scenarios, which have a class of new particles, as they relate bosonic and fermionic degrees of freedom, making the phenomenology interesting, rich and well-motivated. Specifically, in the wake of the discovery of the Higgs boson in 2012, viability of different versions of SUSY scenarios has become an important objective of recent phenomenological studies. Several studies have been performed within different SUSY models, like the MSSM, and the NMSSM, to explain the LHC Higgs data. These models can have a SM-like Higgs boson with mass around 125 GeV and also accommodate potential slight disagreement between the data and SM predictions in different decay channels of the observed Higgs boson. Within the CP-conserving

MSSM, such solutions indicate the presence of relatively heavy stop and large tanβ. On the other hand, as shown in chapter 2, the CP-violating MSSM could provide a viable solution with relatively lighter stop and smaller tanβ, at the same time satisfying stringent flavor and electric dipole moment constraints. Besides the fact that the CP-violating MSSM is more compatible with the LHC Higgs studies, CP violation is one of main conditions required to generate the baryon asymmetry of the universe. In the SM, CP violation based on the Cabibbo-Kobayashi-Maskawa matrix is too small to explain quantitatively the baryon asymmetry. Also, the presence of non-observable parameters in the SUSY potential implying the complex nature of those parameters, which can justify the existence of CP violation naturally. These facts lure to focus particularly on those BSM scenarios which contain additional sources of CP violation. Even though the LHC Run 2 data tightly constrain the CP-conserving MSSM parameter space excluding regions with $\tan\beta$ above 9, we have shown in chapter 2 that the CP-violating MSSM is a viable candidate for a large span of its parameter space region. On the other hand, the NMSSM performs much better than the MSSM. Firstly, it is theoretically more formidable, having advantage over the MSSM, with no $\mu-$problem and the little hierarchy problem arising, and possessing novel collider signatures, like, a light possible pseudoscalar state. Moreover, CP violation can be invoked in the NMSSM Higgs sector at the tree-level by assuming the Higgs self-couplings λ and κ to be complex, unlike the MSSM, where CP violation enters via Higgs-sfermion couplings at one-loop level. Recent investigations on explicit CP violation in the NMSSM Higgs sector suggest that any one of the three lightest neutral Higgs bosons could be the observed one, or two lightest Higgs bosons around 125 GeV could actually be visible as a single resonance at the LHC. We explore such a possibility of mass-degenerate scenario in chapter 3, where apart from the individual contributions of the two closely lying resonances, their possible quantum interference effects through mixing in the propagator is considered. It is well known that flavor observables such as the branching ratios of flavor changing neutral current processes, like, $B_s \to \mu^+\mu^-$, along with the EDM measurements play a crucial role in determining the viable regions of the SUSY parameter space. Taking these possibilities into account, different phenomenological scenarios within the framework of the CP-violating NMSSM, make it a particularly interesting model for exploration at the LHC Run 2 and future colliders. In all these viable SUSY frameworks, additional scalar resonances are possible in sub-TeV region. The possibilities of heavy and mass-degenerate resonances and quantum interference effects could also

be important, as explored in chapter 4. Focusing on this philosophy, the thesis aims to connect the existing theoretical studies with the experiments at the LHC and future colliders in order to extract any novel BSM signature in the context of the MSSM and the NMSSM with a special attention to the CP-nature of the Higgs sector.

In chapter 1 we have provided a brief introduction of the standard model of particle physics along with its main drawbacks. Describing the standard mechanism of electroweak symmetry breaking we have briefly discussed how the elementary particles acquire their masses through the Higgs mechanism. This chapter also describes the theoretical background of the models considered in this thesis, viz., the MSSM and the NMSSM, as enlisted above. We have presented a clear picture of the present status of the related works available in the literature, and provided the experimental status of the scenarios being considered.

In chapter 2, in order to probe the 125 GeV Higgs resonance discovered at the LHC in the context of the MSSM, we study the CPV-MSSM parameter space in order to accommodate the 125 GeV Higgs boson with signal event rates consistent with the observed LHC data and all other available experimental bounds till date, including the different EDM constraints, namely the electron, neutron, mercury and thallium EDMs. We further impose several low energy constraints, mainly those coming from different flavor physics processes. We vary the CPV phases of the gluino mass parameter M_3, trilinear couplings A_t, A_b and A_τ from 0^o to 90^o, which affect the Higgs sector strongly. We perform two separate parameter space scans: (a) with some of the CPV phases setting to their maximal value (90^o) and (b) varying these phases from 0^o to 90^o. For both of these scans, other parameters vary randomly within some specified ranges. Our study conclude that the maximal phase scenario (case (a)) is ruled out by the current EDM measurements, especially the updated electron EDM measurement. However, we find significant span of parameter space points in case (b) satisfying all the constraints including those coming from the EDM measurements. Working within the parameter space region respecting the above constraints, we select out a few illustrative benchmark points to compute the signal rates of the Higgs boson in the $gg \to h_1 \to \gamma\gamma$, $gg \to h_1 \to ZZ^* \to 4\ell$, $gg \to h_1 \to WW^* \to \ell\nu\ell\nu$, $qq \to h_1 \to b\bar{b}$ and $qq \to h_1 \to \tau^+\tau^-$ channels. It is found that over a large span of the CP-violating MSSM parameter space, our results are compatible within 1σ-2σ error levels of the observed data analyzed

by the ATLAS and CMS collaborations, providing a much broader scope for the CP-violating MSSM compared to its CP-conserving counterpart.

Looking into the details, we find some interesting results in terms of some of the observables of the CP-violating MSSM. The couplings of the Higgs boson with the bottom quark and top quark are very important to probe any nuanced BSM signature associated with the SM-like boson discovered at the LHC. We find that the imaginary part of the top and bottom Yukawa couplings can take very small but non-zero values even after satisfying all the latest updates from both the CMS and ATLAS collaborations within $1\sigma - 2\sigma$ uncertainty. Moreover, we find an interesting result from the correlation plots of the different signal strength variables. We do not find any significant excess in the $\gamma\gamma$, W^+W^- and ZZ^* decay modes, but we do see excess of events over the SM predictions for both the $b\bar{b}$ and $\tau^+\tau^-$ channels, when the Higgs boson is produced through vector boson fusion (VBF). The suppression in the di-photon decay mode with simultaneous enhancement in $b\bar{b}$ and $\tau^+\tau^-$ decay modes with respect to the SM prediction and presence of non-zero imaginary parts of the top and bottom Yukawa couplings, could be interesting signatures of this model. In addition to that, we also find that it is possible to have a Higgs mass of about 125 GeV with relatively small $\tan\beta$, large A_t and a light stop, which is consistent with the current supersymmetric searches at the LHC. Thus, these findings point to the fact that the CPV-MSSM provides a viable solution to the updated LHC Higgs data, in fact offering very little in the way of distinction between these two SUSY models at the current LHC Run 2. Improvement in different Higgs coupling measurements is necessary in order to test the possibility of probing the mild dependence of these CPV phases in the Higgs sector of the minimal SUSY realization.

In the third chapter of the thesis, we scrutinize in detail the proton-proton to di-photon process, through which a 125 GeV resonance consistent with the SM Higgs boson has been discovered at the LHC. Indeed, it is the process for which the Higgs mass resolution is highest amongst all those accessible at the CERN colliders. Measurements of its cross section, at both the inclusive and exclusive level, however, do not exclude the possibility of non-SM explanations. Amongst these, particularly intriguing are those invoking two Higgs bosons produced via gluon fusion, with such a small mass difference that they cannot be resolved by the experimental apparata. This scenario can emerge only in non-minimal realizations of SUSY, such as the NMSSM, wherein, unlike the MSSM, two coexisting Higgs

bosons can contribute to the 125 GeV signal. In this case, an accurate treatment of the propagation of the two states is required, which not only goes beyond the narrow width approximation but also allows for full interference between these. Hence, we have studied the quantitative impact of interference between two Higgs states near 125 GeV, with and without mixing effects, relative to the simplistic approach where the two resonant objects are treated independently of each other. For a full treatment, including the possibility of complex couplings as well, we have considered both real and complex NMSSM.

Our analysis involved scanning of the parameter space of the model for finding possible solutions consistent not only with the LHC exclusion limits on the additional Higgs bosons but also with the constraints from EDM measurements. These scans further collected only model solutions yielding two Higgs bosons with masses lying within the uncertainty of the measurements of the 125 GeV resonance. This was followed by a dedicated computation, performed with the help of a locally developed MC program, producing both integrated and differential cross sections for the full process $pp(gg) \to H_1, H_2 \to \gamma\gamma$. We have found that the aforementioned interference effects can be sizable, with some of the selected BPs providing a difference of around 40% in inclusive rates between the standard approach consisting in treating the two resonances as separate Breit-Wigner functions and the full propagator one including all non-trivial quantum effects. We also considered the possibility of a shape analysis of the emerging profile, which could reveal the presence of multiple resonances, assuming realistic, current and prospective, di-photon mass resolutions of the LHC detectors. This revealed some long-term potential to see the difference between the generally exploited simplistic case of assuming two separate resonances and the one where the two nearly mass-degenerate states interfere due to the inclusion of the complete propagator matrix in the amplitude calculation. These differences are in fact more visible with a smaller di-photon mass resolution and a larger data sample, both of which can only be achieved with upgraded detectors. Finally, in attempting to distinguish the two approaches, we have also noted a tension in the underlying dynamics. Any distortion effect of a single BW shape can only be exploited when the mass difference is sufficiently larger than the assumed width of the bins (which should naturally be consistent with the available experimental mass resolution) in the distribution of the differential cross section. However, a larger mass difference leads to smaller interference effects.

In the fourth chapter, we consider the specific example of the NMSSM, wherein nearly identical-mass pairs of CP-even or CP-odd Higgs bosons are viable over large regions of the parameter space. These regions were found by numerical scanning of broad ranges of the model parameters, while imposing the most important experimental constraints, including those from the LHC pertaining to the Higgs, exotic and flavor sectors as well as those from the DM searches. Here the commonly adopted approach of calculating the cross section for a given $2 \to 2$ process by factorizing it into the production and decay parts, assuming a narrow width(s) of the mediator(s), by construction cannot account for the possible quantum interference among the propagators of several mass-degenerate states.

By analyzing six illustrative benchmark points, we have highlighted the importance of taking the interference effects into account. This was done by including the full propagator matrix in the calculation of the cross section for the process of production of $\tau^+\tau^-$ in gluon fusion at the 14 TeV LHC. We have shown that this cross section can deviate considerably from the one obtained by employing the NWA, and even from the one obtained assuming BW propagators, an approach most experimental searches are based on. This deviation, in fact, implies a reduction in the cross section in the case of two mass-degenerate CP-even Higgs bosons, as the interference is always destructive. In the case of CP-odd states, on the other hand, no interference effects appear. We have also reasserted the fact that the smaller the mass-splitting between two nearby Higgs bosons compared to the sum of their widths, the larger the interference effects. The reason for considering the $\tau^+\tau^-$ decay channel of the Higgs bosons is that the $\gamma\gamma$ channel, while cleaner, has a prohibitively smaller decay rate for Higgs bosons with masses close to 1 TeV. The BR for the $\tau^+\tau^-$ is significantly larger, but the price to pay is a poor experimental resolution and mass reconstruction. As a result of which, we have concluded that the LHC will be unable to disentangle the two resonances, even if they have a mass splitting of a few GeV and the integrated luminosity is as large as $3000\,\text{fb}^{-1}$. Thus, even though the $gg \to \tau^+\tau^-$ channel is an effective search instrument for heavy Higgs bosons, in the particular scenario with closely mass-degenerate states, this channel would not be able to resolve them. Alternative Higgs boson production and decay modes will be required for this purpose, which is left for a future study.

In summary, our study has established that the MSSM and the NMSSM, with CP violation is included in their Higgs sectors, are very much consistent with

the measurements performed at the LHC, at the same time compatible with all other known measurements in the EDM and flavor sectors. Further, we have established that possibilities of multiple resonances which are closely degenerate in their masses are viable solutions within both the CPC and CPV versions of NMSSM. Conclusions drawn without considering the effects of such degenerate resonances, especially their quantum interference effects, may lead to erroneous results, as such effects can be significant. Further, extending such possibilities, we have studied possibilities with heavy Higgs states with mass close to a TeV in their decay to a pair of tau leptons, showing distinct effects of quantum interference between the degenerate states.

Appendix A

Chapter 1

A.1 CPC-NMSSM Higgs mass matrix at tree-level

The explicit expressions for the Higgs mass matrices and the tadpoles coefficients are given below. [74, 75, 299].

Tree-level expressions: In the CPC-NMSSM the Higgs mass matrices, $\mathbf{M}_H, \mathbf{M}_A, \mathbf{M}_{H^\pm}$, are hermitian 3×3 and 2×2 matrices, respectively. Their independent entries read for the CP-even fields

$$(\mathbf{M}_H)_{11} = \widetilde{m}_1^2 + \lambda^2 v_u^2 + \frac{1}{4}\left(g_1^2 + g_2^2\right)\left(3v_d^2 - v_u^2\right) , \tag{A.1a}$$

$$(\mathbf{M}_H)_{22} = \widetilde{m}_2^2 + \lambda^2 v_d^2 + \frac{1}{4}\left(g_1^2 + g_2^2\right)\left(3v_u^2 - v_d^2\right) , \tag{A.1b}$$

$$(\mathbf{M}_H)_{33} = m_s^2 + \lambda^2\left(v_u^2 + v_d^2\right) - 2\lambda\kappa v_u v_d + 6\kappa^2 s^2 + 2\kappa s A_\kappa , \tag{A.1c}$$

$$(\mathbf{M}_H)_{12} = (\mathbf{M}_H)_{21} = -\mu_{\text{eff}} B + 2\lambda^2 v_u v_d - \frac{1}{2}\left(g_1^2 + g_2^2\right) v_u v_d , \tag{A.1d}$$

$$(\mathbf{M}_H)_{13} = (\mathbf{M}_H)_{31} = -\frac{v_u}{s}\mu_{\text{eff}} B + \lambda s(2\lambda v_d - \kappa v_u) , \tag{A.1e}$$

$$(\mathbf{M}_H)_{23} = (\mathbf{M}_H)_{32} = -\frac{v_d}{s}\mu_{\text{eff}} B + \lambda s(2\lambda v_u - \kappa v_d) , \tag{A.1f}$$

for the CP-odd fields

$$(\mathbf{M}_A)_{11} = \widetilde{m}_1^2 + \lambda^2 v_u^2 - \frac{1}{4}\left(g_1^2 + g_2^2\right)\left(v_d^2 - v_u^2\right) , \tag{A.2a}$$

$$(\mathbf{M}_A)_{22} = \widetilde{m}_2^2 + \lambda^2 v_d^2 - \frac{1}{4}\left(g_1^2 + g_2^2\right)\left(v_u^2 - v_d^2\right) , \tag{A.2b}$$

$$(\mathbf{M}_A)_{33} = m_s^2 + \lambda^2\left(v_u^2 + v_d^2\right) + 2\lambda\kappa v_u v_d + 2\kappa^2 s^2 - 2\kappa s A_\kappa , \tag{A.2c}$$

$$(\mathbf{M}_A)_{12} = (\mathbf{M}_A)_{21} = -\mu_{\text{eff}} B , \tag{A.2d}$$

$$(\mathbf{M}_A)_{13} = (\mathbf{M}_A)_{31} = -\frac{v_u}{s}\mu_{\text{eff}} B + 2\kappa v_u s , \tag{A.2e}$$

$$(\mathbf{M}_A)_{23} = (\mathbf{M}_A)_{32} = \frac{v_d}{s}\mu_{\text{eff}} B - 2\lambda\kappa v_d s , \tag{A.2f}$$

and for the charged fields

$$(\mathbf{M}_{H^\pm})_{11} = \widetilde{m}_1^2 + \frac{1}{4}g_1^2\left(v_d^2 - v_u^2\right) + \frac{1}{4}g_2^2\left(v_u^2 + v_d^2\right) , \tag{A.3a}$$

$$(\mathbf{M}_{H^\pm})_{22} = \widetilde{m}_2^2 + \frac{1}{4}g_1^2\left(v_u^2 - v_d^2\right) + \frac{1}{4}g_2^2\left(v_u^2 + v_d^2\right) , \tag{A.3b}$$

$$(\mathbf{M}_{H^\pm})_{12} = (\mathbf{M}_A)_{21} = -\mu_{\text{eff}} B + \lambda^2 v_u v_d - \frac{1}{2}g_2 v_u v_d , \tag{A.3c}$$

where $\widetilde{m}_1^2 = m_{H_{dR}}^2 + \lambda^2 s^2$, $\widetilde{m}_2^2 = m_{H_{uR}}^2 + \lambda^2 s^2$ and $\mu_{\text{eff}} B = \lambda s(\kappa s + A_\lambda)$. The Higgs mass matrices are diagonalized according to Eq. 1.58.

Charged Higgs mass: The relation between parameter A_λ or $\mu_{\text{eff}} B$, and the charged Higgs mass at lowest order is obtained by diagonalizing the charged Higgs mass matrix $\mathbf{M}_{H^\pm}$ from Eq. A.3a. With the real angle β_c, the masses of the charged Higgs and unphysical Goldstone pairs read

$$M_{H^\pm}^2 = (\mathbf{M}_{H^\pm})_{11}\sin^2\beta_c + (\mathbf{M}_{H^\pm})_{22}\cos^2\beta_c - 2(\mathbf{M}_{H^\pm})_{12}\sin\beta_c\cos\beta_c , \tag{A.4a}$$

$$M_{G^\pm}^2 = (\mathbf{M}_{H^\pm})_{11}\cos^2\beta_c + (\mathbf{M}_{H^\pm})_{22}\sin^2\beta_c + 2(\mathbf{M}_{H^\pm})_{12}\sin\beta_c\cos\beta_c . \tag{A.4b}$$

The explicit value for β_c can be obtained by the requirement that the mass of the charged Goldstone pair depends only on the tadpole coefficients and thus vanishes at tree-level for the contribution from the Higgs sector. In general there are also contributions from the gauge-fixing term. In case of β, $\beta_c \in [0, 2\pi)$ this is true, if $\beta_c = \beta$, which yields

$$M_{H^\pm}^2 = -\frac{1}{\sqrt{2}v}\left(\frac{\sin^2\beta}{\cos\beta}T_{H_{dR}} + \frac{\cos^2\beta}{\sin\beta}T_{H_{uR}}\right)\frac{\mu_{\text{eff}} B}{\sin\beta\cos\beta} + m_W^2 + \lambda^2 v^2 , \tag{A.5a}$$

$$M_{G^\pm}^2 = -\frac{1}{\sqrt{2}v}\left(T_{H_{dR}}\cos\beta + T_{H_{uR}}\sin\beta\right) , \tag{A.5b}$$

where $v^2 = v_u^2 + v_d^2$ and the tadpole coefficients $T_{H_{dR}}, T_{H_{uR}}$ are given below. By solving Eq. A.5a for $\mu_{\text{eff}} B$ one obtains

$$\mu_{\text{eff}} B = \frac{1}{\sqrt{2}v}\left(\sin^3\beta T_{H_{dR}} + \cos^3\beta T_{H_{uR}}\right) + \left(m_{H^\pm}^2 - m_W^2 + \lambda^2 v^2\right)\sin\beta\cos\beta\,. \quad \text{(A.6)}$$

Note that the angle β_c is not an independent parameter.

Tadpole coefficients: The tadpole coefficients in the interaction basis are defined as the first derivatives of the Higgs potential with respect to the Higgs fields taken in the classical minimum, where all fields vanish. In order to obtain a stable minimum all first derivatives with respect to the Higgs fields have to vanish,

$$T_{H_i} = \frac{\partial}{\partial H_i} V_H \Big|_{H_j, A_m, H_l^\pm = 0} = 0\,, \quad \text{(A.7a)}$$

$$T_{A_i} = \frac{\partial}{\partial A_i} V_H \Big|_{H_j, A_m, H_l^\pm = 0} = 0\,, \quad \text{(A.7b)}$$

$$T_{H_i^\pm} = \frac{\partial}{\partial H_i^\pm} V_H \Big|_{H_j, A_m, H_l^\pm = 0} = 0\,, \quad \text{(A.7c)}$$

with $H_i = H_{dR}, H_{uR}, S_R$, $A_i = H_{dI}, H_{uI}, S_I$ and $H_i^\pm = H_u^+, H_d^-$.

At tree-level all tadpole coefficients are zero, but they receive higher order corrections. Thus it is necessary to treat them as non-vanishing quantities and neglect them only after their renormalization transformations are applied.

In the NMSSM with real parameters, Eq. A.7b & A.7c are always fulfilled due to CP- and C-conservation. However, this is not true for Eq. A.7a. In order to fulfill these conditions for the CP-even fields it is necessary to choose three free parameters, normally the soft Higgs masses, such that the tadpoles for the CP-even fields vanish. If Eq. A.7a is fulfilled, the soft Higgs masses are given by

$$\widetilde{m}_1^2 = -\frac{T_{H_{dR}}}{\sqrt{2}v_u} + \frac{v_u}{v_d}\mu_{\text{eff}} B - \lambda^2 v_u^2 + \frac{1}{4}\left(g_1^2 + g_2^2\right)\left(v_u^2 - v_d^2\right)\,, \quad \text{(A.8a)}$$

$$\widetilde{m}_2^2 = -\frac{T_{H_{uR}}}{\sqrt{2}v_d} + \frac{v_d}{v_u}\mu_{\text{eff}} B - \lambda^2 v_d^2 + \frac{1}{4}\left(g_1^2 + g_2^2\right)\left(v_d^2 - v_u^2\right)\,, \quad \text{(A.8b)}$$

$$m_s^2 = -\frac{T_{S_R}}{\sqrt{2}s} + \frac{v_u v_d}{s^2}\mu_{\text{eff}} B - \lambda^2\left(v_u^2 + v_d^2\right) + \lambda\kappa v_u v_d - 2\kappa^2 s^2 - \kappa s A_\kappa\,. \quad \text{(A.8c)}$$

The expressions for the soft SUSY breaking parameters given in Eq. A.8 in terms of the new set of independent parameters (namely, $\tan\beta$ and v) read

$$\widetilde{m}_1^2 = -\frac{T_{H_{dR}}}{\sqrt{2}v\sin\beta} + \mu_{\rm eff}B\tan\beta - \lambda^2v^2\sin^2\beta + \frac{1}{4}m_Z^2\left(\sin^2\beta - \cos^2\beta\right), \quad \text{(A.9a)}$$

$$\widetilde{m}_2^2 = -\frac{T_{H_{uR}}}{\sqrt{2}v\cos\beta} + \mu_{\rm eff}B\cot\beta - \lambda^2v^2\cos^2\beta + \frac{1}{4}m_Z^2\left(\cos^2\beta - \sin^2\beta\right), \quad \text{(A.9b)}$$

$$m_s^2 = -\frac{\lambda T_{S_R}}{\sqrt{2}\mu_{\rm eff}} + \left(\mu_{\rm eff}B\frac{\lambda^2v^2}{\mu_{\rm eff}^2} + \lambda\kappa v^2\right)\sin\beta\cos\beta - \lambda^2v^2 - \frac{2\kappa^2\mu_{\rm eff}^2}{\lambda^2} + \frac{\kappa\mu_{\rm eff}A_\kappa}{\lambda}. \quad \text{(A.9c)}$$

Higgs mass matrices: In the final set of independent parameters the Higgs mass matrix elements for the CP-even fields read

$$\begin{aligned}(\mathbf{M}_H)_{11} &= \frac{1}{\sqrt{2}v}\left(-\frac{1-\sin^4\beta}{\cos\beta}T_{H_{dR}} + \cos^2\beta\sin\beta T_{H_{uR}}\right)\\ &\quad + \left(m_{H^\pm}^2 - m_W^2 + \lambda^2v^2\right)\sin^2\beta + m_Z^2\cos^2\beta, \quad \text{(A.10a)}\\ (\mathbf{M}_H)_{22} &= \frac{1}{\sqrt{2}v}\left(\sin^2\beta\cos\beta T_{H_{dR}} - \frac{1-\cos^4\beta}{\sin\beta}T_{H_{uR}}\right)\\ &\quad + \left(m_{H^\pm}^2 - m_W^2 + \lambda^2v^2\right)\cos^2\beta + m_Z^2\sin^2\beta, \quad \text{(A.10b)}\\ (\mathbf{M}_H)_{33} &= \frac{\lambda}{\sqrt{2}\mu_{\rm eff}}\left[-T_{S_R} + \frac{\lambda v}{\mu_{\rm eff}}\sin\beta\cos\beta\left(\sin^3\beta T_{H_{dR}} + \cos^3\beta T_{H_{uR}}\right)\right]\\ &\quad + \frac{\lambda^2v^2}{\mu_{\rm eff}^2}\sin^2\beta\cos^2\beta\left(m_{H^\pm}^2 - m_W^2 + \lambda^2v^2\right)\\ &\quad - \lambda\kappa v^2\sin\beta\cos\beta + \frac{4\kappa^2\mu_{\rm eff}^2}{\lambda} + \frac{\kappa\mu_{\rm eff}A_\kappa}{\lambda}, \quad \text{(A.10c)}\\ (\mathbf{M}_H)_{12} &= (\mathbf{M}_H)_{21} = -\frac{1}{\sqrt{2}v}\left(T_{H_{dR}}\sin^3\beta + T_{H_{uR}}\cos^3\beta\right)\\ &\quad - \left(m_{H^\pm}^2 - m_W^2 + \lambda^2v^2 + m_Z^2\right)\sin\beta\cos\beta, \quad \text{(A.10d)}\\ (\mathbf{M}_H)_{13} &= (\mathbf{M}_H)_{31} = -\frac{\lambda}{\sqrt{2}\mu_{\rm eff}}\sin\beta\left(\sin^3\beta T_{H_{dR}} + \cos^3\beta T_{H_{uR}}\right)\\ &\quad + \frac{\lambda v}{\mu_{\rm eff}}\left(m_{H^\pm}^2 - m_W^2 + \lambda^2v^2\right)\sin^2\beta\cos\beta\\ &\quad - \kappa v\sin\beta\mu_{\rm eff} + 2\lambda v\cos\beta\mu_{\rm eff}, \quad \text{(A.10e)}\\ (\mathbf{M}_H)_{23} &= (\mathbf{M}_H)_{32} = -\frac{\lambda}{\sqrt{2}\mu_{\rm eff}}\cos\beta\left(\sin^3\beta T_{H_{dR}} + \cos^3\beta T_{H_{uR}}\right)\\ &\quad + \frac{\lambda v}{\mu_{\rm eff}}\left(m_{H^\pm}^2 - m_W^2 + \lambda^2v^2\right)\cos^2\beta\sin\beta\\ &\quad - \kappa v\cos\beta\mu_{\rm eff} + 2\lambda v\sin\beta\mu_{\rm eff}. \quad \text{(A.10f)}\end{aligned}$$

For the CP-odd fields the Higgs mass-matrix elements read

$$
\begin{aligned}
(\mathbf{M}_A)_{11} &= \frac{1}{\sqrt{2}v}\left(-\frac{1-\sin^4\beta}{\cos\beta}T_{H_{dR}} + \cos^2\beta\sin\beta T_{H_{uR}}\right) \\
&\quad + \left(m_{H^\pm}^2 - m_W^2 + \lambda^2 v^2\right)\sin^2\beta\,, \qquad \text{(A.11a)} \\
(\mathbf{M}_A)_{22} &= \frac{1}{\sqrt{2}v}\left(\sin^2\beta\cos\beta T_{H_{dR}} - \frac{1-\cos^4\beta}{\sin\beta}T_{H_{uR}}\right) \\
&\quad + \left(m_{H^\pm}^2 - m_W^2 + \lambda^2 v^2\right)\cos^2\beta\,, \qquad \text{(A.11b)} \\
(\mathbf{M}_A)_{33} &= \frac{\lambda}{\sqrt{2}\mu_{\text{eff}}}\left[-T_{S_R} + \frac{\lambda v}{\mu_{\text{eff}}}\sin\beta\cos\beta\left(\sin^3\beta T_{H_{dR}} + \cos^3\beta T_{H_{uR}}\right)\right] \\
&\quad + \frac{\lambda^2 v^2}{\mu_{\text{eff}}^2}\sin^2\beta\cos^2\beta\left(m_{H^\pm}^2 - m_W^2 + \lambda^2 v^2\right) \\
&\quad + 3\lambda\kappa v^2\sin\beta\cos\beta - \frac{3\kappa\mu_{\text{eff}}A_\kappa}{\lambda}\,, \qquad \text{(A.11c)} \\
(\mathbf{M}_A)_{12} &= (\mathbf{M}_A)_{21} = -\frac{1}{\sqrt{2}v}\left(T_{H_{dR}}\sin^3\beta + T_{H_{uR}}\cos^3\beta\right) \\
&\quad - \left(m_{H^\pm}^2 - m_W^2 + \lambda^2 v^2\right)\sin\beta\cos\beta\,, \qquad \text{(A.11d)} \\
(\mathbf{M}_A)_{13} &= (\mathbf{M}_A)_{31} = -\frac{\lambda}{\sqrt{2}\mu_{\text{eff}}}\sin\beta\left(\sin^3\beta T_{H_{dR}} + \cos^3\beta T_{H_{uR}}\right) \\
&\quad + \frac{\lambda v}{\mu_{\text{eff}}}\left(m_{H^\pm}^2 - m_W^2 + \lambda^2 v^2\right)\sin^2\beta\cos\beta + 3\kappa v\sin\beta\mu_{\text{eff}}\,, \qquad \text{(A.11e)} \\
(\mathbf{M}_A)_{23} &= (\mathbf{M}_A)_{32} = \frac{\lambda}{\sqrt{2}\mu_{\text{eff}}}\cos\beta\left(\sin^3\beta T_{H_{dR}} + \cos^3\beta T_{H_{uR}}\right) \\
&\quad + \frac{\lambda v}{\mu_{\text{eff}}}\left(m_{H^\pm}^2 - m_W^2 + \lambda^2 v^2\right)\cos^2\beta\sin\beta - 3\kappa v\cos\beta\mu_{\text{eff}}\,. \qquad \text{(A.11f)}
\end{aligned}
$$

Appendix B

Chapter 3

B.1 Tree-level CPV-NMSSM Higgs mass matrix

The tadpole conditions given in Eq. 3.5 result the following relations [244]

$$\begin{aligned}
\frac{1}{v_d}\left\langle\frac{\partial V_H}{\partial H_{dR}}\right\rangle &= m_{H_d}^2+\frac{g^2}{4}(v_d^2-v_u^2)-\mathcal{R}_\lambda\frac{v_u s}{v_d}+\frac{|\lambda|^2}{2}(v_u^2+s^2)-\frac{\mathcal{R}}{2}\frac{v_u s^2}{v_d}=0,\\
\frac{1}{v_u}\left\langle\frac{\partial V_H}{\partial H_{uR}}\right\rangle &= m_{H_u}^2-\frac{g^2}{4}(v_d^2-v_u^2)-\mathcal{R}_\lambda\frac{v_d s}{v_u}+\frac{|\lambda|^2}{2}(v_d^2+s^2)-\frac{\mathcal{R}}{2}\frac{v_d s^2}{v_u}=0,\\
\frac{1}{s}\left\langle\frac{\partial V_H}{\partial S_R}\right\rangle &= m_S^2-\mathcal{R}_\lambda\frac{v_d v_u}{s}+\frac{|\lambda|^2}{2}(v_d^2+v_u^2)+|\kappa|^2 s^2-\mathcal{R}v_d v_u+\mathcal{R}_\kappa s=0,\\
\frac{1}{v_u}\left\langle\frac{\partial V_H}{\partial H_{dI}}\right\rangle &= \frac{1}{v_d}\left\langle\frac{\partial V_H}{\partial H_{uI}}\right\rangle=\mathcal{I}_\lambda s+\frac{\mathcal{I}s^2}{2}=0,\\
\frac{1}{s}\left\langle\frac{\partial V_H}{\partial S_I}\right\rangle &= \mathcal{I}_\lambda\frac{v_d v_u}{s}-\mathcal{I}v_d v_u-\mathcal{I}_\kappa s=0,
\end{aligned}\tag{B.1}$$

where the parameters read

$$\begin{aligned}
\mathcal{R}&=|\lambda||\kappa|\cos(\phi'_\lambda-\phi'_\kappa), & \mathcal{I}&=|\lambda||\kappa|\sin(\phi'_\lambda-\phi'_\kappa),\\
\mathcal{R}_\lambda&=\frac{|\lambda||A_\lambda|}{\sqrt{2}}\cos(\phi'_\lambda+\phi_{A_\lambda}), & \mathcal{R}_\kappa&=\frac{|\kappa||A_\kappa|}{\sqrt{2}}\cos(\phi'_\kappa+\phi_{A_\kappa}),\\
\mathcal{I}_\lambda&=\frac{|\lambda||A_\lambda|}{\sqrt{2}}\sin(\phi'_\lambda+\phi_{A_\lambda}), & \mathcal{I}_\kappa&=\frac{|\kappa||A_\kappa|}{\sqrt{2}}\sin(\phi'_\kappa+\phi_{A_\kappa}),
\end{aligned}\tag{B.2}$$

with

$$\phi'_\lambda=\phi_\lambda+\phi_u+\phi_s, \qquad \phi'_\kappa=\phi_\kappa+3\phi_s. \tag{B.3}$$

$\mathcal{I}_\lambda$ and $\mathcal{I}_\kappa$ can be reparameterized in terms of $\mathcal{I}$ using the last tadpole condition given in Eq. B.1 as

$$\mathcal{I}_\lambda = -\frac{1}{2}\mathcal{I}s, \qquad \mathcal{I}_\kappa = -\frac{3}{2}\mathcal{I}\frac{v_d v_u}{s}. \tag{B.4}$$

The phase combinations $\phi'_\lambda + \phi_{A_\lambda}$ and $\phi'_\kappa + \phi_{A_\kappa}$ can be determined by $\phi'_\lambda - \phi'_\kappa$. Thus $\phi'_\lambda - \phi'_\kappa$ is the only physical CPV phase that appears at tree-level of the NMSSM Higgs sector.

The elements of the CP-even block $\mathbf{M}_S^2$ in the squared-mass matrix given in Eq. 3.6 are

$$\begin{aligned}
\mathbf{M}^2_{S,11} &= \frac{g^2}{2}v_d^2 + \left(\mathcal{R}_\lambda + \frac{\mathcal{R}s}{2}\right) s\,\tan\beta, \\
\mathbf{M}^2_{S,22} &= \frac{g^2}{2}v_u^2 + \left(\mathcal{R}_\lambda + \frac{\mathcal{R}s}{2}\right) \frac{s}{\tan\beta}, \\
\mathbf{M}^2_{S,33} &= \mathcal{R}_\lambda \frac{v_d v_u}{s} + 2|\kappa|^2 s^2 + \mathcal{R}_\kappa s, \\
\mathbf{M}^2_{S,12} &= \mathbf{M}^2_{S,21} = \left(-\frac{g^2}{2} + |\lambda|^2\right) v_d v_u - \left(\mathcal{R}_\lambda + \frac{\mathcal{R}s}{2}\right) s, \\
\mathbf{M}^2_{S,13} &= \mathbf{M}^2_{S,31} = -\mathcal{R}_\lambda v_u + |\lambda|^2 v_d s - \mathcal{R} v_u s, \\
\mathbf{M}^2_{S,23} &= \mathbf{M}^2_{S,32} = -\mathcal{R}_\lambda v_d + |\lambda|^2 v_u s - \mathcal{R} v_d s.
\end{aligned} \tag{B.5}$$

Similarly, the elements of the CP-odd block $\mathbf{M}_P^2$ are

$$\begin{aligned}
\mathbf{M}^2_{P,11} &= \left(\mathcal{R}_\lambda + \frac{\mathcal{R}s}{2}\right) s\,\tan\beta, \\
\mathbf{M}^2_{P,22} &= \left(\mathcal{R}_\lambda + \frac{\mathcal{R}s}{2}\right) \frac{s}{\tan\beta}, \\
\mathbf{M}^2_{P,33} &= \mathcal{R}_\lambda \frac{v_d v_u}{s} + 2\mathcal{R} v_d v_u - 3\mathcal{R}_\kappa s, \\
\mathbf{M}^2_{P,12} &= \mathbf{M}^2_{P,21} = \left(\mathcal{R}_\lambda + \frac{\mathcal{R}s}{2}\right) s, \\
\mathbf{M}^2_{P,13} &= \mathbf{M}^2_{P,31} = (\mathcal{R}_\lambda - \mathcal{R}s)\, v_u, \\
\mathbf{M}^2_{P,23} &= \mathbf{M}^2_{P,32} = (\mathcal{R}_\lambda - \mathcal{R}s)\, v_d,
\end{aligned} \tag{B.6}$$

and the off-diagonal CP-mixed block reads

$$\mathbf{M}^2_{SP} = \begin{pmatrix} 0 & 0 & -\frac{3}{2}\mathcal{I} v_u s \\ 0 & 0 & -\frac{3}{2}\mathcal{I} v_d s \\ \frac{1}{2}\mathcal{I} v_u s & \frac{1}{2}\mathcal{I} v_d s & 2\mathcal{I} v_u v_d \end{pmatrix}. \tag{B.7}$$

Appendix C

Chapter 3

C.1 Self-energies of Higgs bosons

The absorptive part of the Higgs propagator matrix can be written as

$$\mathfrak{Im}\hat{\Pi}_{ij}(s) = \mathfrak{Im}\hat{\Pi}_{ij}^{ff}(s) + \mathfrak{Im}\hat{\Pi}_{ij}^{VV}(s) + \mathfrak{Im}\hat{\Pi}_{ij}^{HV}(s) + \mathfrak{Im}\hat{\Pi}_{ij}^{HH}(s) + \mathfrak{Im}\hat{\Pi}_{ij}^{\tilde{f}\tilde{f}}(s)\,. \tag{C.1}$$

We reproduce here the expressions for the individual contributions from [36], where those to vector bosons as well as associated Higgs and vector boson pairs were derived using the Pinch Technique [300–307], which ensures their linear dependence on s. These two contributions are given as

$$\begin{aligned}\mathfrak{Im}\hat{\Pi}_{ij}^{VV}(s) &= \frac{g^2 g_{H_iVV} g_{H_jVV}\delta_V\beta_V}{128\pi m_W^2}\Big\{-4m_V^2\Big(2s-3m_V^2\Big)+2m_V^2\Big(m_{H_i}^2+m_{H_j}^2\Big)\\ &+ m_{H_i}^2 m_{H_j}^2\Big\}\,\Theta\Big(s-4m_V^2\Big)\,,\end{aligned} \tag{C.2}$$

with $\beta_V = \sqrt{1-4\kappa_V}$ and $\delta_W = 2,\ \delta_Z = 1$, and

$$\begin{aligned}
\mathfrak{Im}\hat{\Pi}_{ij}^{HV}(s) &= \frac{g^2}{64\pi m_W^2} \sum_{k=1-5} g_{H_iH_kZ} g_{H_jH_kZ}\ \lambda^{1/2}\Big(1,\kappa_Z,\kappa_{H_k}\Big) \\
&\times \Big\{-4sm_Z^2 + \Big(m_Z^2 - m_{H_k}^2\Big)^2 + \Big(m_Z^2 - m_{H_k}^2\Big)\Big(m_{H_i}^2 + m_{H_j}^2\Big) \\
&+ m_{H_i}^2 m_{H_j}^2\Big\}\ \Theta\Big(s-(m_Z+m_{H_k})^2\Big) \\
&+ \frac{g^2}{32\pi m_W^2} \mathfrak{Re}\Big(g_{H_iH^+W^-} g^*_{H_jH^+W^-}\Big)\ \lambda^{1/2}\Big(1,\kappa_W,\kappa_{H^\pm}\Big) \\
&\times \Big\{-4\hat{s}m_W^2 + \Big(m_W^2 - m_{H^\pm}^2\Big)^2 \\
&+ \Big(m_W^2 - m_{H^\pm}^2\Big)\Big(m_{H_i}^2 + m_{H_j}^2\Big) + m_{H_i}^2 m_{H_j}^2\Big\} \\
&\times \Theta\Big(s-(m_W+m_{H^\pm})^2\Big)\,. \qquad \text{(C.3)}
\end{aligned}$$

The contribution from loops of Higgs boson pairs reads

$$\begin{aligned}
\mathfrak{Im}\hat{\Pi}_{ij}^{HH}(s) &= \frac{v^2}{16\pi} \sum_{k\geq l=1-5} \frac{S_{ij;kl}}{1+\delta_{kl}} g_{H_iH_kH_l} g_{H_jH_kH_l}\ \lambda^{1/2}\Big(1,\kappa_{H_k},\kappa_{H_l}\Big) \\
&\times \Theta\Big(s-(m_{H_k}+m_{H_{H_l}})^2\Big)\,, \qquad \text{(C.4)}
\end{aligned}$$

where the symmetry factor $S_{ij;kl}$ is equal to 2 for $i=j$ and $k\neq l$, or $i\neq j$ and $k=l$, to 4 for $i=j$ and $k=l$, and to 1 otherwise.

Finally, the loops of fermions (omitting the QCD K-factors) and sfermions give

$$\begin{aligned}
\mathfrak{Im}\hat{\Pi}_{ij}^{ff}(s) &= \frac{s}{8\pi} \sum_{f,f'} g_f^2 \Delta_{ff'} N_{cf}\ \lambda^{1/2}\Big(1,\kappa_f,\kappa_{f'}\Big) \\
&\times \Big\{\Big(1-\kappa_f-\kappa_{f'}\Big)\Big(g^S_{H_if\bar{f}'} g^{S*}_{H_jf\bar{f}'} + g^P_{H_if\bar{f}'} g^{P*}_{H_jf\bar{f}'}\Big) \\
&- 2\sqrt{\kappa_f\kappa_{f'}}\Big(g^S_{H_if\bar{f}'} g^{S*}_{H_jf\bar{f}'} - g^P_{H_if\bar{f}'} g^{P*}_{H_jf\bar{f}'}\Big)\Big\} \\
&\times \Theta\Big(s-(m_f+m_{f'})^2\Big)\,, \qquad \text{(C.5)}
\end{aligned}$$

where $g_f = \frac{gm_f}{2m_W}$, $\Delta_{ff'} = \delta_{ff'}$ $(f,f' = t,b,c,s,\tau,\mu)$, $\frac{4}{1+\delta_{ff'}}$ $(f,f' = \tilde{\chi}^0_{1,2,3,4,5})$, 1 $(f,f' = \tilde{\chi}^+_{1,2})$, $\lambda(x,y,z) = x^2+y^2+z^2-2(xy+yz+zx)$ and $\kappa_x = \frac{m_x^2}{\hat{s}}$, and

$$\mathfrak{Im}\hat{\Pi}_{ij}^{\tilde{f}\tilde{f}}(s) = \frac{v^2}{16\pi} \sum_{\tilde{f}} \sum_{k,l=1-2} N_{cf} g_{H_i\tilde{f}_k\tilde{f}_l^*} g^*_{H_jf_k\tilde{f}_l^*}\ \lambda^{1/2}\Big(1,\kappa_{\tilde{f}_k},\kappa_{\tilde{f}_l}\Big)\ \Theta\Big(s-(m_{\tilde{f}_k}+m_{\tilde{f}_l})^2\Big)\,. \qquad \text{(C.6)}$$

Appendix D

Chapter 3

D.1 Convolution

Here we briefly address the technique used for convolving the distribution for differential cross sections with respect to the invariant mass of the decay products as discussed in chapter 3 and chapter 4 [308].

The Breit-Wigner function is defined as

$$P_{\mathrm{BW}}(x;\Gamma,x_0) = \frac{1}{\pi}\frac{\Gamma/2}{(x-x_0)^2+\Gamma^2/4}\,, \tag{D.1}$$

with the two parameters, x_0 corresponding to the most probable value (at which the peak of the distribution appears) and the width Γ.

The BW function is a useful formalism to describe the resonant processes, like the invariant mass of decay products from an resonant intermediate state. For a resonant state, x_0 and Γ represent its mass and width, respectively.

Convolution of a BW function with a Gaussian one is defined by another function, called the Voigtian function which can be given as

$$P_{\mathrm{Voigt}}(x;x_0,\Gamma,\sigma) = \int_{-\infty}^{+\infty} dx' P_{\mathrm{Gauss}}(x';0,\sigma)P_{\mathrm{BW}}(x-x';x_0,\Gamma)\,. \tag{D.2}$$

Thus in addition to x_0 and Γ, the third parameter that characterizes the Voigtian function is the resolution σ. While there is no straightforward analytical implementation of the Voigtian, there are many numerical techniques available,

e.g., the `TMath::Voigt` function in the `ROOT` data analysis framework [309], the `RooVoigtian` class in the `RooFit` toolkit for data modeling [310], the `Convolve` and the `ListConvolve` functions in `Mathematica` [279].

When the instrumental resolution is sufficiently well described by a Gaussian distribution function, a Voigtian distribution can give a fair description for an observed distribution of a resonant process.

Bibliography

[1] **ATLAS Collaboration**, G. Aad *et al.*, "Observation of a new particle in the search for the Standard Model Higgs boson with the ATLAS detector at the LHC," *Phys.Lett.* **B716** (2012) 1–29, arXiv:1207.7214 [hep-ex].

[2] **CMS Collaboration**, S. Chatrchyan *et al.*, "Observation of a new boson at a mass of 125 GeV with the CMS experiment at the LHC," *Phys. Lett.* **B716** (2012) 30–61, arXiv:1207.7235 [hep-ex].

[3] A. Arbey, M. Battaglia, A. Djouadi and F. Mahmoudi, "An update on the constraints on the phenomenological MSSM from the new LHC Higgs results," Phys. Lett. B **720**, 153 (2013), arXiv:1211.4004 [hep-ph].

[4] M. Drees, "A Supersymmetric Explanation of the Excess of Higgs–Like Events at the LHC and at LEP," Phys. Rev. D **86**, 115018 (2012), arXiv:1210.6507 [hep-ph].

[5] A. Arbey, M. Battaglia, A. Djouadi, F. Mahmoudi, "The Higgs sector of the phenomenological MSSM in the light of the Higgs boson discovery," JHEP **1209**, 107 (2012), arXiv:1207.1348 [hep-ph].

[6] M. Carena, S. Gori, N. R. Shah, C. E. M. Wagner, "A 125 GeV SM-like Higgs in the MSSM and the $\gamma\gamma$ rate," JHEP **1203**, 014 (2012), arXiv:1112.3336 [hep-ph].

[7] U. Ellwanger, C. Hugonie and A. M. Teixeira, "The Next-to-Minimal Supersymmetric Standard Model," *Phys.Rept.* **496** (2010) 1–77, arXiv:0910.1785 [hep-ph].

[8] M. Maniatis, "The Next-to-Minimal Supersymmetric extension of the Standard Model reviewed," *Int.J.Mod.Phys.* **A25** (2010) 3505–3602, arXiv:0906.0777 [hep-ph].

[9] A. Elsayed, S. Khalil and S. Moretti, "Higgs Mass Corrections in the SUSY B-L Model with Inverse Seesaw," Phys. Lett. B **715**, 208 (2012), arXiv:1106.2130 [hep-ph]. L. Basso and F. Staub, "Enhancing $h \to \gamma\gamma$ with staus in SUSY models with extended gauge sector," arXiv:1210.7946 [hep-ph].

[10] A. Chakraborty, B. Das, J. L. Diaz-Cruz, D. K. Ghosh, S. Moretti *et al.*, "125 GeV Higgs signal at the LHC in the CP-violating MSSM," *Phys.Rev.* **D90** no. 5, (2014) 055005, arXiv:1301.2745 [hep-ph].

[11] M. Aaboud *et al.* [ATLAS Collaboration], "Search for Minimal Supersymmetric Standard Model Higgs bosons H/A and for a Z' boson in the $\tau\tau$ final state produced in pp collisions at $\sqrt{s} = 13$ TeV with the ATLAS Detector," Eur. Phys. J. C **76**, no. 11, 585 (2016), arXiv:1608.00890 [hep-ex].

[12] J. E. Kim and H. P. Nilles, "The mu Problem and the Strong CP Problem," *Phys. Lett.* **B138** (1984) 150–154.

[13] P. Fayet, "Supergauge Invariant Extension of the Higgs Mechanism and a Model for the electron and Its Neutrino," *Nucl.Phys.* **B90** (1975) 104–124

[14] J. R. Ellis, J. Gunion, H. E. Haber, L. Roszkowski and F. Zwirner, "Higgs Bosons in a Nonminimal Supersymmetric Model," *Phys.Rev.* **D39** (1989) 844

[15] J. F. Gunion, Y. Jiang and S. Kraml, "Could two NMSSM Higgs bosons be present near 125 GeV?," *Phys.Rev.* **D86** (2012) 071702, arXiv:1207.1545 [hep-ph]

[16] S. King, M. Muhlleitner, R. Nevzorov and K. Walz, "Natural NMSSM Higgs Bosons," *Nucl.Phys.* **B870** (2013) 323–352, arXiv:1211.5074 [hep-ph]

[17] L. Wu, J. M. Yang, C.-P. Yuan and M. Zhang, "Higgs self-coupling in the MSSM and NMSSM after the LHC Run 1," *Phys. Lett.* **B747** (2015) 378–389, arXiv:1504.06932 [hep-ph]

[18] F. Domingo and G. Weiglein, "NMSSM interpretations of the observed Higgs signal," *JHEP* **04** (2016) 095, arXiv:1509.07283 [hep-ph].

[19] S. Munir, L. Roszkowski and S. Trojanowski, "Simultaneous enhancement in gamma.gamma, b.b-bar and tau+.tau- rates in the NMSSM with nearly degenerate scalar and pseudoscalar Higgs bosons," *Phys. Rev.* **D88** (2013) 055017, arXiv:1305.0591 [hep-ph].

[20] A. Pilaftsis, "CP odd tadpole renormalization of Higgs scalar - pseudoscalar mixing," Phys. Rev. D **58**, 096010 (1998), hep-ph/9803297.

[21] A. Pilaftsis and C. E. M. Wagner, "Higgs bosons in the minimal supersymmetric standard model with explicit CP violation," Nucl. Phys. B **553**, 3 (1999), hep-ph/9902371.

[22] S. Y. Choi, M. Drees and J. S. Lee, "Loop corrections to the neutral Higgs boson sector of the MSSM with explicit CP violation," Phys. Lett. B **481**, 57 (2000), hep-ph/0002287.

[23] A. D. Sakharov, "Violation of CP Invariance, c Asymmetry, and Baryon Asymmetry of the Universe," Pisma Zh. Eksp. Teor. Fiz. **5**, 32 (1967) [JETP Lett. **5**, 24 (1967)] [Sov. Phys. Usp. **34**, 392 (1991)] [Usp. Fiz. Nauk **161**, 61 (1991)].

[24] M. Kobayashi and T. Maskawa, "CP Violation in the Renormalizable Theory of Weak Interaction," Prog. Theor. Phys. **49**, 652 (1973).

[25] S. K. Lamoreaux and R. Golub, "Comment on 'An Improved experimental limit on the electric-dipole moment of the neutron', C.A.Baker et al.," Phys. Rev. Lett. **98**, 149101 (2007), hep-ex/0609055.

[26] E. D. Commins, "Electric dipole moments of elementary particles, nuclei, atoms, and molecules," J. Phys. Soc. Jap. **76**, 111010 (2007).

[27] W. C. Griffith, M. D. Swallows, T. H. Loftus, M. V. Romalis, B. R. Heckel and E. N. Fortson, "Improved Limit on the Permanent Electric Dipole Moment of Hg-199," Phys. Rev. Lett. **102**, 101601 (2009).

[28] S. Abel, S. Khalil and O. Lebedev, "EDM constraints in supersymmetric theories," Nucl. Phys. B **606**, 151 (2001), hep-ph/0103320.

[29] S. Moretti, S. Munir and P. Poulose, "125 GeV Higgs Boson signal within the complex NMSSM," *Phys.Rev.* **D89** no. 1, (2014) 015022, arXiv:1305.0166 [hep-ph].

[30] D. A. Demir, "Effects of the supersymmetric phases on the neutral Higgs sector," Phys. Rev. D **60**, 055006 (1999), hep-ph/9901389.

[31] G. L. Kane and L. -T. Wang, "Implications of supersymmetry phases for Higgs boson signals and limits," Phys. Lett. B **488**, 383 (2000), hep-ph/0003198.

[32] S. Moretti and S. Munir, "Two Higgs Bosons near 125 GeV in the Complex NMSSM and the LHC Run I Data," *Adv. High Energy Phys.* **2015** (2015) 509847, arXiv:1505.00545 [hep-ph].

[33] B. Das, S. Moretti, S. Munir, and P. Poulose, "Two Higgs bosons near 125 GeV in the NMSSM: beyond the narrow width approximation," *Eur. Phys. J.* **C77** no. 8, (2017) 544, arXiv:1704.02941 [hep-ph].

[34] P. Bechtle, S. Heinemeyer, O. Stål, T. Stefaniak, G. Weiglein, *et al.*, "MSSM Interpretations of the LHC Discovery: Light or Heavy Higgs?," *Eur.Phys.J.* **C73** (2013) 2354.

[35] P. Bechtle, H. E. Haber, S. Heinemeyer, O. Stål, T. Stefaniak, G. Weiglein, and L. Zeune, "The Light and Heavy Higgs Interpretation of the MSSM," *Eur. Phys. J.* **C77** no. 2, (2017) 67, arXiv:1608.00638 [hep-ph].

[36] J. R. Ellis, J. S. Lee and A. Pilaftsis, "CERN LHC signatures of resonant CP violation in a minimal supersymmetric Higgs sector," Phys. Rev. D **70**, 075010 (2004), hep-ph/0404167.

[37] E. Fuchs, S. Thewes and G. Weiglein, "Interference effects in BSM processes with a generalised narrow-width approximation," *Eur. Phys. J.* **C75** (2015) 254, arXiv:1411.4652 [hep-ph]

[38] E. Fuchs and G. Weiglein, "Breit-Wigner approximation for propagators of mixed unstable states," arXiv:1610.06193 [hep-ph].

[39] D. J. Miller, R. Nevzorov, and P. M. Zerwas, "The Higgs sector of the next-to-minimal supersymmetric standard model," *Nucl. Phys.* **B681** (2004) 3–30, arXiv:hep-ph/0304049 [hep-ph].

[40] B. Das, S. Moretti, S. Munir and P. Poulose, "Quantum interference amongst heavy NMSSM Higgs bosons," arXiv:1804.10393 [hep-ph].

[41] N. Cabibbo, "Unitary Symmetry and Leptonic Decays," Phys. Rev. Lett. **10**, 531 (1963).

[42] L. L. Chau and W. Y. Keung, Phys. Rev. Lett. **53**, 1802 (1984). doi:10.1103/PhysRevLett.53.1802

[43] M. Tanabashi *et al.*, "Review of Particle Physics," Phys. Rev. D **98**, no. 3, 030001 (2018).

[44] S. Schael *et al.* [ALEPH and DELPHI and L3 and OPAL and SLD Collaborations and LEP Electroweak Working Group and SLD Electroweak Group and SLD Heavy Flavour Group], "Precision electroweak measurements on the Z resonance," Phys. Rept. **427**, 257 (2006), hep-ex/0509008.

[45] J. Alcaraz *et al.* [ALEPH and DELPHI and L3 and OPAL Collaborations and LEP Electroweak Working Group], "A Combination of preliminary electroweak measurements and constraints on the standard model," hep-ex/0612034.

[46] S. Chatrchyan *et al.* [CMS Collaboration], "Study of the Mass and Spin-Parity of the Higgs Boson Candidate Via Its Decays to Z Boson Pairs," Phys. Rev. Lett. **110**, no. 8, 081803 (2013), arXiv:1212.6639 [hep-ex].

[47] **ATLAS and CMS Collaborations**, G. Aad *et al.*, "Combined Measurement of the Higgs Boson Mass in pp Collisions at $\sqrt{s} = 7$ and 8 TeV with the ATLAS and CMS Experiments," *Phys. Rev. Lett.* **114** (2015) 191803, arXiv:1503.07589 [hep-ex].

[48] **ATLAS and CMS Collaborations**, G. Aad *et al.*, "Measurements of the Higgs boson production and decay rates and constraints on its couplings from a combined ATLAS and CMS analysis of the LHC pp collision data at $\sqrt{s} = 7$ and 8 TeV," *JHEP* **08** (2016) 045, arXiv:1606.02266 [hep-ex].

[49] **CMS Collaboration**, A. M. Sirunyan *et al.*, "Measurements of Higgs boson properties in the diphoton decay channel in proton-proton collisions at $\sqrt{s} =$ 13 TeV," arXiv:1804.02716 [hep-ex].

[50] **ATLAS Collaboration**, M. Aaboud *et al.*, "Measurements of Higgs boson properties in the diphoton decay channel with 36 fb^{-1} of pp collision data at $\sqrt{s} = 13$ TeV with the ATLAS detector," arXiv:1802.04146 [hep-ex].

[51] The ATLAS collaboration [ATLAS Collaboration], "Combined measurements of Higgs boson production and decay using up to 80 fb^{-1} of proton–proton collision data at $\sqrt{s} = 13$ TeV collected with the ATLAS experiment," ATLAS-CONF-2018-031.

[52] A. Djouadi, "The Anatomy of electro-weak symmetry breaking. I: The Higgs boson in the standard model," Phys. Rept. **457**, 1 (2008). [hep-ph/0503172].

[53] J. Wess and B. Zumino, "Supergauge Transformations in Four-Dimensions," Nucl. Phys. B **70**, 39 (1974).

[54] S. R. Coleman and J. Mandula, "All Possible Symmetries of the S Matrix," Phys. Rev. **159**, 1251 (1967).

[55] R. Haag, J. T. Lopuszanski and M. Sohnius, "All Possible Generators of Supersymmetries of the s Matrix," Nucl. Phys. B **88**, 257 (1975).

[56] P. Van Nieuwenhuizen, "Supergravity," Phys. Rept. **68**, 189 (1981).

[57] J. R. Ellis, J. S. Hagelin, D. V. Nanopoulos, K. A. Olive and M. Srednicki, "Supersymmetric Relics from the Big Bang," Nucl. Phys. B **238**, 453 (1984).

[58] G. Jungman, M. Kamionkowski and K. Griest, "Supersymmetric dark matter," Phys. Rept. **267**, 195 (1996), hep-ph/9506380.

[59] J. R. Ellis, S. Kelley and D. V. Nanopoulos, "Probing the desert using gauge coupling unification," Phys. Lett. B **260**, 131 (1991).

[60] J. Hisano, H. Murayama and T. Yanagida, "Nucleon decay in the minimal supersymmetric SU(5) grand unification," Nucl. Phys. B **402**, 46 (1993), hep-ph/9207279.

[61] E. Witten, "Dynamical Breaking of Supersymmetry," Nucl. Phys. B **188**, 513 (1981).

[62] S. P. Martin, "A Supersymmetry primer," hep-ph/9709356 [hep-ph].

[63] A. Djouadi, "The Anatomy of electro-weak symmetry breaking. II. The Higgs bosons in the minimal supersymmetric model," Phys. Rept. **459**, 1 (2008), hep-ph/0503173.

[64] L. J. Hall, J. D. Lykken and S. Weinberg, "Supergravity as the Messenger of Supersymmetry Breaking," Phys. Rev. D **27**, 2359 (1983).

[65] H. P. Nilles, "Dynamically Broken Supergravity and the Hierarchy Problem," Phys. Lett. **115B**, 193 (1982).

[66] M. Dine and A. E. Nelson, "Dynamical supersymmetry breaking at low-energies," Phys. Rev. D **48**, 1277 (1993), hep-ph/9303230.

[67] G. F. Giudice and R. Rattazzi, "Theories with gauge mediated supersymmetry breaking," Phys. Rept. **322**, 419 (1999), hep-ph/9801271.

[68] L. E. Ibanez and G. G. Ross, "$SU(2) - L \times U(1)$ Symmetry Breaking as a Radiative Effect of Supersymmetry Breaking in Guts," Phys. Lett. **110B**, 215 (1982).

[69] F. Zwirner, "The quest for low-energy supersymmetry and the role of high-energy e^+e^- colliders," In *Saariselkae 1991, Proceedings, Physics and experiments with linear colliders, vol. 1* 309-351 and CERN Geneva - TH. 6357 (91/12,rec.Mar.92) 28 p, hep-ph/9203204.

[70] G. F. Giudice and A. Masiero, "A Natural Solution to the mu Problem in Supergravity Theories," Phys. Lett. B **206**, 480 (1988).

[71] Y. Nir, "Gauge unification, Yukawa hierarchy and the mu problem," *Phys. Lett.* **B354** (1995) 107–110, arXiv:hep-ph/9504312 .

[72] L. Durand and J. L. Lopez, "Upper Bounds on Higgs and Top Quark Masses in the Flipped $SU(5) \times U(1)$ Superstring Model," *Phys.Lett.* **B217** (1989) 463

[73] M. Drees, "Supersymmetric Models with Extended Higgs Sector," *Int.J.Mod.Phys.* **A4** (1989) 3635.

[74] M. Frank, T. Hahn, S. Heinemeyer, W. Hollik, H. Rzehak and G. Weiglein, "The Higgs Boson Masses and Mixings of the Complex MSSM in the Feynman-Diagrammatic Approach," JHEP **0702**, 047 (2007), hep-ph/0611326.

[75] S. Heinemeyer, W. Hollik and G. Weiglein, "The Masses of the neutral CP - even Higgs bosons in the MSSM: Accurate analysis at the two loop level," Eur. Phys. J. C **9**, 343 (1999), hep-ph/9812472.

[76] E. P. Shabalin, "Electric Dipole Moment of Quark in a Gauge Theory with Left-Handed Currents," Sov. J. Nucl. Phys. **28**, 75 (1978) [Yad. Fiz. **28**, 151 (1978)].

[77] E. P. Shabalin, "The Electric Dipole Moment Of The Neutron In A Gauge Theory," Sov. Phys. Usp. **26**, 297 (1983) [Usp. Fiz. Nauk **139**, 561 (1983)].

[78] L. I. Schiff, "Measurability of Nuclear Electric Dipole Moments," Phys. Rev. **132**, 2194 (1963).

[79] S. Ban, J. Dobaczewski, J. Engel and A. Shukla, Phys. Rev. C **82**, 015501 (2010) doi:10.1103/PhysRevC.82.015501, arXiv:1003.2598 [nucl-th].

[80] J. Ellis, J. S. Lee and A. Pilaftsis, "Maximal Electric Dipole Moments of Nuclei with Enhanced Schiff Moments," JHEP **1102**, 045 (2011), arXiv:1101.3529 [hep-ph].

[81] V. A. Dzuba and V. V. Flambaum, "Parity violation and electric dipole moments in atoms and molecules," Int. J. Mod. Phys. E **21**, 1230010 (2012), arXiv:1209.2200 [physics.atom-ph].

[82] J. S. M. Ginges and V. V. Flambaum, "Violations of fundamental symmetries in atoms and tests of unification theories of elementary particles," Phys. Rept. **397**, 63 (2004), physics/0309054.

[83] M. Jung, "A robust limit for the electric dipole moment of the electron," JHEP **1305**, 168 (2013), arXiv:1301.1681[hep-ph].

[84] B. C. Regan, E. D. Commins, C. J. Schmidt and D. DeMille, "New limit on the electron electric dipole moment," Phys. Rev. Lett. **88**, 071805 (2002).

[85] T. Ibrahim and P. Nath, "The Neutron and the lepton EDMs in MSSM, large CP violating phases, and the cancellation mechanism," Phys. Rev. D **58**, 111301 (1998), hep-ph/9807501.

[86] G. F. Giudice and A. Romanino, "Electric dipole moments in split supersymmetry," Phys. Lett. B **634**, 307 (2006), hep-ph/0510197.

[87] Y. Li, S. Profumo and M. Ramsey-Musolf, "Higgs-Higgsino-Gaugino Induced Two Loop Electric Dipole Moments," Phys. Rev. D **78**, 075009 (2008), arXiv:0806.2693 [hep-ph].

[88] G. F. Giudice and A. Romanino, "Split supersymmetry," Nucl. Phys. B **699**, 65 (2004), hep-ph/0406088.

[89] M. Pospelov and A. Ritz, "Electric dipole moments as probes of new physics," Annals Phys. **318**, 119 (2005), hep-ph/0504231.

[90] M. Raidal, A. van der Schaaf, I. Bigi, M. L. Mangano, Y. K. Semertzidis, S. Abel, S. Albino and S. Antusch *et al.*, "Flavour physics of leptons and dipole moments," Eur. Phys. J. C **57**, 13 (2008), arXiv:0801.1826 [hep-ph].

[91] T. Fukuyama, "Searching for New Physics beyond the Standard Model in Electric Dipole Moment," Int. J. Mod. Phys. A **27**, 1230015 (2012), arXiv:1201.4252 [hep-ph].

[92] J. Engel, M. J. Ramsey-Musolf and U. van Kolck, "Electric Dipole Moments of Nucleons, Nuclei, and Atoms: The Standard Model and Beyond," Prog. Part. Nucl. Phys. **71**, 21 (2013), arXiv:1303.2371 [nucl-th].

[93] J. R. Ellis, J. S. Lee and A. Pilaftsis, "Electric Dipole Moments in the MSSM Reloaded," JHEP **0810**, 049 (2008), arXiv:0808.1819 [hep-ph].

[94] J. Hisano, M. Nagai and P. Paradisi, "Flavor effects on the electric dipole moments in supersymmetric theories: A beyond leading order analysis," Phys. Rev. D **80**, 095014 (2009), arXiv:0812.4283 [hep-ph].

[95] J. Hisano, M. Nagai and P. Paradisi, "New Two-loop Contributions to Hadronic EDMs in the MSSM," Phys. Lett. B **642**, 510 (2006), hep-ph/0606322.

[96] W. Altmannshofer, A. J. Buras, S. Gori, P. Paradisi and D. M. Straub, "Anatomy and Phenomenology of FCNC and CPV Effects in SUSY Theories," Nucl. Phys. B **830**, 17 (2010).

[97] Y. Li, S. Profumo and M. Ramsey-Musolf, "A Comprehensive Analysis of Electric Dipole Moment Constraints on CP-violating Phases in the MSSM," JHEP **1008**, 062 (2010), arXiv:1006.1440 [hep-ph].

[98] L. Mercolli and C. Smith, "EDM constraints on flavored CP-violating phases," Nucl. Phys. B **817**, 1 (2009), arXiv:0902.1949 [hep-ph].

[99] A. Ilakovac, A. Pilaftsis and L. Popov, "Lepton Dipole Moments in Supersymmetric Low-Scale Seesaw Models," arXiv:1308.3633 [hep-ph].

[100] V. VFlambaum, "On Enhancement of the electron Electric Dipole Moment in Heavy Atoms," Yad. Fiz. **24**, 383 (1976).

[101] J. J. Hudson, D. M. Kara, I. J. Smallman, B. E. Sauer, M. R. Tarbutt and E. A. Hinds, "Improved measurement of the shape of the electron," Nature **473**, 493 (2011).

[102] C. A. Baker, D. D. Doyle, P. Geltenbort, K. Green, M. G. D. van der Grinten, P. G. Harris, P. Iaydjiev and S. N. Ivanov *et al.*, "An Improved experimental limit on the electric dipole moment of the neutron," Phys. Rev. Lett. **97**, 131801 (2006), hep-ex/0602020.

[103] M. Jung and A. Pich, "Electric Dipole Moments in Two-Higgs-Doublet Models," arXiv:1308.6283 [hep-ph].

[104] A. P. Serebrov, E. A. Kolomenskiy, A. N. Pirozhkov, I. A. Krasnoshekova, A. V. Vasiliev, A. O. Polyushkin, M. S. Lasakov and A. K. Fomin *et al.*, "New measurements of neutron electric dipole moment," arXiv:1310.5588 [nucl-ex].

[105] V. V. Flambaum and I. B. Khriplovich, "New Limits on the Electron Dipole Moment and T Nonconserving Electron - Nucleon Interaction," Sov. Phys. JETP **62**, 872 (1985). [Zh. Eksp. Teor. Fiz. **89**, 1505 (1985)].

[106] J. Baron *et al.* [ACME Collaboration], "Order of Magnitude Smaller Limit on the Electric Dipole Moment of the Electron," Science **343**, no. 6168, 269 (2014); arXiv:1310.7534 [physics.atom-ph].

[107] B. Graner, Y. Chen, E. G. Lindahl and B. R. Heckel, "Reduced Limit on the Permanent Electric Dipole Moment of Hg199," Phys. Rev. Lett. **116**, no. 16, 161601 (2016); arXiv:1601.04339 [physics.atom-ph].

[108] D. A. Demir, O. Lebedev, K. A. Olive, M. Pospelov and A. Ritz, "Electric dipole moments in the MSSM at large tan beta," Nucl. Phys. B **680**, 339 (2004), hep-ph/0311314.

[109] S. Chatrchyan *et al.* CMS Collaboration, "Observation of a new boson at a mass of 125 GeV with the CMS experiment at the LHC," Phys. Lett. B **716**, 30 (2012). [arXiv:1207.7235 [hep-ex]].

[110] G. Aad *et al.* ATLAS Collaboration, "Observation of a new particle in the search for the Standard Model Higgs boson with the ATLAS detector at the LHC," Phys. Lett. B **716**, 1 (2012).

[111] S. Chatrchyan *et al.* [CMS Collaboration], "Observation of a new boson with mass near 125 GeV in pp collisions at $\sqrt{s} = 7$ and 8 TeV," JHEP **1306**, 081 (2013). [arXiv:1303.4571 [hep-ex]].

[112] ATLAS Collaboration: ATLAS-CONF-2013-014.

[113] CMS Collaboration, CMS-PAS-HIG-13-001.

[114] CMS Collaboration, CMS-PAS-HIG-13-002.

[115] CMS Collaboration, CMS-PAS-HIG-13-003.

[116] CMS Collaboration, CMS-PAS-HIG-13-004.

[117] CMS Collaboration, CMS-PAS HIG-13-012.

[118] CMS Collaboration, CMS-PAS-HIG-13-005.

[119] ATLAS Collaboration, ATLAS-CONF-2013-012.

[120] ATLAS Collaboration, ATLAS-CONF-2013-013.

[121] ATLAS Collaboration, ATLAS-CONF-2013-030.

[122] ATLAS Collaboration, ATLAS-CONF-2013-079.

[123] ATLAS Collaboration, ATLAS-CONF-2012-160.

[124] ATLAS Collaboration, ATLAS-CONF-2013-014.

[125] ATLAS Collaboration, ATLAS-CONF-2014-009.

[126] For reviews on supersymmetry, see, J. Wess and J. Bagger, *Supersymmetry and Supergravity*, 2nd ed. (Princeton University Press, Princeton, 1991); M. Drees, P. Roy and R. M. Godbole, *Theory and Phenomenology of Sparticles*, (World Scientific, Singapore, 2005); H. E. Haber and G. Kane, Phys. Rep. (117,75,1985); H. P. Nilles, Phys. Rep. (110,1,1984).

[127] K. Schmidt-Hoberg, F. Staub and M. W. Winkler, "Enhanced diphoton rates at Fermi and the LHC," JHEP **1301**, 124 (2013). [arXiv:1211.2835 [hep-ph]].

[128] Z. Heng, "A 125 GeV Higgs and its di-photon signal in different SUSY models: a mini review," arXiv:1210.3751 [hep-ph].

[129] K. Schmidt-Hoberg and F. Staub, "Enhanced $h \to \gamma\gamma$ rate in MSSM singlet extensions," JHEP **1210**, 195 (2012).

[130] M. Carena, I. Low, C. E. M. Wagner, "Implications of a Modified Higgs to Diphoton Decay Width," JHEP **1208**, 060 (2012), [arXiv:1206.1082 [hep-ph]].

[131] L. J. Hall, D. Pinner, J. T. Ruderman, "A Natural SUSY Higgs Near 126 GeV," JHEP **1204**, 131 (2012), [arXiv:1112.2703 [hep-ph]].

[132] S. Heinemeyer, O. Stal, G. Weiglein, "Interpreting the LHC Higgs Search Results in the MSSM," Phys. Lett. B **710**, 201 (2012), [arXiv:1112.3026 [hep-ph]].

[133] A. Arbey, M. Battaglia, A. Djouadi, F. Mahmoudi, J. Quevillon, "Implications of a 125 GeV Higgs for supersymmetric models," Phys. Lett. B **708**, 162 (2012), [arXiv:1112.3028 [hep-ph]].

[134] P. Draper, P. Meade, M. Reece, D. Shih, "Implications of a 125 GeV Higgs for the MSSM and Low-Scale SUSY Breaking," Phys. Rev. D **85**, 095007 (2012), [arXiv:1112.3068 [hep-ph]].

[135] N. Chen, H. -J. He, "LHC Signatures of Two-Higgs-Doublets with Fourth Family," JHEP **1204**, 062 (2012), [arXiv:1202.3072 [hep-ph]].

[136] G. Guo, B. Ren, X. -G. He, "LHC Evidence Of A 126 GeV Higgs Boson From $H \to \gamma\gamma$ With Three And Four Generations," arXiv:1112.3188 [hep-ph].

[137] X. -G. He, B. Ren, J. Tandean "Hints of Standard Model Higgs Boson at the LHC and Light Dark Matter Searches," Phys. Rev. D **85**, 093019 (2012), [arXiv:1112.6364 [hep-ph]].

[138] A. Djouadi, O. Lebedev, Y. Mambrini, J. Quevillon, "Implications of LHC searches for Higgs–portal dark matter," Phys. Lett. B **709**, 65 (2012), [arXiv:1112.3299 [hep-ph]].

[139] K. Cheung, T. -C. Yuan, "Could the excess seen at 124-126 GeV be due to the Randall-Sundrum Radion?," Phys. Rev. Lett. **108**, 141602 (2012), [arXiv:1112.4146 [hep-ph]].

[140] M. Hemeda, S. Khalil and S. Moretti, "Light Chargino Effects onto $H \to \gamma\gamma$ in the MSSM," Phys. Rev. D **89**, 011701 (2014), [arXiv:1312.2504 [hep-ph]].

[141] A. Belyaev, S. Khalil, S. Moretti and M. Thomas, "Light sfermion interplay in the 125 GeV MSSM Higgs production and decay at the LHC," arXiv:1312.1935 [hep-ph].

[142] B. Batell, S. Gori, L. -T. Wang, "Exploring the Higgs Portal with 10/fb at the LHC," JHEP **1206**, 172 (2012).

[143] M. Kadastik, K. Kannike, A. Racioppi, M. Raidal, "Implications of the 125 GeV Higgs boson for scalar dark matter and for the CMSSM phenomenology," JHEP **1205**, 061 (2012), [arXiv:1112.3647 [hep-ph]]. H. Baer, V. Barger, A. Mustafayev, "Implications of a 125 GeV Higgs scalar for LHC SUSY and neutralino dark matter searches," Phys. Rev. D **85**, 075010 (2012), [arXiv:1112.3017 [hep-ph]]. J. F. Gunion, Y. Jiang, S. Kraml, "The Constrained NMSSM and Higgs near 125 GeV," Phys. Lett. B **710**, 454 (2012); [arXiv:1201.0982 [hep-ph]]. L. Aparicio, D. G. Cerdeno, L. E. Ibanez, "A 119-125 GeV Higgs from a string derived slice of the CMSSM," JHEP **1204**, 126 (2012); [arXiv:1202.0822 [hep-ph]]. J. Ellis, K. A. Olive, "Revisiting the Higgs Mass and Dark Matter in the CMSSM," Eur. Phys. J. C **72**, 2005 (2012); [arXiv:1202.3262 [hep-ph]]. H. Baer, V. Barger, A. Mustafayev, "Neutralino dark matter in mSUGRA/CMSSM with a 125 GeV light Higgs scalar," JHEP **1205**, 091 (2012); [arXiv:1202.4038 [hep-ph]]. N. Desai, B. Mukhopadhyaya, S. Niyogi, "Constraints on Invisible Higgs Decay in MSSM in the Light of Diphoton Rates from the LHC," arXiv:1202.5190 [hep-ph]. J. Cao, Z. Heng, D. Li, J. M. Yang, "Current experimental constraints on the lightest Higgs boson mass in the constrained MSSM," Phys. Lett. B **710**, 665 (2012), [arXiv:1112.4391 [hep-ph]].

[144] S. F. King, M. Muhlleitner, R. Nevzorov, K. Walz, "Natural NMSSM Higgs Bosons," Nucl. Phys. B **870**, 323 (2013); [arXiv:1211.5074 [hep-ph]]. G. Belanger, U. Ellwanger, J. F. Gunion, Y. Jiang, S. Kraml, J. H. Schwarz, "Higgs Bosons at 98 and 125 GeV at LEP and the LHC," JHEP **1301**, 069 (2013); [arXiv:1210.1976 [hep-ph]]. J. F. Gunion, Y. Jiang, S. Kraml, "The Constrained NMSSM and Higgs near 125 GeV," Phys. Lett. B **710**, 454 (2012); [arXiv:1201.0982 [hep-ph]]. U. Ellwanger, C. Hugonie, "Higgs bosons near 125 GeV in the NMSSM with constraints at the GUT scale," Adv. High Energy Phys. **2012**, 625389 (2012); [arXiv:1203.5048 [hep-ph]]. U. Ellwanger, "A Higgs boson near 125 GeV with enhanced di-photon signal in the NMSSM," JHEP **1203**, 044 (2012); [arXiv:1112.3548 [hep-ph]]. J. -J. Cao, Z. -X. Heng, J. M. Yang, Y. -M. Zhang, J. -Y. Zhu, "A SM-like Higgs near 125 GeV in low energy SUSY: a comparative study for MSSM

and NMSSM," JHEP **1203**, 086 (2012); [arXiv:1202.5821 [hep-ph]]. Z. Kang, J. Li and T. Li, "On Naturalness of the MSSM and NMSSM," JHEP **1211**, 024 (2012); [arXiv:1201.5305 [hep-ph]].

[145] A. Dedes and S. Moretti, "Effects of CP violating phases on Higgs boson production at hadron colliders in the minimal supersymmetric standard model," Nucl. Phys. B **576**, 29 (2000); [hep-ph/9909418].

[146] A. Dedes and S. Moretti, "Effect of large supersymmetric phases on Higgs production.," Phys. Rev. Lett. **84**, 22 (2000); [hep-ph/9908516].

[147] S. Hesselbach, S. Moretti, S. Munir and P. Poulose, "CP-violating Higgs sector of the MSSM through g g $\to$H$_1$ $\to\gamma\gamma$," J. Phys. Conf. Ser. **335**, 012020 (2011); [arXiv:1103.4437 [hep-ph]].

[148] S. Hesselbach, S. Moretti, S. Munir and P. Poulose, "Explicit CP violation in the MSSM Higgs sector," AIP Conf. Proc. **1200**, 498 (2010); [arXiv:0910.0230 [hep-ph]].

[149] S. Moretti, S. Munir and P. Poulose, "Explicit CP Violation in the MSSM Through Higgs $\to$ $\gamma\gamma$," Phys. Lett. B **649**, 206 (2007); hep-ph/0702242 [hep-ph].

[150] S. Hesselbach, S. Moretti, S. Munir and P. Poulose, "Exploring the Di-Photon Decay of a Light Higgs Boson in the MSSM With Explicit CP Violation," Eur. Phys. J. C **54**, 129 (2008); [arXiv:0706.4269 [hep-ph]].

[151] S. Hesselbach, S. Moretti, S. Munir and P. Poulose, "Explicit CP violation in the MSSM through $gg \to H(1) \to \gamma\gamma$," Phys. Rev. D **82**, 074004 (2010); [arXiv:0903.0747 [hep-ph]].

[152] O. Kittel, "CP violation in production and decay of supersymmetric particles," hep-ph/0504183.

[153] I. Hinchliffe and N. Kersting, "Constraining CP violating phases of the MSSM," Phys. Rev. D **63**, 015003 (2001); [hep-ph/0003090].

[154] S. W. Ham, S. G. Jo, S. K. OH and D. Son, "The Higgs search of the MSSM with explicit CP violation at the LHC and ILC," arXiv:0711.3951 [hep-ph].

[155] T. Gajdosik, R. M. Godbole and S. Kraml, "Fermion polarization in sfermion decays as a probe of CP phases in the MSSM," JHEP **0409**, 051 (2004); [hep-ph/0405167].

[156] T. -F. Feng, X. -Q. Li and J. Maalampi, "Mixing among the neutral Higgs bosons and rare B decays in the CP violating MSSM," Phys. Rev. D **73**, 035011 (2006); [hep-ph/0602056].

[157] S. Baek and P. Ko, "Probing SUSY induced CP violations at B factories," Phys. Rev. Lett. **83**, 488 (1999); [hep-ph/9812229].

[158] W. Altmannshofer, A. J. Buras and P. Paradisi, "Low Energy Probes of CP Violation in a Flavor Blind MSSM," Phys. Lett. B **669**, 239 (2008); [arXiv:0808.0707 [hep-ph]].

[159] D. A. Demir, A. Masiero and O. Vives, 2"CP conserving constraints on supersymmetric CP violation in the MSSM," Phys. Rev. D **61**, 075009 (2000); [hep-ph/9909325].

[160] S. Y. Choi and J. S. Lee, "MSSM Higgs boson production at hadron colliders with explicit CP violation," Phys. Rev. D **61**, 115002 (2000); [hep-ph/9910557].

[161] S. Y. Choi, K. Hagiwara and J. S. Lee, "Observability of the lightest MSSM Higgs boson with explicit CP violation via gluon fusion at the LHC," Phys. Lett. B **529**, 212 (2002); [hep-ph/0110138].

[162] M. S. Carena, J. R. Ellis, A. Pilaftsis and C. E. M. Wagner, "CP violating MSSM Higgs bosons in the light of LEP-2," Phys. Lett. B **495**, 155 (2000); [hep-ph/0009212].

[163] J. R. Ellis, J. S. Lee and A. Pilaftsis, "Resonant CP violation in Higgs radiation at e+ e- linear collider," Phys. Rev. D **72**, 095006 (2005); [hep-ph/0507046].

[164] R. M. Godbole, S. Kraml, S. D. Rindani and R. K. Singh, "Probing CP-violating Higgs contributions in $\gamma\gamma \to$ f anti-f through fermion polarization," Phys. Rev. D **74**, 095006 (2006); [hep-ph/0609113].

[165] A. G. Akeroyd and A. Arhrib, "Probing scalar pseudoscalar mixing in the CP violating MSSM at high-energy e+ e- colliders," Phys. Rev. D **64**, 095018 (2001); [hep-ph/0107040].

[166] S. Y. Choi, K. Hagiwara and J. S. Lee, "Higgs boson decays in the minimal supersymmetric standard model with radiative Higgs sector CP violation," Phys. Rev. D **64**, 032004 (2001); [hep-ph/0103294].

[167] S. Y. Choi, M. Drees, J. S. Lee and J. Song, "Supersymmetric Higgs boson decays in the MSSM with explicit CP violation," Eur. Phys. J. C **25**, 307 (2002); [hep-ph/0204200].

[168] F. Deppisch and O. Kittel, "Probing SUSY CP Violation in Two-Body Stop Decays at the LHC," JHEP **0909**, 110 (2009); [arXiv:0905.3088 [hep-ph]].

[169] D. K. Ghosh, R. M. Godbole and D. P. Roy, "Probing the CP-violating light neutral Higgs in the charged Higgs decay at the LHC," Phys. Lett. B **628**, 131 (2005); [hep-ph/0412193].

[170] D. K. Ghosh and S. Moretti, "Probing the light neutral Higgs boson scenario of the CP-violating MSSM Higgs sector at the LHC," Eur. Phys. J. C **42**, 341 (2005); [hep-ph/0412365].

[171] A. Arhrib, D. K. Ghosh and O. C. W. Kong, "Observing CP violating MSSM Higgs bosons at hadron colliders?," Phys. Lett. B **537**, 217 (2002); [hep-ph/0112039].

[172] B. Bhattacherjee, A. Chakraborty, D. Kumar Ghosh and S. Raychaudhuri, "Using Jet Substructure at the LHC to Search for the Light Higgs Bosons of the CP-Violating MSSM," Phys. Rev. D **86**, 075012 (2012); [arXiv:1204.3369 [hep-ph]].

[173] A. Bartl, S. Hesselbach, K. Hidaka, T. Kernreiter and W. Porod, "Top squarks and bottom squarks in the MSSM with complex parameters," Phys. Rev. D **70**, 035003 (2004); [hep-ph/0311338].

[174] A. Bartl, S. Hesselbach, K. Hidaka, T. Kernreiter and W. Porod, "Impact of CP phases on the search for top and bottom squarks," hep-ph/0409347.

[175] C. -H. Chen, "Impact of CP phases on a light sbottom and gluino sector," Phys. Lett. B **579**, 371 (2004); [hep-ph/0311107].

[176] A. Bartl, S. Hesselbach, K. Hidaka, T. Kernreiter and W. Porod, "Impact of CP phases on stop and sbottom searches," Phys. Lett. B **573**, 153 (2003); [hep-ph/0307317].

[177] A. Bartl, S. Hesselbach, K. Hidaka, T. Kernreiter and W. Porod, "Impact of SUSY CP phases on stop and sbottom decays in the MSSM," hep-ph/0306281.

[178] T. Ibrahim, U. Chattopadhyay and P. Nath, "Constraints on explicit CP violation from the Brookhaven muon g-2 experiment," Phys. Rev. D **64**, 016010 (2001); [hep-ph/0102324].

[179] T. Ibrahim, "Mixing of the CP even and the CP odd Higgs bosons and the EDM constraints," Phys. Rev. D **64**, 035009 (2001); [hep-ph/0102218].

[180] T. Ibrahim and P. Nath, "Large CP phases and the cancellation mechanism in EDMs in SUSY, string and brane models," Phys. Rev. D **61**, 093004 (2000); [hep-ph/9910553].

[181] A. Romanino and A. Strumia, "Electric dipole moments from Yukawa phases in supersymmetric theories," Nucl. Phys. B **490**, 3 (1997); [hep-ph/9610485].

[182] S. Yaser Ayazi and Y. Farzan, "Reconciling large CP-violating phases with bounds on the electric dipole moments in the MSSM," Phys. Rev. D **74**, 055008 (2006); [hep-ph/0605272].

[183] H. Georgi, A. Pais,Phys. Rev. D **10** (1974) 1246; N. Maekawa, Phys. Lett. B **282**, 387 (1992); A. Pilaftsis, Phys. Lett. B **435**, 88 (1998).

[184] O. C.W. Kong, F. L. Lin, Phys. Lett. B **418**, 217 (1998); N. Haba, Phys. Lett. B **398**, 305 (1997); A. Pomarol, Phys. Lett. B **287**, 331 (1992).

[185] M. S. Carena, J. R. Espinosa, M. Quiros and C. E. M. Wagner, "Analytical expressions for radiatively corrected Higgs masses and couplings in the MSSM," Phys. Lett. B **355**, 209 (1995); [hep-ph/9504316].

[186] S. Y. Choi, J. Kalinowski, Y. Liao and P. M. Zerwas, "H/A Higgs mixing in CP-noninvariant supersymmetric theories," Eur. Phys. J. C **40**, 555 (2005); [hep-ph/0407347].

[187] M. S. Carena, J. R. Ellis, A. Pilaftsis and C. E. M. Wagner, "Higgs boson pole masses in the MSSM with explicit CP violation," Nucl. Phys. B **625**, 345 (2002); [hep-ph/0111245].

[188] M. S. Carena, J. R. Ellis, A. Pilaftsis and C. E. M. Wagner, "Renormalization group improved effective potential for the MSSM Higgs sector with explicit CP violation," Nucl. Phys. B **586**, 92 (2000); [hep-ph/0003180].

[189] K. E. Williams, H. Rzehak and G. Weiglein, "Higher order corrections to Higgs boson decays in the MSSM with complex parameters," Eur. Phys. J. C **71**, 1669 (2011); [arXiv:1103.1335 [hep-ph]].

[190] D. Chang, W. -Y. Keung and A. Pilaftsis, "New two loop contribution to electric dipole moment in supersymmetric theories," Phys. Rev. Lett. **82**, 900 (1999); [hep-ph/9811202].

[191] A. Pilaftsis, "Higgs mediated electric dipole moments in the MSSM: An application to baryogenesis and Higgs searches," Nucl. Phys. B **644**, 263 (2002); [hep-ph/0207277].

[192] K. A. Olive, M. Pospelov, A. Ritz and Y. Santoso, "CP-odd phase correlations and electric dipole moments," Phys. Rev. D **72**, 075001 (2005); [hep-ph/0506106].

[193] A. Sopczak [ALEPH and DELPHI and L3 and OPAL Collaborations], "MSSM Higgs boson searches at LEP," hep-ph/0602136.

[194] S. Schael *et al.* [ALEPH and DELPHI and L3 and OPAL and LEP Working Group for Higgs Boson Searches Collaborations], "Search for neutral MSSM Higgs bosons at LEP," Eur. Phys. J. C **47**, 547 (2006); [hep-ex/0602042].

[195] J. Beringer et al. (Particle Data Group), Phys. Rev. D86, 010001 (2012).

[196] A. J. Buras, J. Girrbach, D. Guadagnoli and G. Isidori, "On the Standard Model prediction for BR($B_{s,d} \to \mu^+\mu^-$)," Eur. Phys. J. C **72**, 2172 (2012); arXiv:1208.0934 [hep-ph].

[197] K. S. Babu and C. F. Kolda, "Higgs mediated $B^0 \to \mu^+\mu^-$ in minimal supersymmetry," Phys. Rev. Lett. **84**, 228 (2000); [hep-ph/9909476].

[198] S. R. Choudhury and N. Gaur, "Dileptonic decay of B(s) meson in SUSY models with large tan Beta," Phys. Lett. B **451**, 86 (1999); [hep-ph/9810307].

[199] W. Altmannshofer, M. Carena, N. R. Shah and F. Yu, "Indirect Probes of the MSSM after the Higgs Discovery," JHEP **1301**, 160 (2013); [arXiv:1211.1976 [hep-ph]].

[200] The ATLAS collaboration, "Search for charged Higgs bosons in the τ+jets final state with pp collision data recorded at $\sqrt{s} = 8$ TeV with the ATLAS experiment," ATLAS-CONF-2013-090.

[201] CMS Collaboration [CMS Collaboration], "Higgs to tau tau (MSSM)," CMS-PAS-HIG-13-021.

[202] **LHCb Collaboration**, R. Aaij *et al.*, "Measurement of the $B^0_s \to \mu^+\mu^-$ branching fraction and effective lifetime and search for $B^0 \to \mu^+\mu^-$ decays," *Phys. Rev. Lett.* **118** no. 19, (2017) 191801, arXiv:1703.05747 [hep-ex].

[203] S. Bertolini, F. Borzumati and A. Masiero, "QCD Enhancement of Radiative b Decays," Phys. Rev. Lett. **59**, 180 (1987); N. G. Deshpande, P. Lo, J. Trampetic, G. Eilam and P. Singer, "$B \to K\gamma$ and the Top-Quark Mass," Phys. Rev. Lett. **59**, 183 (1987); B. Grinstein and M. B. Wise, "Weak Radiative B Meson Decay as a Probe of the Higgs Sector," Phys. Lett. B **201**, 274 (1988); B. Grinstein, R. P. Springer and M. B. Wise, "Effective Hamiltonian for Weak Radiative B Meson Decay," Phys. Lett. B **202**, 138 (1988); W. -S. Hou and R. S. Willey, "Effects of Charged Higgs Bosons on the Processes $b \to s\gamma, b \to sg^*$ and $b \to s$ Lepton+ Lepton-," Phys. Lett. B **202**, 591 (1988); B. Grinstein, R. P. Springer and M. B. Wise, "STRONG INTERACTION EFFECTS IN WEAK RADIATIVE anti-B MESON DECAY," Nucl. Phys. B **339**, 269 (1990).

[204] S. Bertolini, F. Borzumati, A. Masiero and G. Ridolfi, "Effects of supergravity induced electroweak breaking on rare B decays and mixings," Nucl. Phys. B **353**, 591 (1991); R. Barbieri and G. F. Giudice, "$b \to s\gamma$ decay and supersymmetry," Phys. Lett. B **309**, 86 (1993); hep-ph/9303270; R. Garisto and J. N. Ng, "Supersymmetric $b \to s\gamma$ with large chargino contributions," Phys. Lett. B **315**, 372 (1993); hep-ph/9307301; P. Nath and R. L. Arnowitt, "$b \to s\gamma$ decay in supergravity grand unification and dark matter," Phys. Lett. B **336**, 395 (1994); hep-ph/9406389; M. Ciuchini, G. Degrassi, P. Gambino and G. F. Giudice, "Next-to-leading QCD corrections to $B \to X_s\gamma$ in supersymmetry," Nucl. Phys. B **534**, 3 (1998); [hep-ph/9806308].

[205] M. S. Carena, D. Garcia, U. Nierste and C. E. M. Wagner, "b —¿ s gamma and supersymmetry with large tan Beta," Phys. Lett. B **499**, 141 (2001); [hep-ph/0010003].

[206] **HFLAV Collaboration**, Y. Amhis *et al.*, "Averages of b-hadron, c-hadron, and τ-lepton properties as of summer 2016," *Eur. Phys. J.* **C77** no. 12, (2017) 895, arXiv:1612.07233 [hep-ex].

[207] A. J. Buras, P. H. Chankowski, J. Rosiek and L. Slawianowska, "$\Delta M_{d,s}, B^0 d, s \to \mu^+\mu^-$ and $B \to X_s\gamma$ in supersymmetry at large $\tan\beta$," Nucl. Phys. B **659**, 3 (2003); [hep-ph/0210145].

[208] P. Ball and R. Fleischer, "Probing new physics through B mixing: Status, benchmarks and prospects," Eur. Phys. J. C **48**, 413 (2006); [hep-ph/0604249].

[209] G. Isidori and F. Teubert, "Status of indirect searches for New Physics with heavy flavour decays after the initial LHC run," Eur. Phys. J. Plus **129**, 40 (2014); [arXiv:1402.2844 [hep-ph]].

[210] Y. Amhis *et al.* [Heavy Flavor Averaging Group Collaboration]. "Averages of B-Hadron, C-Hadron, and tau-lepton properties as of early 2012," arXiv:1207.1158 [hep-ex]

[211] M. Bona *et al.* [UTfit Collaboration], "The Unitarity Triangle Fit in the Standard Model and Hadronic Parameters from Lattice QCD: A Reappraisal after the Measurements of Δm_s and BR($B \to \tau\nu_\tau$)," JHEP **0610**, 081 (2006); [hep-ph/0606167].

[212] R. Aaij *et al.* [LHCb Collaboration], "Precision measurement of the B_s^0-$\bar{B}_s^0$ oscillation frequency with the decay $B_s^0 \to D_s^-\pi^+$," New J. Phys. **15**, 053021 (2013); [arXiv:1304.4741 [hep-ex]].

[213] A. Lenz and U. Nierste, "Numerical Updates of Lifetimes and Mixing Parameters of B Mesons," arXiv:1102.4274 [hep-ph].

[214] G. Isidori and P. Paradisi, "Hints of large tan(beta) in flavour physics," Phys. Lett. B **639**, 499 (2006); [hep-ph/0605012].

[215] N. Fornengo, S. Scopel and A. Bottino, "Discussing direct search of dark matter particles in the Minimal Supersymmetric extension of the Standard Model with light neutralinos," Phys. Rev. D **83**, 015001 (2011); [arXiv:1011.4743 [hep-ph]].

[216] M. Chakraborti, U. Chattopadhyay and R. M. Godbole, "Implication of a Higgs boson at 125 GeV within the stochastic superspace framework," Phys. Rev. D **87**, no. 3, 035022 (2013); [arXiv:1211.1549 [hep-ph]].

[217] J. S. Lee, M. Carena, J. Ellis, A. Pilaftsis and C. E. M. Wagner, "CPsuperH2.3: an Updated Tool for Phenomenology in the MSSM with Explicit CP Violation," Comput. Phys. Commun. **184**, 1220 (2013); [arXiv:1208.2212 [hep-ph]]; J. S. Lee, M. Carena, J. Ellis, A. Pilaftsis and C. E. M. Wagner, "CPsuperH2.0: an Improved Computational Tool for Higgs Phenomenology

in the MSSM with Explicit CP Violation," Comput. Phys. Commun. **180**, 312 (2009); [arXiv:0712.2360 [hep-ph]]. J. S. Lee, A. Pilaftsis, M. S. Carena, S. Y. Choi, M. Drees, J. R. Ellis and C. E. M. Wagner, "CPsuperH: A Computational tool for Higgs phenomenology in the minimal supersymmetric standard model with explicit CP violation," Comput. Phys. Commun. **156**, 283 (2004); [hep-ph/0307377].

[218] CMS Collaboration CMS-PAS-SUS-12-005, CMS-PAS-SUS-13-012.

[219] ATLAS Collaboration ATLAS-CONF-2012-109, ATLAS-CONF-2013-047, ATLAS-CONF-2013-062.

[220] G. Aad *et al.* [ATLAS Collaboration], "Search for the neutral Higgs bosons of the Minimal Supersymmetric Standard Model in pp collisions at $\sqrt{s} = 7$ TeV with the ATLAS detector," JHEP **1302**, 095 (2013); [arXiv:1211.6956 [hep-ex]].

[221] CMS Collaboration [CMS Collaboration], "Measurements of properties of the Higgs boson in the diphoton decay channel with the full 2016 data set," CMS-PAS-HIG-16-040.

[222] CMS Collaboration [CMS Collaboration], "Measurements of properties of the Higgs boson decaying into four leptons in pp collisions at sqrts = 13 TeV," CMS-PAS-HIG-16-041.

[223] CMS Collaboration [CMS Collaboration], "Measurements of properties of the Higgs boson decaying to a W boson pair in pp collisions at $\sqrt{s} = 13$ TeV," CMS-PAS-HIG-16-042.

[224] CMS Collaboration [CMS Collaboration], "Evidence for the decay of the Higgs Boson to Bottom Quarks," CMS-PAS-HIG-16-044.

[225] A. M. Sirunyan *et al.* [CMS Collaboration], "Observation of the Higgs boson decay to a pair of τ leptons with the CMS detector," Phys. Lett. B **779**, 283 (2018) [arXiv:1708.00373 [hep-ex]].

[226] K. Hagiwara, J. S. Lee and J. Nakamura, "Properties of 125 GeV Higgs boson in non-decoupling MSSM scenarios," JHEP **1210**, 002 (2012); [arXiv:1207.0802 [hep-ph]].

[227] M. Carena, S. Gori, N. R. Shah, C. E. M. Wagner and L. -T. Wang, "Light Stops, Light Staus and the 125 GeV Higgs," JHEP **1308**, 087 (2013) [arXiv:1303.4414 [hep-ph]].

[228] **ATLAS Collaboration**, M. Aaboud *et al.*, "Measurement of the Higgs boson coupling properties in the $H \to ZZ^* \to 4\ell$ decay channel at $\sqrt{s} = 13$ TeV with the ATLAS detector," *JHEP* **03** (2018) 095, arXiv:1712.02304 [hep-ex]

[229] The ATLAS collaboration [ATLAS Collaboration], "Measurement of gluon fusion and vector boson fusion Higgs boson production cross-sections in the $H \to WW^* \to e\nu\mu\nu$ decay channel in pp collisions at $\sqrt{s} = 13$ TeV with the ATLAS detector," ATLAS-CONF-2018-004.

[230] M. Aaboud *et al.* [ATLAS Collaboration], "Evidence for the $H \to b\bar{b}$ decay with the ATLAS detector," JHEP **1712**, 024 (2017) [arXiv:1708.03299 [hep-ex]].

[231] The ATLAS collaboration [ATLAS Collaboration], "Cross-section measurements of the Higgs boson decaying to a pair of tau leptons in proton–proton collisions at $\sqrt{s} = 13$ TeV with the ATLAS detector," ATLAS-CONF-2018-021.

[232] G. Aad *et al.* [ATLAS Collaboration], "Measurements of Higgs boson production and couplings in diboson final states with the ATLAS detector at the LHC," Phys. Lett. B **726**, 88 (2013) [arXiv:1307.1427 [hep-ex]].

[233] S. Chatrchyan *et al.* [CMS Collaboration], "Measurement of the properties of a Higgs boson in the four-lepton final state," Phys. Rev. D **89**, 092007 (2014) [arXiv:1312.5353 [hep-ex]].

[234] A. Freitas and P. Schwaller, "Higgs CP Properties From Early LHC Data," Phys. Rev. D **87**, no. 5, 055014 (2013) [arXiv:1211.1980 [hep-ph]].

[235] G. Belanger, B. Dumont, U. Ellwanger, J. F. Gunion and S. Kraml, "Higgs Couplings at the End of 2012," JHEP **1302**, 053 (2013) [arXiv:1212.5244 [hep-ph]].

[236] K. Cheung, J. S. Lee and P. Y. Tseng, "Higgs Precision (Higgcision) Era begins," JHEP **1305**, 134 (2013) [arXiv:1302.3794 [hep-ph]].

[237] K. Cheung, J. S. Lee and P. Y. Tseng, "Higgcision Updates 2014," arXiv:1407.8236 [hep-ph].

[238] K. Cheung, J. S. Lee, E. Senaha and P. Y. Tseng, "Confronting Higgcision with Electric Dipole Moments," JHEP **1406**, 149 (2014) [arXiv:1403.4775 [hep-ph]].

[239] M. J. Dolan, P. Harris, M. Jankowiak and M. Spannowsky, "Constraining CP-violating Higgs Sectors at the LHC using gluon fusion," arXiv:1406.3322 [hep-ph].

[240] J. Shu and Y. Zhang, "Impact of a CP Violating Higgs Sector: From LHC to Baryogenesis," Phys. Rev. Lett. **111**, no. 9, 091801 (2013) [arXiv:1304.0773 [hep-ph]].

[241] T. Gherghetta, B. von Harling, A. D. Medina, and M. A. Schmidt, "The Scale-Invariant NMSSM and the 126 GeV Higgs Boson," *JHEP* **1302** (2013) 032, arXiv:1212.5243 [hep-ph].

[242] T. Fritzsche, S. Heinemeyer, H. Rzehak and C. Schappacher, "Heavy Scalar Top Quark Decays in the Complex MSSM: A Full One-Loop Analysis," *Phys. Rev.* **D86** (2012) 035014, arXiv:1111.7289 [hep-ph]

[243] T. Graf, R. Grober, M. Muhlleitner, H. Rzehak and K. Walz, "Higgs Boson Masses in the Complex NMSSM at One-Loop Level," *JHEP* **1210** (2012) 122, arXiv:1206.6806 [hep-ph].

[244] S. Munir, "Novel Higgs-to-125 GeV Higgs boson decays in the complex NMSSM," *Phys.Rev.* **D89** (2014) 095013, arXiv:1310.8129 [hep-ph].

[245] P. Bechtle, S. Heinemeyer, O. Stal, T. Stefaniak and G. Weiglein, "*HiggsSignals*: Confronting arbitrary Higgs sectors with measurements at the Tevatron and the LHC," *Eur.Phys.J.* **C74** no. 2, (2014) 2711, arXiv:1305.1933 [hep-ph].

[246] G. Cacciapaglia, A. Deandrea and S. De Curtis, "Nearby resonances beyond the Breit-Wigner approximation," *Phys. Lett.* **B682** (2009) 43–49, arXiv:0906.3417 [hep-ph]

[247] N. Chen and Z. Liu, "Degenerate Higgs bosons: hiding a second Higgs at 125 GeV," arXiv:1607.02154 [hep-ph]

[248] U. Ellwanger and C. Hugonie, "Yukawa induced radiative corrections to the lightest Higgs boson mass in the NMSSM," *Phys. Lett.* **B623** (2005) 93–103, arXiv:hep-ph/0504269 [hep-ph].

[249] G. Degrassi and P. Slavich, "On the radiative corrections to the neutral Higgs boson masses in the NMSSM," *Nucl.Phys.* **B825** (2010) 119–150, arXiv:0907.4682 [hep-ph].

[250] M. D. Goodsell, K. Nickel and F. Staub, "Two-loop corrections to the Higgs masses in the NMSSM," *Phys.Rev.* **D91** no. 3, (2015) 035021, arXiv:1411.4665 [hep-ph].

[251] S. Ham, S. Oh and D. Son, "Neutral Higgs sector of the next-to-minimal supersymmetric standard model with explicit CP violation," *Phys.Rev.* **D65** (2002) 075004, arXiv:hep-ph/0110052

[252] K. Funakubo and S. Tao, "The Higgs sector in the next-to-MSSM," *Prog.Theor.Phys.* **113** (2005) 821–842, arXiv:hep-ph/0409294.

[253] K. Cheung, T.-J. Hou, J. S. Lee and E. Senaha, "The Higgs Boson Sector of the Next-to-MSSM with CP Violation," *Phys.Rev.* **D82** (2010) 075007, arXiv:1006.1458 [hep-ph].

[254] K. Cheung, T.-J. Hou, J. S. Lee and E. Senaha, "Higgs Mediated EDMs in the Next-to-MSSM: An Application to Electroweak Baryogenesis," *Phys.Rev.* **D84** (2011) 015002, arXiv:1102.5679 [hep-ph].

[255] F. Domingo, "A New Tool for the study of the CP-violating NMSSM," *JHEP* **06** (2015) 052, arXiv:1503.07087 [hep-ph].

[256] M. Muhlleitner, D. T. Nhung, H. Rzehak and K. Walz, "Two-loop contributions of the order $\mathcal{O}(\alpha_t\alpha_s)$ to the masses of the Higgs bosons in the CP-violating NMSSM," *JHEP* **05** (2015) 128, arXiv:1412.0918 [hep-ph].

[257] M. Spira, A. Djouadi, D. Graudenz, and P. Zerwas, "Higgs boson production at the LHC," *Nucl.Phys.* **B453** (1995) 17–82, arXiv:hep-ph/9504378.

[258] J. Baglio, R. Grober, M. Muhlleitner, D. Nhung, H. Rzehak *et al.*, "NMSSMCALC: A Program Package for the Calculation of Loop-Corrected Higgs Boson Masses and Decay Widths in the (Complex) NMSSM," *Comput.Phys.Commun.* (2014) , arXiv:1312.4788 [hep-ph].

[259] P. Z. Skands *et al.*, "SUSY Les Houches accord: Interfacing SUSY spectrum calculators, decay packages, and event generators," *JHEP* **07** (2004) 036, arXiv:hep-ph/0311123

[260] B. C. Allanach *et al.*, "SUSY Les Houches Accord 2," *Comput. Phys. Commun.* **180** (2009) 8–25, arXiv:0801.0045 [hep-ph].

[261] P. Bechtle, O. Brein, S. Heinemeyer, G. Weiglein and K. E. Williams, "HiggsBounds: Confronting Arbitrary Higgs Sectors with Exclusion Bounds from LEP and the Tevatron," *Comput.Phys.Commun.* **181** (2010) 138–167, arXiv:0811.4169 [hep-ph]

[262] P. Bechtle, O. Brein, S. Heinemeyer, G. Weiglein and K. E. Williams, "HiggsBounds 2.0.0: Confronting Neutral and Charged Higgs Sector Predictions with Exclusion Bounds from LEP and the Tevatron," *Comput.Phys.Commun.* **182** (2011) 2605–2631, arXiv:1102.1898 [hep-ph]

[263] P. Bechtle, O. Brein, S. Heinemeyer, O. Stål, T. Stefaniak *et al.*, "Recent Developments in HiggsBounds and a Preview of HiggsSignals," *PoS* **CHARGED2012** (2012) 024, arXiv:1301.2345 [hep-ph]

[264] P. Bechtle, O. Brein, S. Heinemeyer, O. Stål, T. Stefaniak *et al.*, "HiggsBounds – 4: Improved Tests of Extended Higgs Sectors against Exclusion Bounds from LEP, the Tevatron and the LHC," *Eur.Phys.J.* **C74** (2014) 2693, arXiv:1311.0055 [hep-ph].

[265] **ATLAS Collaboration**, G. Aad *et al.*, "Constraints on the off-shell Higgs boson signal strength in the high-mass ZZ and WW final states with the ATLAS detector," *Eur. Phys. J.* **C75** no. 7, (2015) 335, arXiv:1503.01060 [hep-ex].

[266] **CMS Collaboration**, V. Khachatryan *et al.*, "Limits on the Higgs boson lifetime and width from its decay to four charged leptons," *Phys. Rev.* **D92** no. 7, (2015) 072010, arXiv:1507.06656 [hep-ex]

[267] **CMS Collaboration**, V. Khachatryan *et al.*, "Search for Higgs boson off-shell production in proton-proton collisions at 7 and 8 TeV and derivation of constraints on its total decay width," *JHEP* **09** (2016) 051, arXiv:1605.02329 [hep-ex].

[268] F. Caola and K. Melnikov, "Constraining the Higgs boson width with ZZ production at the LHC," *Phys. Rev.* **D88** (2013) 054024, arXiv:1307.4935 [hep-ph].

[269] C. Englert and M. Spannowsky, "Limitations and Opportunities of Off-Shell Coupling Measurements," *Phys. Rev.* **D90** (2014) 053003, arXiv:1405.0285 [hep-ph].

[270] https://www.netlib.org/lapack/

[271] G. P. Lepage, "A New Algorithm for Adaptive Multidimensional Integration," *J. Comput. Phys.* **27** (1978) 192.

[272] R. V. Harlander, S. Liebler and H. Mantler, "SusHi: A program for the calculation of Higgs production in gluon fusion and bottom-quark annihilation in the Standard Model and the MSSM," *Computer Physics Communications* **184** (2013) 1605–1617, arXiv:1212.3249 [hep-ph]

[273] S. Liebler, "Neutral Higgs production at proton colliders in the CP-conserving NMSSM," *Eur. Phys. J.* **C75** no. 5, (2015) 210, arXiv:1502.07972 [hep-ph]

[274] R. V. Harlander, S. Liebler and H. Mantler, "SusHi Bento: Beyond NNLO and the heavy-top limit," arXiv:1605.03190 [hep-ph].

[275] **LHC Higgs Cross Section Working Group**, J. R. Andersen *et al.*, "Handbook of LHC Higgs Cross Sections: 3. Higgs Properties," arXiv:1307.1347 [hep-ph].

[276] H.-L. Lai, M. Guzzi, J. Huston, Z. Li, P. M. Nadolsky, J. Pumplin and C. P. Yuan, "New parton distributions for collider physics," *Phys. Rev.* **D82** (2010) 074024, arXiv:1007.2241 [hep-ph].

[277] **LHC Higgs Cross Section Working Group**, D. de Florian *et al.*, "Handbook of LHC Higgs Cross Sections: 4. Deciphering the Nature of the Higgs Sector," arXiv:1610.07922 [hep-ph].

[278] A. M. Sirunyan *et al.* [CMS Collaboration], "Measurement of inclusive and differential Higgs boson production cross sections in the diphoton decay channel in proton-proton collisions at $\sqrt{s} = 13$ TeV," arXiv:1807.03825 [hep-ex].

[279] http://reference.wolfram.com/language/ref/ListConvolve.html

[280] F. Gianotti *et al.*, "Physics potential and experimental challenges of the LHC luminosity upgrade," *Eur. Phys. J.* **C39** (2005) 293–333, arXiv:hep-ph/0204087 [hep-ph].

[281] **CMS Collaboration**, "Measurements of properties of the Higgs boson and search for an additional resonance in the four-lepton final state at sqrt(s) = 13 TeV," CMS-PAS-HIG-16-033.

[282] G. Cacciapaglia, A. Deandrea, G. Drieu La Rochelle and J.-B. Flament, "Higgs couplings: disentangling New Physics with off-shell measurements," *Phys. Rev. Lett.* **113** no. 20, (2014) 201802, arXiv:1406.1757 [hep-ph].

[283] H. E. Logan, "Hiding a Higgs width enhancement from off-shell $gg(\to h^*) \to ZZ$ measurements," *Phys. Rev.* **D92** no. 7, (2015) 075038, arXiv:1412.7577 [hep-ph].

[284] C. Englert, I. Low and M. Spannowsky, "On-shell interference effects in Higgs boson final states," *Phys. Rev.* **D91** no. 7, (2015) 074029, arXiv:1502.04678 [hep-ph]

[285] C. Englert, M. McCullough and M. Spannowsky, "Combining LEP and LHC to bound the Higgs Width," *Nucl. Phys.* **B902** (2016) 440–457, arXiv:1504.02458 [hep-ph].
10

[286] E. Fuchs and G. Weiglein, "Impact of CP-violating interference effects on MSSM Higgs searches," *Eur. Phys. J.* **C78** no. 2, (2018) 87, arXiv:1705.05757 [hep-ph].

[287] http://www.th.u-psud.fr/NMHDECAY/nmssmtools.html.

[288] U. Ellwanger, J. F. Gunion, and C. Hugonie, "NMHDECAY: A Fortran code for the Higgs masses, couplings and decay widths in the NMSSM," *JHEP* **0502** (2005) 066, arXiv:hep-ph/0406215 [hep-ph]

[289] U. Ellwanger and C. Hugonie, "NMHDECAY 2.0: An Updated program for sparticle masses, Higgs masses, couplings and decay widths in the NMSSM," *Comput.Phys.Commun.* **175** (2006) 290–303, arXiv:hep-ph/0508022 [hep-ph].

[290] G. Belanger, F. Boudjema, A. Pukhov, and A. Semenov, "MicrOMEGAs 2.0: A Program to calculate the relic density of dark matter in a generic model," *Comput.Phys.Commun.* **176** (2007) 367–382, arXiv:hep-ph/0607059 [hep-ph].

[291] G. Bélanger, F. Boudjema, A. Pukhov, and A. Semenov, "MicrOMEGAs4.1: two dark matter candidates," *Comput. Phys. Commun.* **192** (2015) 322–329, arXiv:1407.6129 [hep-ph].

[292] **Planck Collaboration**, P. Ade *et al.*, "Planck 2015 results. XIII. Cosmological parameters," arXiv:1502.01589 [astro-ph.CO].

[293] **XENON Collaboration**, E. Aprile *et al.*, "First Dark Matter Search Results from the XENON1T Experiment," arXiv:1705.06655 [astro-ph.CO].

[294] **Fermi-LAT and MAGIC Collaborations**, M. L. Ahnen *et al.*, "Limits to dark matter annihilation cross-section from a combined analysis of MAGIC and Fermi-LAT observations of dwarf satellite galaxies," *JCAP* **1602** no. 02, (2016) 039, arXiv:1601.06590 [astro-ph.HE].

[295] **CMS Collaboration**, "Combined measurements of the Higgs boson's couplings at $\sqrt{s} = 13$ TeV," Tech. Rep. CMS-PAS-HIG-17-031, CERN, Geneva, Mar. 2018

[296] **ATLAS Collaboration**, M. Aaboud *et al.*, "Search for electroweak production of supersymmetric states in scenarios with compressed mass spectra at $\sqrt{s} = 13$ TeV with the ATLAS detector," *Phys. Rev.* **D97** no. 5, (2018) 052010, arXiv:1712.08119 [hep-ex].

[297] **CMS Collaboration**, A. M. Sirunyan *et al.*, "Combined search for electroweak production of charginos and neutralinos in proton-proton collisions at $\sqrt{s} = 13$ TeV," *JHEP* **03** (2018) 160, arXiv:1801.03957 [hep-ex].

[298] **ATLAS Collaboration**, M. Aaboud *et al.*, "Search for additional heavy neutral Higgs and gauge bosons in the ditau final state produced in 36 fb^1 of pp collisions at $\sqrt{s} = 13$ TeV with the ATLAS detector," *JHEP* **01** (2018) 055, arXiv:1709.07242 [hep-ex].

[299] K. Ender, T. Graf, M. Muhlleitner and H. Rzehak, "Analysis of the NMSSM Higgs Boson Masses at One-Loop Level," Phys. Rev. D **85**, 075024 (2012) [arXiv:1111.4952 [hep-ph]].

[300] J. M. Cornwall, "Dynamical Mass Generation in Continuum QCD," *Phys. Rev.* **D26** (1982) 1453.

[301] J. M. Cornwall and J. Papavassiliou, "Gauge Invariant Three Gluon Vertex in QCD," *Phys. Rev.* **D40** (1989) 3474

[302] J. Papavassiliou, "Gauge Invariant Proper Selfenergies and Vertices in Gauge Theories with Broken Symmetry," *Phys. Rev.* **D41** (1990) 3179

[303] J. Papavassiliou, "Gauge independent transverse and longitudinal self energies and vertices via the pinch technique," *Phys. Rev.* **D50** (1994) 5958–5970, arXiv:hep-ph/9406258.

[304] G. Degrassi and A. Sirlin, "Gauge invariant selfenergies and vertex parts of the Standard Model in the pinch technique framework," *Phys. Rev.* **D46** (1992) 3104–3116

[305] S. Hashimoto, J. Kodaira, Y. Yasui, and K. Sasaki, "The Background field method: Alternative way of deriving the pinch technique's results," *Phys. Rev.* **D50** (1994) 7066–7076, arXiv:hep-ph/9406271

[306] N. J. Watson, "Universality of the pinch technique gauge boson selfenergies," *Phys. Lett.* **B349** (1995) 155–164, arXiv:hep-ph/9412319

[307] D. Binosi and J. Papavassiliou, "Pinch Technique: Theory and Applications," *Phys. Rept.* **479** (2009) 1–152, arXiv:0909.2536 [hep-ph].

[308] J. Ocariz, "Probability and Statistics for Particle Physicists," CERN-2014-001 and KEK-Proceedings 2013-8, pp. 253-280 [arXiv:1405.3402 [physics.data-an]].

[309] R. Brun and F. Rademakers, "ROOT: An object oriented data analysis framework," Nucl. Instrum. Meth. A **389**, 81 (1997).

[310] W. Verkerke and D. P. Kirkby, eConf C **0303241**, MOLT007 (2003) [physics/0306116].